Forschungszentrum Jülich

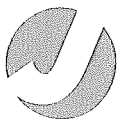

Institut für Chemie und Dynamik der Geosphäre 3:
Atmosphärische Chemie

Measurements of Atmospheric Trace Gas Concentrations during the Field Campaign in Jülich 1990

Jül-3650

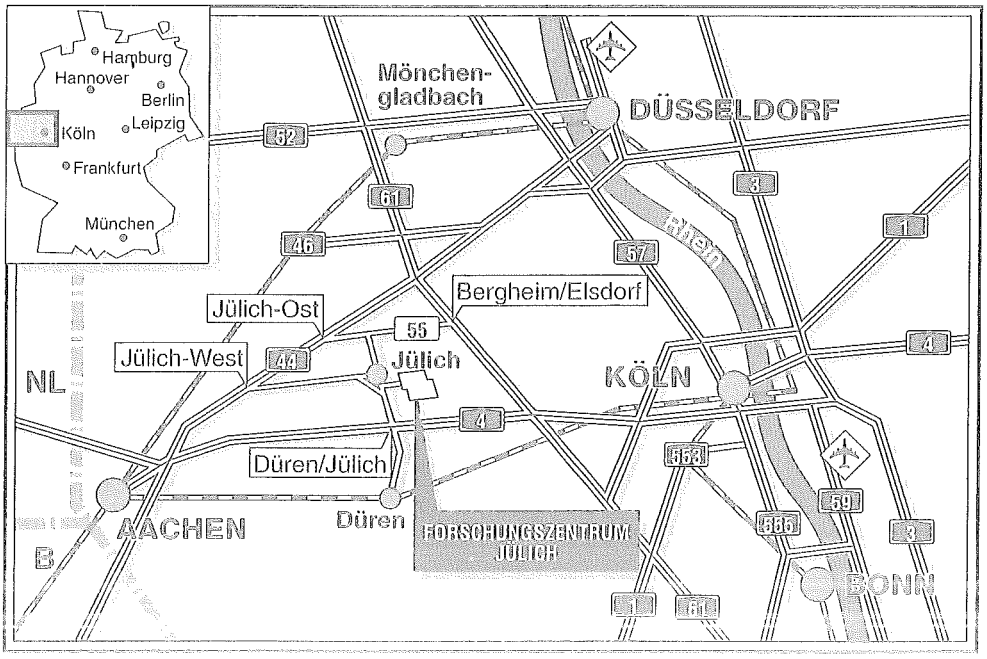

Berichte des Forschungszentrums Jülich ; 3350
ISSN 0944-2952
Institut für Chemie und Dynamik der Geosphäre 3:
Atmosphärische Chemie Jül-3350

Zu beziehen durch: Forschungszentrum Jülich GmbH · Zentralbibliothek
D-52425 Jülich · Bundesrepublik Deutschland
☎ 02461/61-6102 · Telefax: 02461/61-6103 · e-mail: zb-publikation@fz-juelich.de

Measurements of Atmospheric Trace Gas Concentrations during the Field Campaign in Jülich 1990

D. Poppe, R. Bauer, T. Brauers, D. Brüning, J. Callies, H.-P. Dorn, R. Gerlach, A. Hofzumahaus, F.-J. Johnen, A. Khedim, H. Koch, R. Koppmann, H. London, S. Mertes, K.-P. Müller, M. Müller, R. Neuroth, Ch. Plaß-Dülmer, F. Rohrer, J. Rudolph, U. Schmidt, A. Wahner, M. Wallasch, M. Weber, and D.H. Ehhalt

Abstract

Measurements of atmospheric trace gas concentrations, photolysis frequencies, and meteorological parameters from a field campaign in Jülich (lat.: 50.9°N, long.: 6.3°E, alt.: 100 m above sealevel) are presented. The measurements were performed at the earth surface between July 29 and August 13, 1990, a period of fine weather with hardly any precipitation

The objectives of the field study were to probe near surface air masses and determine their trace gas composition and their photochemical activity. Ultimate goal is the comparison with appropriate numerical model calculations to test our current understanding of the trace gas chemistry of the lower atmosphere. They are the same as for the field study in 1988 at the same location (Poppe et al., 1993).

The measured quantities include the concentration of OH, O_3, NO, and NO_2, NO_y, HCHO, SO_2, CH_4, CO, nonmethane hydrocarbons up to C7, peroxy acetylnitrate, and aldehydes. The photolysis frequencies of O_3 and NO_2 were monitored together with pressure, relative humidity, wind speed and wind direction.

The report presents the experimental material and the experimental techniques. A discussion of the experimental uncertainties is also given. The access to the data in computerized form for interpretation and processing is indicated.

Contents

Contents

Contents

1. Introduction

The Institute of Atmospheric Chemistry (ICG-3) has continued its efforts to investigate the atmospheric chemistry of the planetary boundary layer air with a major field campaign in summer 1990 from July 29 to August 13 in Jülich.

The experimental site, the objectives, and the methodology were the same as for the field experiment in 1988 and the reader is refered to the report on that experiment (Poppe et al., 1993). Here we briefly summarize some major characteristics of the trace gas burden and the weather encountered during the field experiment. The abundances of anthropogenic pollutants were quite high. The CO mixing ratio was always larger than 107 ppb with an average of about 300 ppb. Nonmethane hydrocarbons showed also elevated concentrations. For example the light alkanes ($< C_5$) were found with individual mixing ratios that varied between a few hundred ppt and 7 ppb. Similar results were found for the light alkenes. For example mixing ratios for ethene up to 11 ppb and propene up to 1.5 ppb were encountered. The most important biogenically emitted organic compound, isoprene, was also measured. Due to the high temperatures up to 35°C the emissions were substantial and led to mixing ratios of about 8 ppb in the early afternoon, the average, however, was with 0.7 ppb much lower. The weather was characterized by often clear sky with hardly any precipitation. The chemistry exhibited a high photochemical activity which gave rise to considerable photooxidant formation causing strong diurnal variations of ozone with maximum mixing ratios of 140 ppb. Despite the high temperatures peroxyacetylnitrate (PAN) was present with up to 3.5 ppb. Also partly oxidized compounds like formaldehyde and acetaldehyde were formed with maximum mixing ratios of 7 ppb and 2.2 ppb, respectively.

The meteorological conditions divided the campaign into two sections. Until Aug. 6 stable conditions were encountered while a high pressure system was located over middle Europe. The wind came from various directions and the wind speed was low. On Aug. 6 a weak front passed Jülich and unpolluted air was transported to the experimental site. From Aug. 7 on again a stagnant high pressure system with increasing temperatures evolved. In particular the data from the second part of the field experiment are an interesting record of the temporal development of an episode ending with a high burden of photooxidants.

Similar to the report on the data from 1988 we will concentrate on the presentation of the experimental results and the documentation of the experimental techniques. The latter are presented in the next two sections with emphasis on the alterations and improvements relative to the campaign of 1988. In appendix A the measured diurnal cycles of all measured quantities are given. Weather maps (kindly provided by the

Deutscher Wetterdienst) are given in Appendix B. Access to the data in computerized form is indicated in section 4.

2. Measurement Sites

Hydrocarbons, CO, O_3, NO, NO_2, aldehydes, and PAN were measured in-situ. The majority of these measurements were done in the vicinity of the building of the institute (see Figure 1). It is part of the Forschungszentrum Jülich and located in a deciduous forest. Car parks and service roads surround the building. Gas inlets were installed several meters above the ground to prevent contamination from sources of the immediate neighborhood. The photolysis frequencies were measured on the roof of the building.

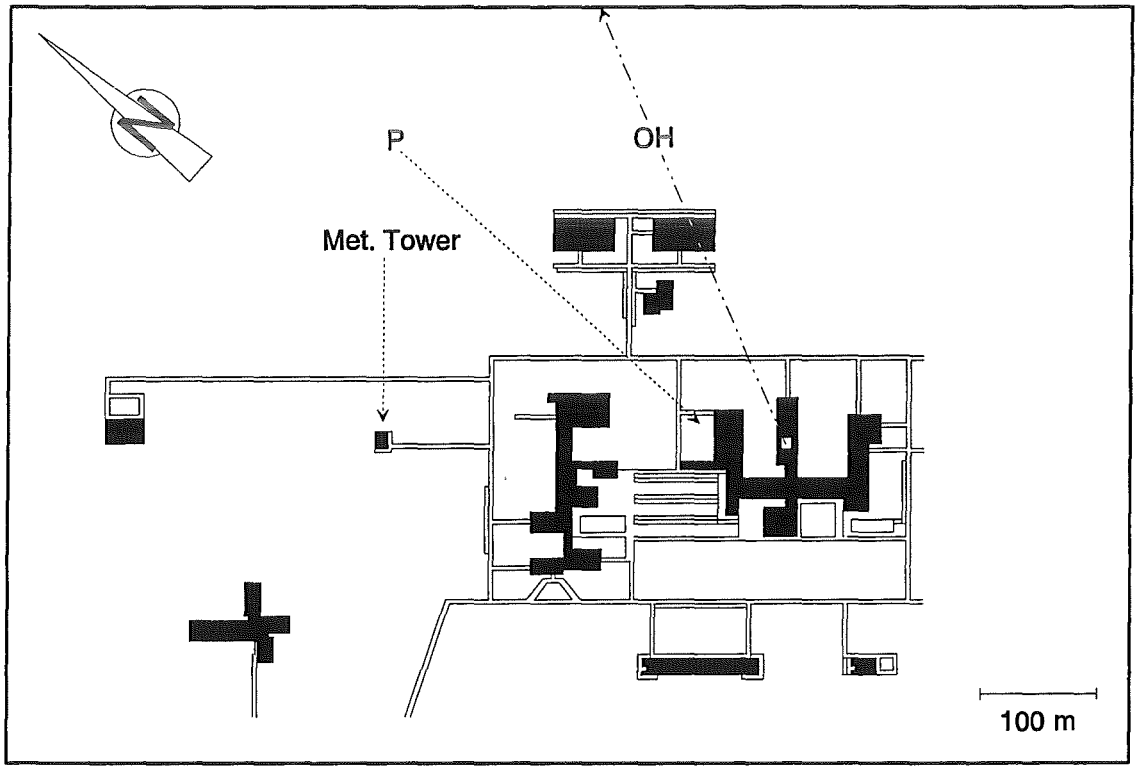

Figure 1: Measurement site. The location of the gas inlets (P) and the two long-path absorption instruments (used for the detection of OH and NO_2, HCHO, O_3, SO_2, respectively) as well as the light path are indicated.

Gas samples for analysis of hydrocarbon abundances were also taken at several places on the Sophienhöhe. It is an artificial hill with a altitude of 285 m above sea level in approximately 3 km distance. It covers an area of 3 km by 4 km. A surface brown coal mine of 12 km^2 size and a depth of roughly 200 m is located south east of the hill. It is known that the topography gives rise to local perturbations of the windfield near the surface. The area is embedded into a rather flat landscape which extends over 10 km in, all directions. The mean height above sea level is about 100 m.

OH, O_3, NO_2, HCHO, and SO_2 were studied by two instruments based on long path optical-absorption. For both instruments, the absorbtion light path was set up between the roof of the institute building within the KFA, where the light sources and optical detection systems were installed, and near the top of the Sophienhöhe where a reflecting mirror was mounted. The mean height of the beam above ground was 50 m. One of the spectrometers, the high resolution system needed for OH detection, suffered from technical problems with the detection device, resulting in a poor detection limit of only $7 \cdot 10^6$ cm^{-3}. Therefore, only upper limits of the OH concentration were determined.

The main sources of pollutants were to some extent the immediate surroundings of the institute, the town of Jülich and several power plants burning brown coal within distances between 10 km and 15 km. The site is surrounded by three motor ways with heavy traffic. The distance to the motorways is between 10 km and 20 km.

Local meteorological data were obtained from sensors at the institute and from the meteorological tower of the KFA (see section 3.3). The horizontal distance to the institute is roughly 270 m. For the height of the PBL, we rely on the data of the Deutscher Wetterdienst station in Essen, which is located about 100 km east of Jülich.

3. Experimental Data

This section presents a brief description of the experimental techniques and an uncertainty analysis of the data. It also discusses the program of the measurements and the performance of the instruments.

An overview over the experimental material is given in Table 1. Frequency and integration time of the measurements and the total number of data obtained are entered for each species.

#	data	measurement technique	file	tot. meas.
1	NO	chemiluminescence	NO____NEW	1349
2	NO_2	chemiluminescence	NO2_CNEW	1071
3	NO_2	DOAS	ALLDOASJ/S5	906
4	NO_y	chemiluminescence	NOY__NEW	1346
5	O_3	DASIBI # 1	O3_D1NEW	1806
6	O_3	DASIBI # 3	O3_D3NEW	1963
7	O_3	DASIBI +) Horiba	O3_HGNEW	1950
8	O_3	DASIBI (courtesy of U Heidelberg) Horiba	O3_HHNEW	1985
9	O_3	DOAS	ALLDOASJ/S7	905
10	O_3 - column density	O3cd, Brewer	O3CD	81
11	HCHO	HPLC	HCHO	383
12	HCHO	DOAS	ALLDOASJ/S6	905
13	CH_3CHO	HPCL	CH3CHO	383
14	CO	GC grab sample	CO_BHLTR	111
15	CO	GC grab sample	CO_SH	13
16	CO	see section 3.1.5	CO	1853
17	CO_2	GC grab sample	CO2	111
18	CO_2	GC grab sample *)	CO2_SH	13
19	CH_4	GC grab sample	METHAN	111
20	CH_4	GC grab sample *)	METHAN_S	12
21	PAN	see section 3.1.6	PAN	1153
22	ethane	GC in-situ	ETHAN	102
23	propane	GC	PROPAN	103
24	i-butane	GC	I-BUTAN	103
25	n-butane	GC	N-BUTAN	103
26	ethene	GC in-situ	ETHEN	103
27	propene	GC	PROPEN	103
28	1-butene	GC	1-BUTEN	103
29	actylene	GC in-situ	ACETYLEN	102
30	isoprene	GC	ISOPREN	101
31	CH_3Cl	GC in-situ	CH3CL	103
32	ROOH	fluorimetric analysis	ROOH	3645
33	HNO_3	see section 3.1.8	HNO3	55
34	totale nitrate	filter technique	NITRAT	55
35	SO_2	DOAS	ALLDOASJ/S8	887
36	Rn activity	Radon - a - counts, cts, cts /sec x ltr, Meteo	RADONNEW	655
37	$J(O^1D)$	filter radiometer	JO1D_JO0	1143
38	$J(O^1D)$	filter radiometer	JO1D_JO1	10776
39	$J(O^1D)$	filter radiometer	JO1D_JO2	10776
40	$J(NO_2)$	filter radiometer	JNO2RNEW	1350

+) Dasibi of the manufacturing company
*) measurement on Sophienhöhe
#) data from Hohenpeißenberg

NO_y : $NO + NO_2 + NO_3 + 2\,N_2O_5 + HNO_2 + HNO_3 + HNO_4 + PAN$ + nitrate aerosol

PAN : Peroxiacetylnitrate

$J(O_3)$: photolysis frequency $O_3 \rightarrow O(^1D) + O_2$

$J(NO_2)$: photolysis frequency $NO_2 \rightarrow NO + O(^3P)$

Table 1: Overview of the measured quantities during the campaign in Jülich 1990.

Table 1 continued

#	data	measurement technique	file	tot. meas.
41	total radiation (2.5 µm)	see section 3.3	GSTR_NEW	1990
42	condensation nuclei	METEO system	CONDNNEW	1989
43	visibility β	nephelometer # 2	NEPH2NEW	1989
44	R.H. (2 m)		RF__2	2149
45	R.H. (20 m)		RF_20	2149
46	R.H. (50 m)		RF_50	2149
47	R.H. (100 m)		RF100	2149
48	temperature (2 m)		T__2	1345
49	temperature (20 m)		T_20	2149
50	temperature (50 m)		T_50	2149
51	temperature (100 m)		T100	2149
52	wind speed (2 m)		WG__2	2144
53	wind speed (20 m)		WG_20	2145
54	wind speed (50 m)		WG_50	2145
55	wind speed (100 m)		WG100	2142
56	wind direction (50 m)		WR_50	2149
57	wind direction (120 m)		WR120	2149

+) Dasibi of the manufacturing company
*) measurement on Sophienhöhe
#) data from Hohenpeißenberg

NO_y : $NO + NO_2 + NO_3 + 2\,N_2O_5 + HNO_2 + HNO_3 + HNO_4 + PAN$ + nitrate aerosol

PAN : Peroxiacetylnitrate

$J(O_3)$: photolysis frequency $O_3 \rightarrow O(^1D) + O_2$

$J(NO_2)$: photolysis frequency $NO_2 \rightarrow NO + O(^3P)$

3.1 Trace Gas Concentrations

3.1.1 Measurement of NO, NO_2, NO_y, and O_3

NO, NO_2 and NO_y were measured by the chemiluminescence technique described by Drummond et al. (1985). Three NO-detector systems were used. They were equipped with a photolytic converter for NO_2-detection and a gold converter for NO_y-detection. Each NO-detector has a sensitivity of about 1 cps/ppt NO. The data were obtained with a time resolution of 30 s. In an alternating sequence, 'background'-signals (including the dark current of the PMT and most of the interfering fluorescences) were measured by placing a prereaction chamber in the ambient air flow. The trace gas signal was derived by subtraction of these background signals from the NO signals and multiplication with the instrument sensitivity. The average (and the standard deviation) of 10 individual

trace gas measurements were used to obtain mixing ratios and variances for an integration time of 10 minutes.

The detectors were calibrated once a day using a mixture of synthetic air and NO calibration gas (2 ppm NO/N_2, SPECTRASEAL). The calibration factors showed day-to-day fluctuations of less than 3%. For the data analysis, the calibration factors were linearly interpolated between the calibration times. The calibration mixture was checked by gas phase titration of NO with ozone with an UV-photometer (Dasibi 1003 AH). The calibration uncertainty is estimated to be approx. 5%.

The inlet point was located 12 m West of the institute building and 10 m above ground. Ambient air was pumped at a flow rate of 4 l/min (1.5 l/min for the NO- and NO_2-detectors, 1 l/min for the NO_y detector) through the 17 m long Teflon (PTFE, inner diameter 4 mm) line with a residence time of 3.2 s.

Measured NO mixing ratios were corrected for the reaction of NO with ozone in the inlet line. Using the measured ozone concentrations (see below) and the ambient temperature at 20 m altitude at the meteorological tower of the KFA, the correction amounts for approx. 7% / 14% at 50 ppb / 100 ppb ozone. The associated error is estimated to be 2% / 4% at 50 ppb / 100 ppb ozone. Combining the different error sources mentioned before, the accuracy of the measured NO mixing ratios is estimated to be 3 ppt (due to the noise of the NO signal) plus 10% / 12% of the NO-value at 50 ppb / 100 ppb ozone.

NO_2 was measured by the second NO-detector using a photolytic converter equipped with a 300 W Xe-arc lamp (Rohrer and Brüning, 1992). The conversion efficiency was determined daily using a NO_2-calibration mixture in synthetic air. The photolytic converter efficiency was typically 0.6 and showed day-to-day fluctuations of less than 5%. This efficiency was corrected for the reaction of NO with ozone in the inlet line and in the converter volume. NO_2 mixing ratios were obtained by subtraction of the simultaneous measured NO of the first detector from the NO detected after the photolytic converter. The noise of the NO_2-detector was around 15 ppt NO_2 at zero ppb NO_X and 50 ppt at 5 ppb NO_X. The overall accuracy of the NO_2-mixing ratios is estimated to be 15 ppt plus 17% of the NO_2-signal. The accuracy of the NO/NO_2-ratio is estimated to be 10% for NO- and NO_2-signals higher than 100 ppt.

NO_y (the sum of NO, NO_2, NO_3, 2 N_2O_5, HNO_2, HNO_3, PAN, organic nitrate, nitrate aerosol ...) was measured by the third NO detector after conversion of NO_y to NO in a heated gold tube (Fahey et al., 1985). Since HNO_3 was absorbed at the surface of the

long inlet line, the detector did not measure any contribution from HNO_3. Potentially this is a source of large errors of the NO_y measurement, possibly up to a factor of 2. On average, the measured HNO_3-mixing ratios were on the order of 10% of NO_y (see Table 4). The conversion efficiency of the NO_y-converter for NO_2 was checked each day resulting in a maximum error of 5%. The accuracy of the NO_y-mixing ratios arising from NO, NO_2 and PAN contributions is estimated to be 100 ppt plus 10% of the NO_y-signal.

Ozone was measured by four UV-photometers (two DASIBI type 1003 and two HORIBA type APOA 350 E). The instruments were located near the DOAS-experiment on the roof of the building. The accuracy and precision of the instruments as specified by the manufacturers are around 3% and 1 ppb ozone, resp. Through a comparison between these instruments and with a reference instrument (DASIBI type 1008 PC), the actual precision of the instruments is estimated to be 3 ppb.

3.1.2 Measurement of Tropospheric OH by Long Path Absorption

The concentration of tropospheric hydroxyl radicals, OH, was measured by differential optical absorption spectroscopy (DOAS). As shown in Figure 1 the absorption path extended from the roof of the institute's building to near the top of the Sophienhöhe where a plane mirror was mounted (Fig. 2).
The total light path length was 5.8 km. The distance to the ground is indicated in Figure 3. Because the instrumental setup is already described in the literature (Perner et al. 1987, Callies 1988, Callies et al. 1989, Dorn et al. 1988, Platt et al. 1988) only a short description will be given here. The instrument consists of four main parts: light source, absorption path, spectrometer, and spectral detector.

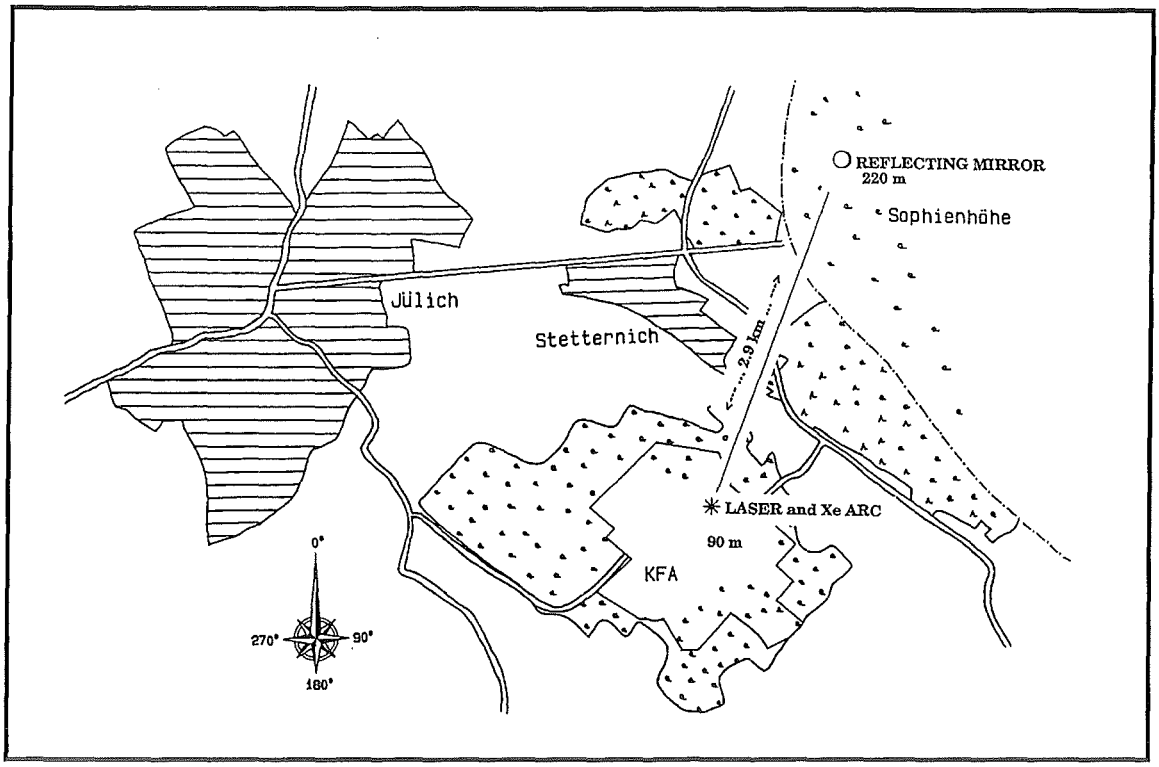

Figure 2: Location of the coincident light paths for the DOAS-experiments. The light sources and the spectrometers were located on the roof of the building of the Institute of Atmospheric Chemistry (altitude 100 m). The reflector was mounted near the top of the Sophienhöhe (altitude 220 m). The total length of each light path was 5.8 km.

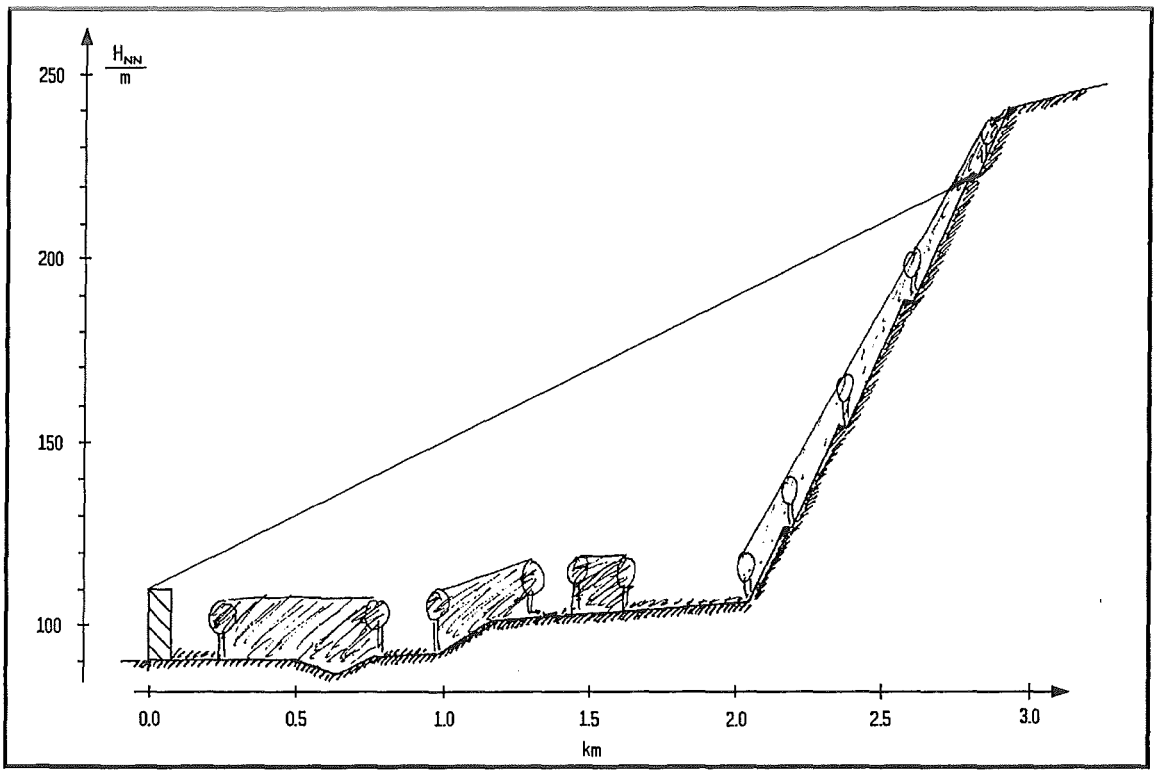

Figure 3: Height profile of the DOAS-absorption path.

Light source

Because the rotational lines of OH have a very narrow bandwidth (2.5 pm under atmospheric conditions) the high spectral irradiance essential for absorption spectroscopy can only be provided by a UV laser. The system used in our measurements was a frequency doubled picosecond dye laser which was synchronously pumped by a mode-locked argon ion laser. The dye laser generated nearly transform limited picosecond pulses with a intensity profile of large bandwidth (about 0.15 nm after frequency doubling to 308 nm) and very little spectral substructures. Both features are of decisive importance for tropospheric trace species measurements especially under polluted conditions. Typical UV output power is 15 mW.

Absorption path

Before entering the free troposphere, the laser beam was expanded by about a factor of 50 using a Cassegrin telescope in order to reduce the beam divergence and light intensity and thus the level of self generated OH radicals by laser induced photolysis of ambient ozone and subsequent formation of OH.

Spectrometer

After passing the absorption path, light was collected by a Newton telescope ($f = 2400$ mm, $d = 300$ mm) and was focused onto the entrance slit of a high resolution double grating spectrometer ($\lambda/\Delta\lambda = 171000$).

Detection system

Spectra were recorded using a linear photodiode array as a multichannel spectrometric detector.

The spectrum was image from the exit plane of the spectrograph onto the diode array using a 3 element UV achromat with a magnification factor of about 11. This resulted in oversampling since the smallest resolvable spectral element was covered by 5-6 diodes of the array.

Sources of error and results of the 1990 campaign

The instrumental setup of the OH instrument used for the 1990 measurements was the same as used for the 1988 campaign. The OH detection limit in 1990 however was considerably higher than in 1988, because of the aging of the photo diode array detector and of the homebuild electronics controlling the detector head. The following sources of error predominantly controlled the OH detection limit in 1990:

1. Artificial structures generated by the detector itself.

   In order to avoid etalon interferences the photo diode array detector was continuously operated without a protective window for more than 3 years. Although the detector chamber was always flushed with aerosol free dry air during that time, we finally observed substantial covering of the semiconductor surface with very small (≤ 20 µm) particles which could not be removed by cleaning.

   A careful examination of the influence of these particles on the signal response of the diode array in laboratory experiments after the OH campaign showed a relatively large effect (Neuroth 1992).

   It is well known that the output signal of even clean new diode arrays depends on the illumination characteristics like angle of incidence, polarization and homogeneity of the detector illumination (Dorn et al., 1994). Diode arrays based spectrometers applied for atmospheric measurements suffer from this peculiarity, because air turbulences change the angle of incidence of the light from the spectrograph onto the detector. Furthermore the image of the light source on the detector surface forms a rapidly changing speckle pattern after the passage of the atmospheric path, which is very pronounced when coherent laser light is used. In consequence the detector is usually not homogeneously illuminated. The resulting 'illumination noise' unfortunately behaves non–statistically (the generated noise background does not improve with the square root of the number of photoelectrons sampled) and therefore the lowest detectable optical density (absorbance) is usually limited to at least $(1\text{-}2)\cdot 10^{-4}$ using diode arrays although the corresponding shot noise limit (calculated from the number of photoelectrons measured) can be as much as 10 times lower for typical measurement conditions.

   The presence of particles on the detector surface which were in the dimension of the width of an individual array pixel (25 µm) enlarged this illumination noise even further.

2. Etalon interferences

   Optical elements like lenses and windows which were placed in the coherent laser beam caused periodic spectral modulations of the received light intensity because they were acting as etalons of very low finesse. Probably due to slight illumination differences of these components during the recording of air and reference spectra a weak residual periodic modulation remained in the quotient although it was theoretically expected that the etalon effect should have cancel after division.

   This effect modulated the spectral baseline and thus appeared like weak 'absorption signals' which increased the noise and enhanced the detection limit for absorbing trace gases.

Altogether those interference effects caused residual structures in the measured spectra which on the average corresponded to an optical density of $4 \cdot 10^{-4}$ (Neuroth, 1992) and reached peak values of up to $(1\text{-}2) \cdot 10^{-3}$. This signal level must be compared with the expected absorbance due to ambient OH radical concetrations. For $3 \cdot 10^{6}$ OH/cm^3 and a light path length of 5800 m the resulting optical density is about $2 \cdot 10^{-4}$.

The high noise level had further consequences for the subtraction of absorption features of SO_2 and HCHO. At high concentrations of these trace gases the subtraction was no longer quantitative leading to spurius signals in the residual spectra which interfered with the OH bands resulting in an even worse OH detection sensitivity.

In summary the instrumental detection sensitivity during the 1990 field campaign was about $7 \cdot 10^{6}$ OH/cm^3 and therefore all the OH concentration data of this campaign only represent upper limits. Therefore these data are not given in the report.

For the measurement of SO_2 the limitations given above are of less relevance. The observed SO_2 mixing ratio during the field campaign ranged from 1-12 ppb corresponding to an absorbance of $(0.5\text{-}3.5) \cdot 10^{-3}$. A comparison of SO_2 data obtained with the OH instrument and the measurements of a low resolution long path instrument (which probed roughly the same air volume; see section 3.1.3) showed a good correlation (Fig. 4). The scatter observed can be explained by different integration times of both instruments and the influence of stray light within the spectrograph of the low resolution instrument.

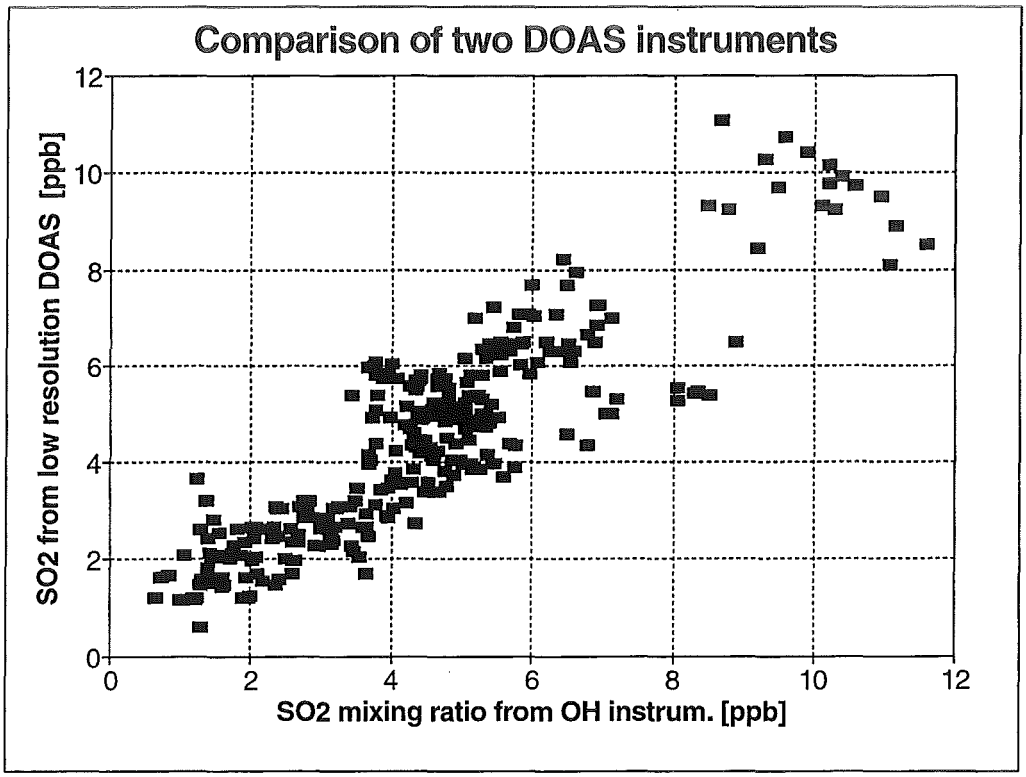

Figure 4: Comparison of SO_2 measurements with low and high resolution DOAS techniques

3.1.3 Measurement of O_3, NO_2, HCHO, and SO_2 by Long Path Differential Absorption

Long Path Differential Optical Absorption Spectroscopy (DOAS) was used for the simultaneous measurements of O_3, NO_2, CH_2O, and SO_2 using nearly the same light path as the OH measurements. DOAS with low spectral resolution (0.3 nm) uses the characteristic vibrational structure of electronic transitions in the visible and ultraviolet spectral region for the detection of trace gases (see cf. review by Platt (1994)). The following section will briefly describe the experimental technique and the evaluation of the data.

Experimental

The collimated beam of a 500 W high pressure Xe arc lamp on the roof of KFA building (see Figure 2) was directed to a remote controlled flat mirror (30 cm diameter) near the top of the Sophienhöhe. This mirror was also used by the OH long path absorption experiment (see section 3.1.2). The reflected light was collected by a Newton type telescope (f = 1.8 m, 30 cm diameter) and focused into a spectrometer (SPEX 1870, f = 0.5 m, 600 l/mm) both located on the same roof. The total absorption path length was 5.8 km. A 60 nm spectral range (300 nm - 360 nm) was repetitively scanned (100 Hz) by a rotating slotted disk mounted in the focal plane of the spectrometer. The light passing the slit was detected using a photomultiplier tube (EMI 9659QB, 2"diameter) and its output signal was digitized with a 12-Bit-ADC at a sampling frequency of 40 kHz. 25000 scans were added and after offset correction this averaged signal was stored on a LSI11 computer as one spectrum. In addition to the air spectra reference spectra of NO_2 were recorded as a wavelength reference.

Data evaluation, calibration, and errors

The concentrations of the trace gases were determined from the spectra by applying Lambert-Beer's-law

$$c = \ln\left(\frac{I'_0}{I}\right) \Big/ L \cdot \sigma'$$

where I'_0 and I are the light intensity beside and in the center of a selected absorption band, respectively, while L denotes the optical path length and σ' the differential absorption cross section of the species being measured. The differential absorption cross sections were taken from the literature and are listed in Table 2.

The spectral range of the DOAS instrument covers absorption features of O_3, NO_2, CH_2O, and SO_2 in one spectrum. To determine the optical densities for each molecule present in ambient air absorption spectra different spectral regions for the evaluation were used (see Table 2). Within each region a multicomponent analysis was performed by simultaneously fitting the absorption spectra of the pure trace gases (reference spectra were recorded during the campaign with the field instrument) and a polynomial of 3rd order (which corrects for a slight curvature of the spectral baseline caused by the lamp profile and broadband unstructured trace gas absorption). The fitting procedure are based on a least-squares algorithm (Press et al., 1992) and are part of the MFC program which was used for the evaluation (Gomer et al., 1995). From the resulting vector of fit coefficients and the known absorbances of the reference spectra, the corresponding optical densities at the reference wavelength for each component were calculated. From those the final concentrations were obtained using the absorption cross sections (Table 2) and light path length (5.8 km).

The errors of the optical densities were calculated from the least square algorithm (Press et al., 1992; Gomer et al., 1995). The 1-σ estimated error of the fitting procedure represents the precision of the measurement and these errors are entered in the data files. However, this error represents a measure of the residual structure which cannot be attributed to the reference spectra (noise, unknown absorbers). The systematic errors caused by the uncertainties of the absorption cross section and the light path are not included. Since the error of the lightpath length is less than 1% the contribution of the absorption cross section to the accuracy of the measurements depends on the species as can be seen from Table 2.

Species	wavelength region used for fit	cross section σ' [10^{-20} cm^2]	Wavelength λ [nm]	reference
NO_2	345 nm - 356 nm	7.1 (± 5%)	348	Schneider et al., 1987
O_3	325 nm - 336 nm	0.65 (± 8%)	323	Molina and Molina, 1986
HCHO	325 nm - 336 nm	7.8 (± 20%)	326	Cantrell et al. 1990
SO_2	302 mn - 356 nm	57 (± 10%)	300	Brassington 1981

Table 2: Absorption bands and differential absorption cross sections (σ') used for the evaluation of the DOAS spectra. The spectral regions for the evaluation of the species are given in column 2. For the NO_2 evaluation only an NO_2 reference and a polynomial was fitted. Ozone and HCHO concentrations were calculated from a simultaneous fit of O_3, HCHO and NO_2 reference spectra in the respective spectral range. The SO_2 fit included reference spectra of NO_2, HCHO, and O_3.

Measurements

During the campaign 1155 air spectra were recorded. After analysis of the spectra and the results of the fitting procedure a number of spectra with low light levels or deviations from usual noise levels were removed from the data set. Finally the data set consists of 905 data points for O_3, NO_2, and CH_2O. The number of SO_2 data is only 887 since the light level in the wavelength region around 310 nm was much lower than at longer wavelength in the same spectrum. In addition the region around 308 nm was sometimes disturbed by scattered laser radiation of OH DOAS experiment.

3.1.4 Measurement of Hydrocarbons

Most of the nonmethane hydrocarbon (NMHC) measurements were made by in-situ gas chromatography. The instrument was installed in a container near the institute building. The air intake was located on top of a mast at 10 m above ground and at a distance of 5 m from the container. The distance to the nearest building was 15 m. The experimental technique is described in detail by Rudolph et al. (1986) and Koppmann et al. (1992).

The time required for one measurement including preconcentration from about 1 dm^3 of air was 3 h. The instrument was operated for 24 h a day from July 30, 1990, 17:30 UT until August 13, 1990, 11:00 UT. The samples were analyzed for the C_2- C_4-alkanes, C_2- C_4-alkenes, acetylene, isoprene, benzene, and toluene.

	error of calibration %	reproducibility %
alkanes		
ethane	10	5
propane	10	10
i-butane	30	9
n-butane	30	7
alkenes		
ethene	10	6
propene	25	19
1-butene	30	19
isoprene	30	< 20
acetylene	10	13
aromatics		
benzene	20	< 20
toluene	30	< 20

Table 3: Calibration error and reproducibility for the measurements of non-methane hydrocarbons.

The atmospheric mixing ratios were calculated by comparing the sample with a reference air of known composition. The mixing ratio of the different hydrocarbons in the reference air were in the range of a fraction of a ppb to a few ppt, comparable with the levels in ambient air. Reproducibility, and calibration errors are given in Table 3.

The raw data were acquired with a personal computer using a commercial chromatography software and stored on tape. During the campaign 141 air samples were measured.

In addition, 148 whole air grab samples were collected in 2 dm^3 stainless steel canisters. 113 samples were collected near to the laboratory container, 35 were collected on the Sophienhöhe. These samples were analyzed for nonmethane hydrocarbons using the same technique as for the in situ measurements and additionally for CO and CH_4 in the laboratory using a gas chromatograph with a molecular sieve column (5 A). For the detection with a flame ionization detector (FID) CO is reduced catalytically into CH_4. The quantization is done by comparing the sample with a reference air with a CO mixing ratio representative for ambient air. The reproducibility for CO and CH_4 was 1.5 % and 0.5 %, the total error of measurement was 1% and 2%, respectively.

3.1.5 In-situ Measurement of Carbon Monoxide

For the measurements of CO two Reduction Gas Analyzers (RGA 3, Trace Analytical Inc., USA) were operated in an automatic mode throughout the full campaign period. The instrument employs the mercury oxide technique developed by Seiler and Junge (1970), which is based on the reaction of CO with mercury oxide (HgO) at elevated temperatures (about 100°C),

$$HgO + CO \rightarrow CO_2 + Hg$$

The mercury vapor released through this reaction is monitored in an optical cell by atomic absorption at 253 nm. Because atmospheric hydrogen also reacts with HgO (Schmidt and Seiler, 1970), both trace gases are separated on a short chromatographic column (molecular sieve, 5 A) before the sample volume passes through the reaction cell. An automated sampling system was used to inject alternatively ambient air or a calibration standard. One measurement was made every 5 minutes. The analytical precision as derived from the series of standard analyses was better than 1%. The difference between the two instruments was smaller than 2%.

The sensitivity of the chemical detector of the RGA 3 changes if water vapor enter the reaction cell. Therefore, the sampled air was dried prior to injection. During this campaign the sampled air was taken from a bulk air flow supplied to the container from the same air intake line as used for the measurements of nonmethane hydrocarbons (cf. section 3.1.4).

3.1.6 Measurement of Peroxyacetylnitrate

The peroxyacetylnitrate (PAN) measurements were made by in situ gaschromatography. The instrument was situated inside the institute. The air intake was located on top of a 10 m mast at a distance of 12 m from the institute's building. The PTFE inlet line had a total length of 25 m. A continuous flow of air was drawn through the line by a pump, resulting in a delay time of about 0.8 s. The experimental technique is described in general by B. Vierkorn-Rudolph et al. (1985). The system used during the 1990 campaign was partially modified as described by K. P. Müller et al. (1989).

The instrument was operated for 24 h a day from July 30, 1990, 11:30 UT until August 13, 1990, 09:16 UT. The analysis time was 15 minutes. Only between July 31, 14:30 UT and August 01, 7:00 UT the analysis time was raised to 30 min. Between August 05, 2:30 UT and August 06, 7:16 UT the instrument was calibrated. Therefore no measurements of PAN were made during that period. A total number of 1153 air samples was taken during this campaign.

The atmospheric mixing ratios of PAN were calculated by comparing the air sample with a reference of a known PAN concentration of about 5 ppb. This reference gas was generated in a dynamic calibration source. After discontinuous hydrolysis it was quantified as nitrite ion by a colorimetric method. The mixing ratio of PAN in ambient air varied between 63 ppt and more than 3 ppb during some sunny periods. Reproducibility, calibration error and detection limits of the instrument were given by Müller et al. (1989). The raw data were acquired with a personal computer using a commercial integration software and stored on tape.

3.1.7 Measurement of Peroxides

For the in situ measurements of peroxides in the gas phase a stripping coil technique in combination with a fluorimetric analysis of peroxides was used. The method as applied to aqueous samples has been described in detail by Lazrus et al. (1985). The H_2O_2 vapor technique incorporates changes which optimize the stripping efficiency within the ambient H_2O_2 concentration range.

The technique is based on the selective catalysis of H_2O_2 decomposition with p-hydroxyphenylacetic acid (POPHA). The reaction products are water and the dimeric product, 6,6'-dihydroxy-3,3'-biphenyldiacetic acid. The dimeric product fluoresces with a peak excitation wavelength of 320 nm and a peak emission wavelength of 400 nm (Guilbault et al., 1968). The peroxide concentration is directly proportional to the fluorescence intensity.

Peroxidase also catalyzes the reaction of organic hydroperoxides to form the fluorescent dimer. In order to distinguish H_2O_2 from organic hydroperoxides, the technique utilizes a dual channel flow system with a dual cell fluorimeter. The reaction described above yields a measure of both the hydrogen peroxide and organic hydroperoxides in the first channel. In the second channel, the enzyme catalase is added to selectively destroy hydrogen peroxide before the peroxidase-catalyzed reaction occurs. The second channel therefore provides an analytical blank for the determination of H_2O_2 and the fluorescent signal is due only to organic hydroperoxides. The two signals are produced simultaneously by the system which is automated by means of a Technicon Autoanalyzer peristaltic pump. The difference between the two signals is a measure of H_2O_2 vapor.

Due to inconsistencies of the data of the second channel (negative data, strong fluctuations of the baseline) during the campaign only the data of the total peroxide channel was evaluated. The standard deviation of the baseline is 10 parts per trillion by volume (pptv) under laboratory conditions and 180 pptv during campaign conditions. The variation of the calibration (performed every 24 hours) was about ± 20%. Therefore the overall error is estimated to be approx. 35% for the total peroxides.

3.1.8 Measurement of Nitric Acid

Gaseous nitric acid (HNO_3) was measured by high volume sampling. The air intake was located on top of a 2 m mast at a distance of 15 m from the institute's building. The filter stack consisting of a PTFE-filter with a pore size of 0.25 µm to remove the particulate matter followed by 3 nylon-filters which absorb HNO_3 was flushed with 100 l STP/min of outside air. The nylon-filters were pretreated with sulfanilamide to reduce the blank

values and to simplify filter extraction. The serial filter scheme allows the control of HNO_3 sampling efficiency.
Analysis was carried out in the laboratory by wet chemical determination of the nitrate-ion content of the filters. They were extracted with 20 ml of blank-free water in an ultrasonic bath for about 20 minutes. The liquid phase was analyzed either by a modified Griess-photometric method or Ion-Chromatography with a detection limit of 2 ng/ml of NO_3^- each. The overall detection limit is determined by the blank values of the filters. The detection limit (3 sigma) for HNO_3 is 5 ppt for a sampling time of 60 minutes.

The collection of air samples was carried out from July 30. 1990, 9:30 UT until August 13. 1990, 07:00 UT. The number of samples normally was 5 a day. The sampling times were at 4:00, 7:00, 11:00, 15:00 and 20:00 UT daily. 64 measurements have been carried out during this campaign, 9 of which had to be rejected due to some breakthrough-events.

The mixing ratio of HNO_3 in ambient air was in the range of 0.05 ppbV up to 8 ppbV during some sunny periods. The nitrate aerosol collected on the Teflon-prefilters ranged from 0.05 to 5 ppbm. Reproducibility, calibration error and detection limits of the method were given by Müller and Rudolph (1991) and Papenbrock et al. (1992). The raw data were aquired with a personal computer using a commercial integration software and stored on tape.

3.1.9 Comparison between NO_2/O_3 - DOAS and in situ measurements

During the campaign NO_2 and O_3 were measured simultaneously by two different techniques: by long-path (DOAS) and local measurements (chemiluminescence detector and UV-photometer). These measurements will be compared, although the air masses which are probed by the different technics can be quite different. The experimental setup of these experiments is described in the sections concerned with the individual measurement technics. Here, only a short outline is given.

Measurement of O_3 and NO_2 by DOAS (Differential Optical Absorption Spectroscopy)
- light source: Xe arc lamp
- lenght of the light path: 5.8 km
- slope of light path 120m / 2.9 km
- detector: 0.5 m spectrograph with slotted disk + PMT
- spectral resolution 0.6 nm

- wavelength region 300 nm-360 nm and differential absorption cross sections

	λ [nm]	σ [10^{-20} cm^2]	accuracy
NO_2	348	7.1	5%
O_3	323	0.65	8%

- values integrated over 4-7 min (25000 individual scans)

Local NO_2 measured by CL (ChemiLuminescence)
- photolytic conversion of NO_2
- time resolution 30 sec
- accuracy 17%, precision 5%
- inlet 10 m above ground, at the institute building near one end of DOAS light path

Local O_3 measured by a UV-photometer
- absorption wavelength 254 nm
- commercial instrument (Horriba)
- data integrated over 10 min
- accuracy 3%, precision 3 ppb
- inlet at the institute building near one end of DOAS light path

Meteorological Data
- measured at the meteorological tower of the KFA
- 270 m from the inlets of the local measurements
- temperature, wind speed, R.H. at 2 m, 20 m, 50 m, and 100 m above ground
- wind direction at 50 m and 120 m above ground

The temperature data measured at 20 m and 100 m altitude were used for the calculation of the potential temperatures $\Delta\Theta$. The difference of the potential temperatures between 100 m and 20 m altitude is an indicator for the occurrence of convective transport ($\Delta\Theta > 0$) or the formation of an inversion layer ($\Delta\Theta < 0$). The diurnal variations of $\Delta\Theta$ ($\Delta\Theta > 0$ during daylight, $\Delta\Theta < 0$ during night) were quite stable during the whole time period.

Comparison of long-path and local measurements

For the comparison the temporal integration interval of DOAS (5 min) was chosen as a common time base for all measurements: For NO_2 (CL) mean and standard deviation were calculated for the 5-min interval. If available the 10 min average data were taken for O_3 (local) provided the integration intervals overlap. Otherwise an interpolation between closest data points was performed.

The scatter plots based on all data points (Fig. 5.1-2) show the large scatter of the whole data set. Fig. 5.1 (NO_2) shows 496 data pairs. Fig. 5.2 (O_3) shows 875 data pairs also with a high amount of scatter. The scatter might be due to the different air masses sampled by DOAS and the in situ techniques if the region covered by the light path of the DOAS and in situ instruments is not well mixed. Therefore we restricted the data set including only data when convective mixing can be assumed ($\Delta\Theta > 0$).

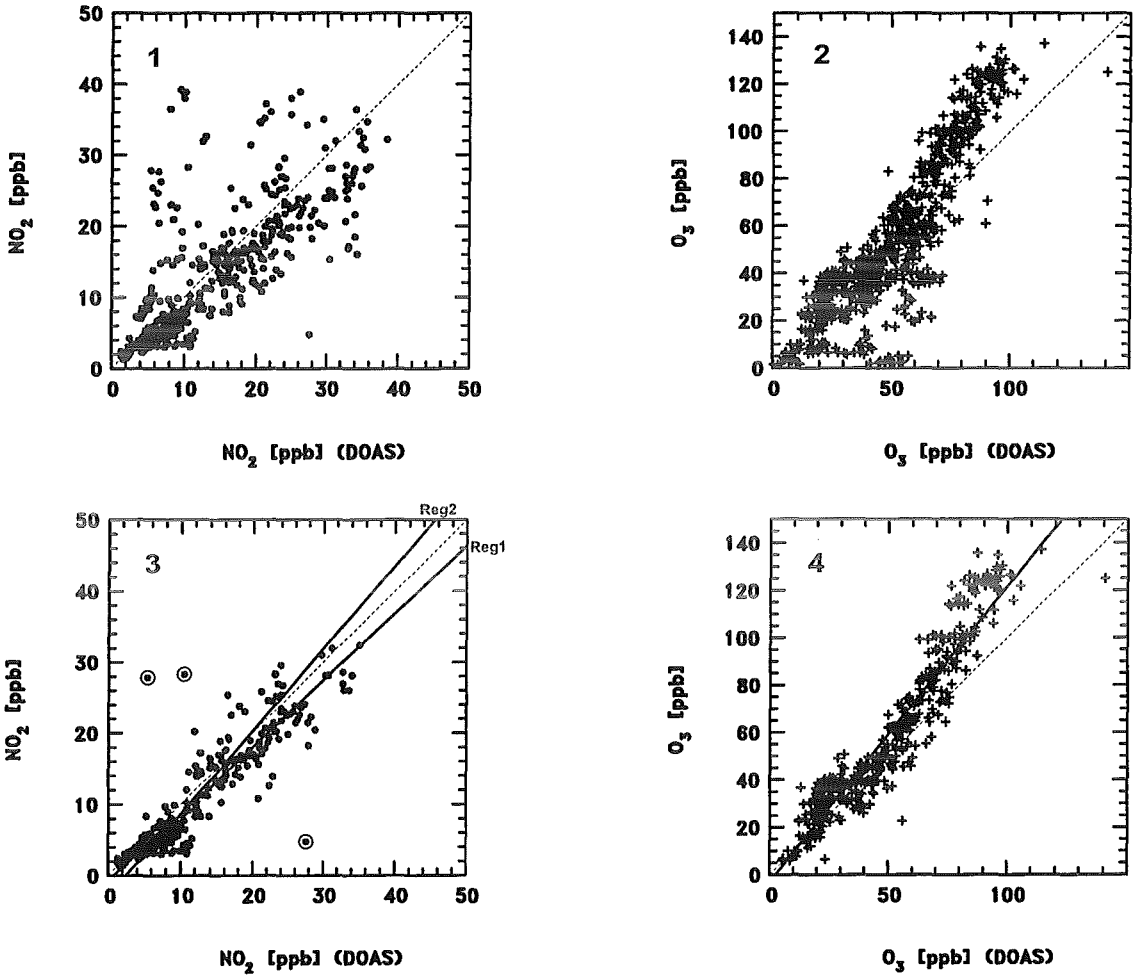

Figure 5.1-4: Comparison of NO_2 and O_3 measurements with DOAS- and in-situ technique, (1,2) all data pairs, (3,4) only data pairs with $\Delta\Theta > 0$

The restricted data set for NO_2 in Fig. 5.3 shows strongly reduced scatter compare to Fig. 5.1. Only 3 obvious outliers (high variances in CL data, probably due to local sources of NO_2) are left over. The correlation is surprisingly good ($R^2 = 0.912$) for the 334 data pairs. We used a linear regression algorithm to compare the results of the two measurement technics. Since linear regression is based on zero-variance of the independent variable it is not possible to calculate the correct fit parameters. Linear

regression tends to underestimate the slope and to overestimate the intercept if the independent variable has a significant variance. Therefore two linear regressions were calculated by interchanging the dependent and independent variable.

independent var.	intercept	slope	
NO_2 (DOAS)	-0.8±1.4	0.941±0.12	[Regression 1]
NO_2 (CL)	2.45±1.4	0.911±0.12	[Regression 2]

These results show that there is no significant deviation from unity slope.

The restricted data set for ozone (Fig. 5.4) shows also reduced scatter. There seems to be no significant deviation from unity slope between 0 and 80 ppb of ozone. But for ozone mixing ratios above 80 ppb there are systematic deviations from a linear relation. DOAS-values are 20-30 ppb lower than local measurements. These deviations are higher than the experimental uncertainties.

Conclusions

The large scatter in the correlation between local and long path measurements of NO_2 and ozone can strongly be reduced by restricting the data set to convective conditions. Inside the confidence limit of this data set, DOAS and CL measure the same values for NO_2. Contrary to this, the ozone measurements show a significant deviation between in-situ and long-path techniques for high ozone values (> 80 ppb). The reason for this deviation is yet unknown.

3.2 Photolysis frequencies of Ozone and Nitrogen Dioxide

$J(O^1D)$, the photolysis frequency of ozone

The photolysis frequency, $J(O(^1D))$, is the rate coefficient of the ozone photolysis leading to the formation of $O(^1D)$,

$$O_3 + h\nu \rightarrow O_2 + O(^1D)$$

It was determined by filter radiometry. The three instruments used during the campaign, named JO05, JO07, and JO08, were designed and built in our laboratory. Since

technical aspects and the calibration procedure have been published already (Junkermann et al., 1989, Schiller, 1987, Müller, 1994), only some details are given here.

Principles

The filter radiometers measure the atmospheric actinic flux from 2π sr in the wavelength range from 290 to 330 nm. The corresponding value for $J(O(^1D))$ is calculated by multiplying the output voltage U of a radiometer by a conversion function B, which has been determined individually for each instrument:

$$J(O(^1D)) = B \cdot U$$

B takes into account:

1. calibration of the instrument's absolute sensitivity either by radiometric characterization in the laboratory or by field comparisons with reference techniques (chemical actinometry or spectroradiometry),
2. correction for the mismatch between the instrument's spectral response and the ozone photodissociation spectrum,
3. correction for the deviation of the instrument's geometrical response from uniformity over one hemisphere.

For B the current values of the solar zenith angle and the ozone column density are used as input parameters. Additionally, an assumption for the spectral shape of the $O(^1D)$ quantum yield for the ozone photolysis reaction has to be made. Controversial data on the quantum yield have been published for the wavelength region 310 to 325 nm. Here the data from Brock and Watson (1980) were used which show $O(^1D)$ formation even at wavelength larger than 320 nm, in contrast to the NASA-JBL recommended $O(^1D)$ quantum yield (DeMore et al., 1992). Our decision is supported by our own recent field study on $O(^1D)$ formation (Müller et al., 1995), new laboratory measurements (Trolier and Wiesenfeld, 1988; Ball et al., 1993; Armerding et al., 1995) and a model by Michelsen et al. (1994). Since the revised quantum yield data have only been measured for room temperature, all $J(O(^1D))$ data determined from the filter radiometers are valid only for room temperature.

Experimental conditions

Instrument JO05 was located on the roof of the institute's building at about 25 m above ground level. It was mounted facing the upper hemisphere, with a completely free field of view. The output signal was read out with 1 Hz sampling rate and stored as mean values over 10 min integration time by the "METEO" data acquisition system.
The instruments JO07 and JO08 were mounted 100 m above the ground on a cantilever of the meteorological observation tower. The cantilever headed into SSW direction, thus no shadowing of the direct sun could occur. JO08 was looking upwards, while JO07 was looking downwards towards the surrounding grass area, woods, roads, and buildings of the KFA. The output signal were recorded at 1 Hz sampling rate by a stand-alone data acquisition system and stored as 1 min mean values. – At the same site, two filter radiometers for measuring $J(NO_2)$ and two instruments for monitoring the global radiation were operated.

Calibration

The determination of the conversion functions B for the instruments JO05, JO07, and JO08 was based on laboratory characterizations of the individual instruments in summer 1993 (Müller, 1994). As input parameters for B, ozone column data from the TOMS instrument on the NASA Nimbus 7 satellite were interpolated to the geographical site of Jülich. For the absolute calibration of the instruments, 19 parallel runs of JO05 and JO07 with a chemical actinometer were evaluated, in autumn 1993 (Kraus, 1994).

Errors

The 1 σ error of $J(O(^1D))$ at 298 K determined by the filter radiometric measurements is $\pm$ 8.7 % (Müller, 1994). This value is based on absolute calibration against chemical actinometry. Also two systematic error contributions have to be taken into account. The first is the uncertainty of the branching ratio for the reaction of $O(^1D)$ with N_2O, which leads to a maximum error of $\pm$ 14% for $J(O(^1D))$ determined by chemical actinometry as discussed by Junkermann et al. (1989). The second is the unknown temperature dependence of the $O(^1D)$ quantum yield. In order to estimate the temperature dependence of $J(O(^1D))$, field measurements by Dickerson et al. (1982) can be used. They indicate a sensitivity of about 0.5 % - 1.5 % K^{-1} at room temperature.

Recommendation

The J(O(^{1}D)) values based on the JO05 (file: JO35ANEW) data should be taken which have a temporal resolution of 10 min. If a higher temporal resolution is required, the JO08 (file: JO3NR8S) based values are recommended. However it should be noted that JO08 was mounted at a different place above ground.

3.3 Meteorological Parameters

Meteorological measurements are continuously carried out by the "Abteilung Sicherheit und Strahlenschutz der KFA Jülich" (Polster et al., 1986 and 1989). The following time series were kindly provided for the duration of the campaign (see Table 4).

3.4 Overview of measured data

#	data	tot	MI	Q16	MD	Q84	MA	ME	SD
1	NO [ppb]	1349	0.0	0.027	0.387	3.570	115.2	3.325	9.559
2	NO_2 [ppb]	1071	1.337	3.778	11.58	21.31	158.9	13.50	11.90
3	NO_2 [cm^{-3}]	906	3.01E10	1.35E11	2.79E11	5.55E11	1.16E12	3.31E12	2.04E11
4	NO_y [ppb]	1346	1.716	7.139	13.62	29.18	159.4	18.96	16.95
5	O_3(Dasibi1) [ppb]	1806	1.921	10.23	33.60	74.69	113.8	41.20	28.75
6	O_3(Dasibi3) [ppb]	1963	2.676	12.62	43.35	89.86	240.7	50.75	34.86
7	O_3(Horiba) [ppb]	1950	1.464	11.27	43.31	94.04	139.8	51.53	36.46
8	O_3(Horiba) [ppb]	1985	0.0	13.76	45.34	94.04	139.5	53.09	35.66
9	O_3 [cm^{-3}]	905	-1.47E11	5.80E11	1.18E12	1.82E12	3.39E12	1.21E12	5.68E11
10	O_3 column density [D.U.]	81	276.0	313.0	325.0	341.0	371.0	326.1	18.15
11	HCHO [ppb]	383	0.553	1.302	2.495	4.573	7.199	2.810	1.472
12	HCHO [cm^{-3}]	905	-4.45E10	3.62E10	9.23E10	1.38E11	4.88E12	9.48E11	6.74E10
13	CH_3CHO [ppb]	383	0.023	0.216	0.539	1.065	2.276	0.641	0.440
14	CO(grab) [ppb]	111	108.0	180.0	281.0	442.0	737.0	312.7	131.4
15	CO [ppb]	13	107.0	162.0	296.0	397.0	591.0	301.0	127.7
16	CO [ppb]	1853	111.3	179.7	282.2	411.6	779.2	301.0	121.5
17	CO_2 [ppm]	111	249.0	350.0	370.0	412.0	649.0	381.1	46.19
18	CO_2 [ppm]	13	340.0	343.0	347.0	370.0	384.0	353.6	14.07
19	CH_4 [ppb]	111	1820.	1870.	1950.	2220.	3070.	2054.	264.0
20	CH_4 [ppb]	12	1860.	1890.	1945.	2040.	2290.	1991.	127.2
21	PAN [ppb]	1153	0.063	0.449	1.182	1.668	3.543	1.147	0.583
22	ethane [ppb]	102	1.043	1.462	2.394	4.691	7.040	2.917	1.571
23	propane [ppb]	103	0.448	0.746	1.364	2.917	6.570	1.867	1.334
24	i-butane [ppb]	103	0.134	0.346	0.710	1.359	4.028	0.838	0.586
25	n-butane [ppb]	103	0.408	0.793	1.531	3.239	5.822	1.955	1.252
26	ethene [ppb]	103	0.177	0.365	1.264	3.065	10.94	1.643	1.613
27	propene [ppb]	103	0.005	0.041	0.180	0.496	1.390	0.280	0.289
28	1-butene [ppb]	103	0.005	0.027	0.071	0.158	0.478	0.092	0.080
29	acetylen [ppb]	102	0.181	0.405	0.855	1.651	3.889	1.011	0.713
30	isoprene [ppb]	101	0.01	0.04	0.42	1.330	8.720	0.719	1.033
31	CH_3Cl [ppb]	103	0.491	0.510	0.564	0.621	0.864	0.572	0.064
32	ROOH [ppb]	3645	-0.11	0.02	0.12	0.87	7.44	0.52	1.02
33	HNO_3 [ppb]	55	0.02	0.299	1.318	3.331	8.025	1.836	1.788
34	nitrate [ppbm]	55	0.008	0.290	0.848	1.331	5.314	1.052	1.074
35	SO_2 [cm^{-3}]	887	1.06E10	5.80E10	1.26E11	2.32E11	5.08E12	1.44E11	8.06E10
36	radon activity [a.u.]	655	22.00	103.0	226.0	506.0	1395.	303.2	238.9

Dasibi: *Commercial instrument*
Q16: *16- Percentile*
MI: *Minimum*
MD: *Median*
tot: *total number of measurements*
SD: *Standard Deviation*
Q84: *84- Percentile*
MA: *Maximum*
ME: *Mean*

Table 4: *Abundances of trace gases and other parameters during the field campaign in Jülich, 1990. The location of the measurement are in the vicinity of the intstitute (see section 2) if not stated otherwise in brackets.*

Table 4 continued

#	data	tot	MI	Q16	MD	Q84	MA	ME	SD
37	$J(O^1D)$(Det.#5) [cts]	1143	1.40E-08	6.12E-07	6.49E-06	1.561E-05	2.55E-05	7.68E-06	6.56E-06
38	$J(O^1D)$(Det.#7) [cts]	10776	0.00E+00	4.24E-08	5.08E-07	1.154E-06	2.11E-06	5.77E-07	4.92E-07
39	$J(O^1D)$(Det.#8) [s^{-1}]	10776	8.98E-09	4.67E-07	5.74E-06	1.506E-05	2.29E-05	7.25E-06	6.54E-06
40	$J(NO_2)$ [s^{-1}]	1350	-2.00E-06	1.00E-06	7.29E-04	5.94E-03	8.95E-03	2.28E-03	2.71E-03
41	global rad. [mW cm^{-2}]	1990	0.0	0.0	10.58	58.81	89.54	23.68	27.10
42	CN [cm^{-3}]	1989	2369.	6374.	9939.	18074.	46760.	12050.	6951.
43	beta [m^{-1}]	1989	1.84E-05	5.35E-05	8.13E-05	1.49E-04	2.42E-04	9.97E-05	5.41E-05
44	R.H. (2 m) [%]	2149	17.70	33.60	56.10	96.90	97.20	61.99	26.55
45	R.H. (20 m) [%]	2149	19.20	35.40	52.70	88.20	95.30	57.58	22.84
46	R.H. (50 m) [%]	2149	22.00	37.70	54.20	81.00	94.60	56.64	19.17
47	R.H. (100 m) [%]	2149	23.70	38.50	53.20	75.00	92.80	55.41	17.23
48	temperature (2 m) [C]	1345	7.400	12.80	19.80	28.10	34.80	20.36	6.92
49	temperature (20 m) [C]	2149	9.100	15.10	21.30	28.20	35.00	21.44	6.19
50	temperature (50 m) [C]	2149	10.40	16.00	22.40	28.00	34.10	22.01	5.67
51	temperature (100 m) [C]	2149	10.30	15.90	22.60	27.20	33.20	21.94	5.39
52	wind speed (2 m) [m/s]	2144	0.0	0.0	0.20	0.70	5.50	0.306	0.36
53	wind speed (20 m) [m/s]	2145	0.0	0.500	1.100	2.000	4.600	1.267	0.79
54	wind speed (50 m) [m/s]	2145	0.0	1.100	2.400	3.800	7.700	2.503	1.39
55	wind speed (100m) [m/s]	2142	0.100	1.500	3.100	5.200	9.700	3.370	1.82
56	wind direction (50m) [°]	2149	0.0	103.0	256.0	309.0	359.0	219.7	96.08
57	wind direction (100m) [°]	2149	0.0	86.00	258.0	310.0	359.0	217.4	101.0

Dasibi: *Commercial instrument*
Q16: *16- Percentile*
MI: *Minimum*
MD: *Median*
tot: *total number of measurements*
SD: *Standard Deviation*
Q84: *84- Percentile*
MA: *Maximum*
ME: *Mean*

4. Access to the Data

The data are entered into clear-text data files with a common format for further evaluation using a computer. The files are also provided with the necessary information on calibration procedures, experimental methods and uncertainties to fully verify the reliability of the entered data. The entries are self-explanatory to a large extent. The whole data set is stored (and also archived) at the computer center (ZAM) of the KFA. For copies of the data on disc, contact D. Poppe, Institut für Atmosphärische Chemie (ICG 3).

Literature:

Armerding, W., Comes, F. J., and Schülke, B., 1995,
O(^{1}D) quantum yield of ozone photolysis in the UV from 300 nm to ist threshold and at 355 nm, J. Phys. Chem., 99, 3137-3143.

Ball, S. M., Hancock, G., Murphy, I. J., and Rayner, S. P., 1993,
The relative quantum yield of O_2 ($^1\Delta_g$) from the photolysis of ozone in the wavelength range 270 nm $\leq \lambda \leq$ 329 nm, GRL 20, 2063-2066.

Brassington, D. J., 1981
Sulfor dioxide absorption cross-section measurements from 290 nm to 6317 nm
Appl. Opt. 2021, 3774-3779.

Brock, J. C., and Watson, R. T., 1980,
Laser flash photolysis of ozone: O(^{1}D) quantum yields in the fall-off region 297-325 nm, Chem. Phys., 46, 477–484.

Callies, J., 1988,
Absorptionsspektroskopischer Nachweis von Hydroxyl-Radikalen in der Troposphäre, Ph. D. Thesis, Universität Köln.

Cantrell, C. A., Davidson, J. A., Mc Daniel, A. H., Shetter, R. E., and Calvert, S. G., 1990
Temperaturedempendent formaldehyde cross section in the near ultraviolet spectral region.
J. Phys. Chem., 94, 3902-3908.

Callies, J., Dorn, H.-P., Platt, U., and Ehhalt, D. H., 1989,
Tropospheric OH-concentration measurements by laser long-path absorption spectroscopy, in R. D. Bojkov and P. Fabian (eds.), Ozone in the Atmosphere, Proc. of the Quadrennial Ozone Symposium 1988 Deepak Publishing, Hampton/VA, pp. 772-775.

DeMore, W. B., Molina, M. J., Sander, S. P., Golden, D. M., Hampson, R. F., Kurylo, M. J., Howard, C. J., and Ravishankara, A. R., 1992,
Chemical kinetics and photochemical data for use in stratospheric modeling, JPL Publ. 92-20.

Dickerson, R. R., Stedman, D. J., and Delany, A. C., 1982,
Direct measurements of ozone and nitrogen dioxide photolysis rates in the troposphere, J. Geophys. Res., 87, 4933–4946.

Dorn, H.-P., Brandenburger, U., Brauers, T., Hausmann, M., and Gerlach, R., 1994,
Multipass folded long-path absorption for the in-situ measurement of tropospheric OH, in Physico-Chemical Behaviour of Atmospheric Pollutants, edited by G. Angeletti and G. Restelli, European Commission Report 15609/2, 787-792.

Dorn, H.-P., Callies, J., Platt, U., and Ehhalt, D. H., 1988,
Measurement of tropospheric OH concentrations by laser long-path absorption spectroscopy, Tellus 40 B, 437-445.

Drummond, J. W., Ehhalt, D. H. and Volz, A., 1985,
An optimized chemiluminescence detector for tropospheric NO measurements, J. Atmos. Chem. 2, 287-306.

Fahey, D. W., Eubank, C. S., Hübler, G., and Fehsenfeld, F. C., 1985,
Evaluation of a catalytic reduction technique for the measurement of total reactive odd-nitrogen NOy in the atmosphere, J. Atmos. Chem. 3, 435-468.

Gomer, T., Brauers, T., Heintz, F., Stutz, J., and Platt, U., 1995,
MFC, Manual Version 1.98, Universität Heidelberg.

Guilbault, G. G., Bignac, P., and Juneau, M., 1968,
Anal. Chem. 40, 1256.

Junkermann, W., Platt, U., and Volz-Thomas, A., 1989,
A photoelectric detector for the measurement of photolysis frequencies of ozone and other atmospheric molecules, J. Atmos. Chem., 8, 203–227.

Kraus, A., 1994,
Direkte Messung der Bildungsrate von $O(^1D)$-Atomen aus der Photolyse von Ozon unter atmosphärischen Bedingungen, Diplom thesis, Universität Köln.

Koppmann, R., Bauer, R., Johnen, F. J., Plass, C., and Rudolf, F, 1992,
The distribution of light nonmethane hydrocarbons over the mid-Atlantic: Results of the Polarstern cruise ANT VII/1, J. Atmos. Chem. 15, 235-251.

Lazrus, A. L., Kok, G. L., Bitlin, S. N., and Lind, J. A., 1985,
Anal. Chem. 57, 917.

Michelsen, H. A., Salawitch, R. S., Wennberg, P. O., and Anderson, J. G., 1994
Production of $O(^1D)$ from photolysis of O_3
Geophys. Res. Lett., 21, 22, 2227-2230

Molina, L. T., and Molina, M. J., 1986,
Absolute absorption cross sections of ozone in the 185- to 350-nm wavelength range,
J. Geophys. Res. 91, 14, 501-14, 508.

Müller, K. P., and Rudolph, J., 1989,
An automated technique for the measurement of peroxyacetylnitrate in ambient air at ppb and ppt levels, Intern. J. Environm. Anal. Chem. 37, 253-262.

Müller, K. P.,and Rudolph, J, 1991,
Application of an improved method for measurements of gaseous nitric acid in the nonurban atmosphere, Fresenius J. Anal. Chem. 339, 661.

Müller, M., Kraus, A., and Hofzumahaus, A., 1995,
$O_3 \rightarrow O(^1D)$ photolysis frequencies determined from spectroradiometric measurements of solar actinic UV-radiation: Comparison with chemical actinometer measurements, Geophys. Res. Lett., 22, 679-682.

Müller, M., 1994,
Messung der aktinischen ultravioletten Strahlung und der Ozon-Photolysefrequenz in der Atmosphäre mittels Filterradiometrie und Spektralradiometrie, Ph.D. thesis, Universität Bonn.

Neuroth, R., 1992,
Messung troposphärischer Hydroxyl Radikale mit Laser-Langweg-Absorption, Ph. D. Thesis, Universität Köln.

Papenbrock, Th., Stuhl, F., Müller, K. P., and Rudolph, J., 1992,
Measurement of Gaseous HNO_3 over the Atlantic Ocean, J. Atmos. Chem. 15, 369-379.

Perner, D., Platt, U., Trainer, M., Huebler, G., Drummond, J. W., Junkermann, W., Rudolph, J., Schubert, B., Volz, A., Ehhalt, D. H., Rumpel, K. J., and Helas, G., 1987, Measurement of Tropospheric OH concentrations: A comparison of field data with model predictions, J. Atmos. Chem. 5, 185-216.

Platt, U., Rateike, M., Junkermann, W., Rudolph, J., and Ehhalt, D. H., 1988, New tropospheric OH measurements, J. Geophys. Res. 93, 5159-5166.

Platt, U., 1994, Differential optical absorption spectroscopy (DOAS), in: M.W. Sigrist (ed.), Air Monitoring by Spectroscopic (Chemical Analysis Series: Techniques), vol. 127 John Wiley & Sons, Inc., pp. 27-83.

Polster, G., Geiß, H., and Heinemann, K., 1986, Der Meteorologische Turm der Kernforschungsanlage Jülich, Jül-Report no. 2035, Jülich.

Polster, G., Bergs, W., and Brunen, E., 1989, Meteorologische Messungen, in: Arbeitsbericht 1988 der Abteilung Sicherheit und Strahlenschutz, p. 177, ASS-Bericht Nr. 0493, Jülich.

D. Poppe, A. Hofzumahaus, A. Khedim, Ch. Plaß-Dülmer, D. Brüning, D. H. Ehhalt, F.-J. Johnen, F. Rohrer, H.-P. Dorn, H. London, J. Callies, J. Rudolph, K.-P. Müller, M. Wallasch, R. Bauer, R. Koppmann, R. Neuroth, T. Brauers, U. Platt, U. Schmidt., 1993, Measurement of atmospheric trace gas concentrations during the field campaign in Jülich 1988, Jül-Report no. 2731, Jülich

Press, W. H., Teukolsky, S. A., Vetterling, W. T., and Flannery, B. P., 1992, Numerical Recipes in C, 2nd ed. Cambridge University Press, Cambridge.

Rohrer, F., and Brüning, D., 1992, Surface NO- and NO_2-mixing ratios measured between 30°N and 30°S in the atlantic region, J. Atmos. Chem. 15, 253-267

Rudolph, J., Johnen, F. J., and Khedim, A., 1986, Problems connected with the analysis of halocarbons and hydrocarbons in the non-urban atmosphere, Intern. J. Environ. Anal. Chem. 27, 97-122.

Schiller, C., 1987,
Messung des Photonenflusses um 300 nm zur Untersuchung der $O(^1D)$-Produktion durch O_3-Photolyse in der Stratosphäre, Diplom thesis, Universität Bonn.

Schmidt, U., and Seiler, W., 1970,
A new method for recording molecular hydrogen in atmospheric air, J. Geophys. Res. 75, 1970, 1713-1716.

Schneider, W., Moortgat, G. K., Tyndall, G. S., and Burrows, J. P., 1987,
Absorption cross-sections of NO2 in the UV and visible region (200 - 700 nm) at 298 K, J. Photochem. Photobiol. 40, 195-217.

Seiler, W., and Junge, C., 1970,
Carbon monoxide in the atmosphere, J. Geophys. Res. 75, 1970, 2217-2226.

Trolier, M., and Wiesenfeld, J. R., 1988,
Relative quantum yield of $O(^1D_2)$ following ozone photolysis between 275 and 325 nm, J. Geophys. Res., 93, 7119–7124.

Umweltbundesamt (ed.), 1989,
Daten zur Umwelt 1988/89, Berlin.

Vierkorn-Rudolph, B., Rudolph, J., and Diederich, S., 1985,
Determination of peroxyacetylnitrate in unpolluted areas, Intern. J. Environm. Anal. Chem. 20, 131-148.

Appendix A Diurnal Cycles of all Measured Quantities during the Campaign. The time is given in UT.

In this appendix the diurnal cycles of all measured quantities are shown in diagrams for each quantity separately on a daily basis. For easy comparison between different days the same scale was used for all diagrams of a species with a few exceptions where the variability is very large. The time is given in UT and the date is indicated below the corresponding diagram. The quantity and the unit used are given at the bottom together with the name of the file which contains the data. The entry *"Dataset"* refers to the numbering of the files in table 1 and 4.

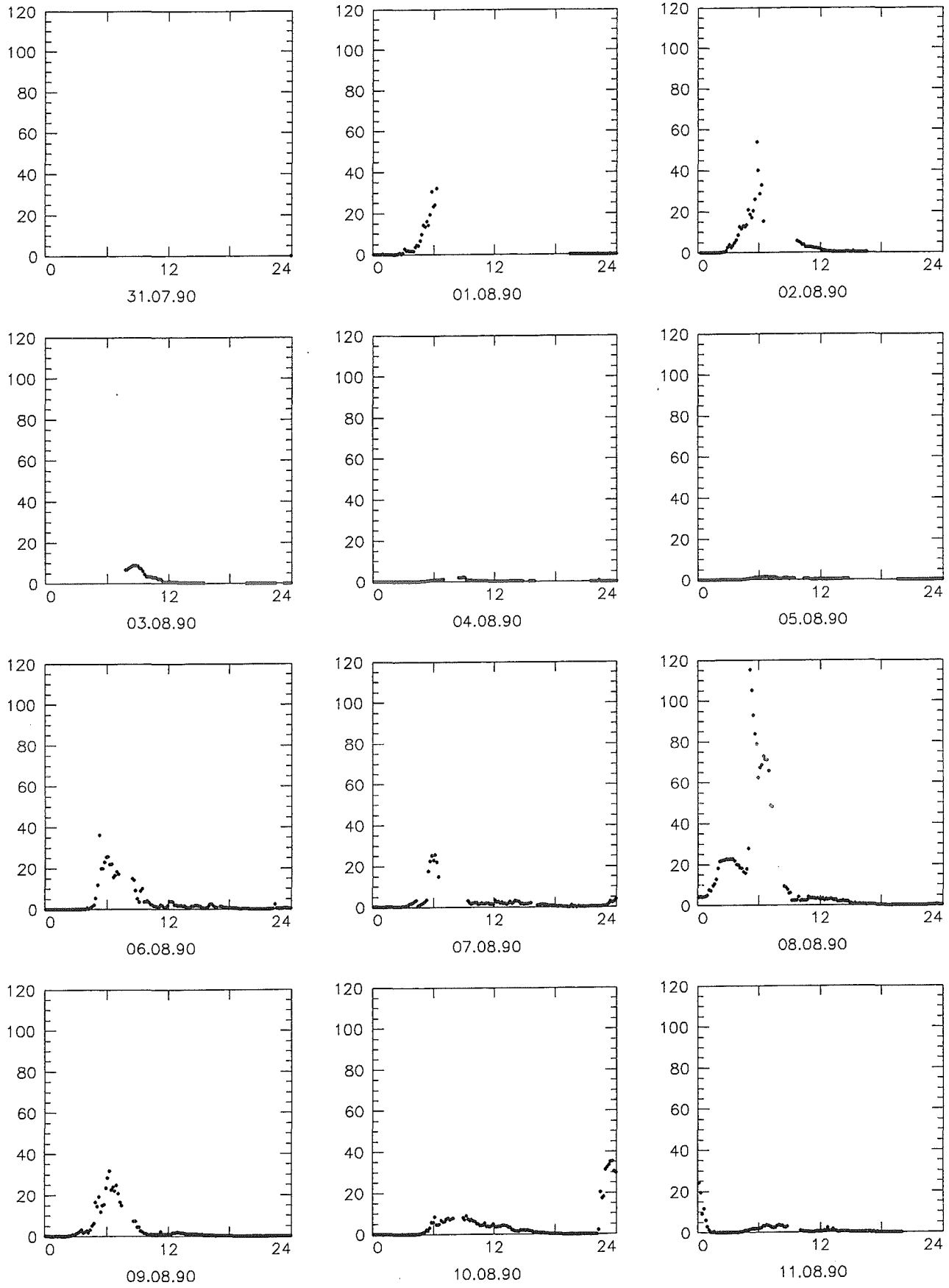

NO/ppb

File: NO___NEW ENZ90JUE

Dataset: 1

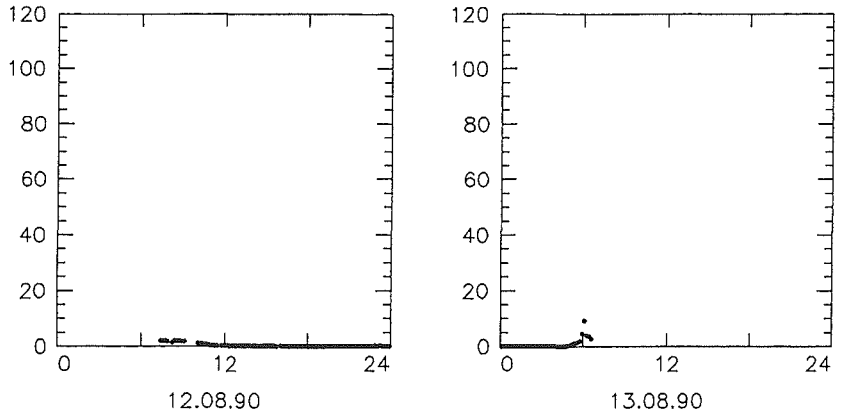

NO/ppb

File: NO___NEW ENZ90JUE

Dataset: 1

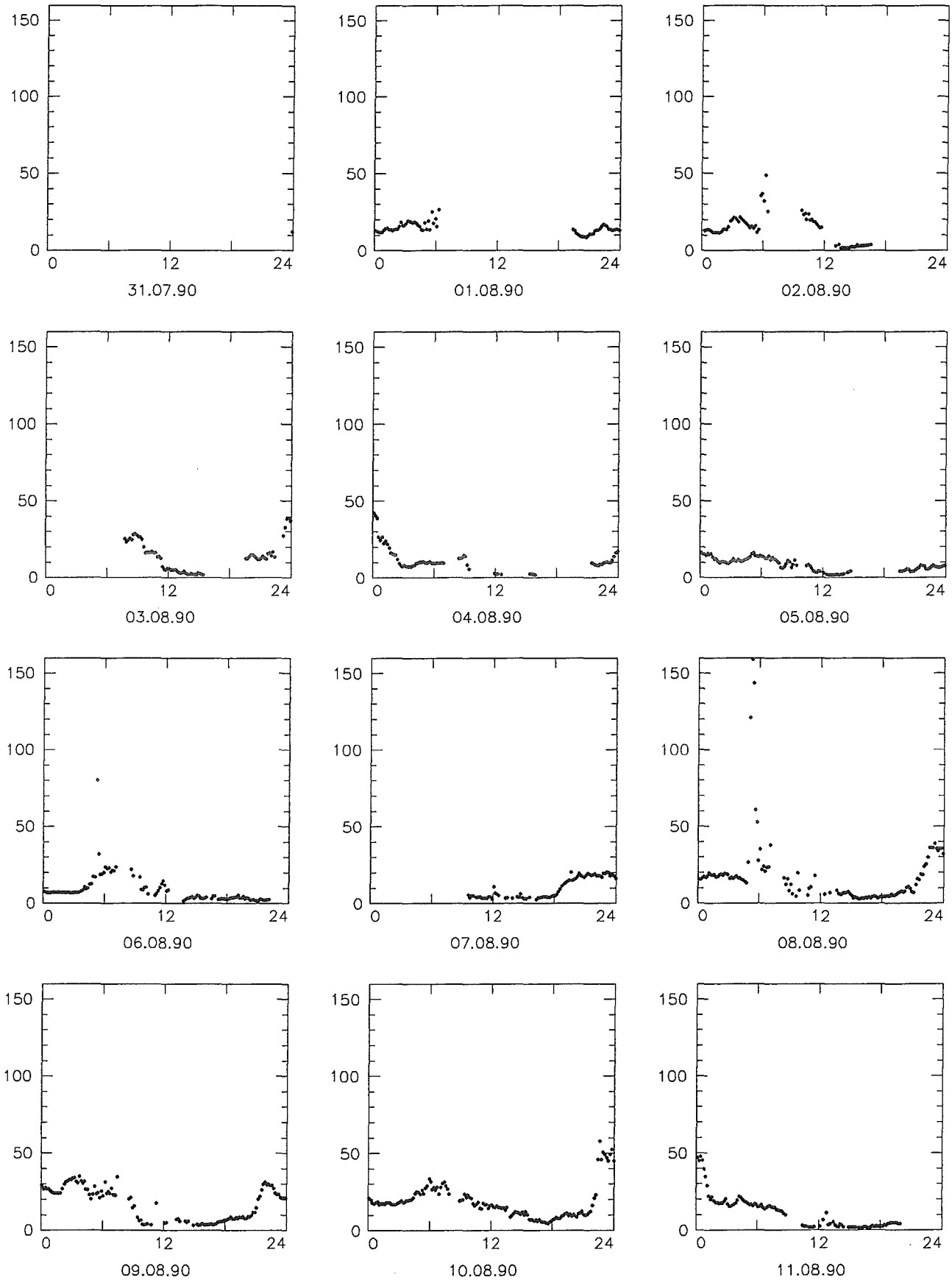

NO_2/ppb

File: NO2_CNEW ENZ90JUE

Dataset: 2

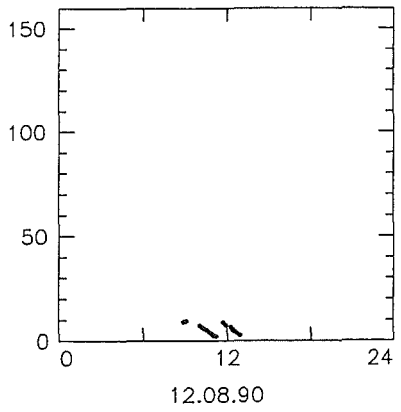

NO_2/ppb

File: NO2_CNEW ENZ90JUE

Dataset: 2

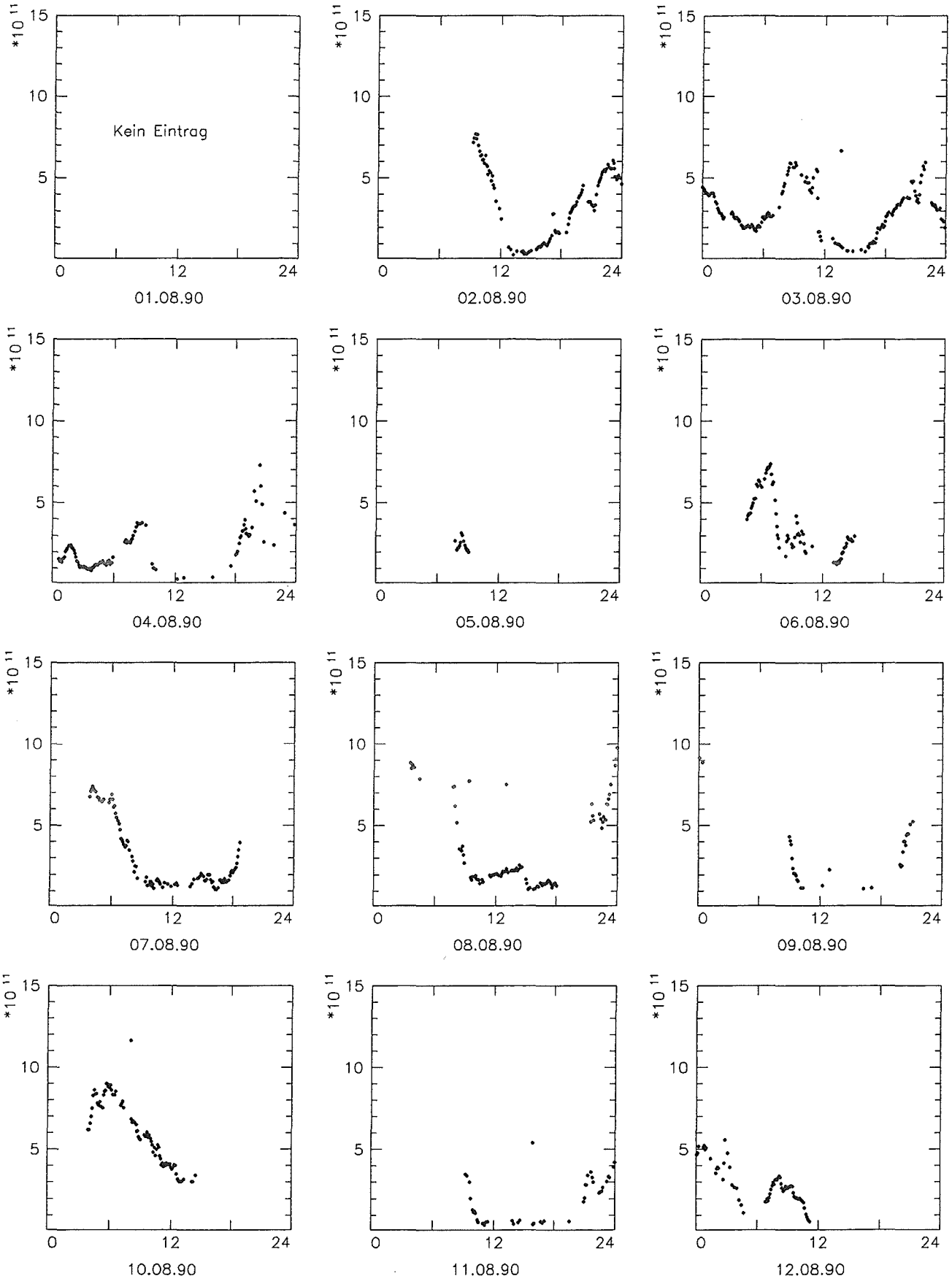

NO_2/cm^{-3}

File: ALLDOASJ ZUS90JUY

Dataset: 3

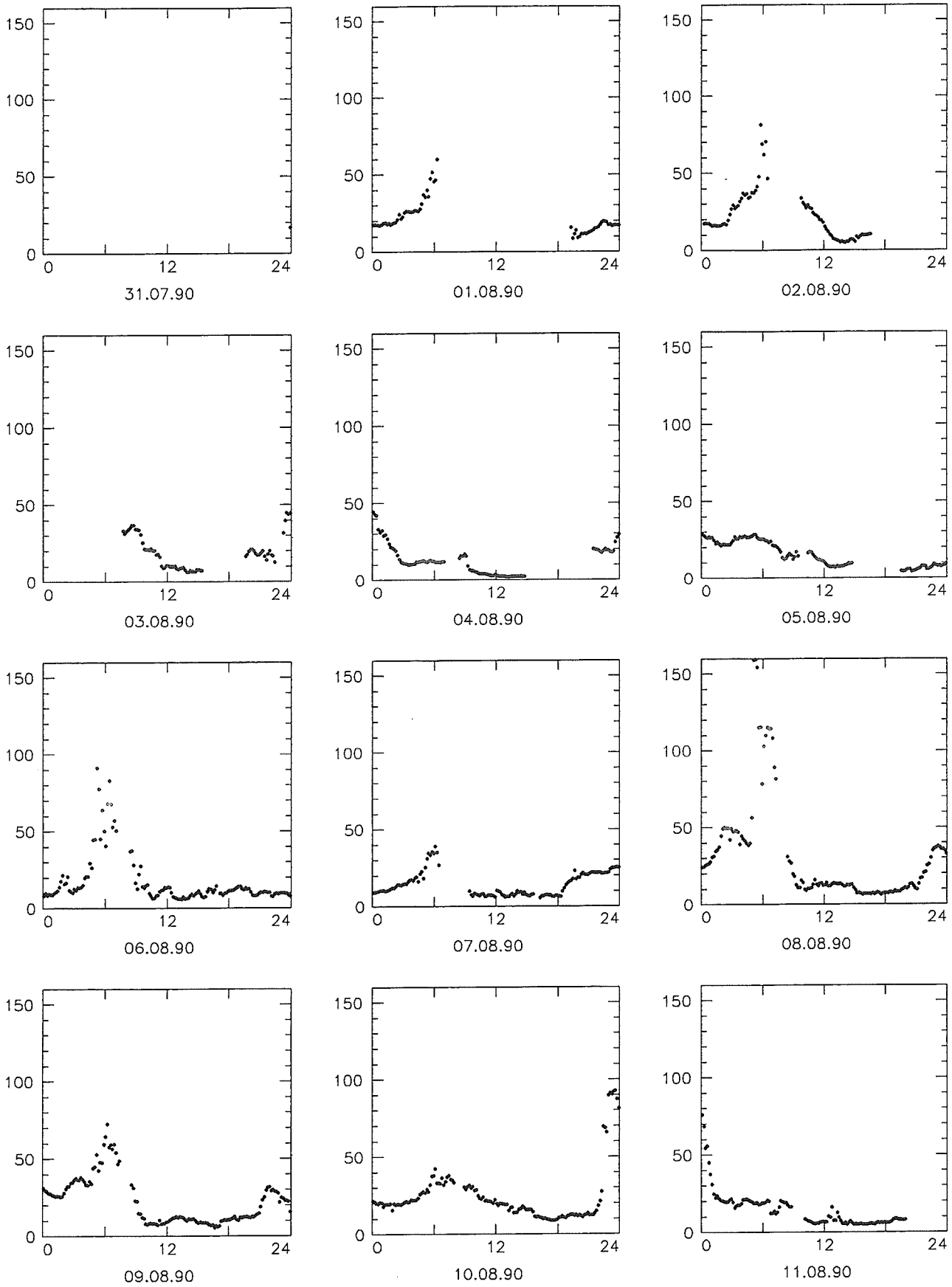

NO_y/ppb

File: NOY__NEW ENZ90JUE

Dataset: 4

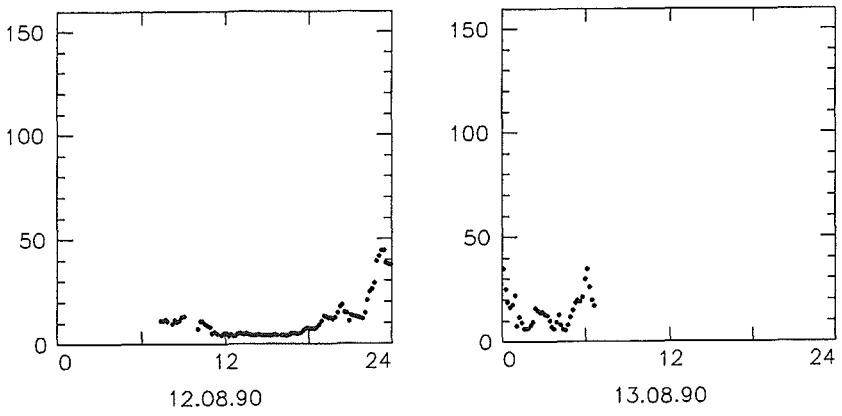

NO_y/ppb

File: NOY__NEW ENZ90JUE

Dataset: 4

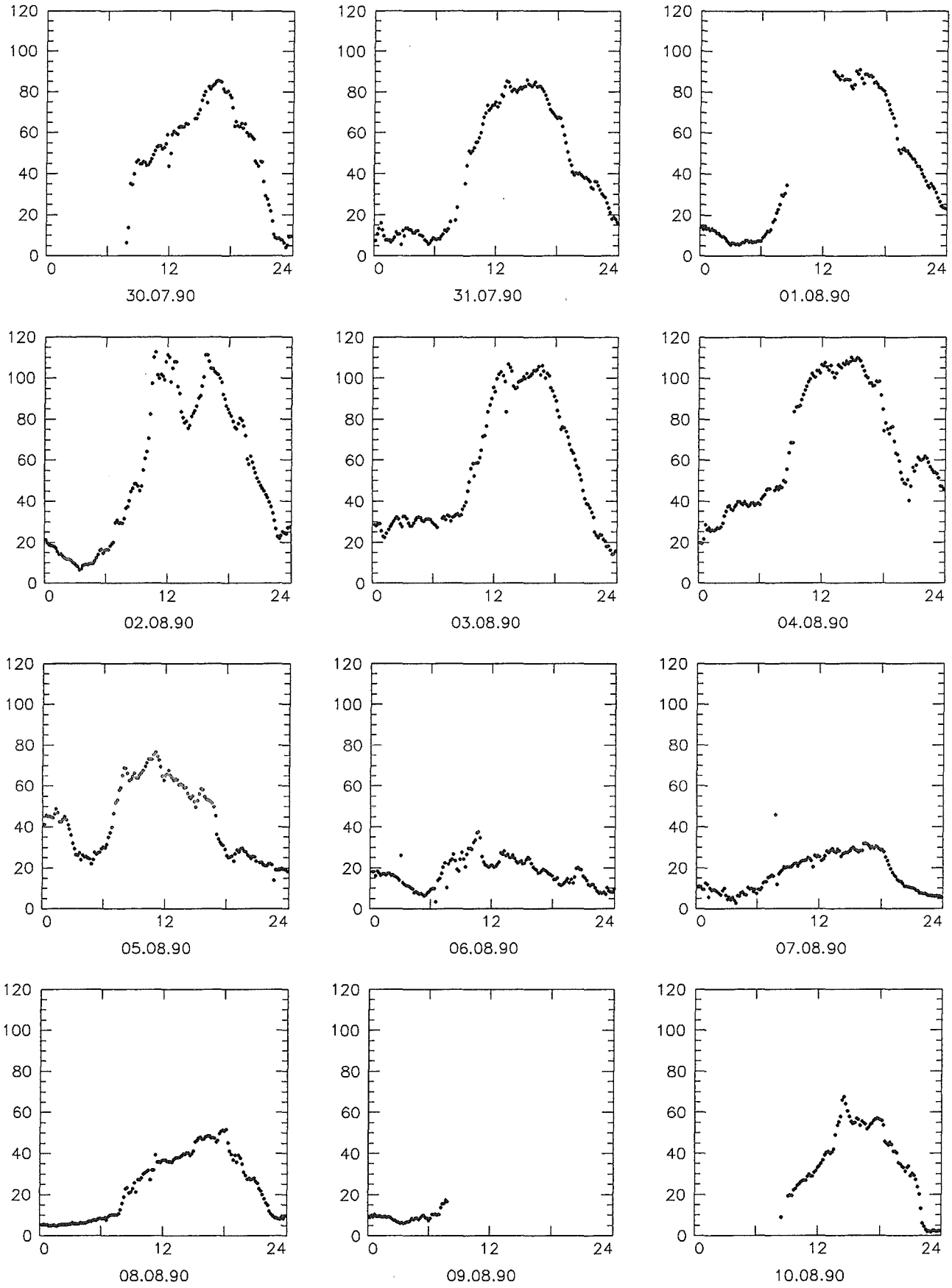

O_3/ppb

File: 03_D1NEW ENZ90JUE

Dataset: 5

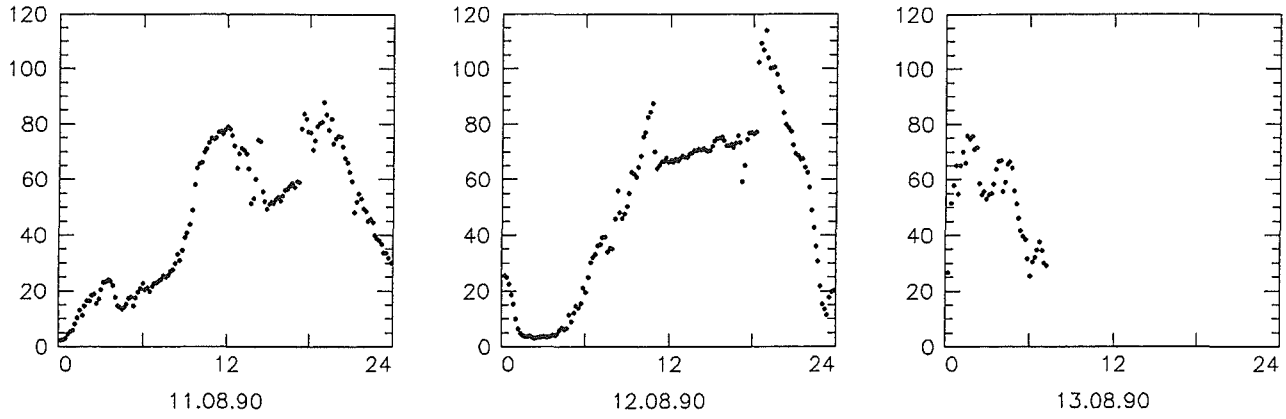

O_3/ppb

File: 03_D1NEW ENZ90JUE

Dataset: 5

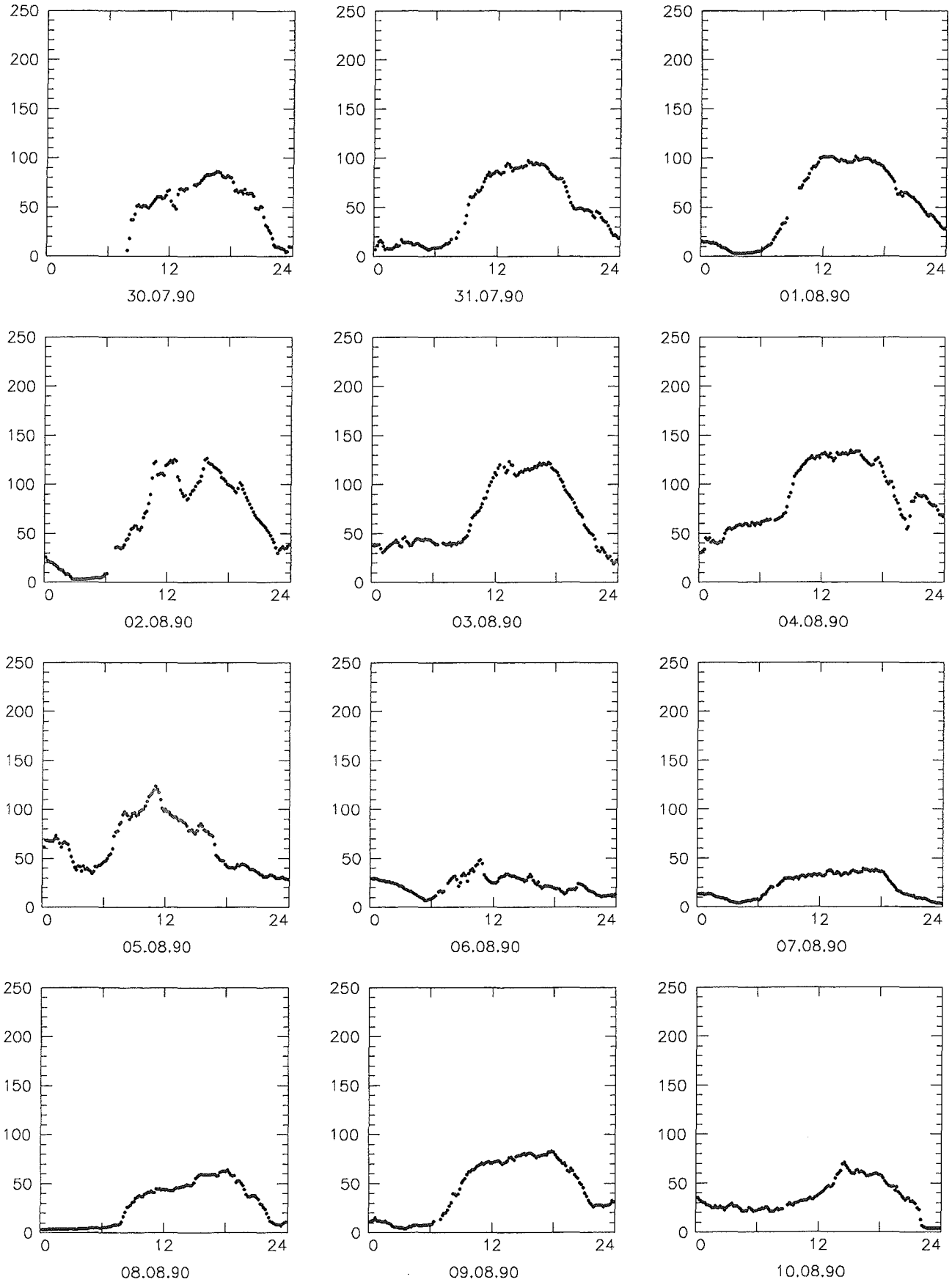

O_3/ppb

File: 03_D3NEW ENZ90JUE

Dataset: 6

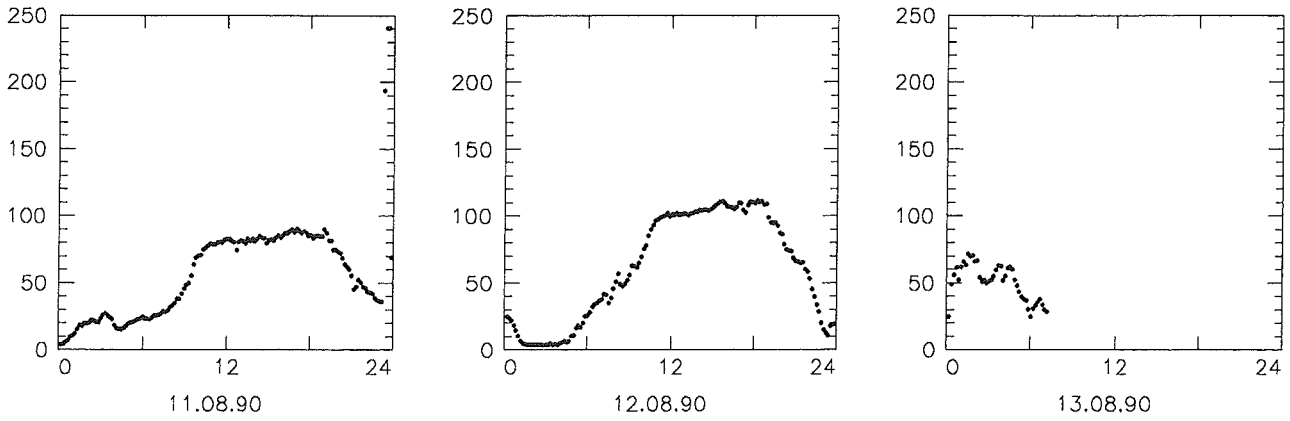

O_3/ppb

File: 03_D3NEW ENZ90JUE

Dataset: 6

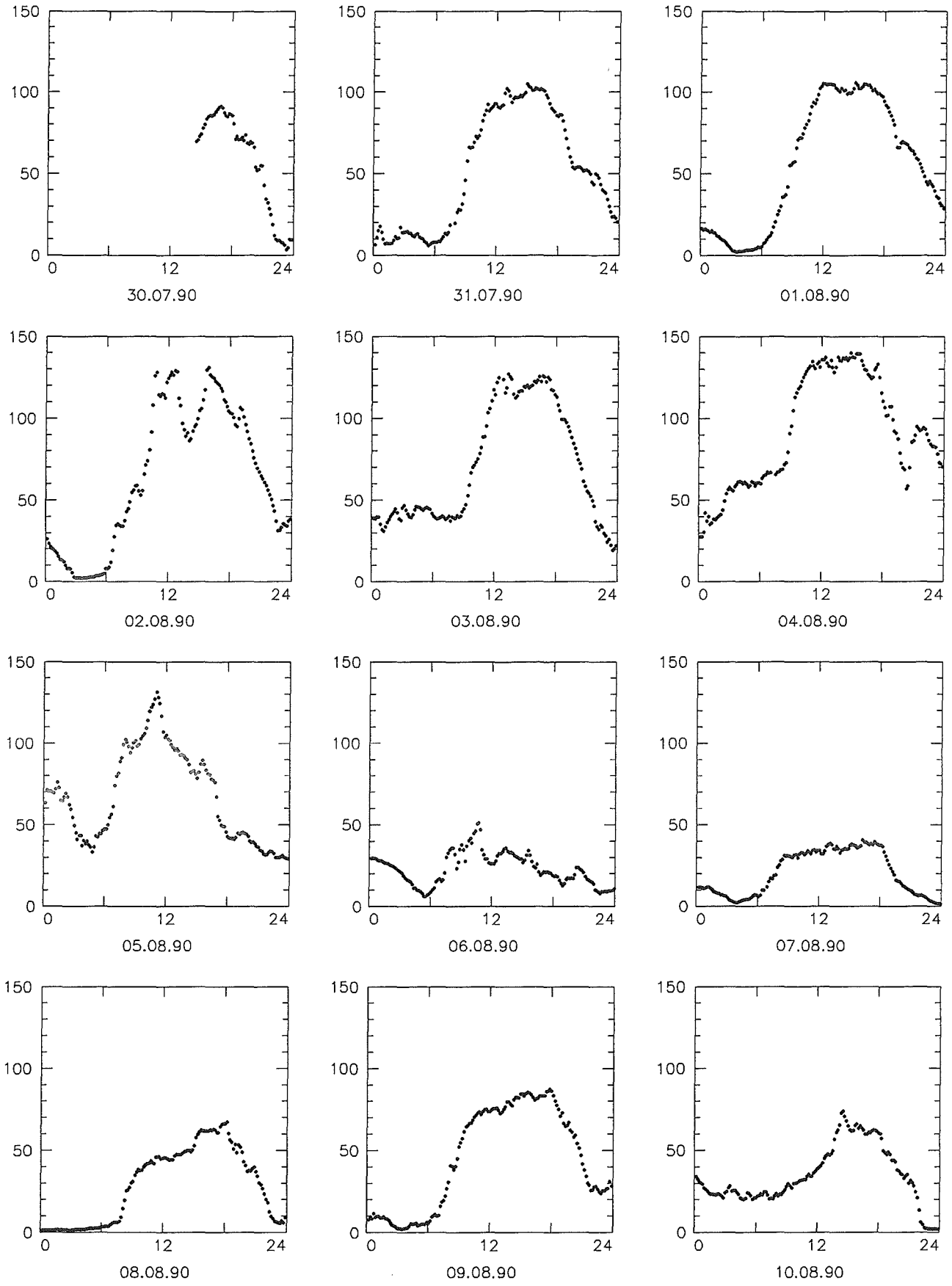

O_3/ppb

File: 03_HGNEW ENZ90JUE

Dataset: 7

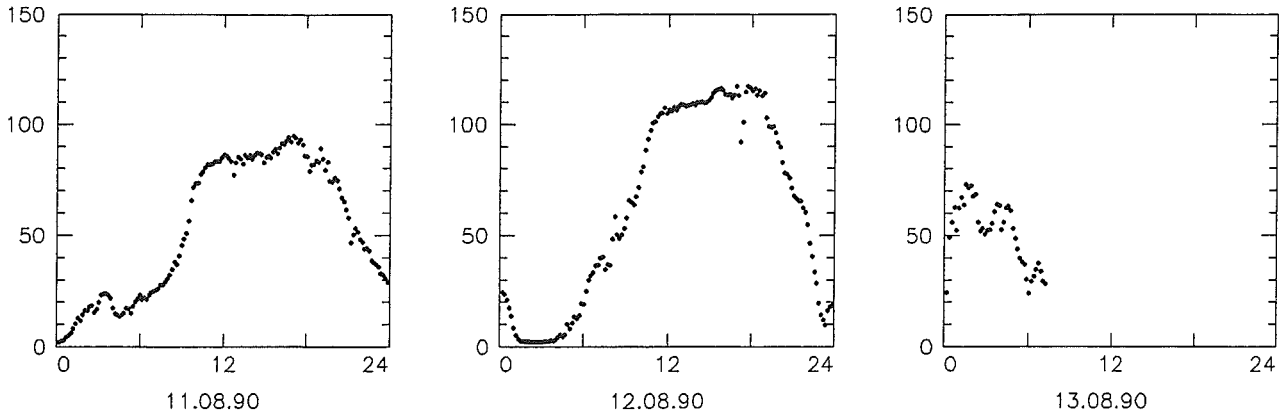

O_3/ppb

File: 03_HGNEW ENZ90JUE

Dataset: 7

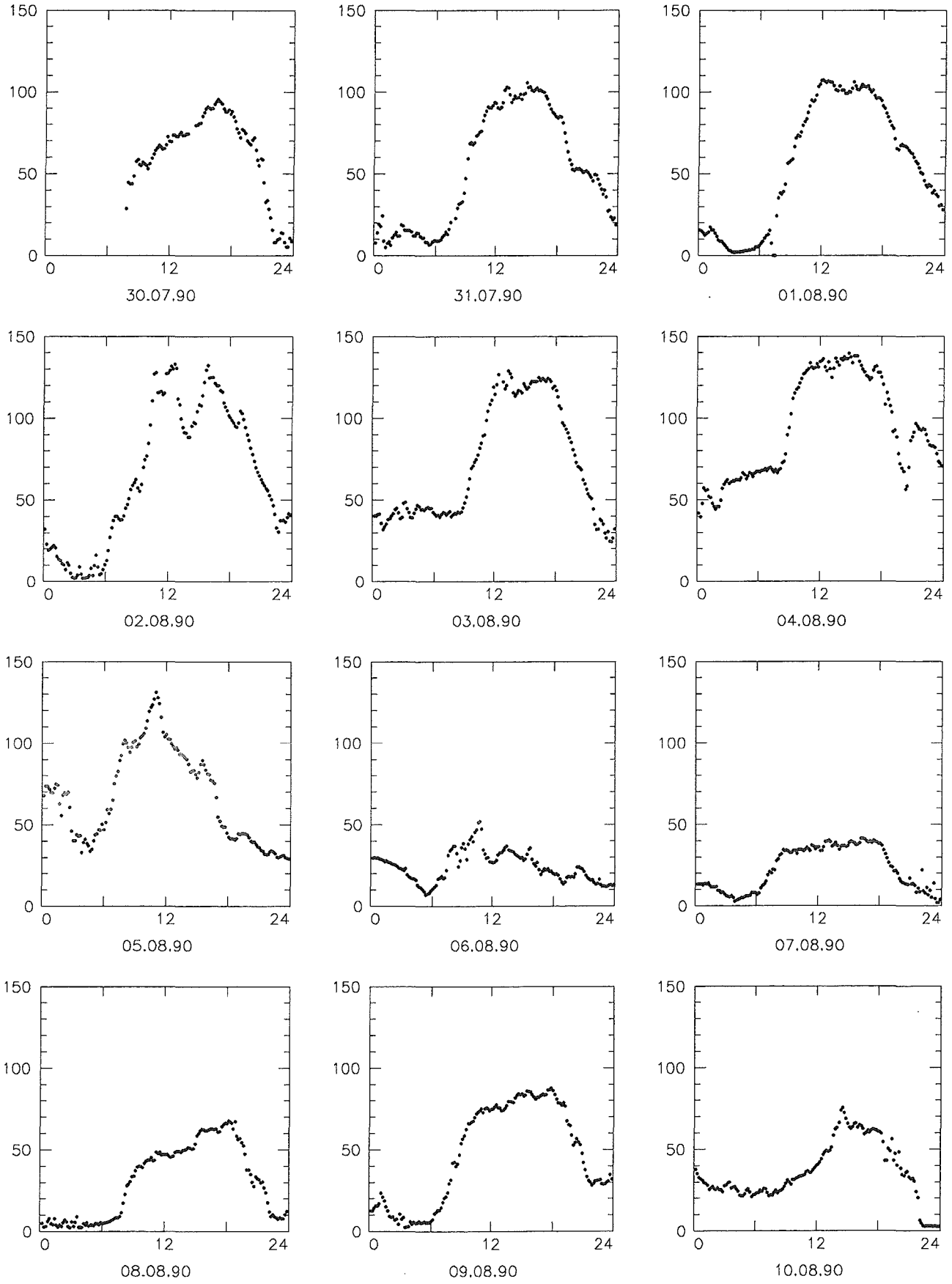

O_3/ppb

File: 03_HHNEW ENZ90JUE

Dataset: 8

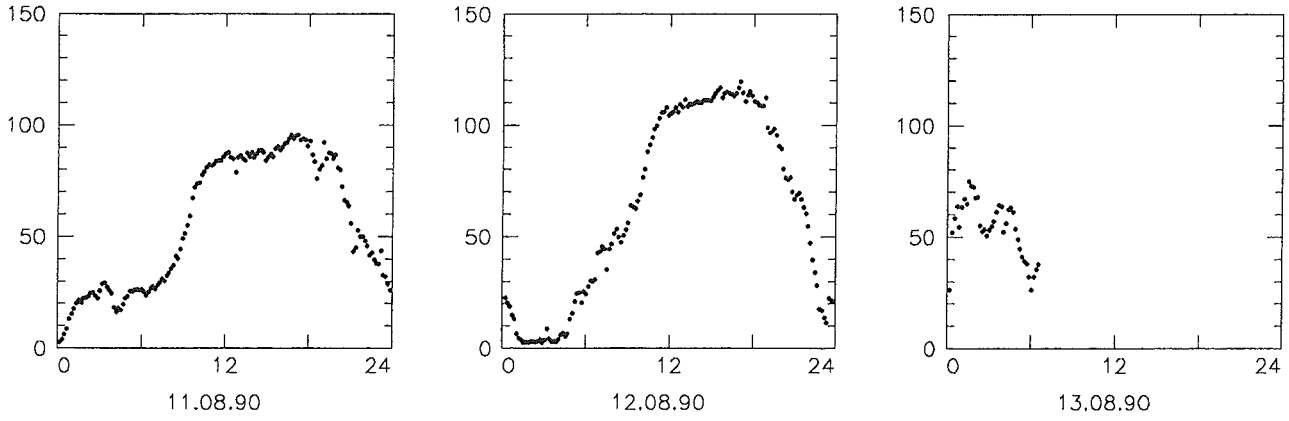

O_3/ppb

File: 03_HHNEW ENZ90JUE

Dataset: 8

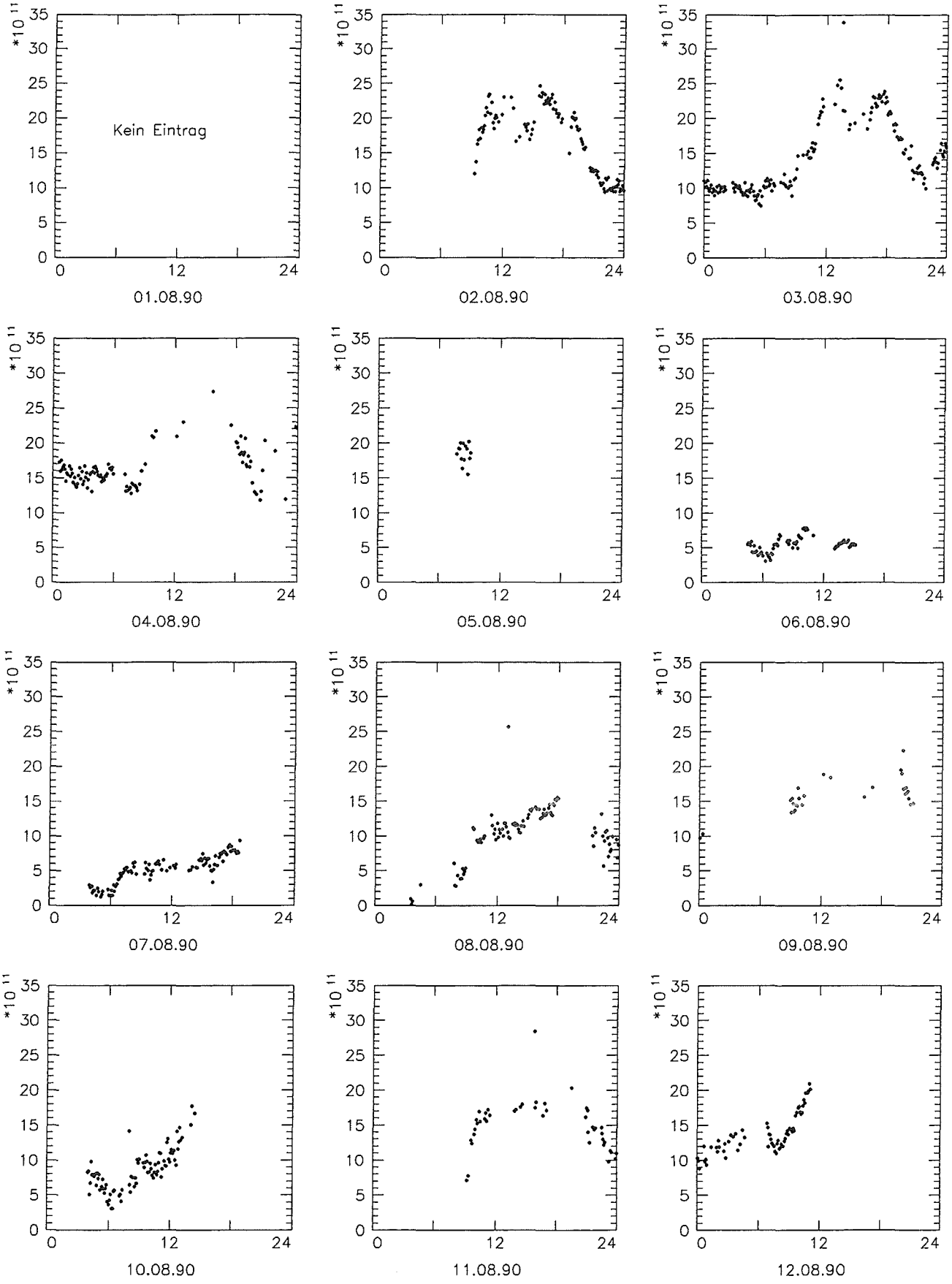

O_3/cm^{-3}

File: ALLDOASJ ZUS90JUY

Dataset: 9

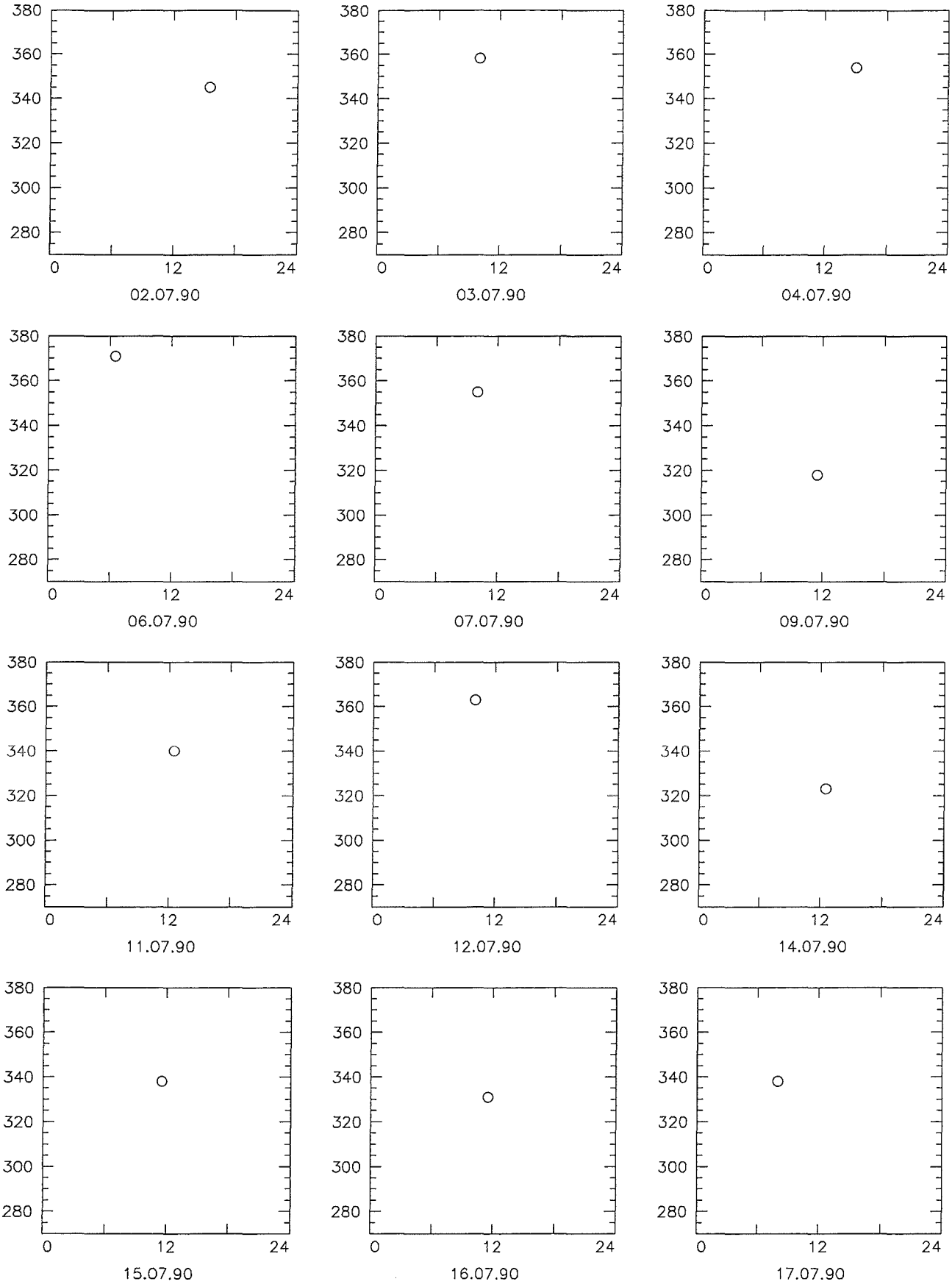

O_3 column density / DU

File: 03CD ENZ90JUE

Dataset: 10

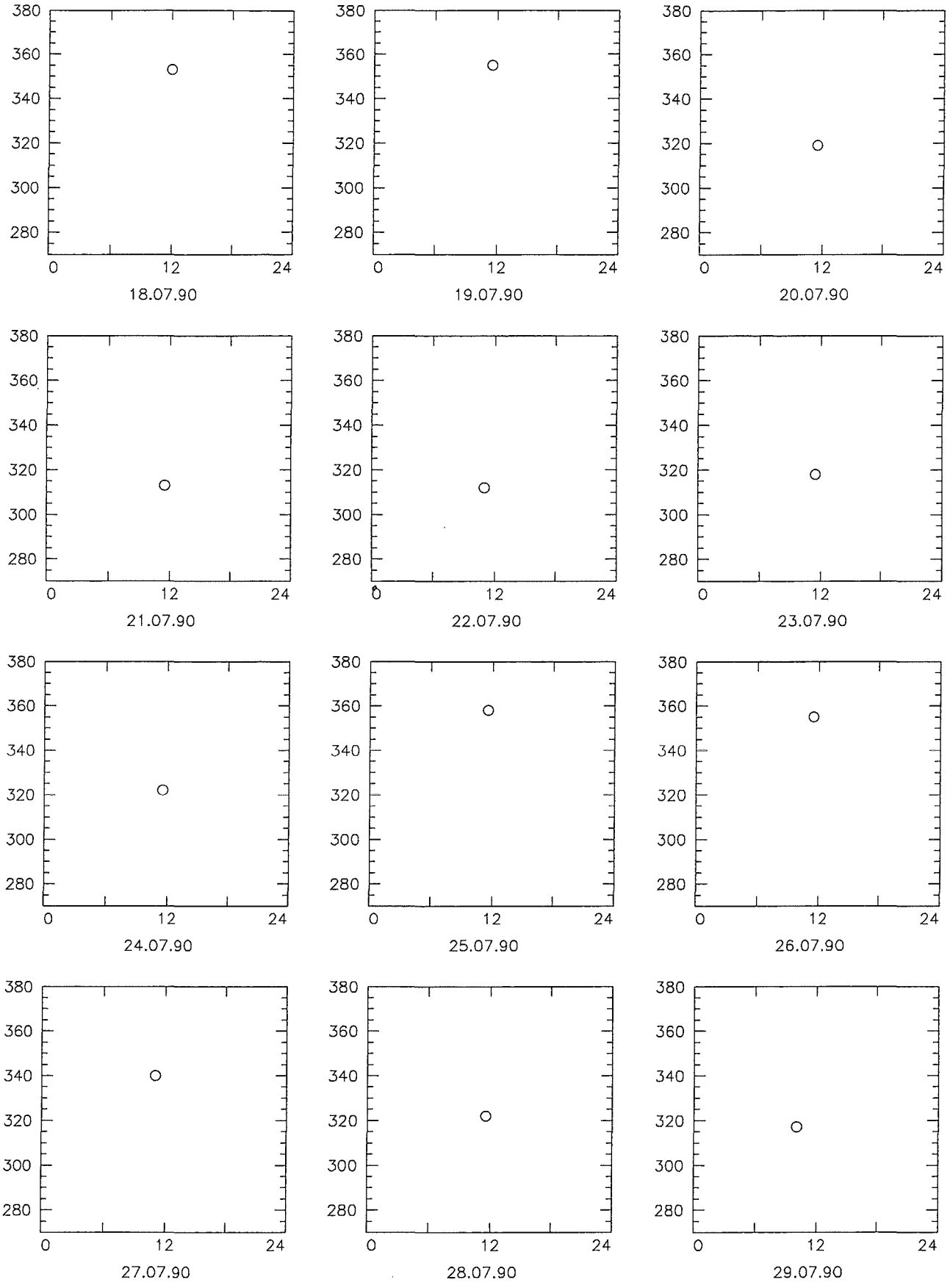

O_3 column density / DU

File: 03CD ENZ90JUE

Dataset: 10

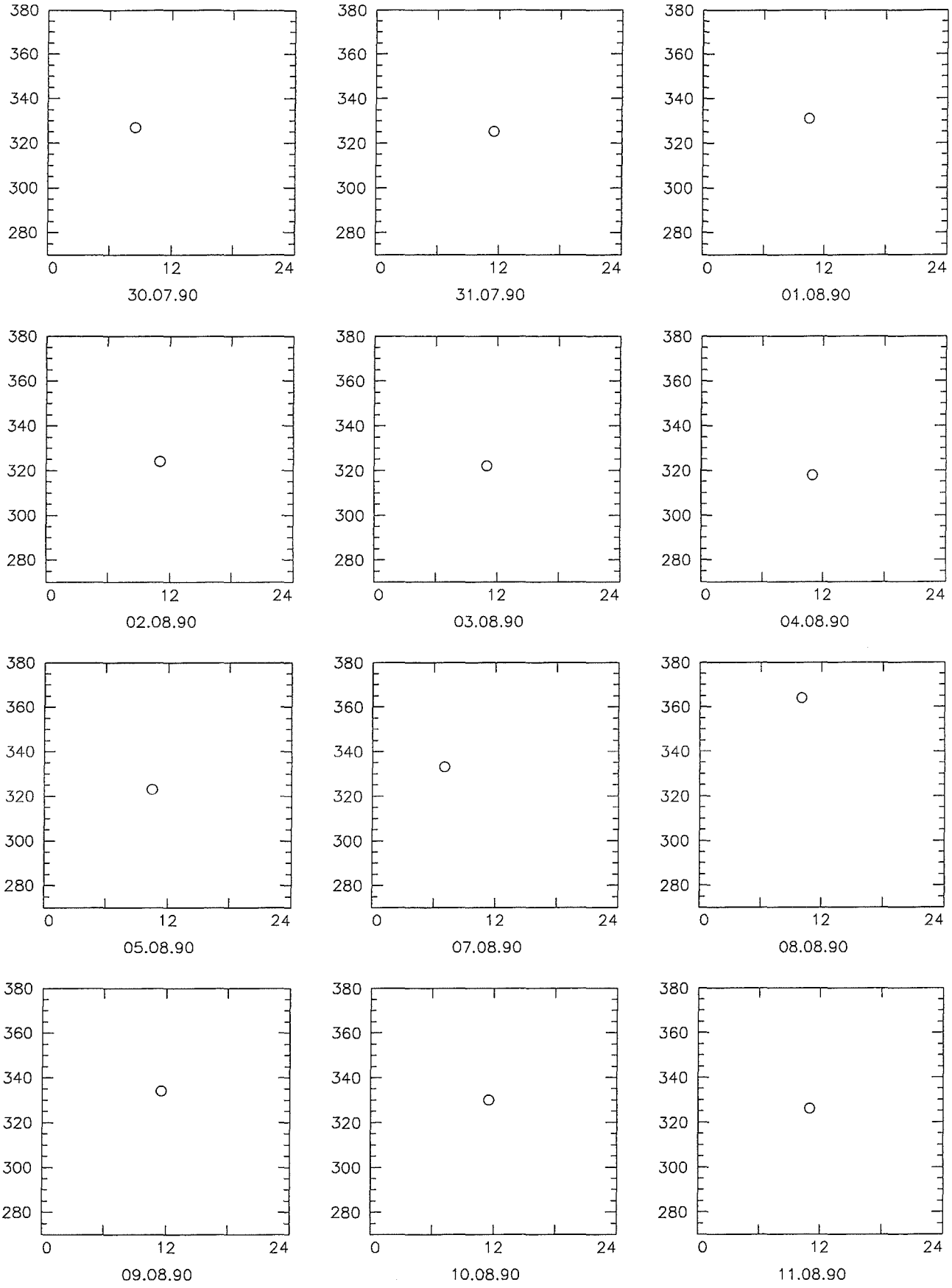

O_3 column density / DU

File: O3CD ENZ90JUE

Dataset: 10

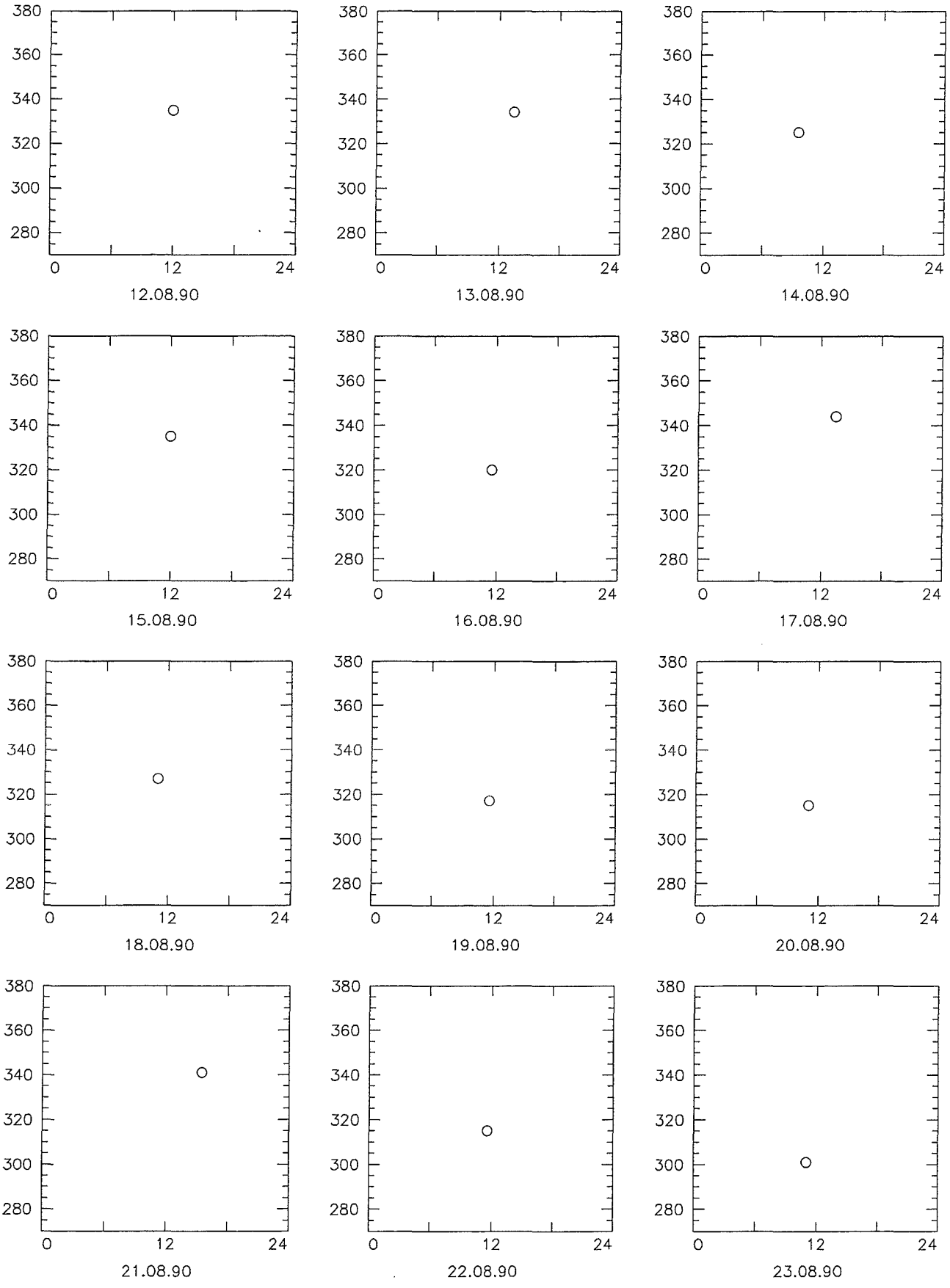

O_3 column density / DU

File: 03CD ENZ90JUE

Dataset: 10

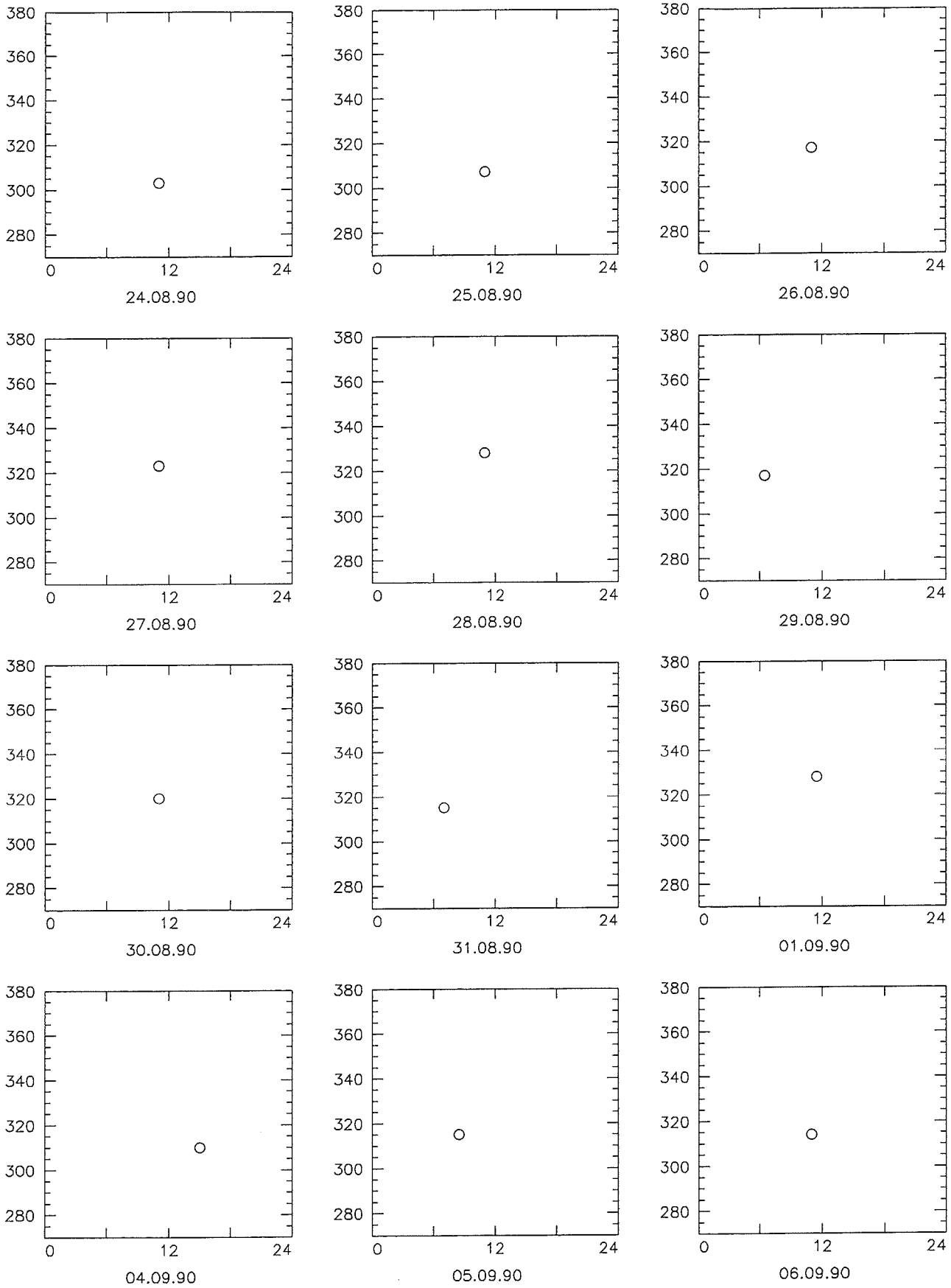

O_3 column density / DU

File: 03CD ENZ90JUE

Dataset: 10

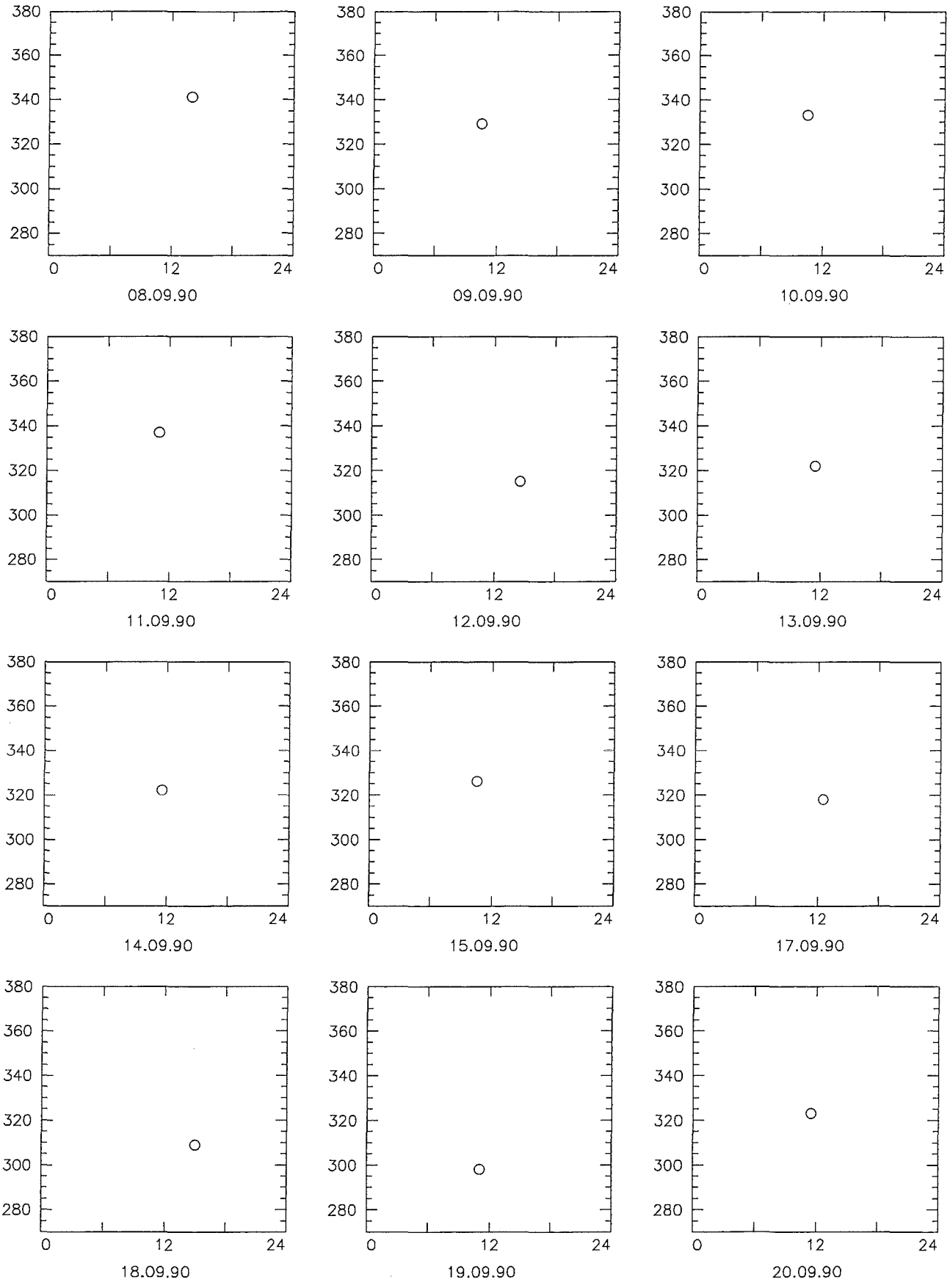

O_3 column density / DU

File: 03CD ENZ90JUE

Dataset: 10

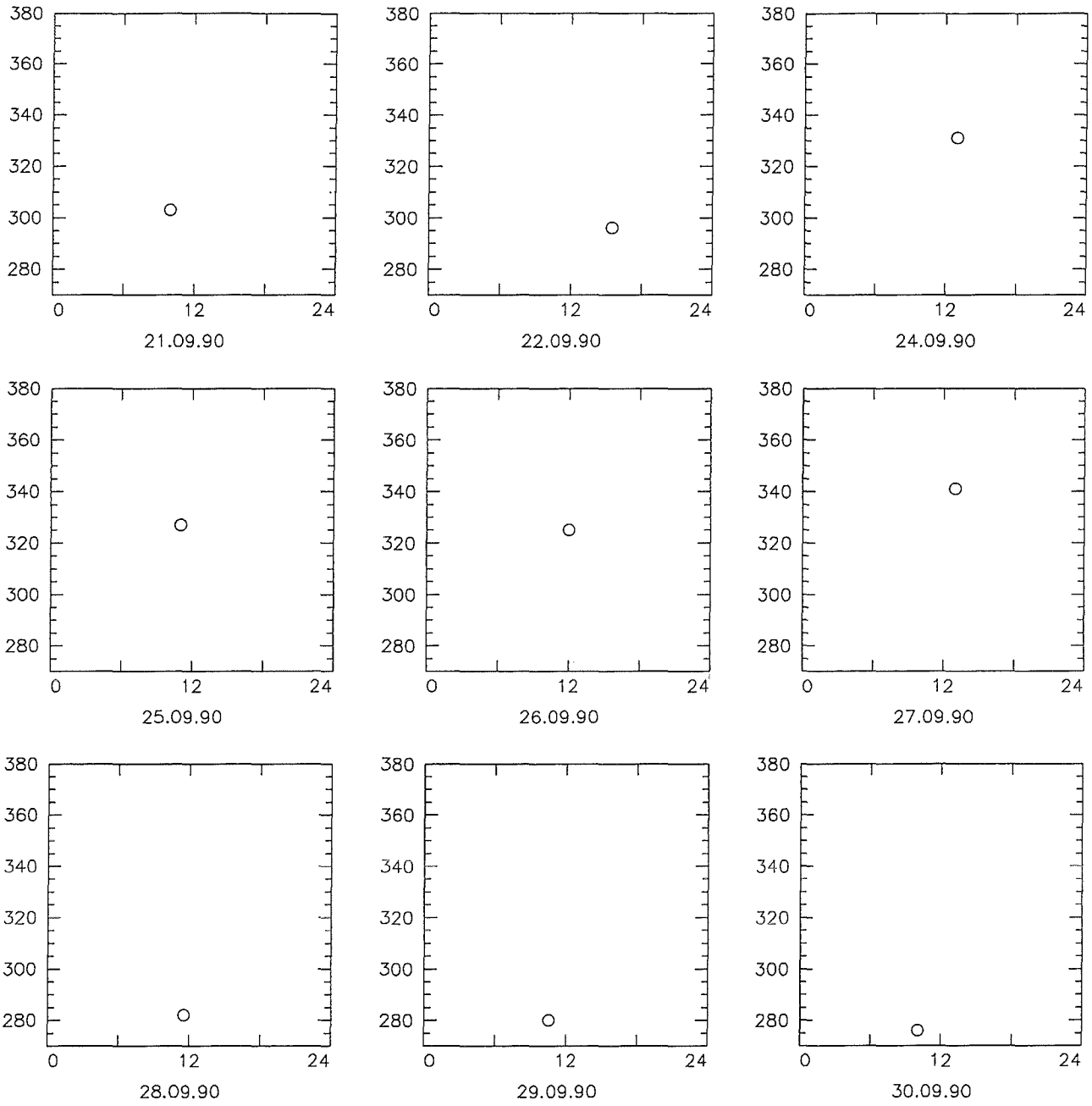

O_3 column density / DU

File: 03CD ENZ90JUE

Dataset: 10

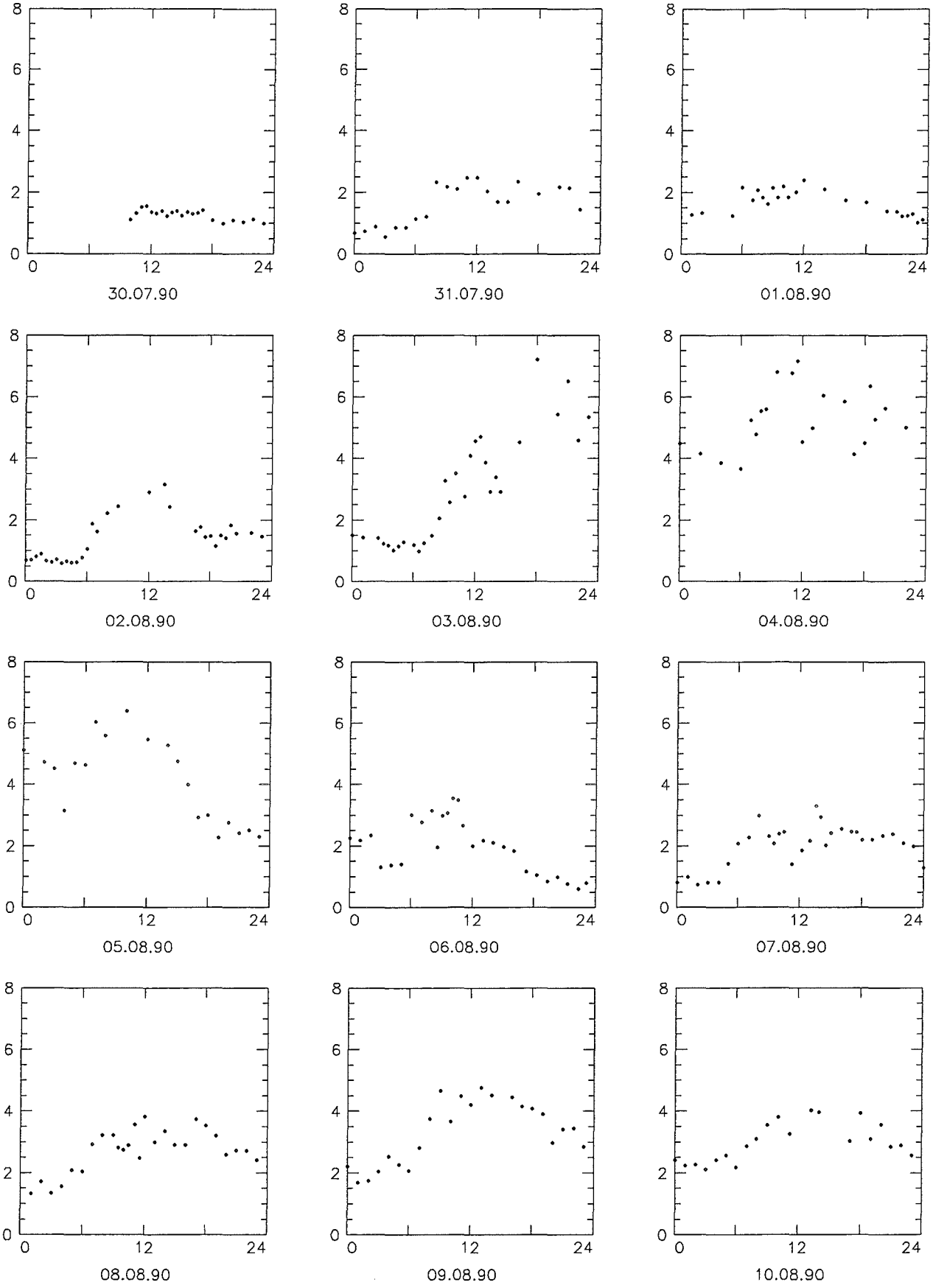

HCHO/ppb

File: HCHO ENZ90JUE

Dataset: 11

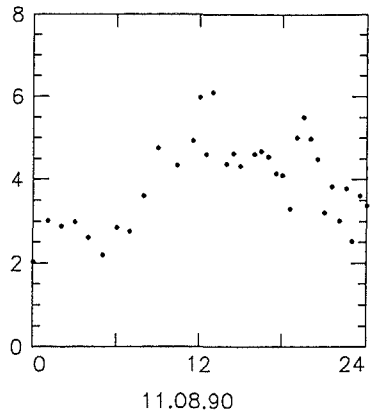

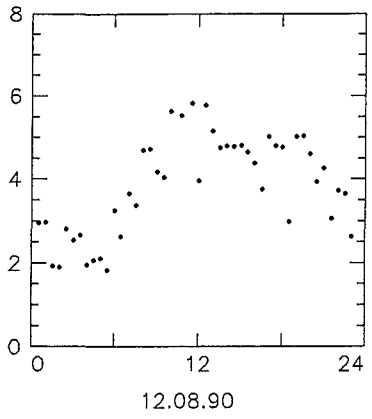

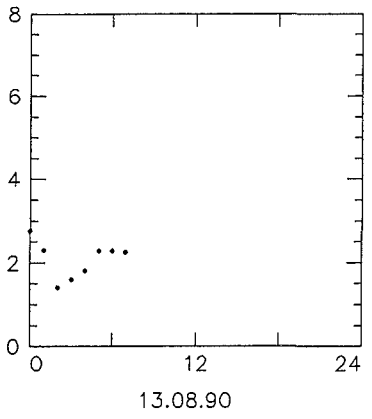

HCHO/ppb

File: HCHO ENZ90JUE

Dataset: 11

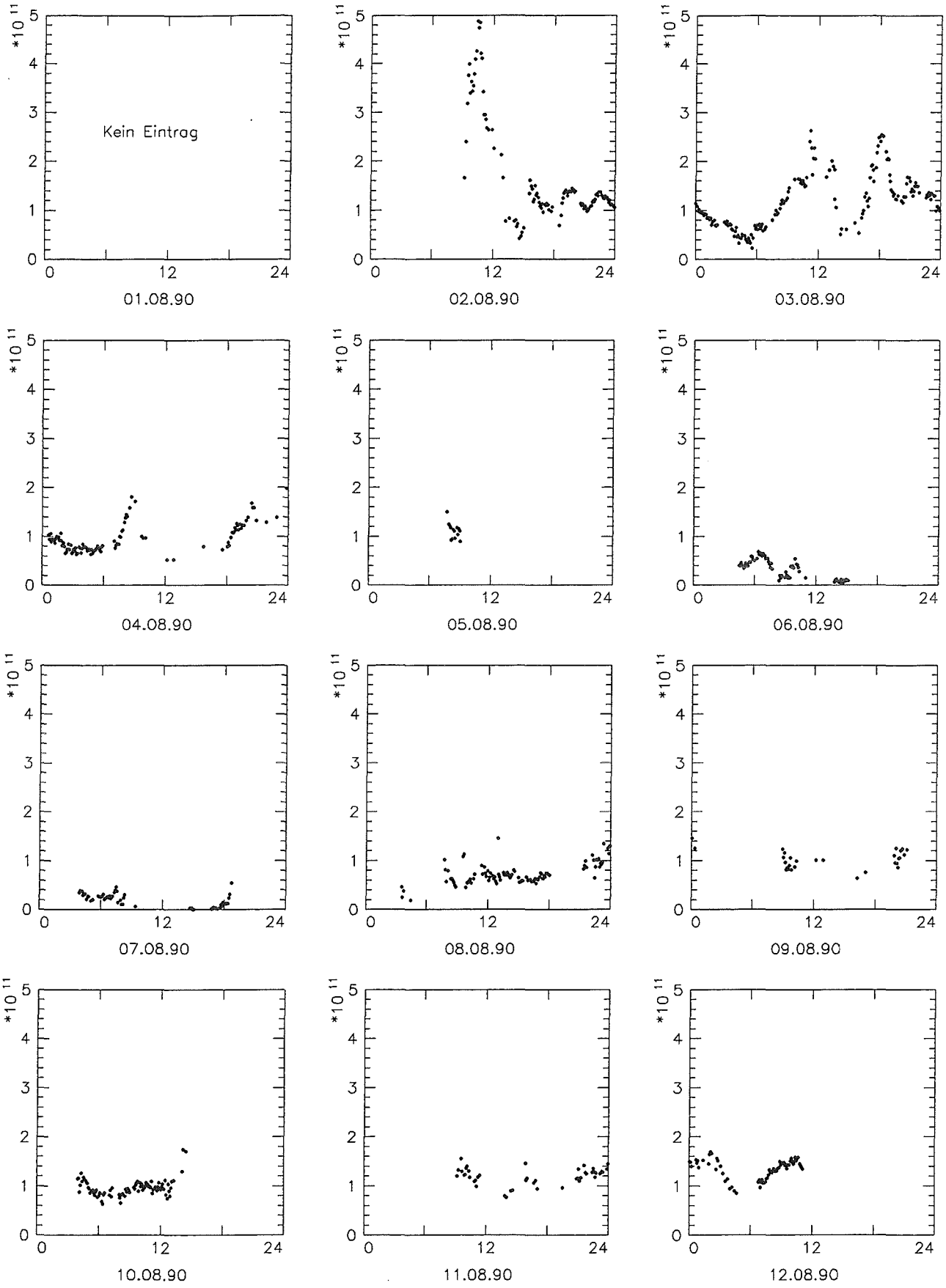

$HCHO/cm^{-3}$

File: ALLDOASJ ZUS90JUY

Dataset: 12

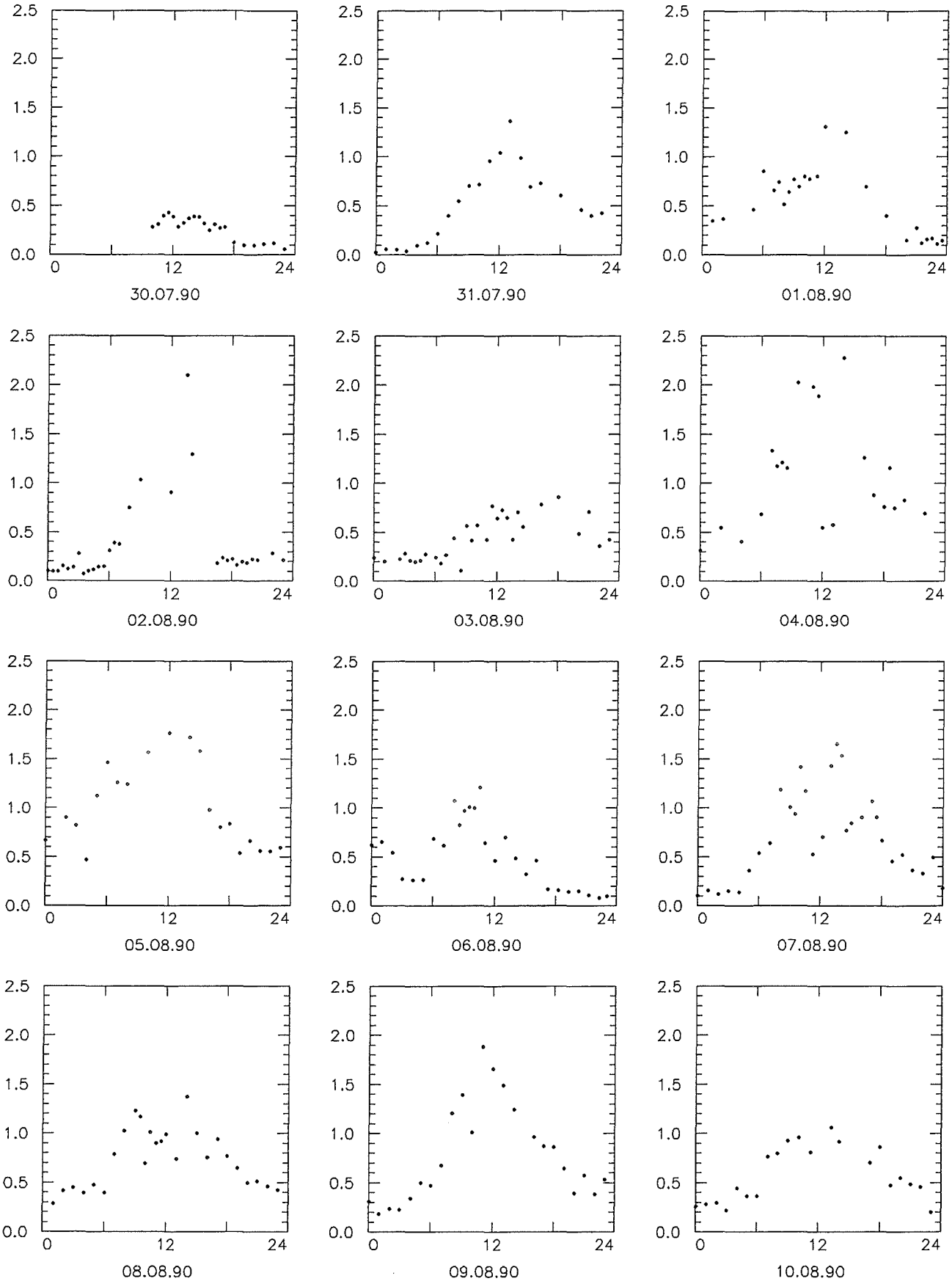

CH_3CHO/ppb

File: CH3CHO ENZ90JUE

Dataset: 13

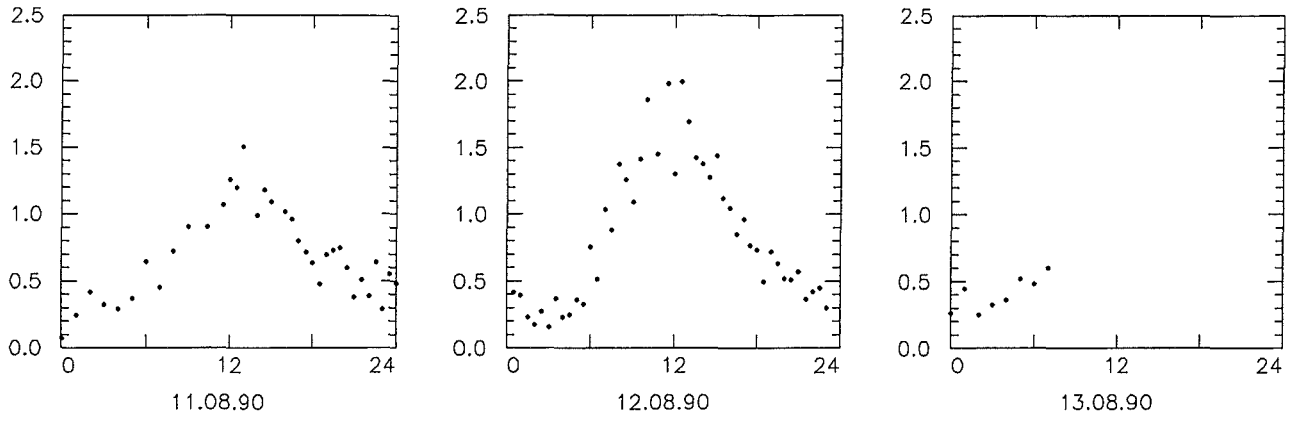

CH_3CHO/ppb

File: CH3CHO ENZ90JUE

Dataset: 13

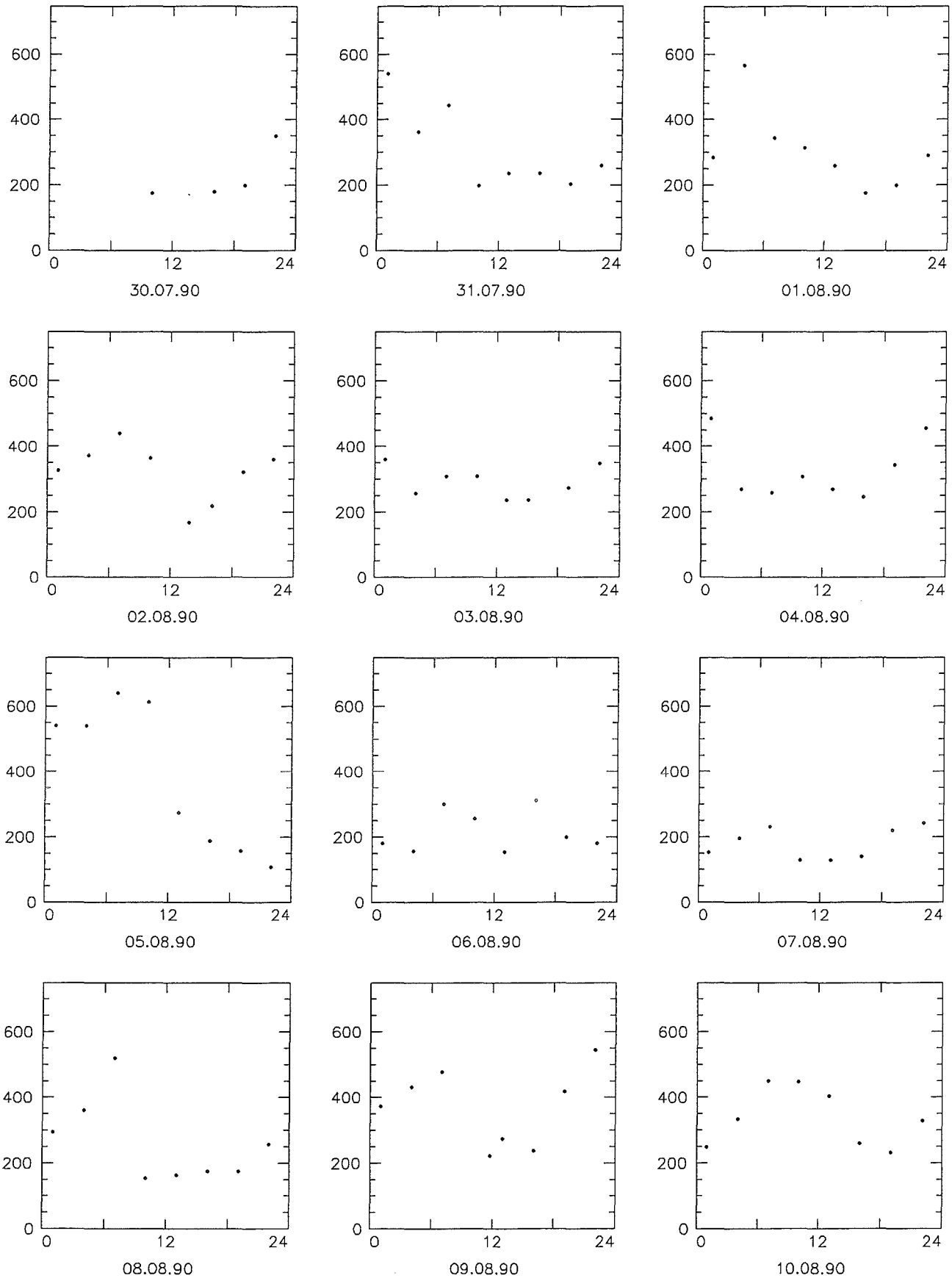

CO/ppb

File: CO_BHLTR ENZ90JUE

Dataset: 14

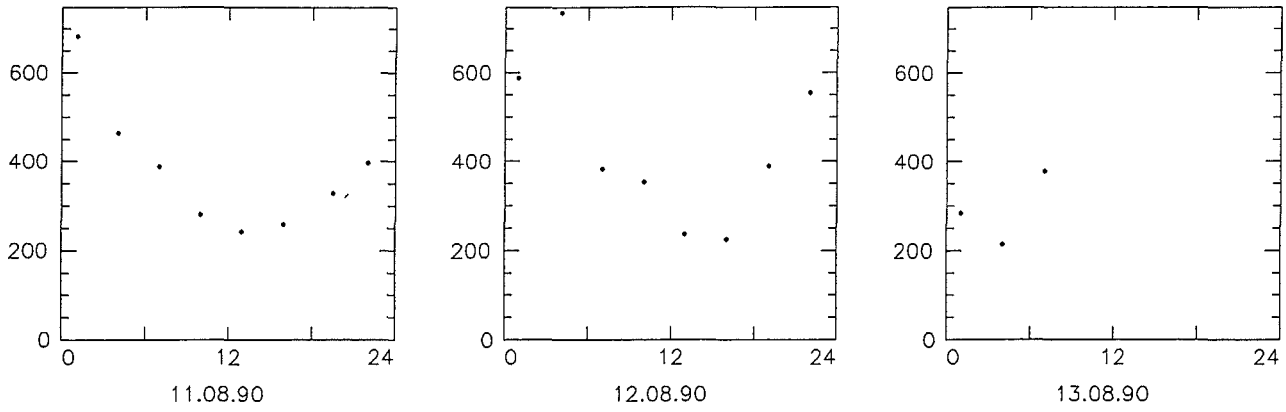

CO/ppb

File: CO_BHLTR ENZ90JUE

Dataset: 14

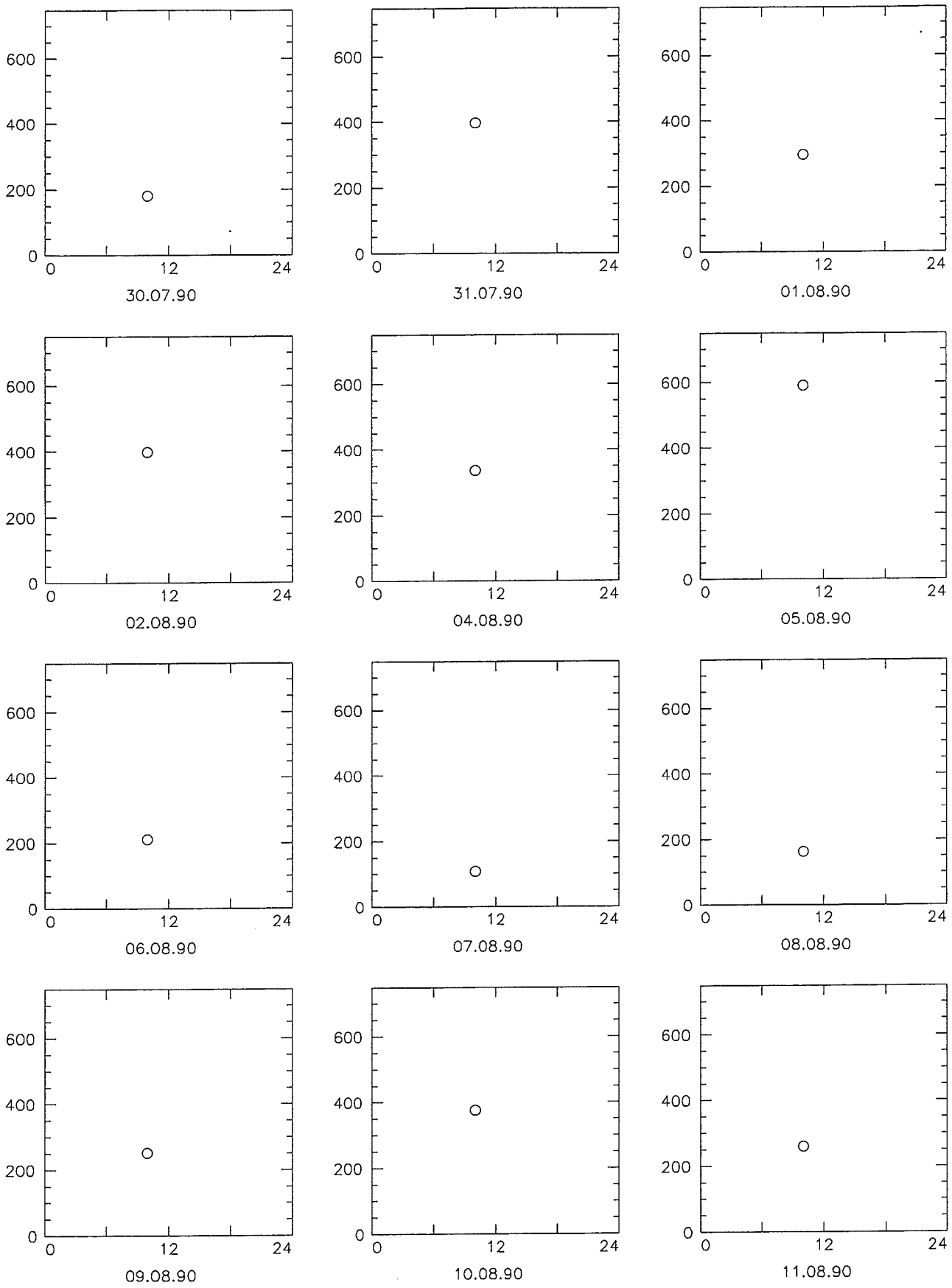

CO/ppb

File: CO_SH ENZ90JUE

Dataset: 15

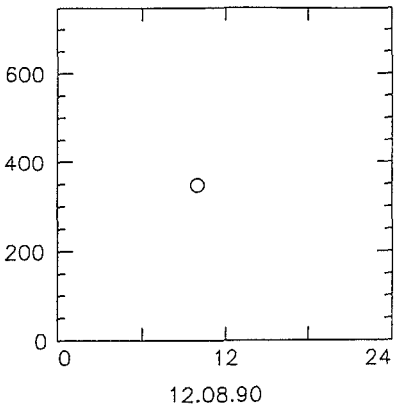

CO/ppb

File: CO_SH ENZ90JUE

Dataset: 15

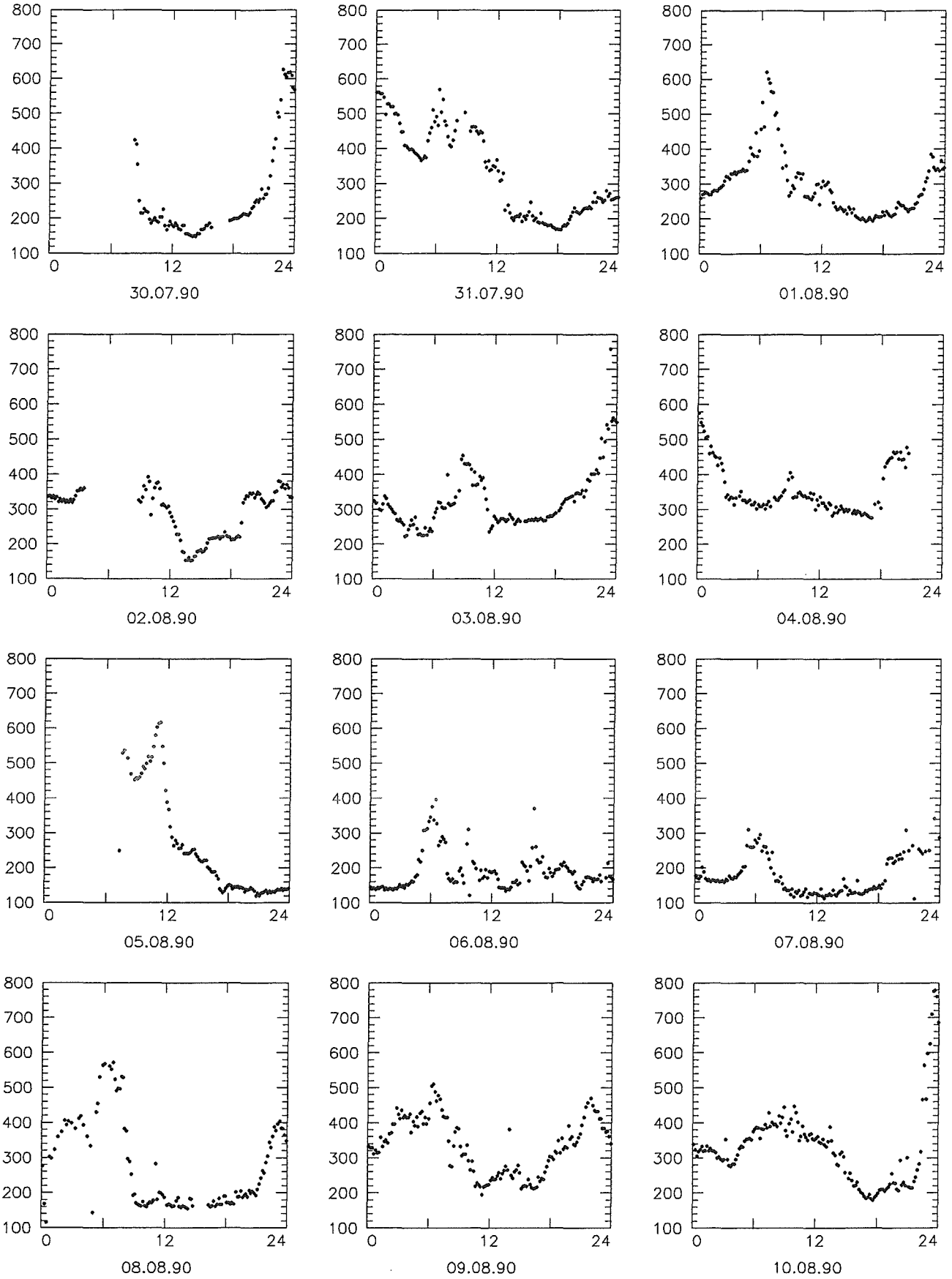

CO/ppb

File: CO ENZ90JUE

Dataset: 16

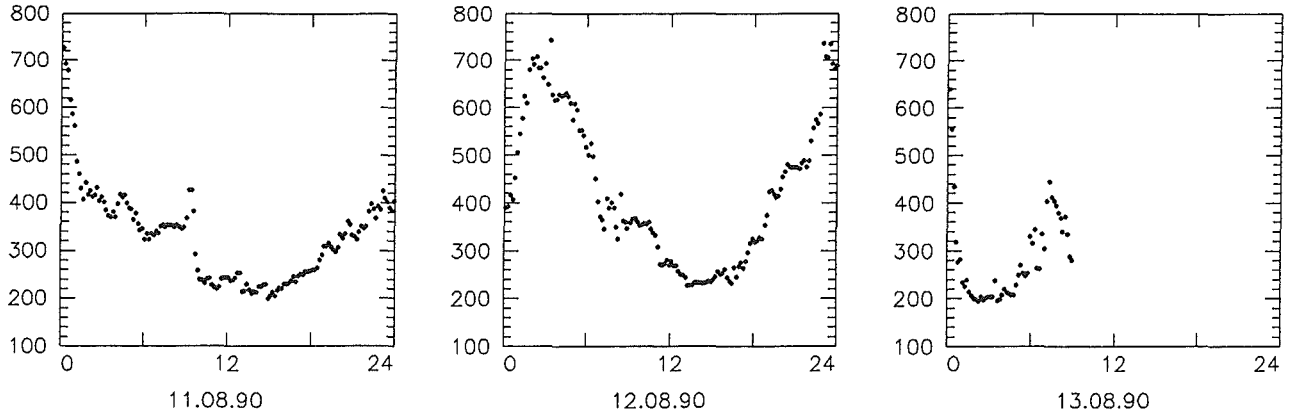

CO/ppb

File: CO ENZ90JUE

Dataset: 16

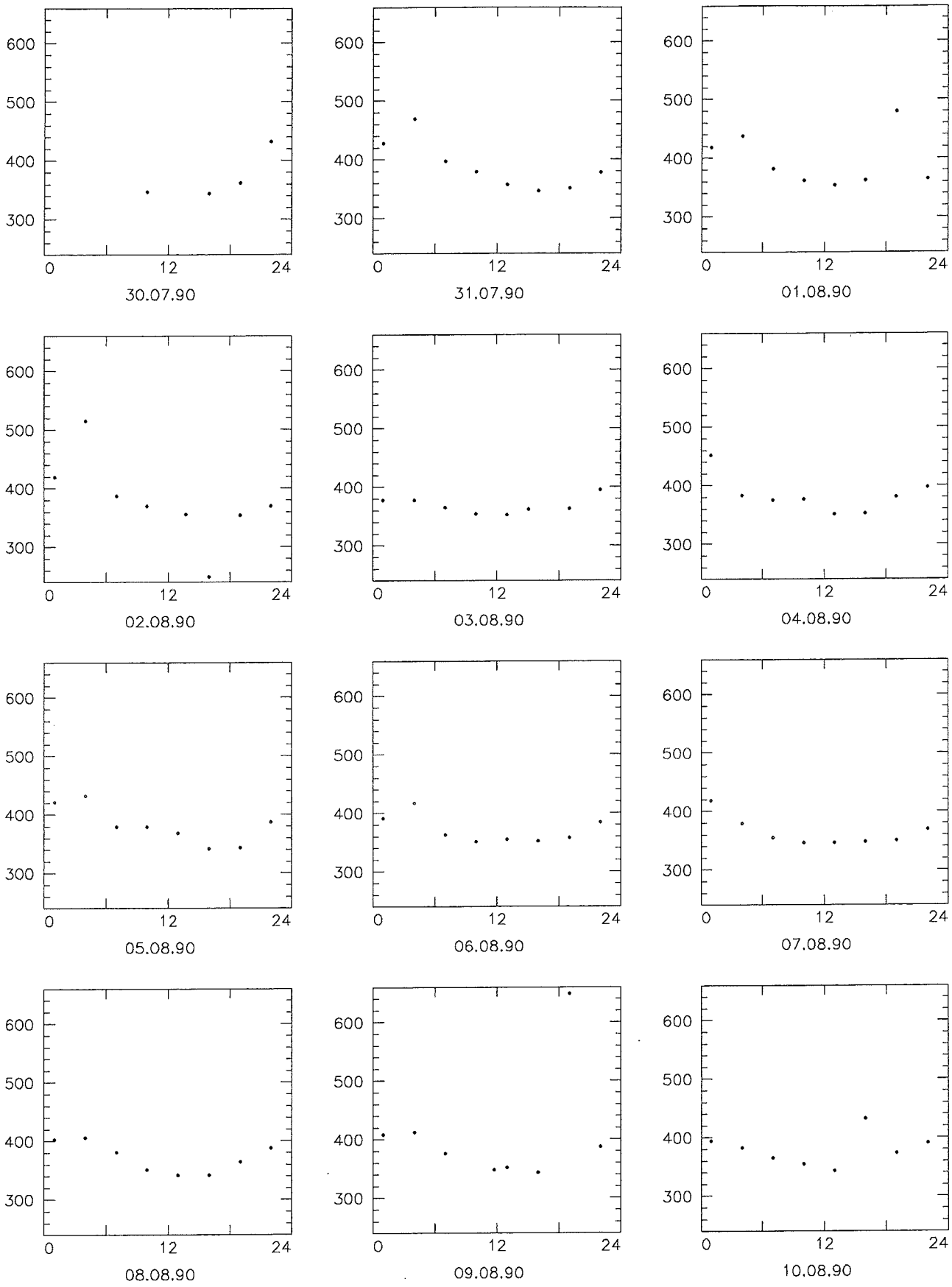

CO_2/ppm

File: C02 ENZ90JUE

Dataset: 17

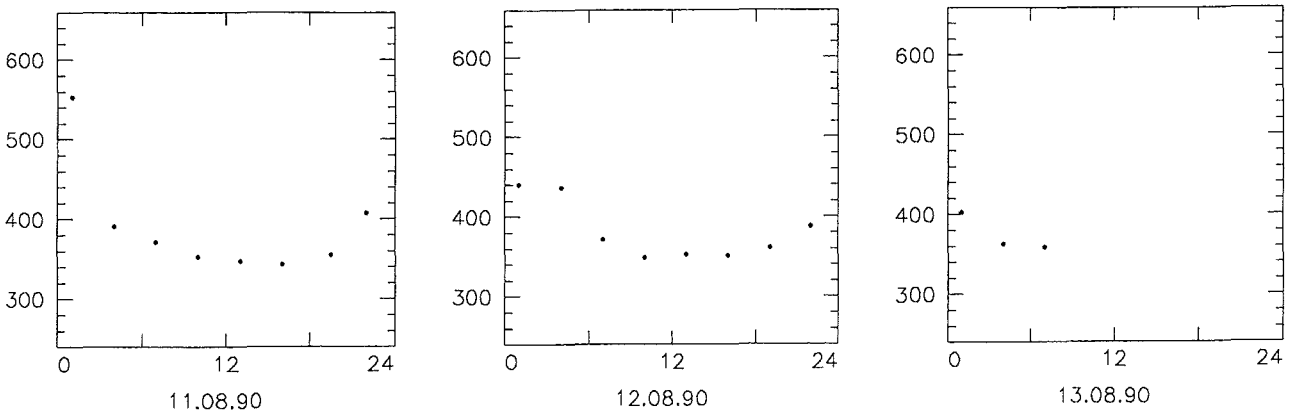

CO_2/ppm

File: CO2 ENZ90JUE

Dataset: 17

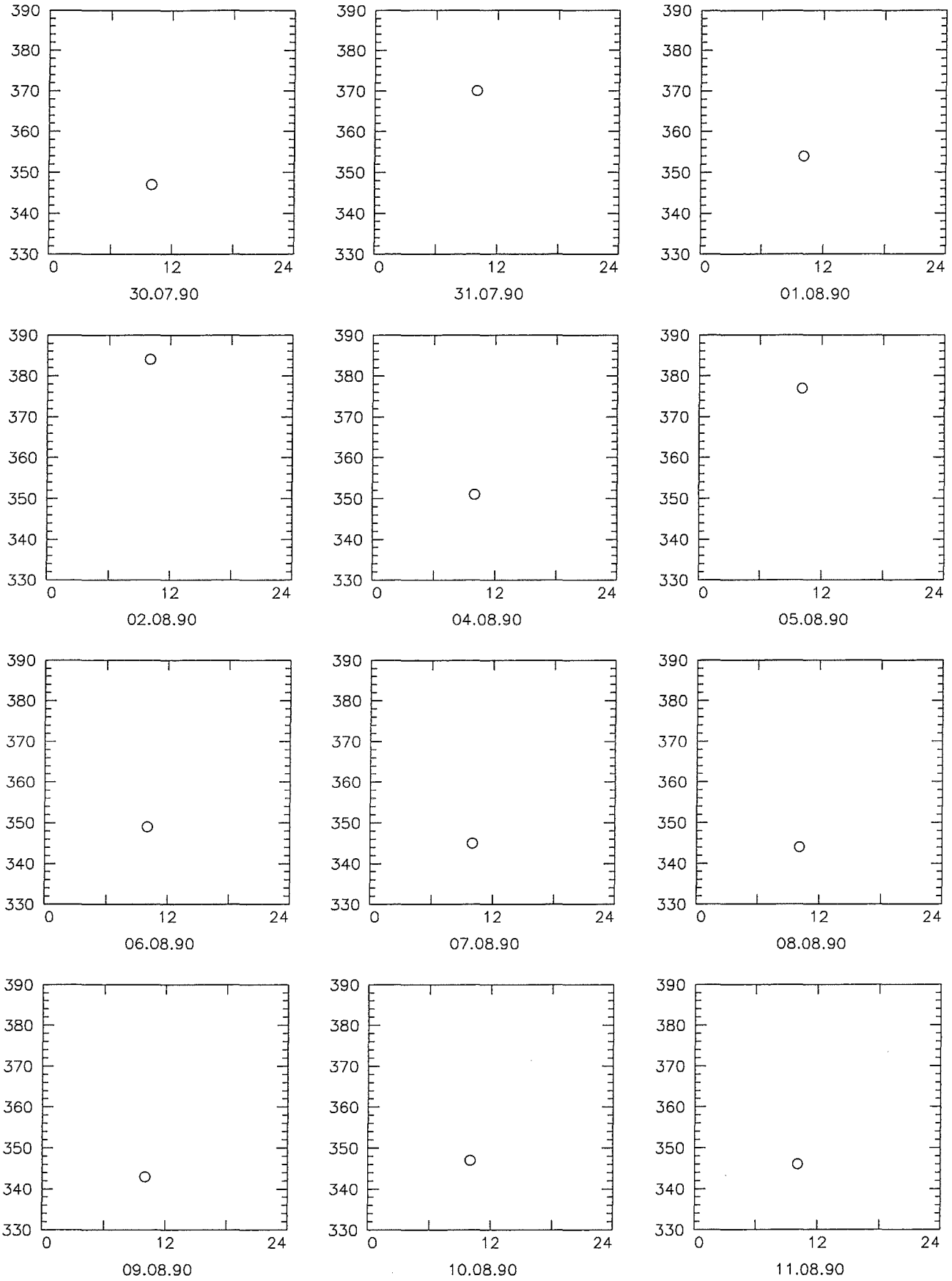

CO_2/ppm

File: CO2_SH ENZ90JUE

Dataset: 18

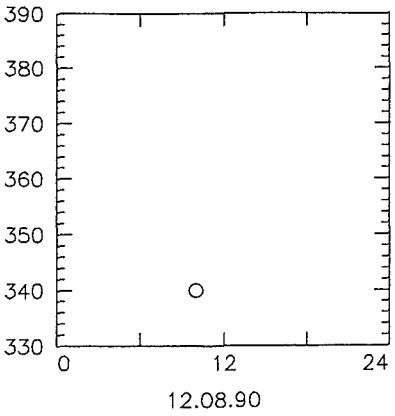

CO_2/ppm

File: CO2_SH ENZ90JUE

Dataset: 18

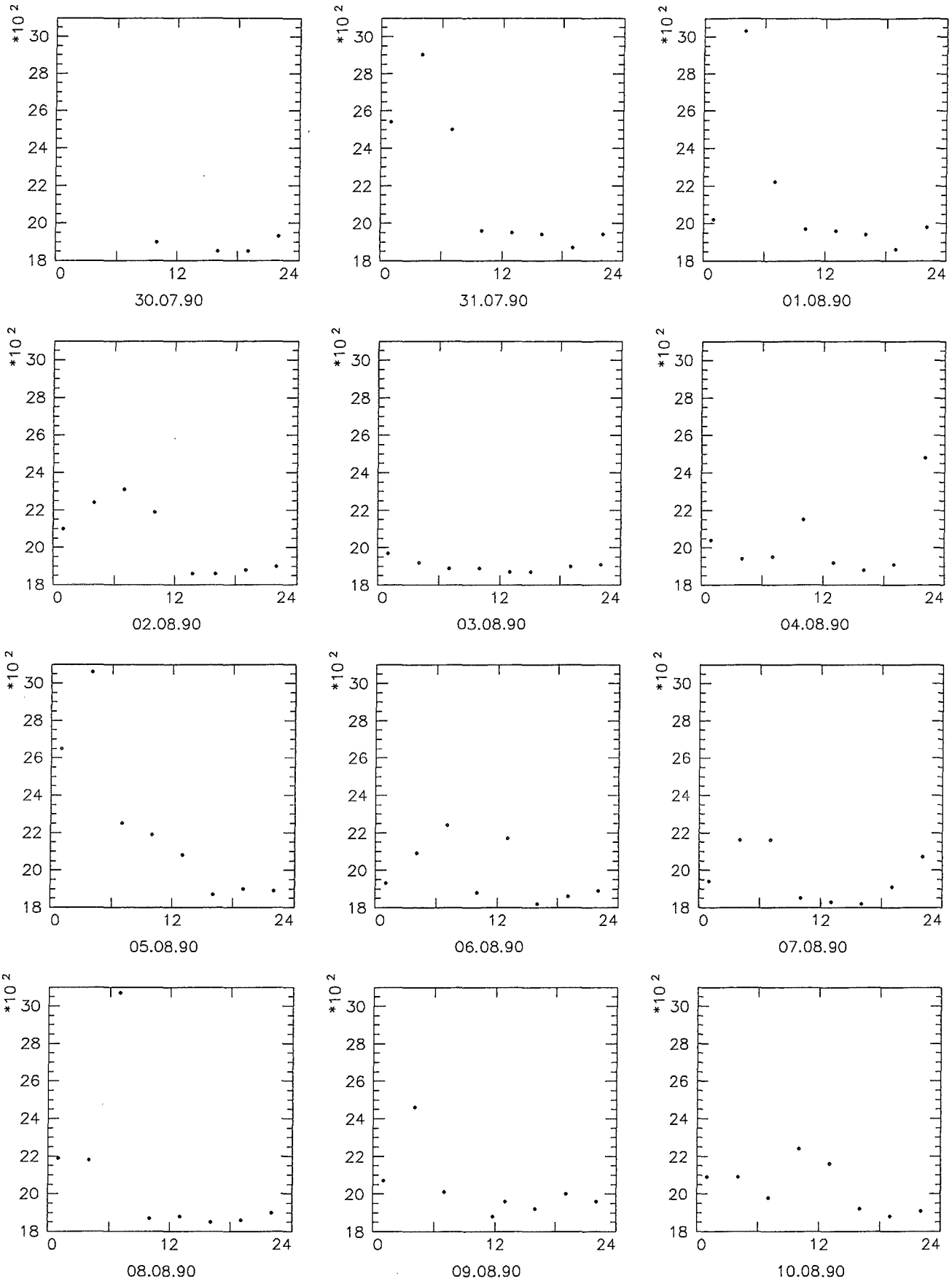

CH_4/ppb

File: METHAN ENZ90JUE

Dataset: 19

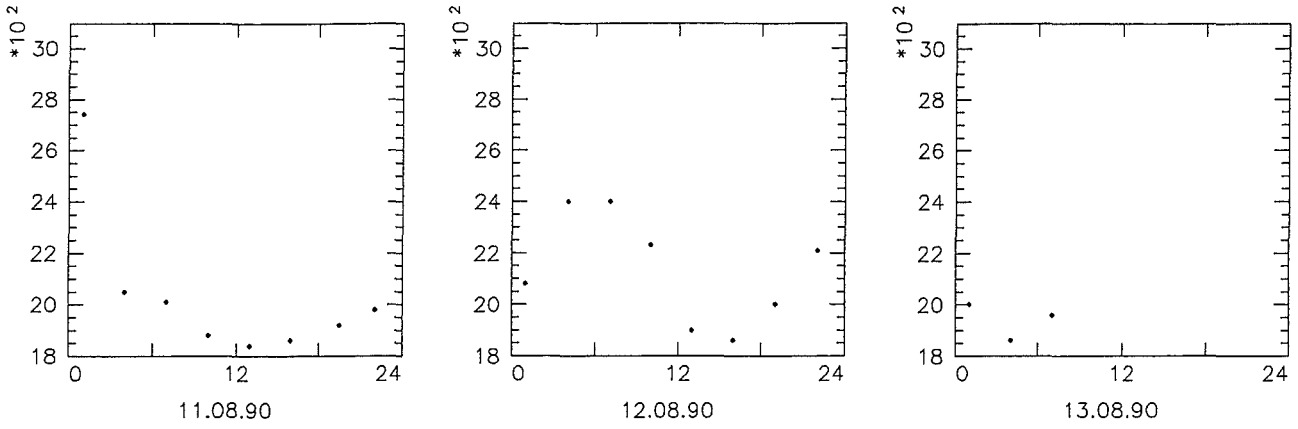

CH_4/ppb

File: METHAN ENZ90JUE

Dataset: 19

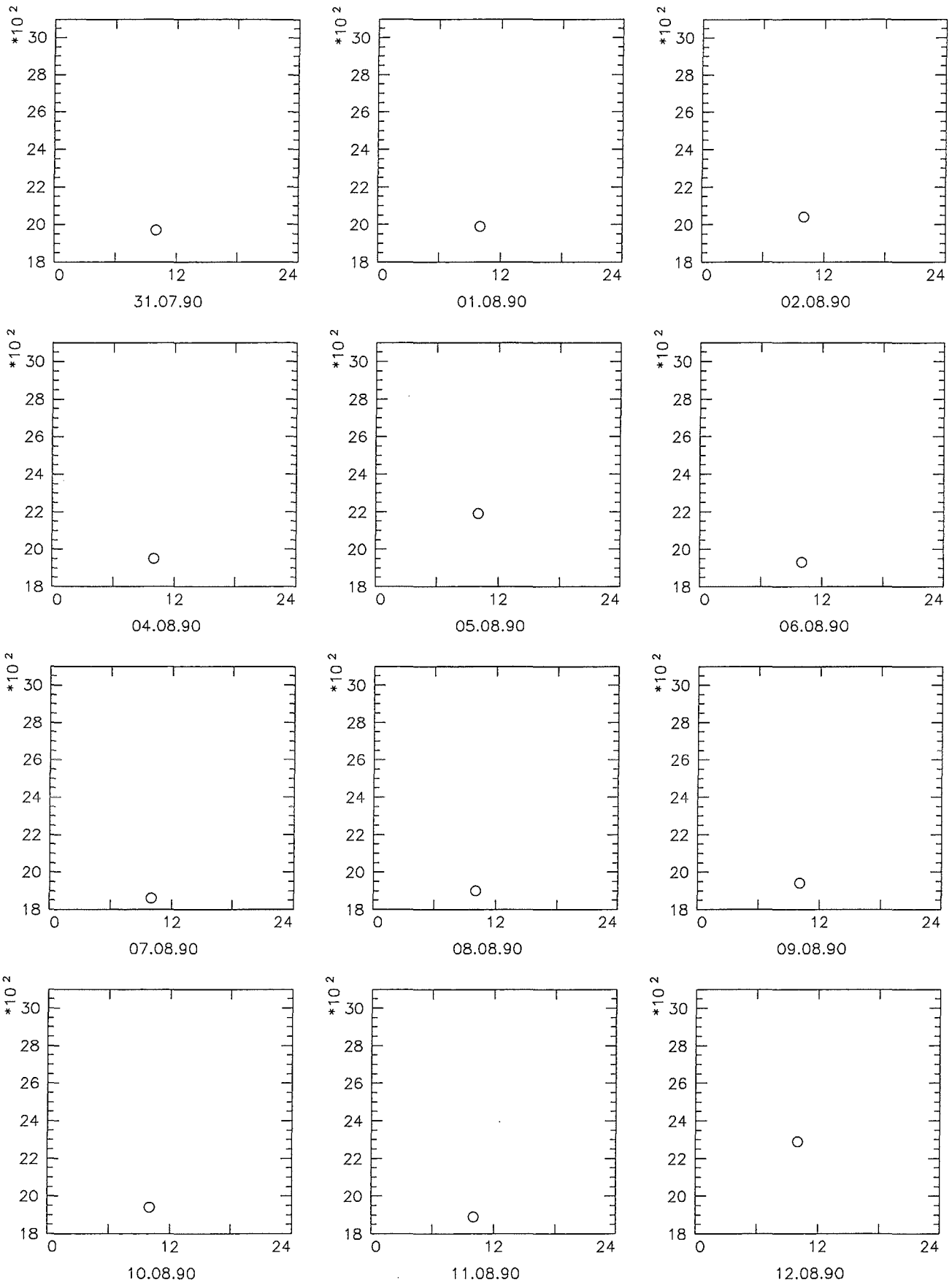

CH_4/ppb

File: METHAN_S ENZ90JUE

Dataset: 20

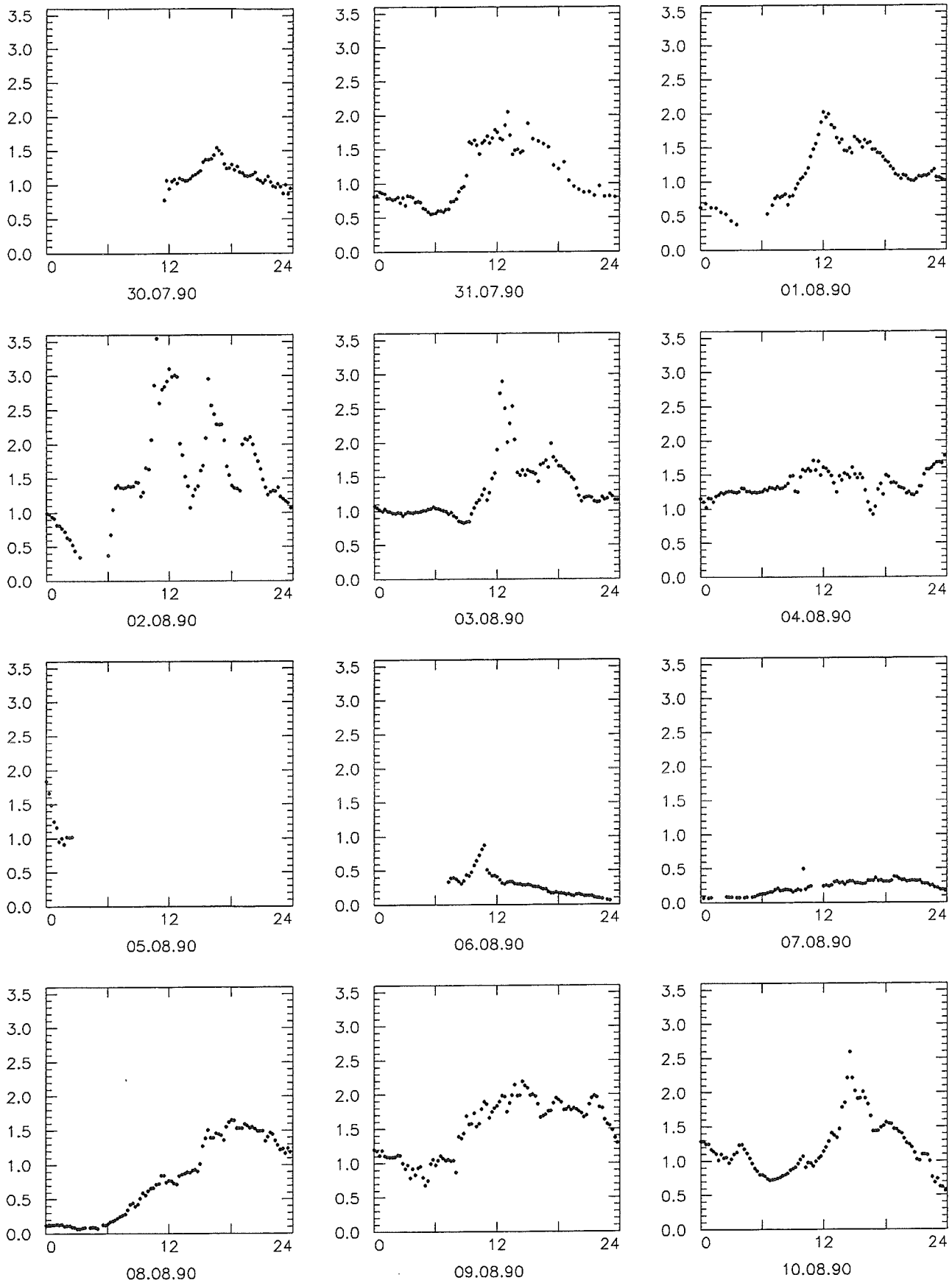

PAN/ppb

File: PAN ENZ90JUE

Dataset: 21

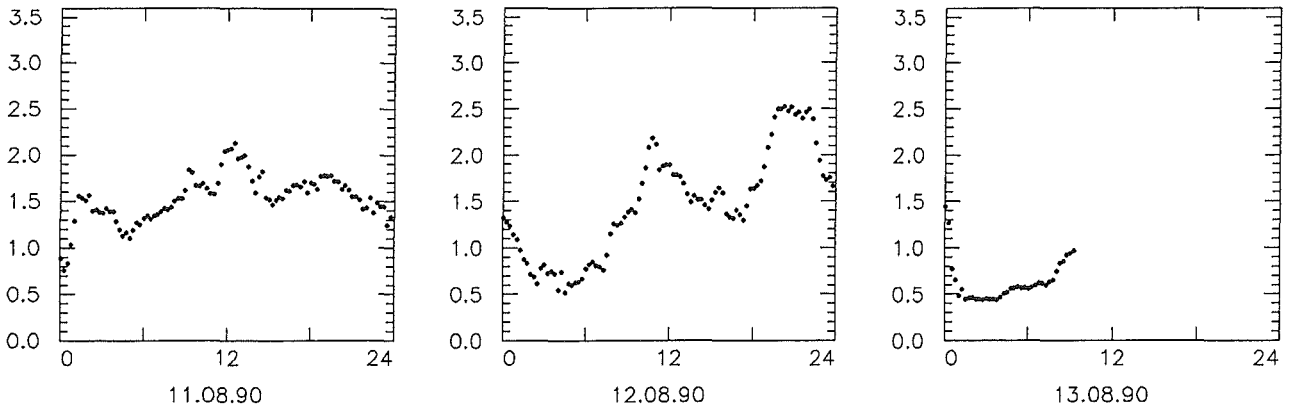

PAN/ppb

File: PAN ENZ90JUE

Dataset: 21

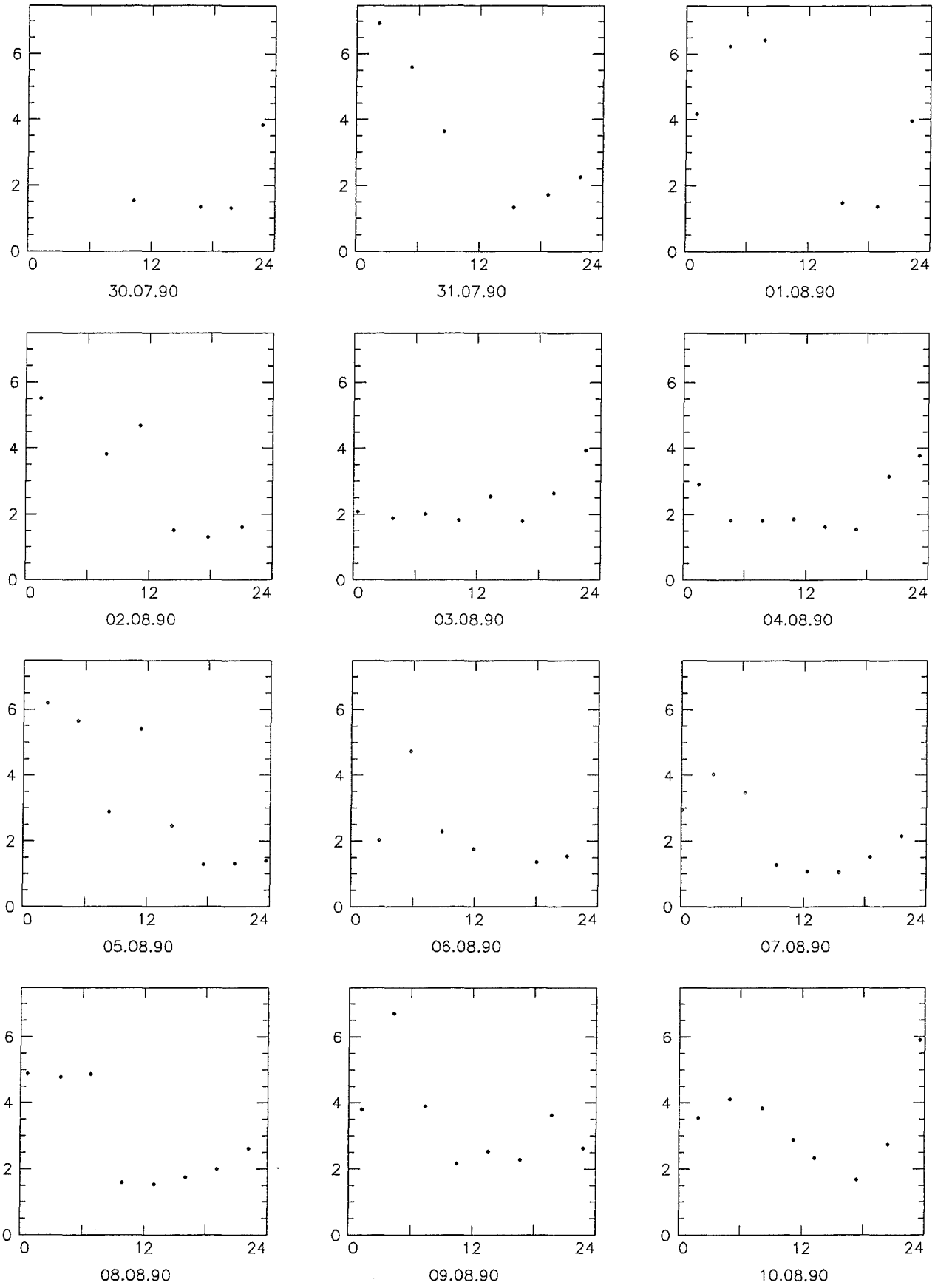

ethane/ppb

File: ETHAN ENZ90JUE

Dataset: 22

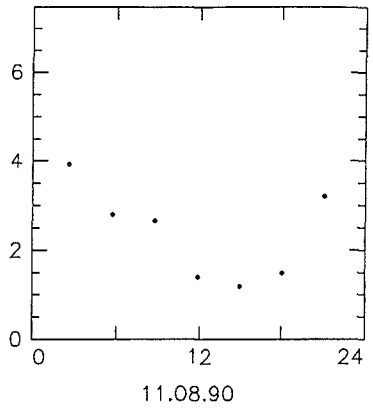

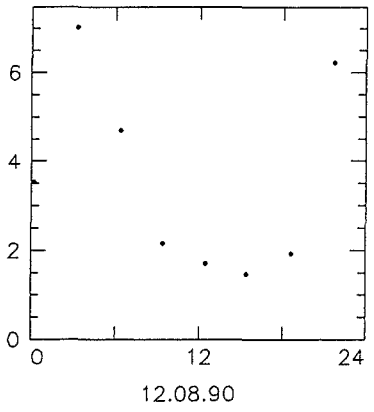

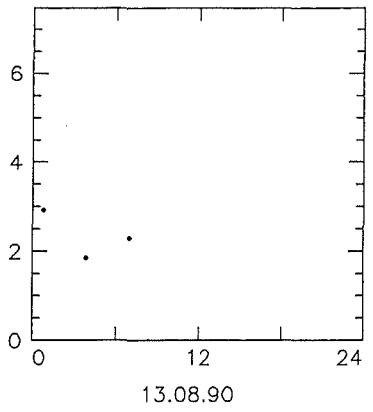

ethane/ppb

File: ETHAN ENZ90JUE

Dataset: 22

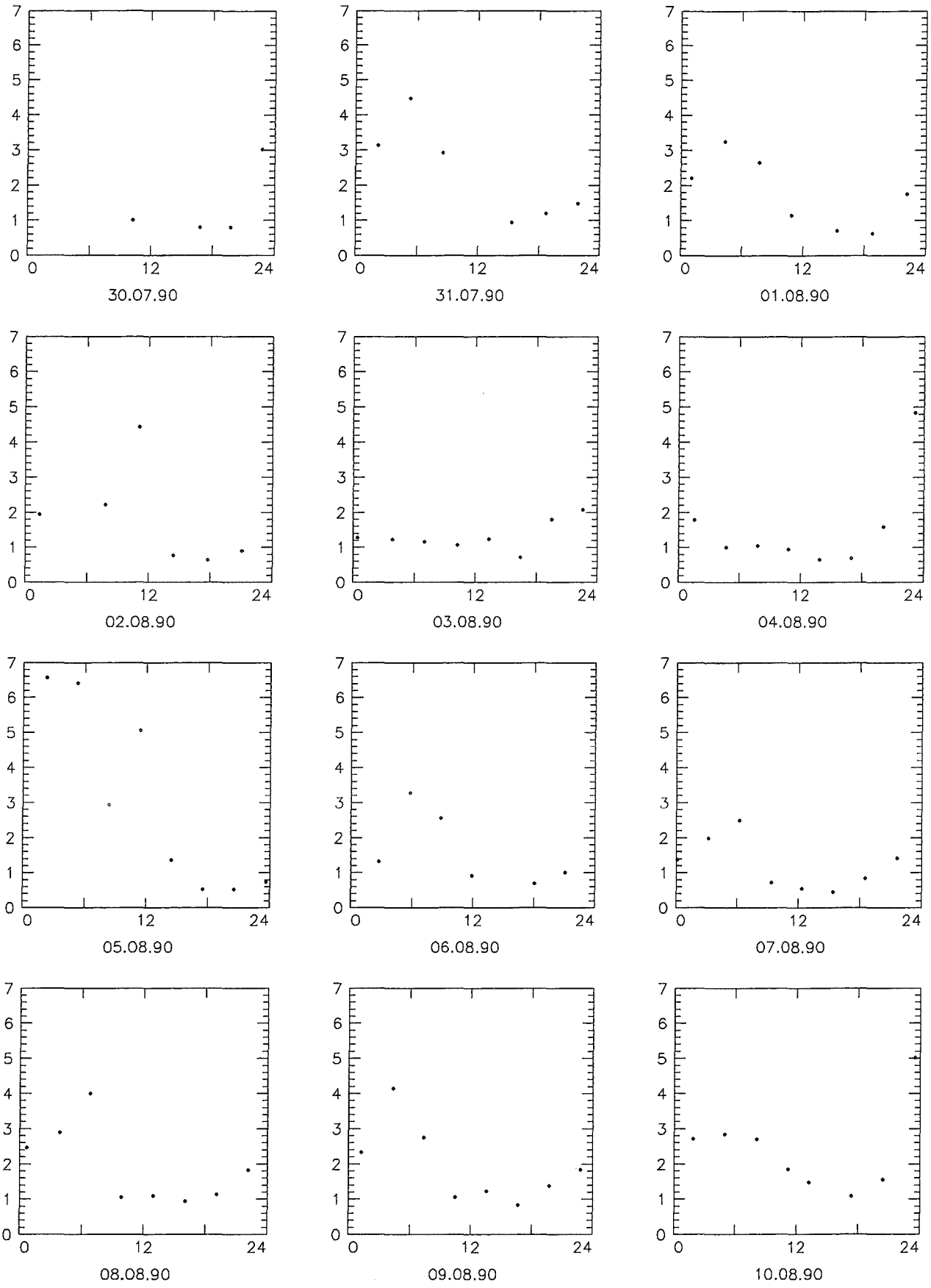

propane/ppb

File: PROPAN ENZ90JUE

Dataset: 23

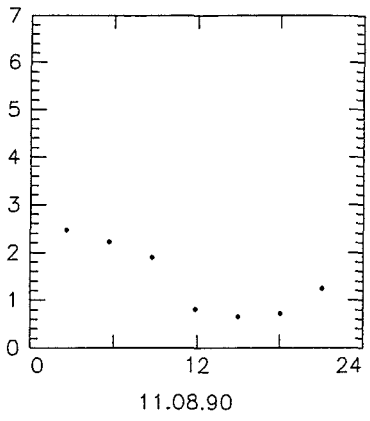

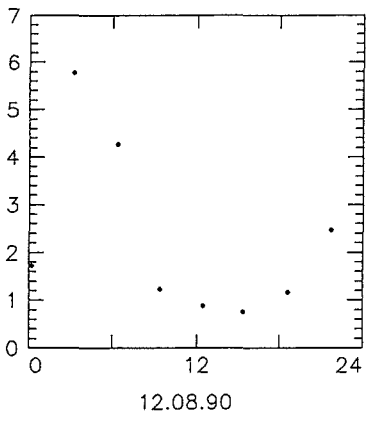

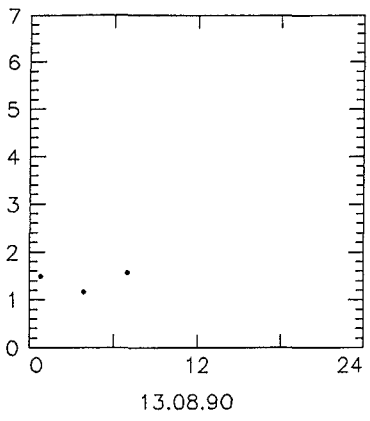

propane/ppb

File: PROPAN ENZ90JUE

Dataset: 23

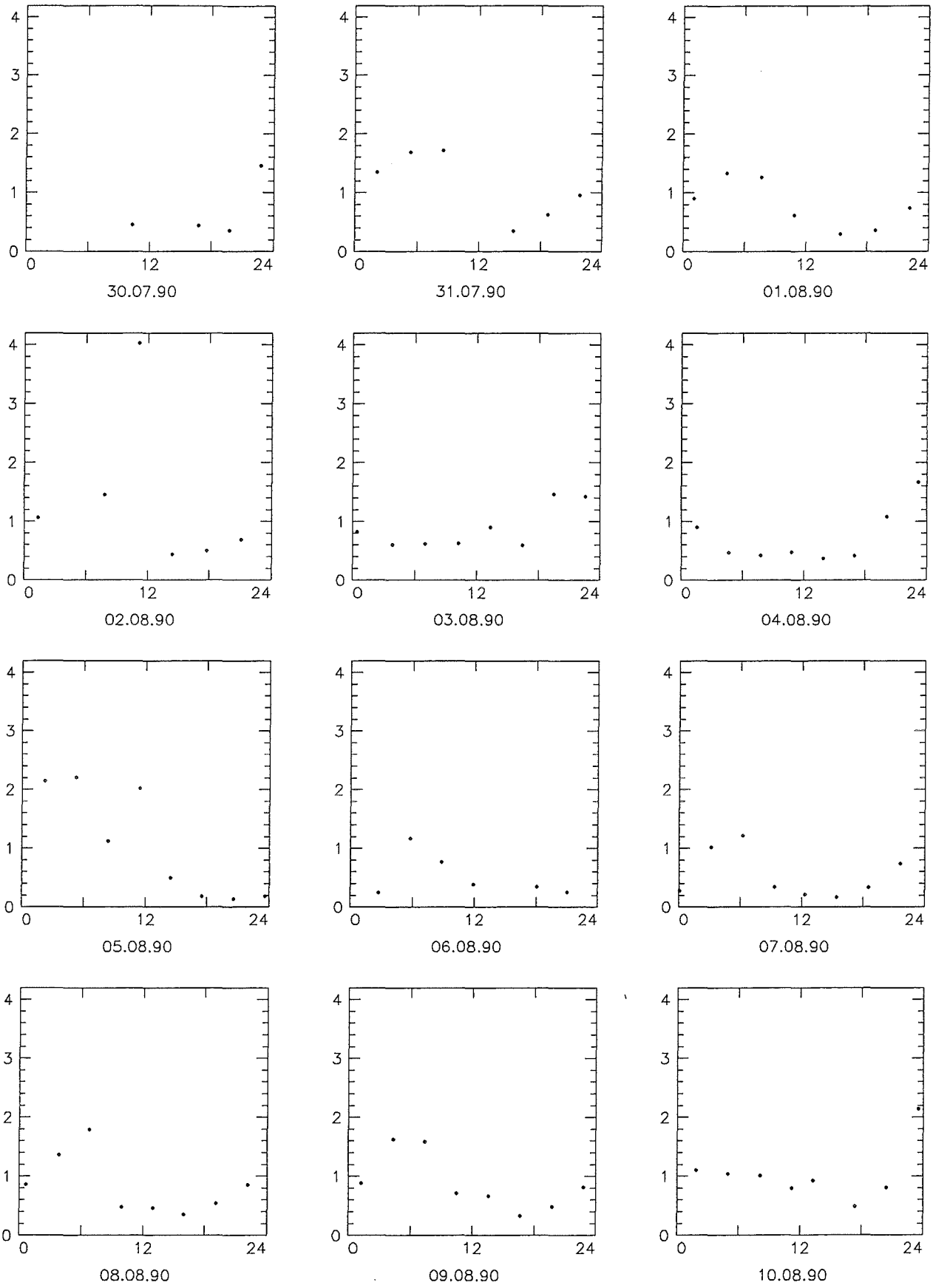

i–butane/ppb

File: I–BUTAN ENZ90JUE

Dataset: 24

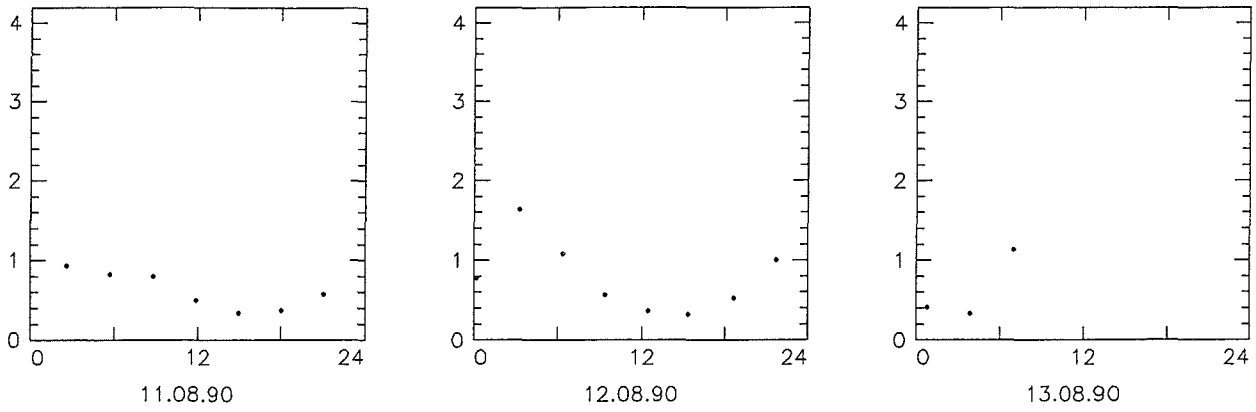

i–butane/ppb

File: I–BUTAN ENZ90JUE

Dataset: 24

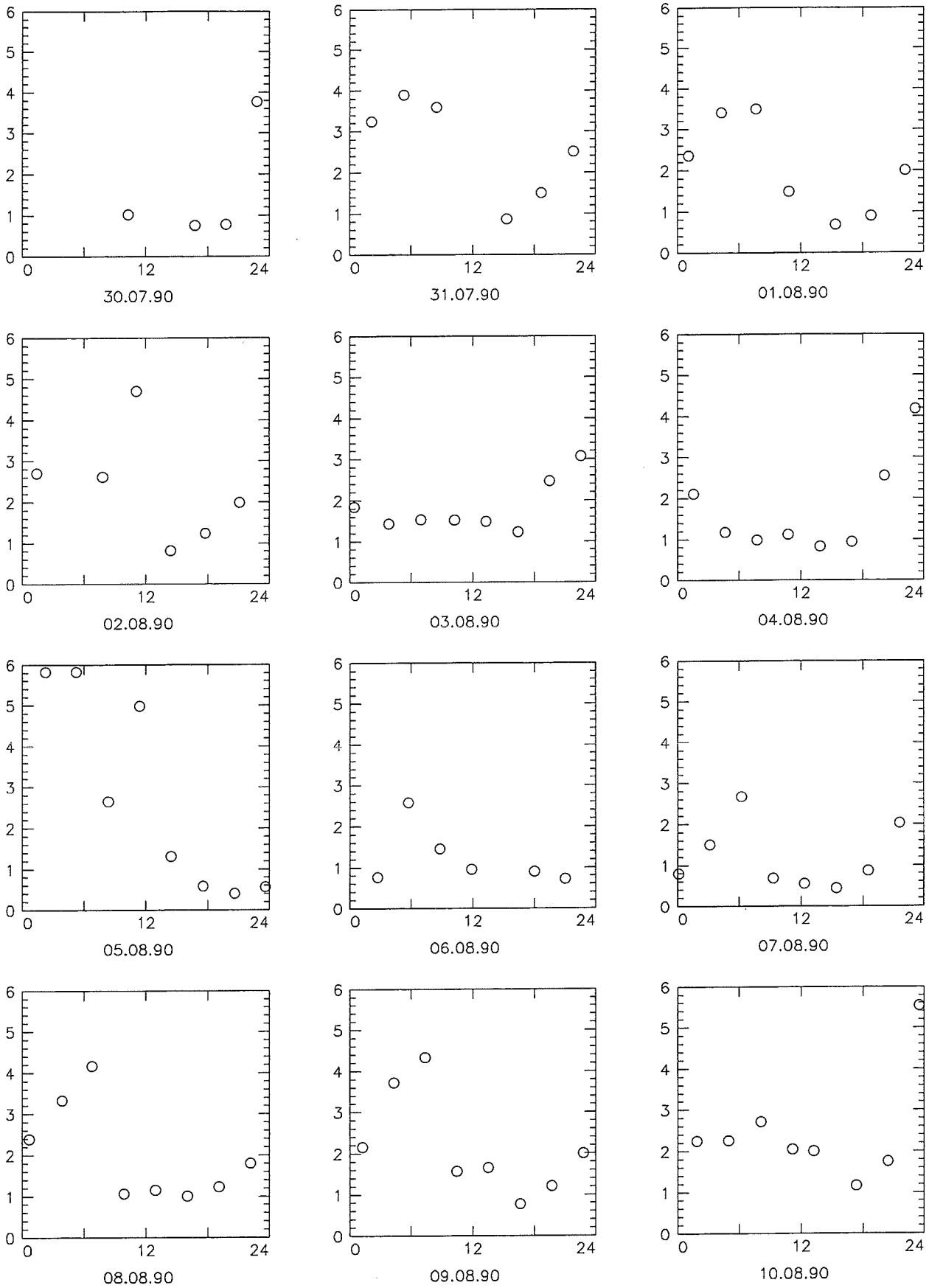

n–butane/ppb

File: N–BUTAN ENZ90JUE

Dataset: 25

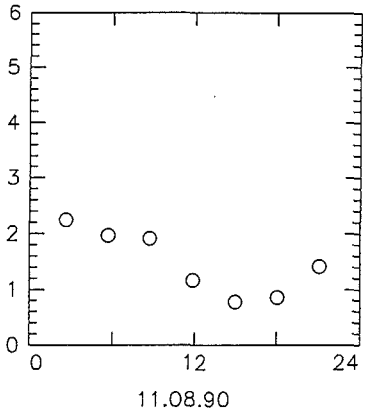

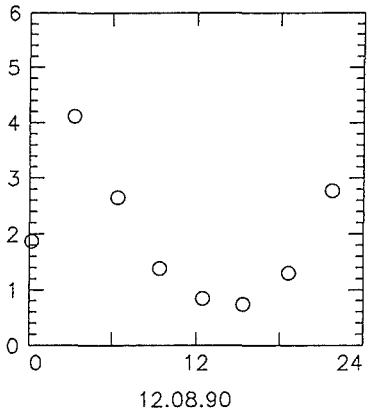

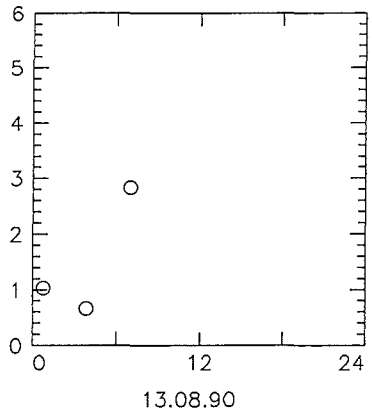

n−butane/ppb

File: N−BUTAN ENZ90JUE

Dataset: 25

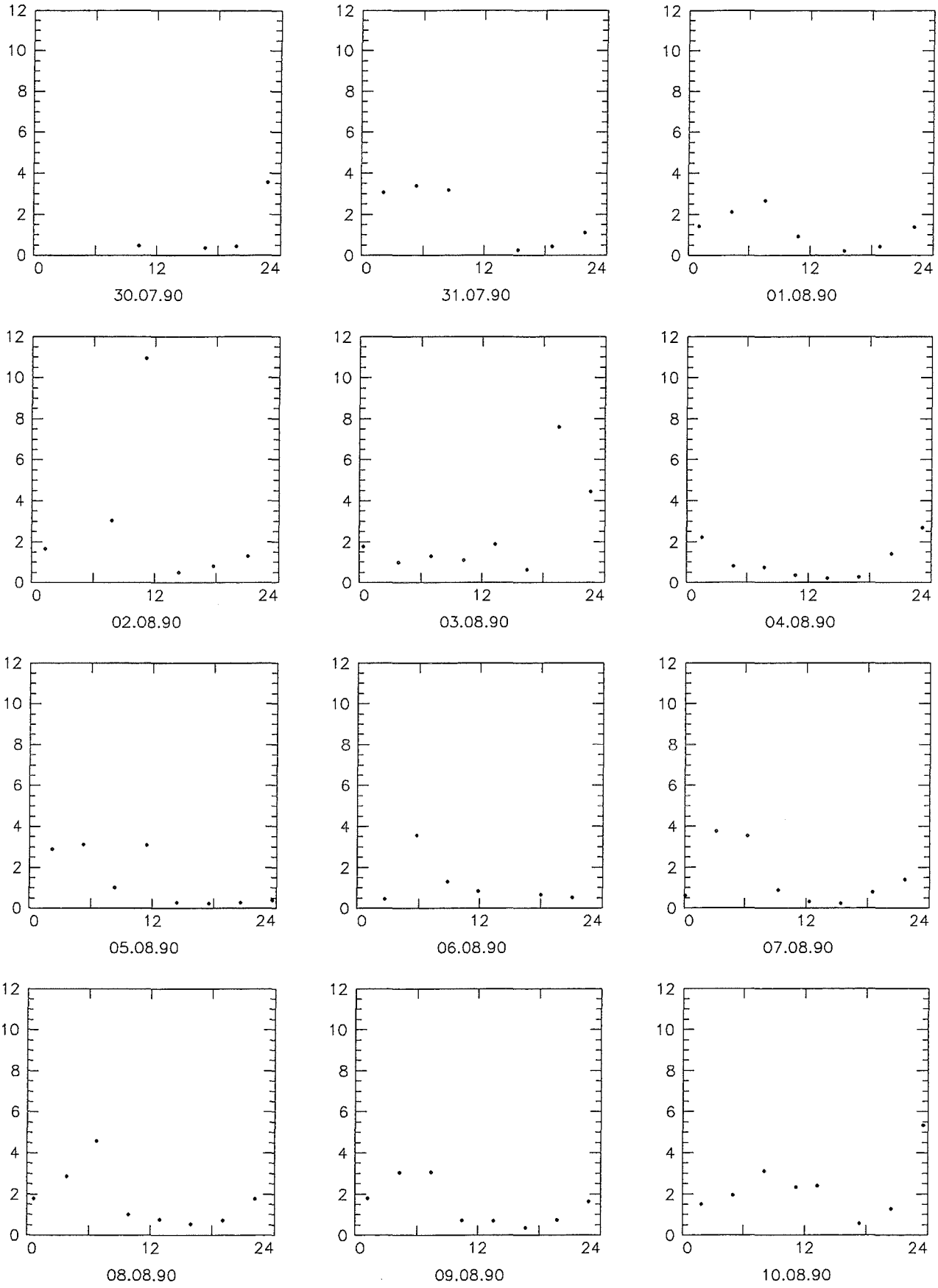

ethene/ppb

File: ETHEN ENZ90JUE

Dataset: 26

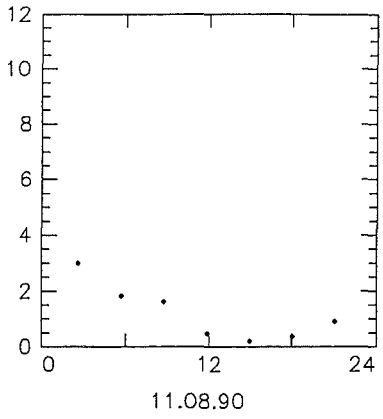

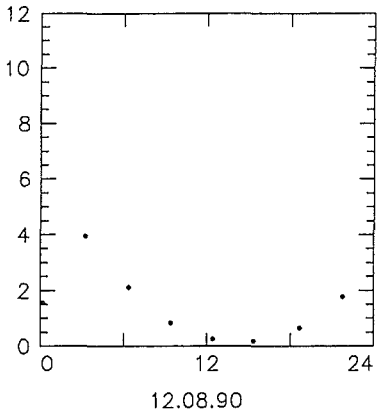

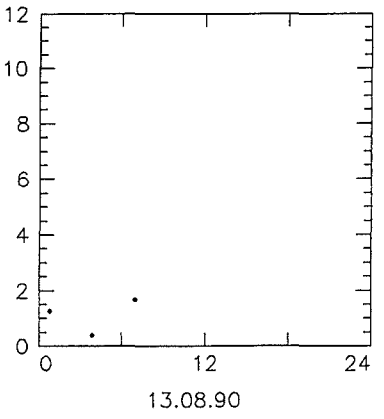

ethene/ppb

File: ETHEN ENZ90JUE

Dataset: 26

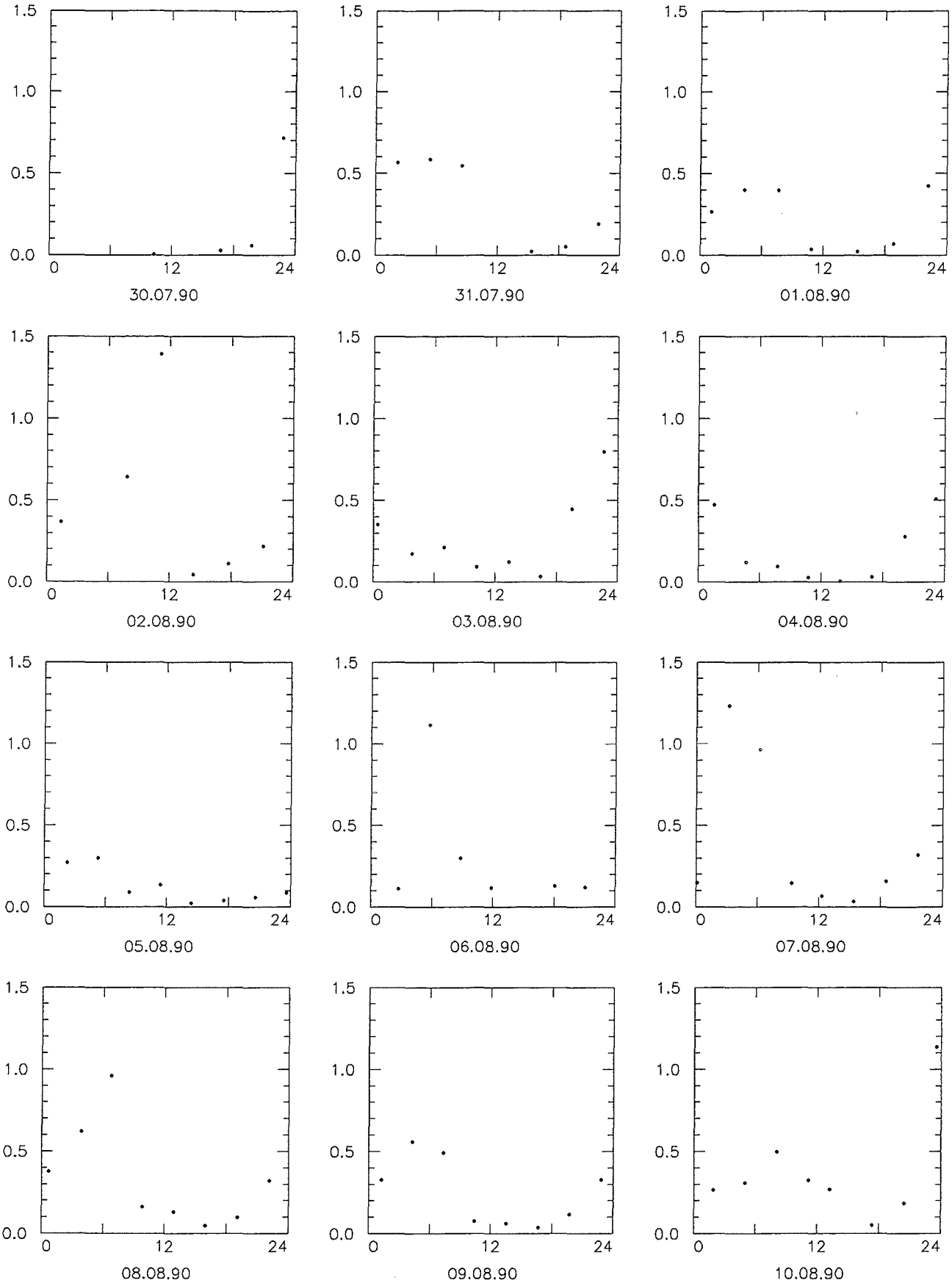

propene/ppb

File: PROPEN ENZ90JUE

Dataset: 27

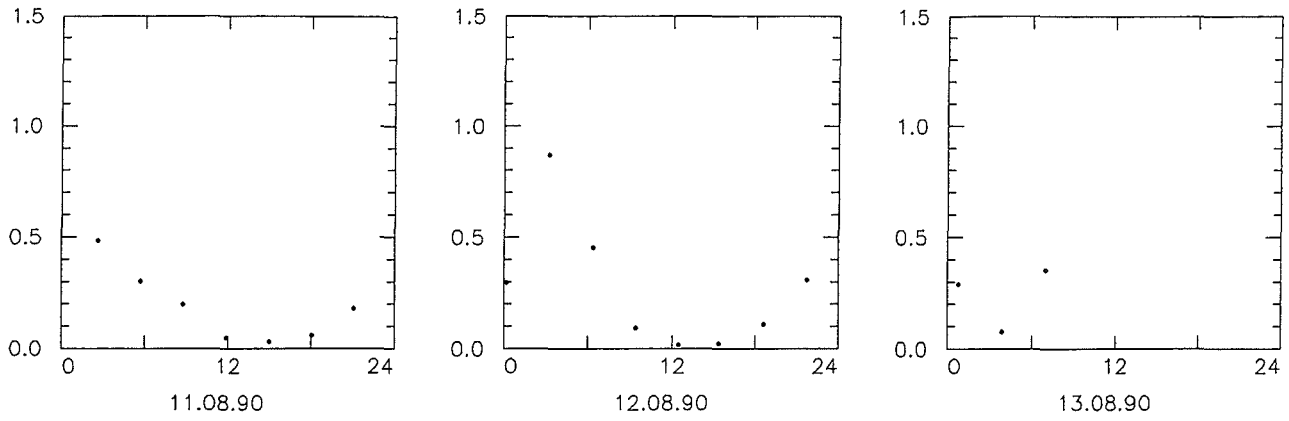

propene/ppb

File: PROPEN ENZ90JUE

Dataset: 27

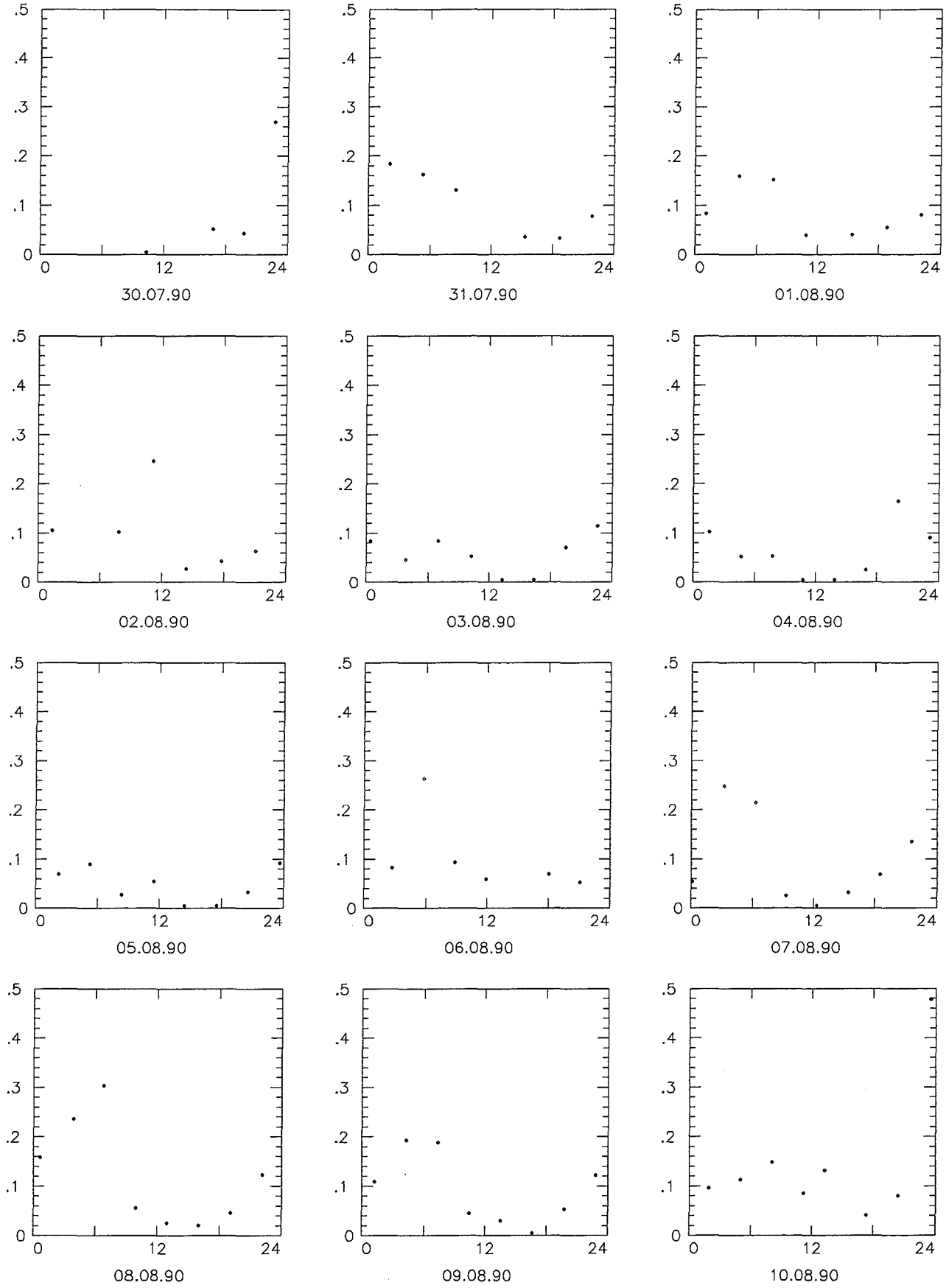

1-butene/ppb

File: 1-BUTEN ENZ90JUE

Dataset: 28

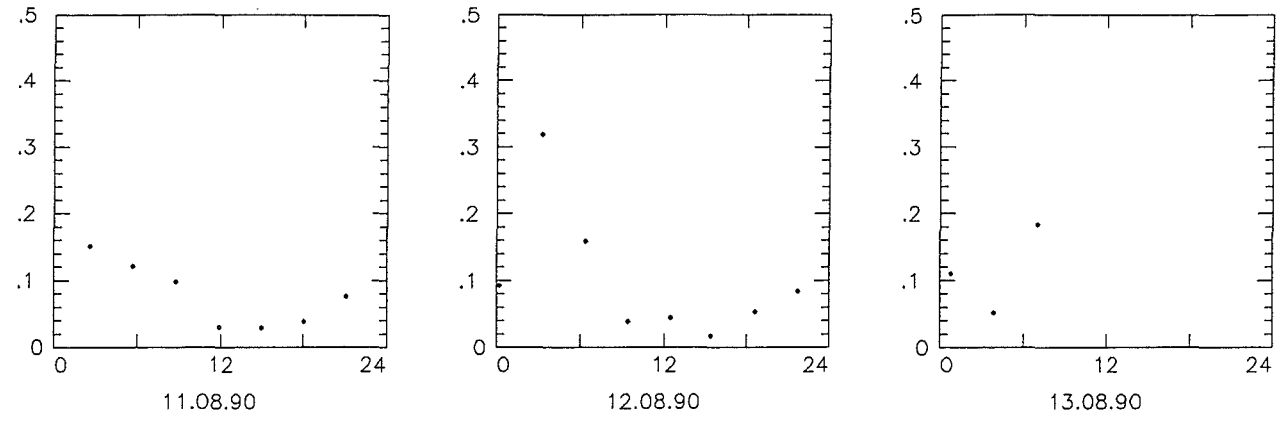

1-butene/ppb

File: 1-BUTEN ENZ90JUE

Dataset: 28

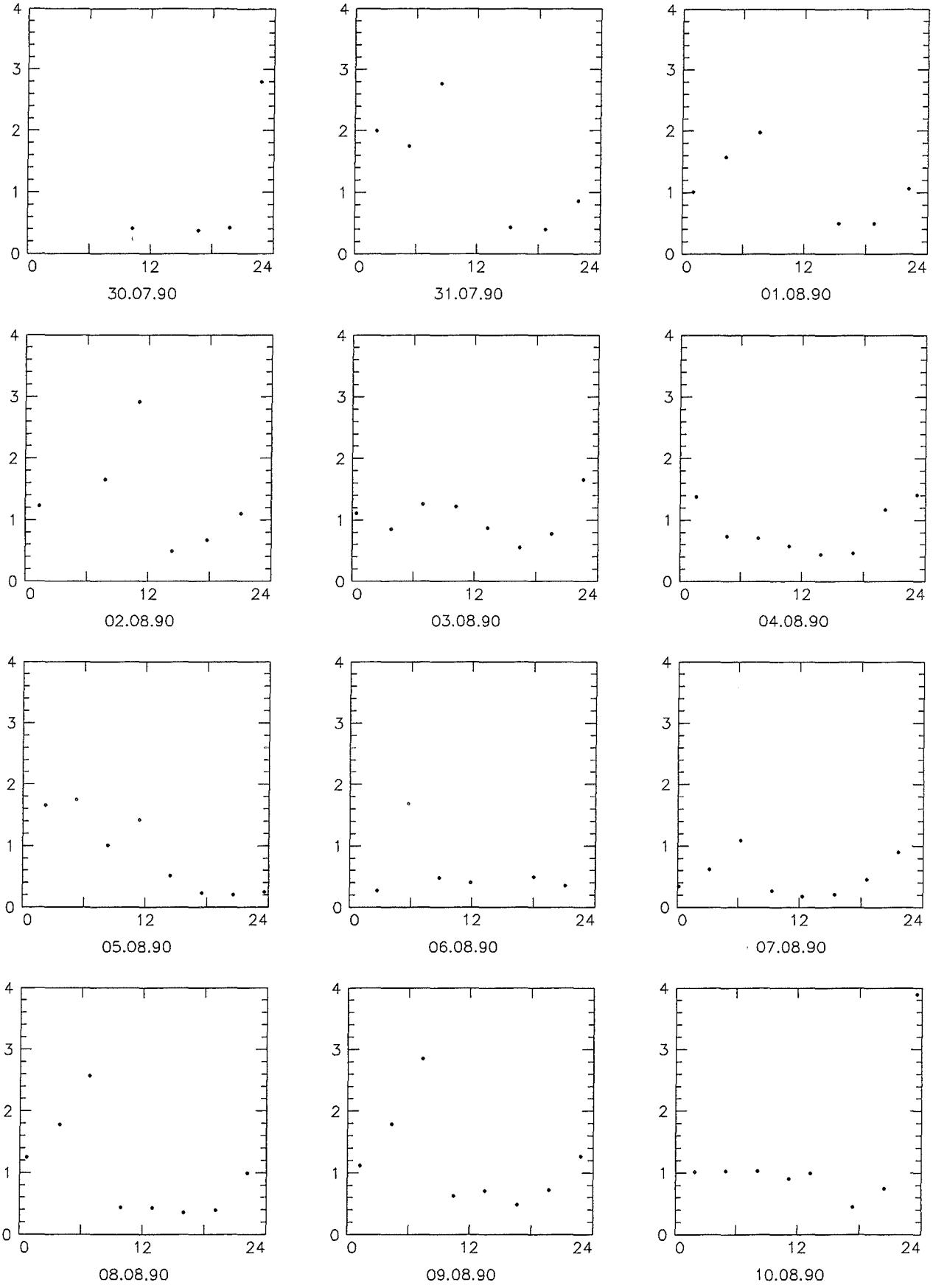

acetylene/ppb

File: ACETYLEN ENZ90JUE

Dataset: 29

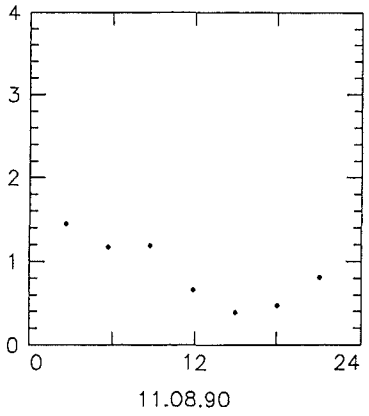

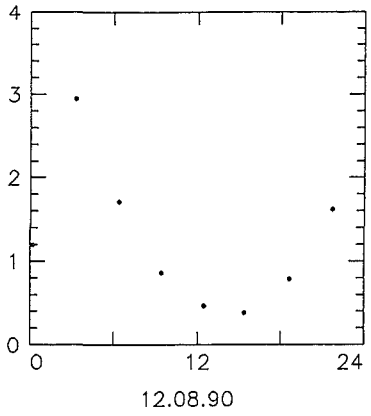

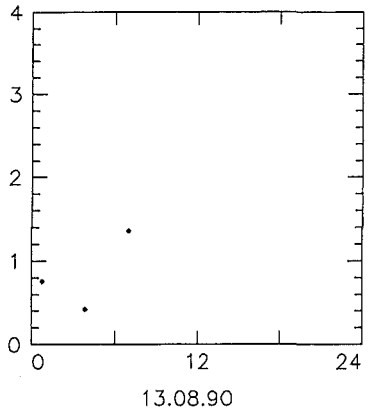

acetylene/ppb

File: ACETYLEN ENZ90JUE

Dataset: 29

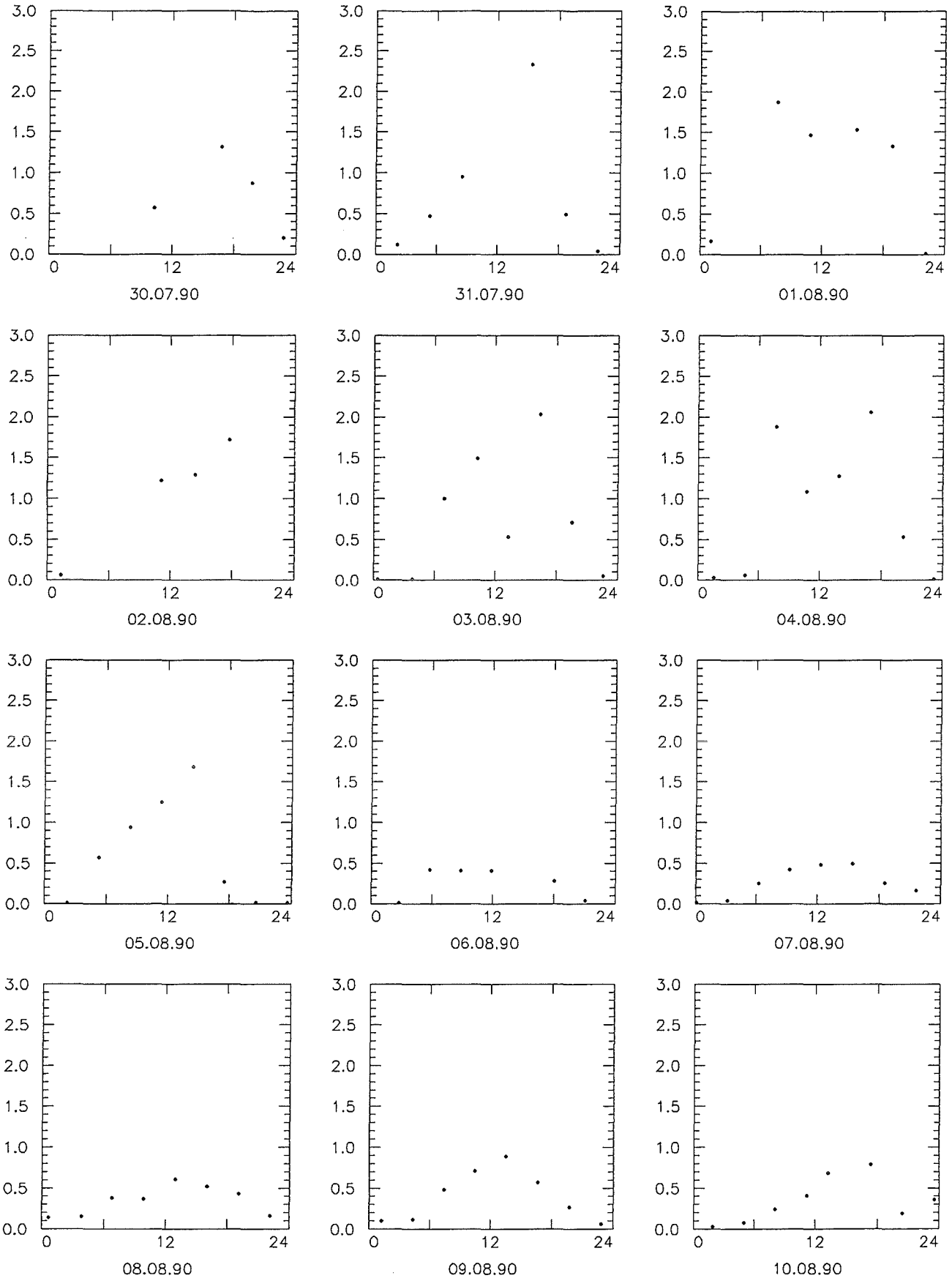

isoprene/ppb

File: ISOPREN ENZ90JUE

Dataset: 30

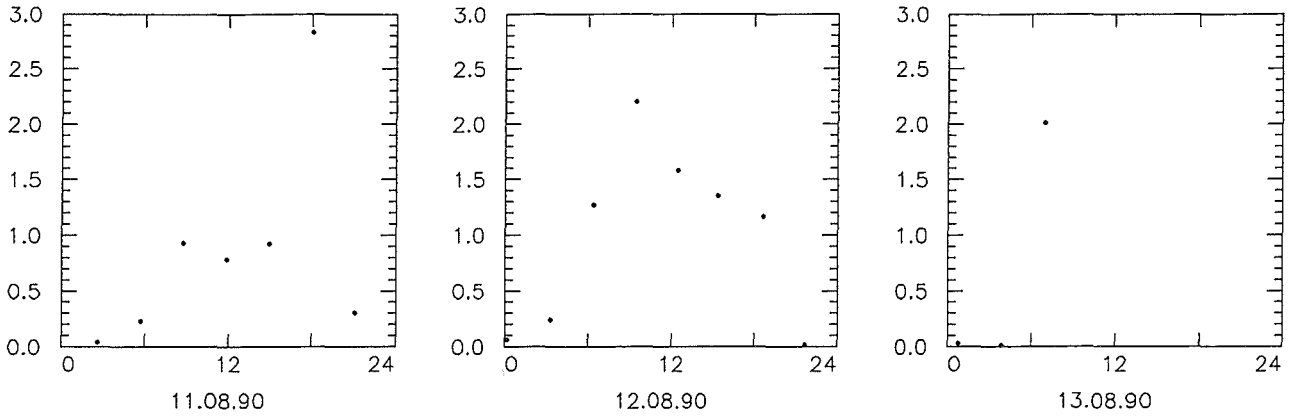

isoprene/ppb

File: ISOPREN ENZ90JUE

Dataset: 30

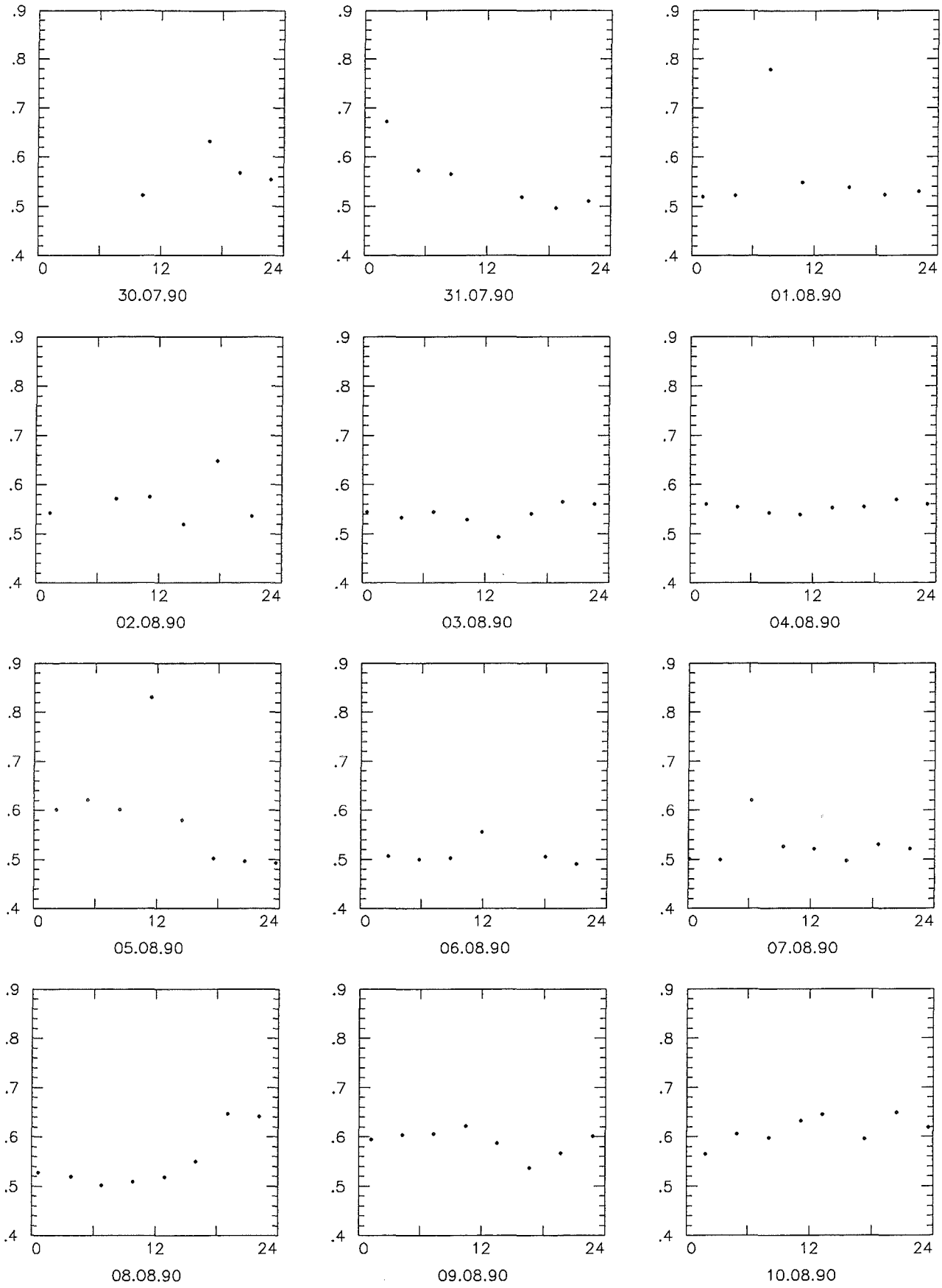

CH_3Cl/ppb

File: CH3CL ENZ90JUE

Dataset: 31

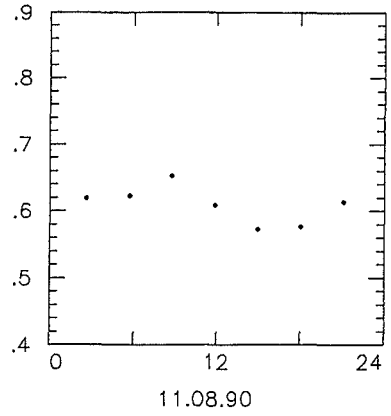

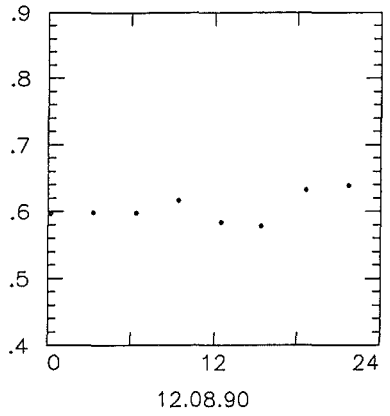

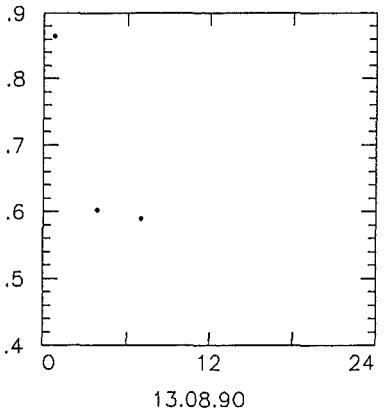

CH_3Cl/ppb

File: CH3CL ENZ90JUE

Dataset: 31

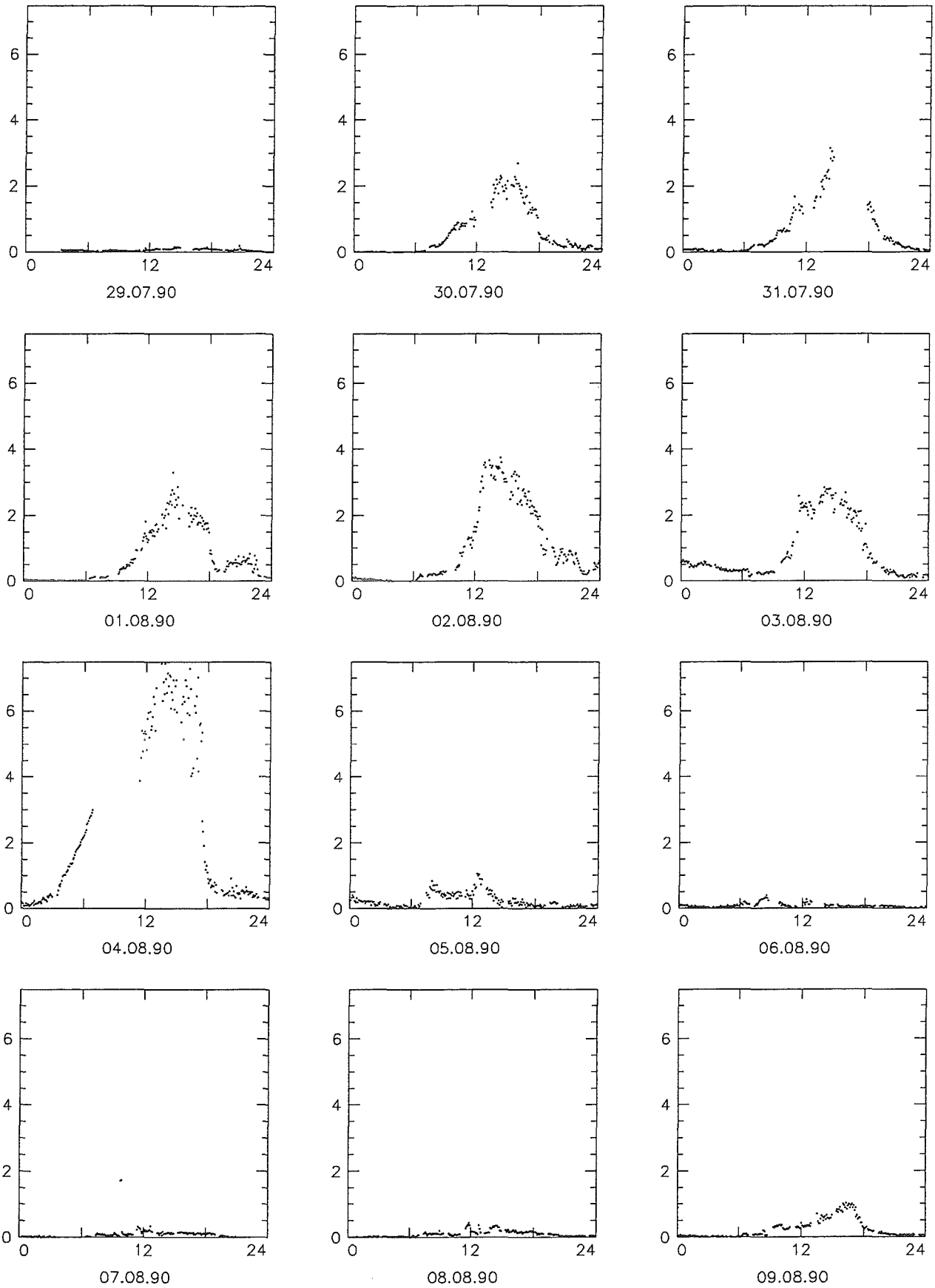

ROOH/ppb

File: ROOH ENZ90JUE

Dataset: 32

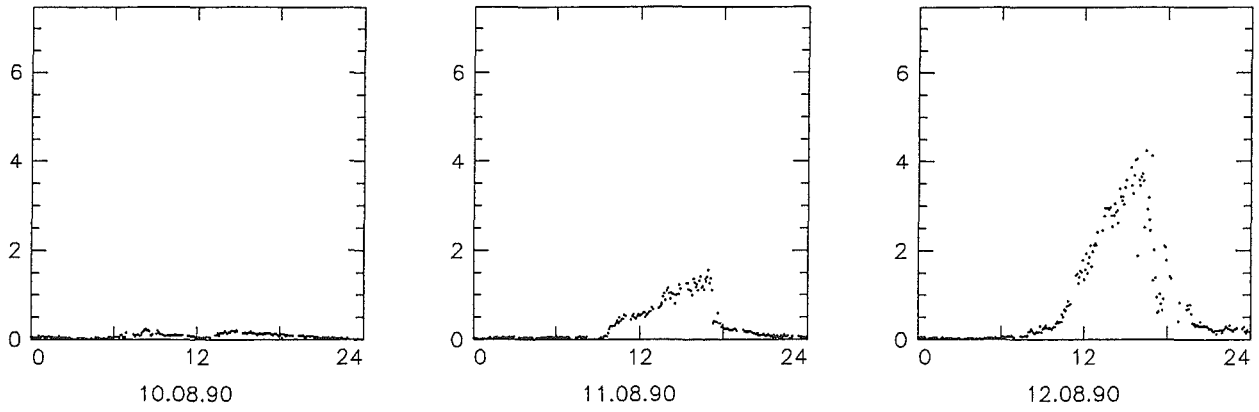

ROOH/ppb

File: ROOH ENZ90JUE

Dataset: 32

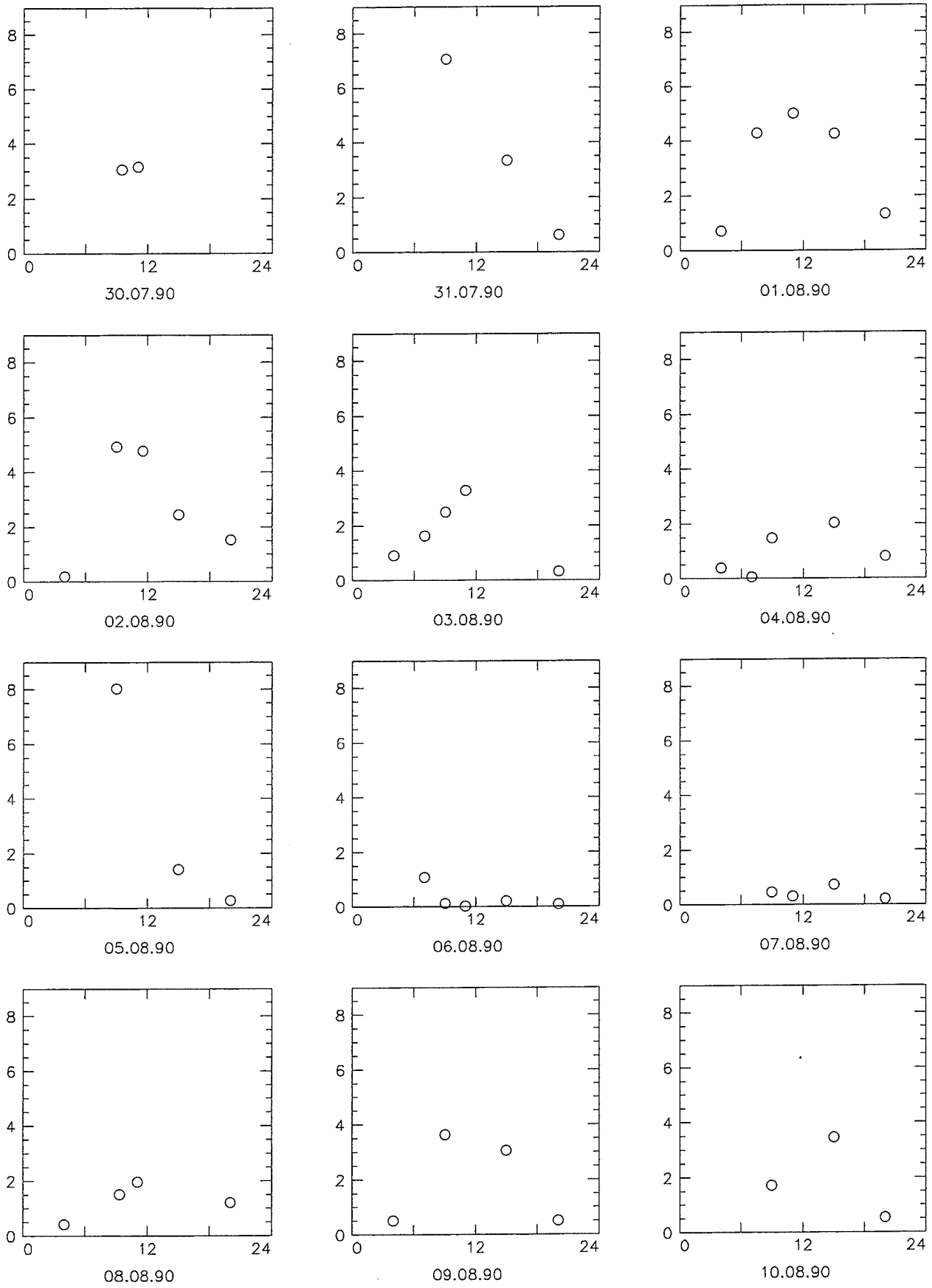

HNO_3/ppb

File: HNO3 ENZ90JUE

Dataset: 33

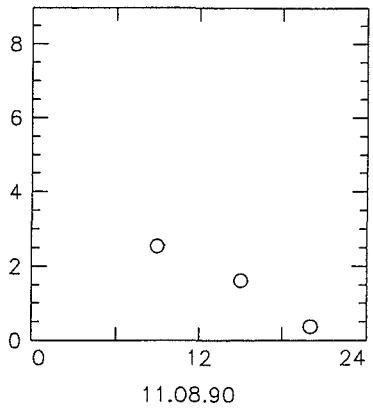

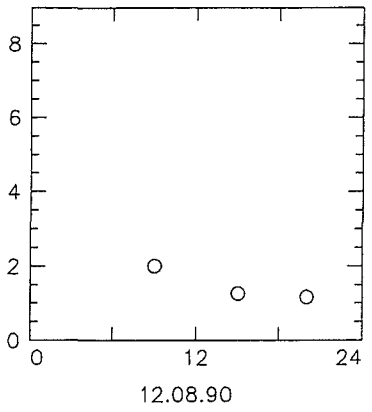

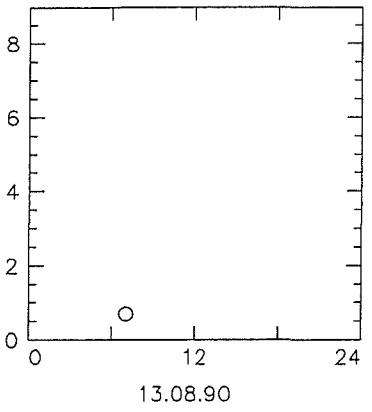

HNO_3/ppb

File: HNO3 ENZ90JUE

Dataset: 33

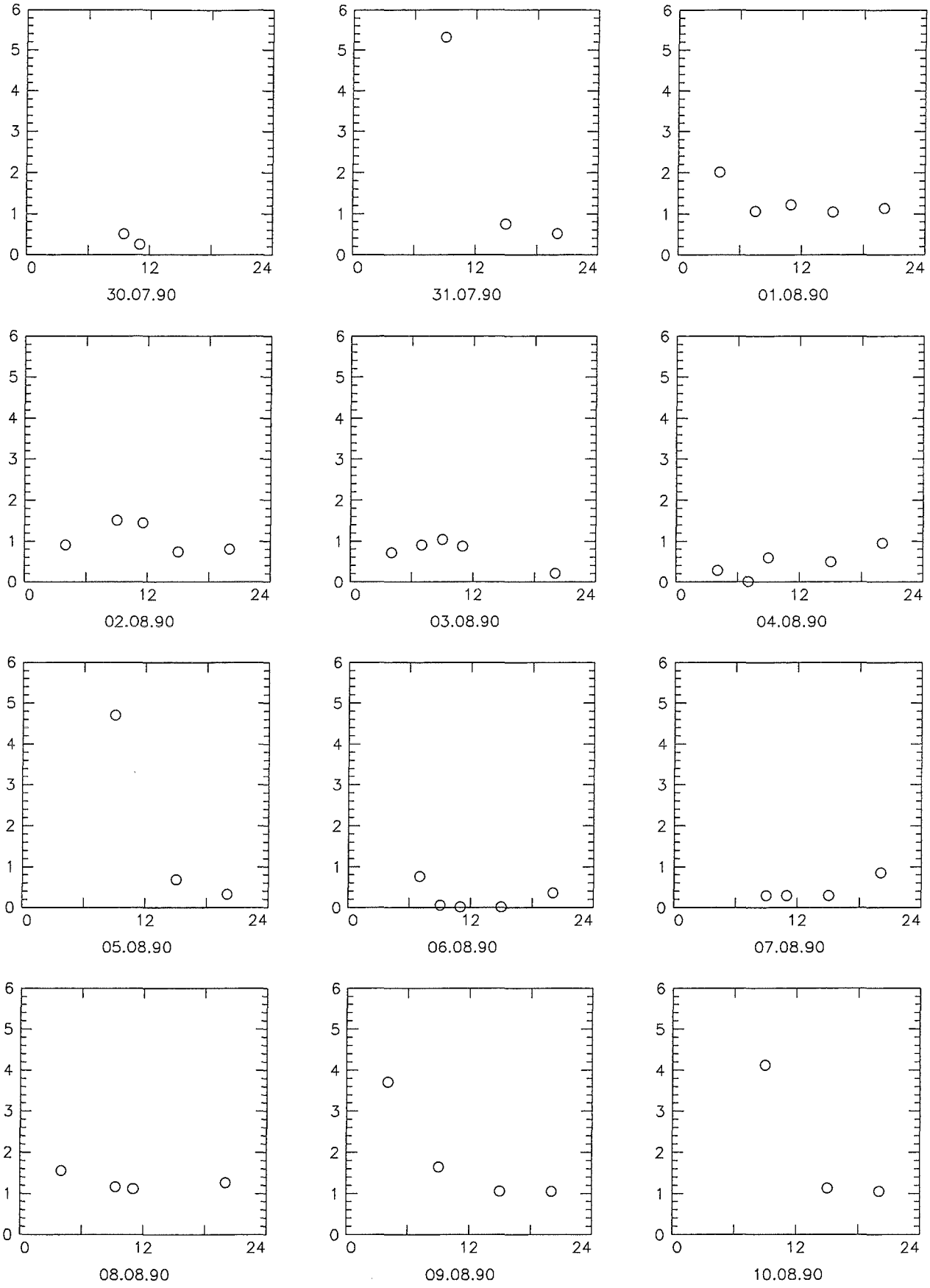

total nitrate / ppbm

File: NITRAT ENZ90JUE

Dataset: 34

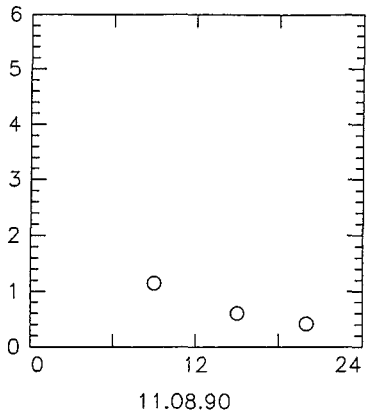

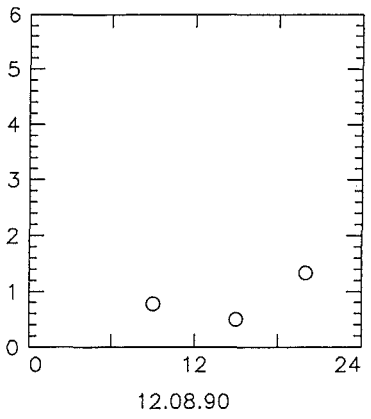

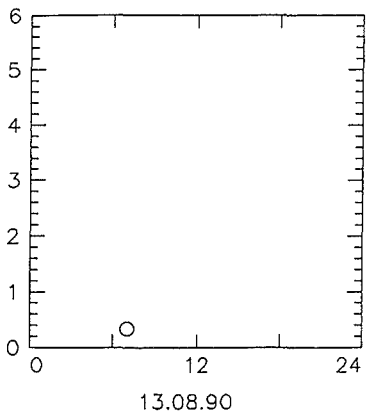

total nitrate / ppbm

File: NITRAT ENZ90JUE

Dataset: 34

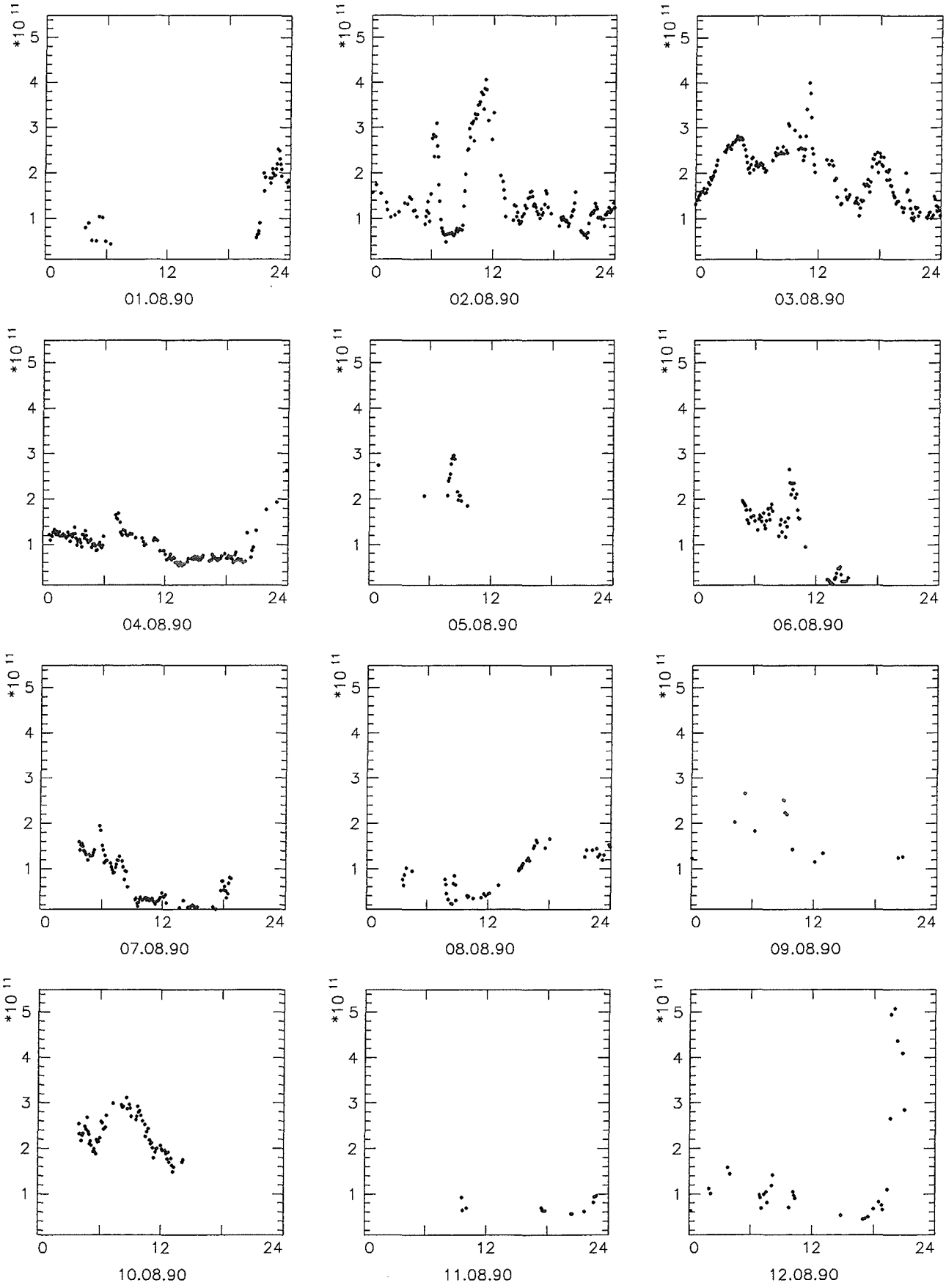

SO_2/cm^{-3}

File: ALLDOASJ ZUS90JUY

Dataset: 35

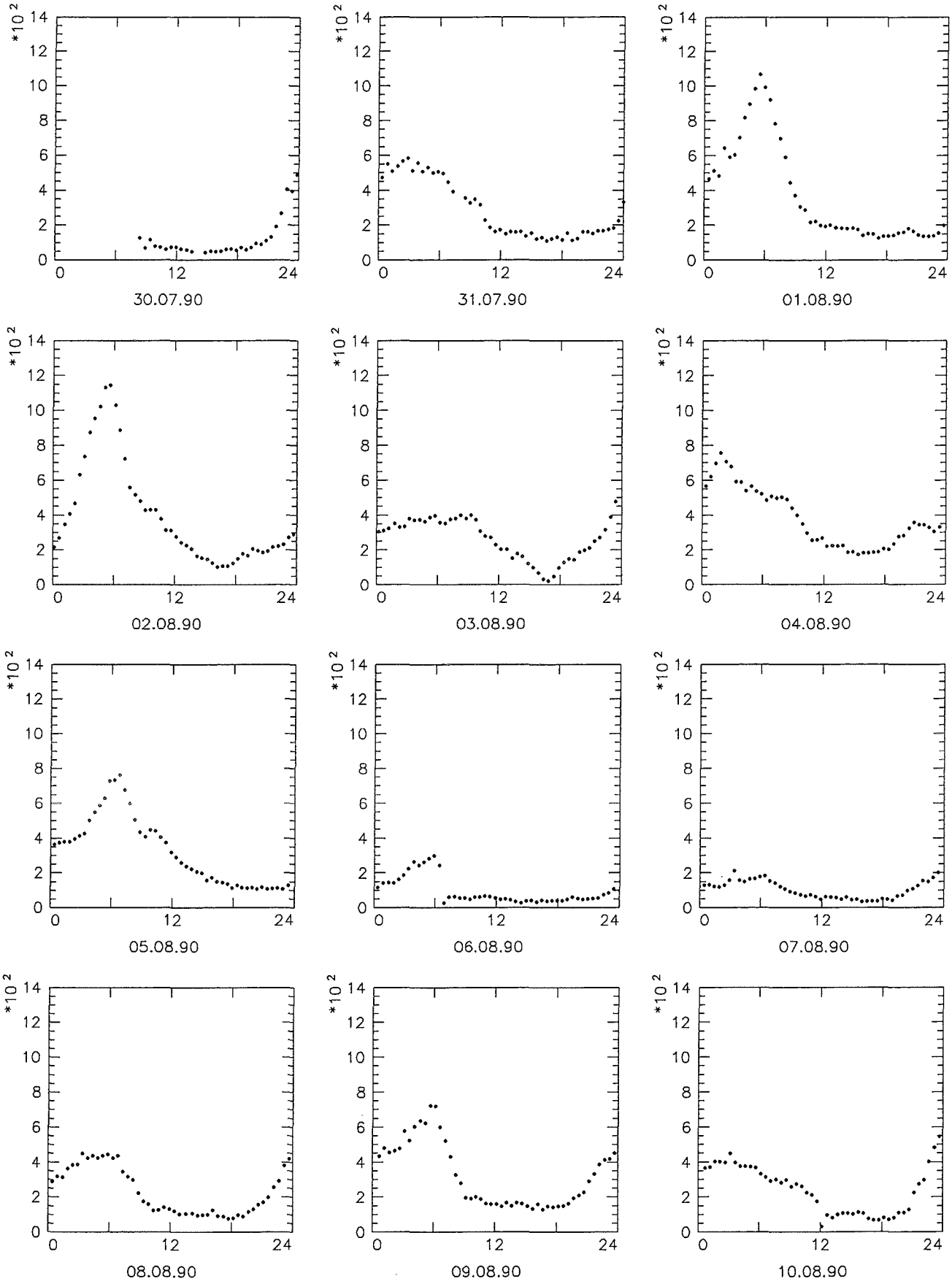

Rn/a.u.

File: RADONNEW ENZ90JUE

Dataset: 36

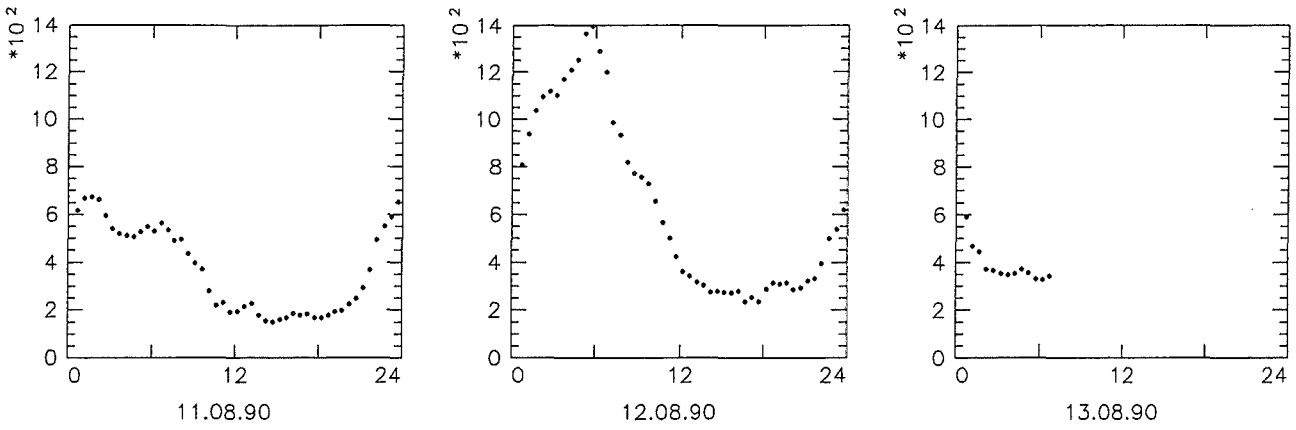

Rn/a.u.

File: RADONNEW ENZ90JUE

Dataset: 36

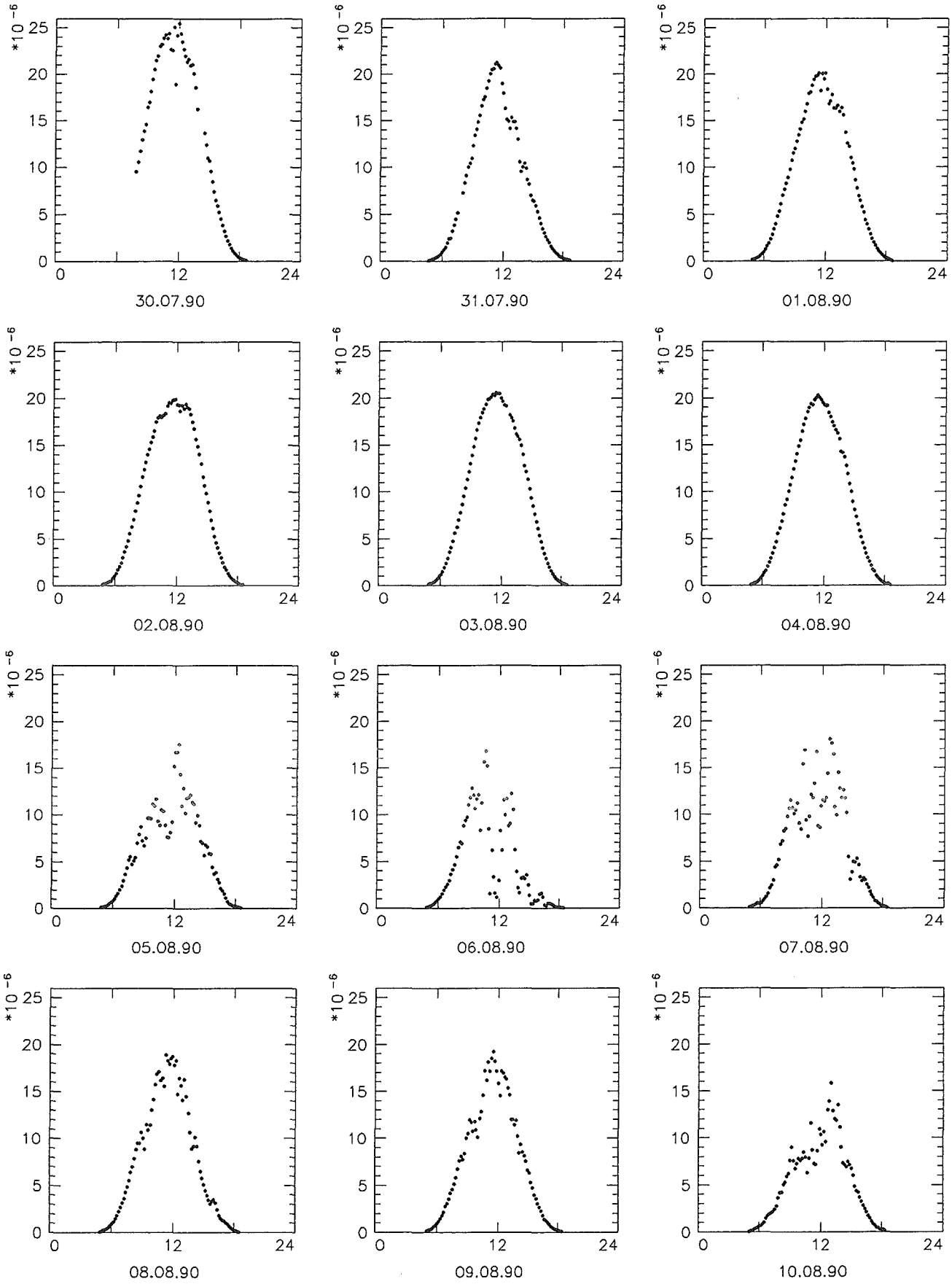

J(O¹D) / s⁻¹ (detector 5)

File: J01D_J00 ENZ90JUE

Dataset: 37

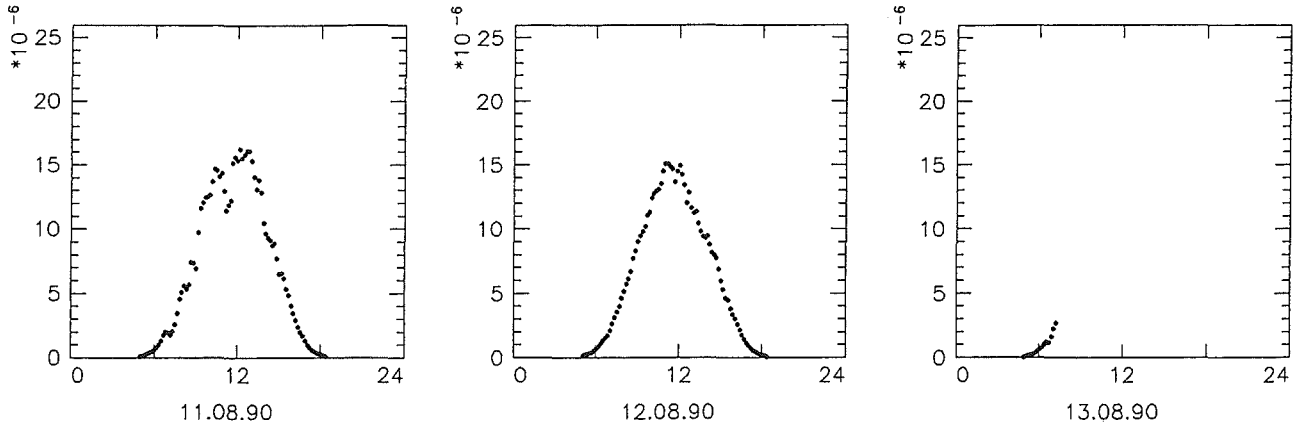

$J(O^1D)$ / s^{-1} *(detector 5)*

File: J01D_J00 ENZ90JUE

Dataset: 37

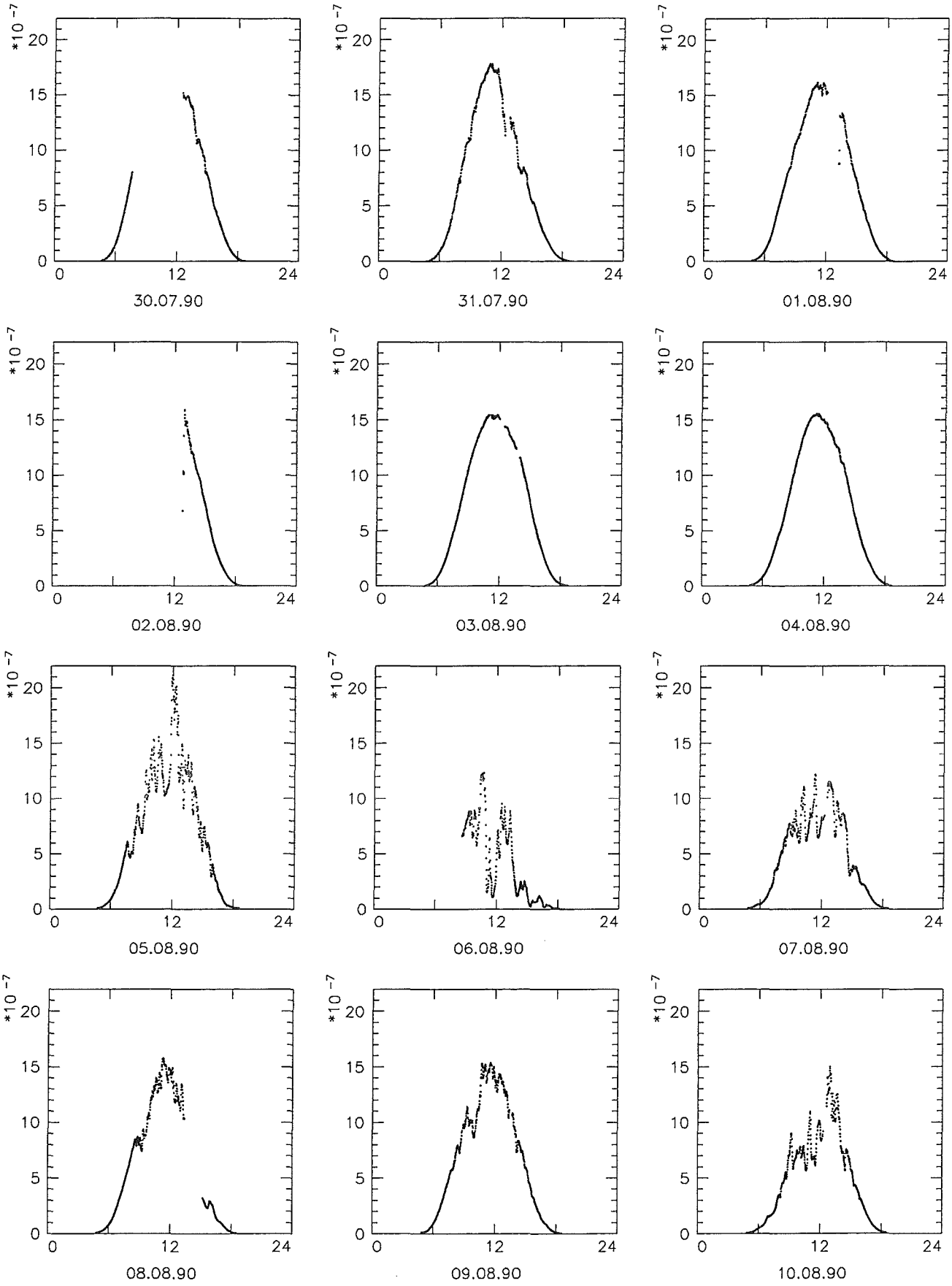

$J(O^1D)$ / s^{-1} (detector 7)

File: J01D_J01 ENZ90JUE

Dataset: 38

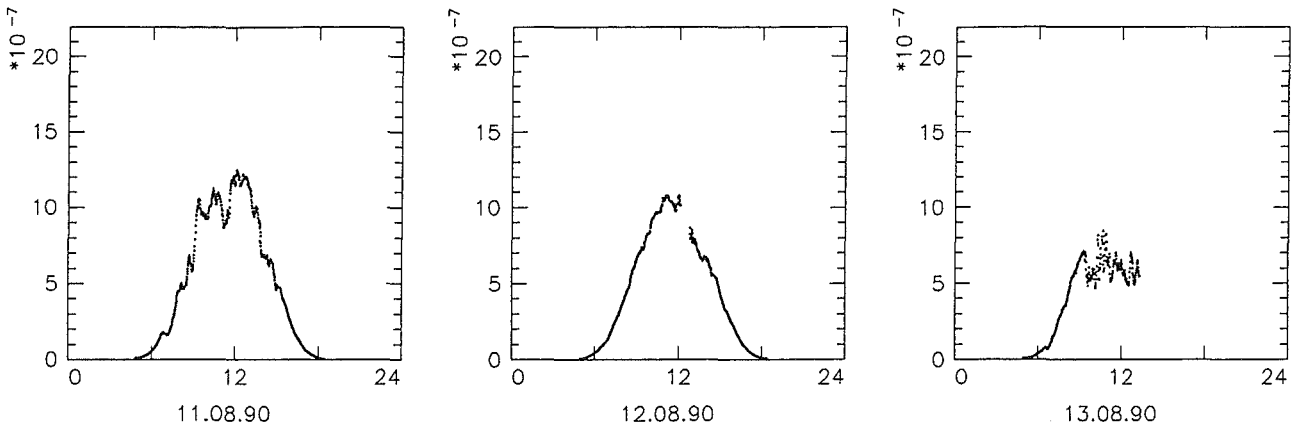

$J(O^1D)$ / s^{-1} (detector 7)

File: J01D_J01 ENZ90JUE

Dataset: 38

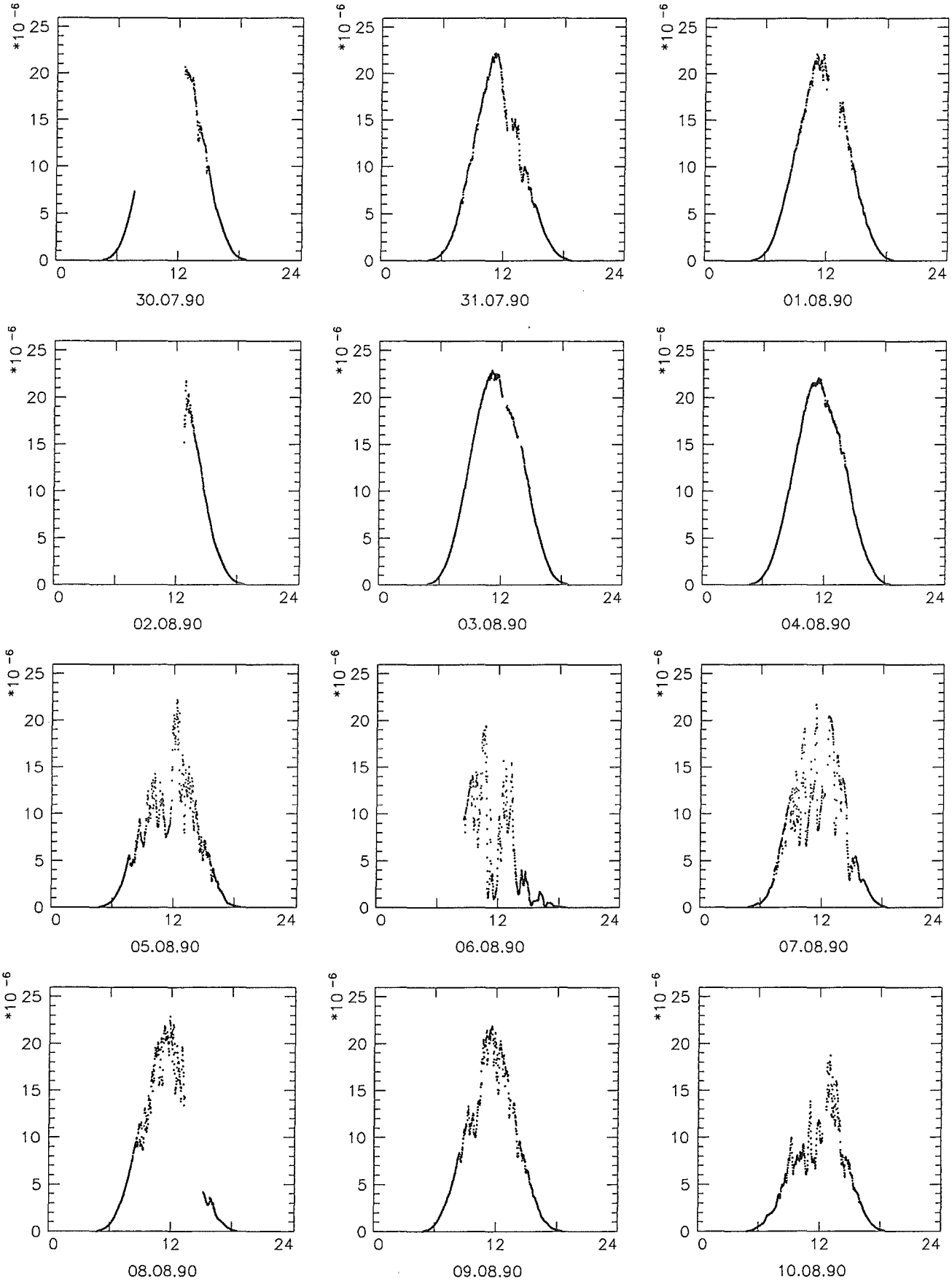

J(O^{1}D) / s^{-1} (detector 8)

File: J01D_J02 ENZ90JUE

Dataset: 39

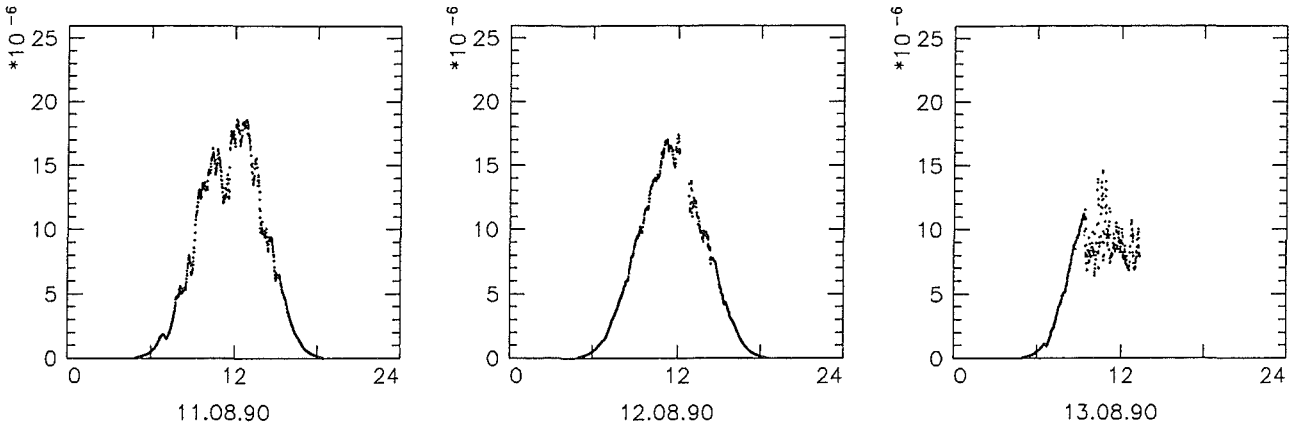

$J(O^1D)$ / s^{-1} (detector 8)

File: J01D_J02 ENZ90JUE

Dataset: 39

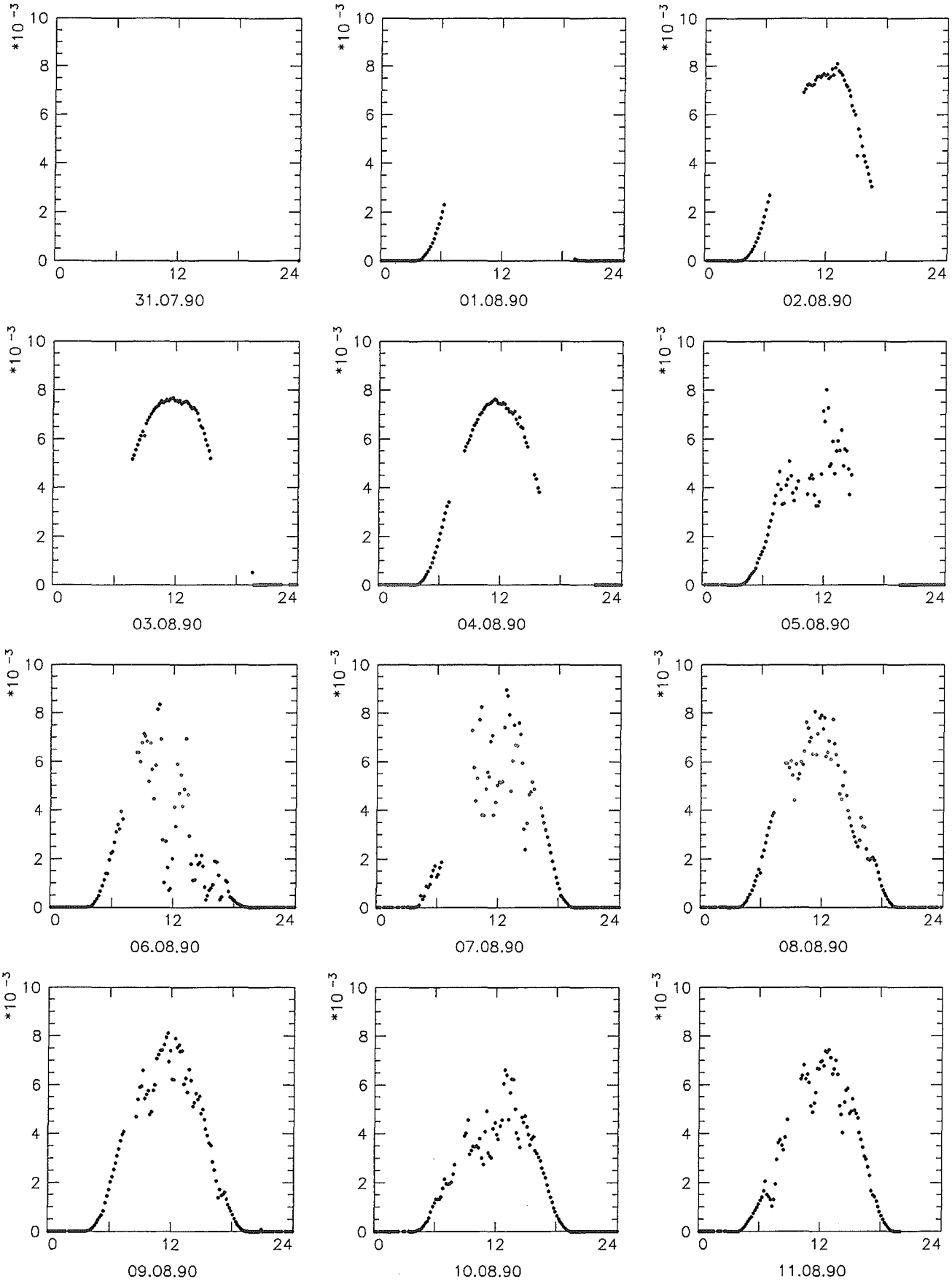

$J(NO_2)/s^{-1}$

File: JNO2RNEW ENZ90JUE

Dataset: 40

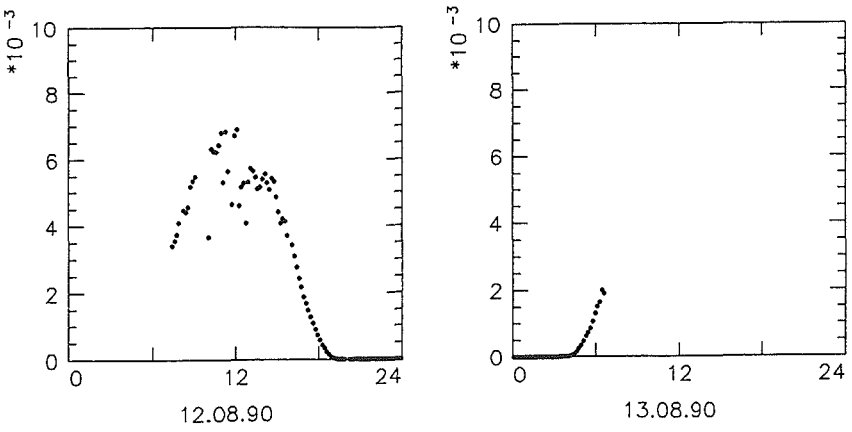

$J(NO_2)/s^{-1}$

File: JNO2RNEW ENZ90JUE

Dataset: 40

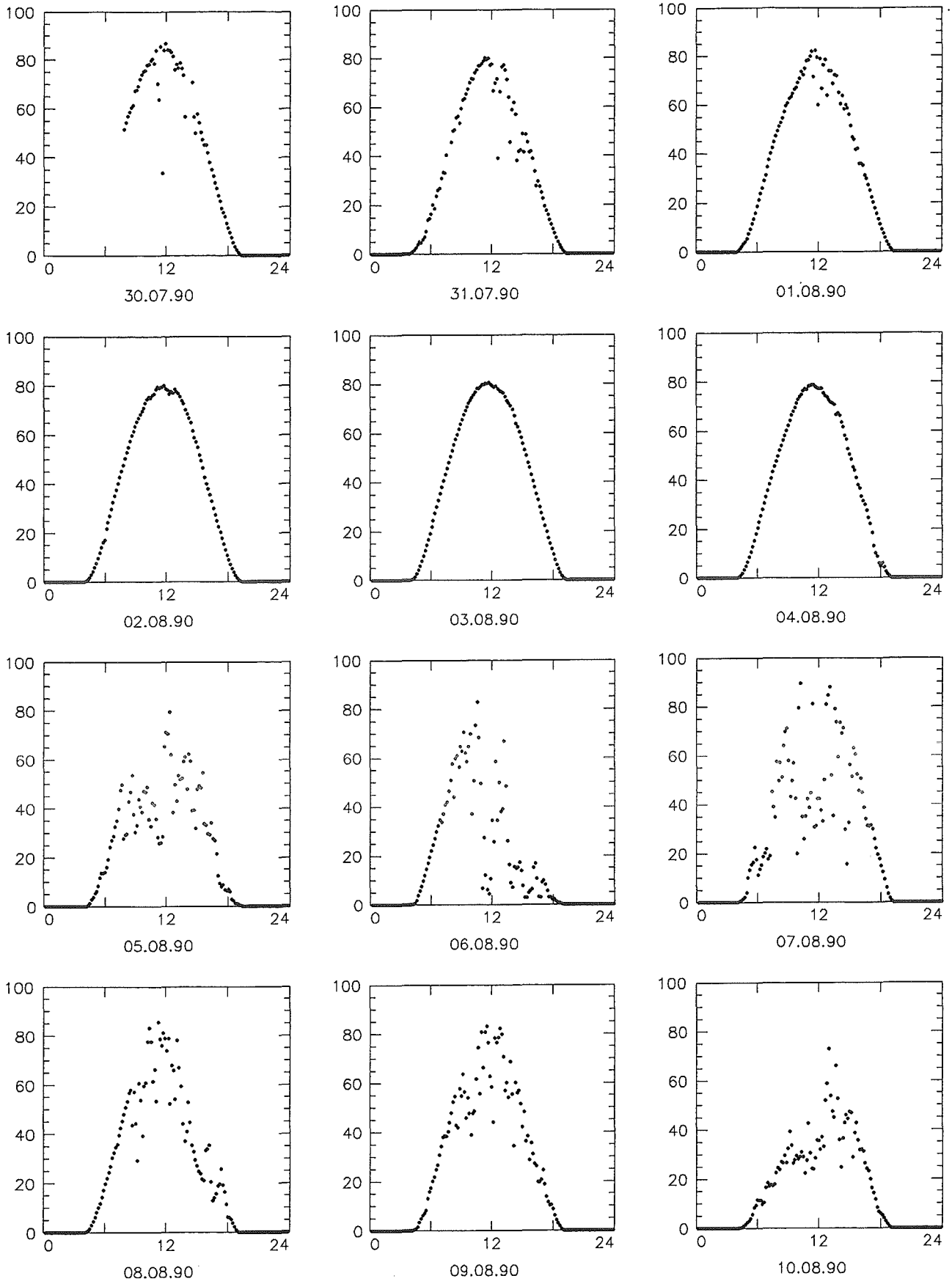

total radiation / mW cm^{-2}

File: GSTR_NEW ENZ90JUE

Dataset: 41

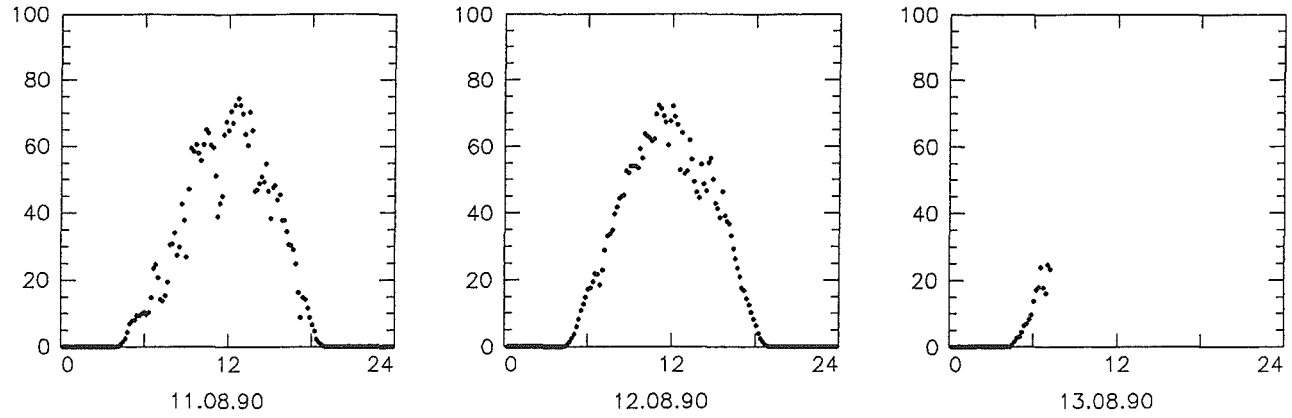

total radiation / mW cm^{-2}

File: GSTR_NEW ENZ90JUE

Dataset: 41

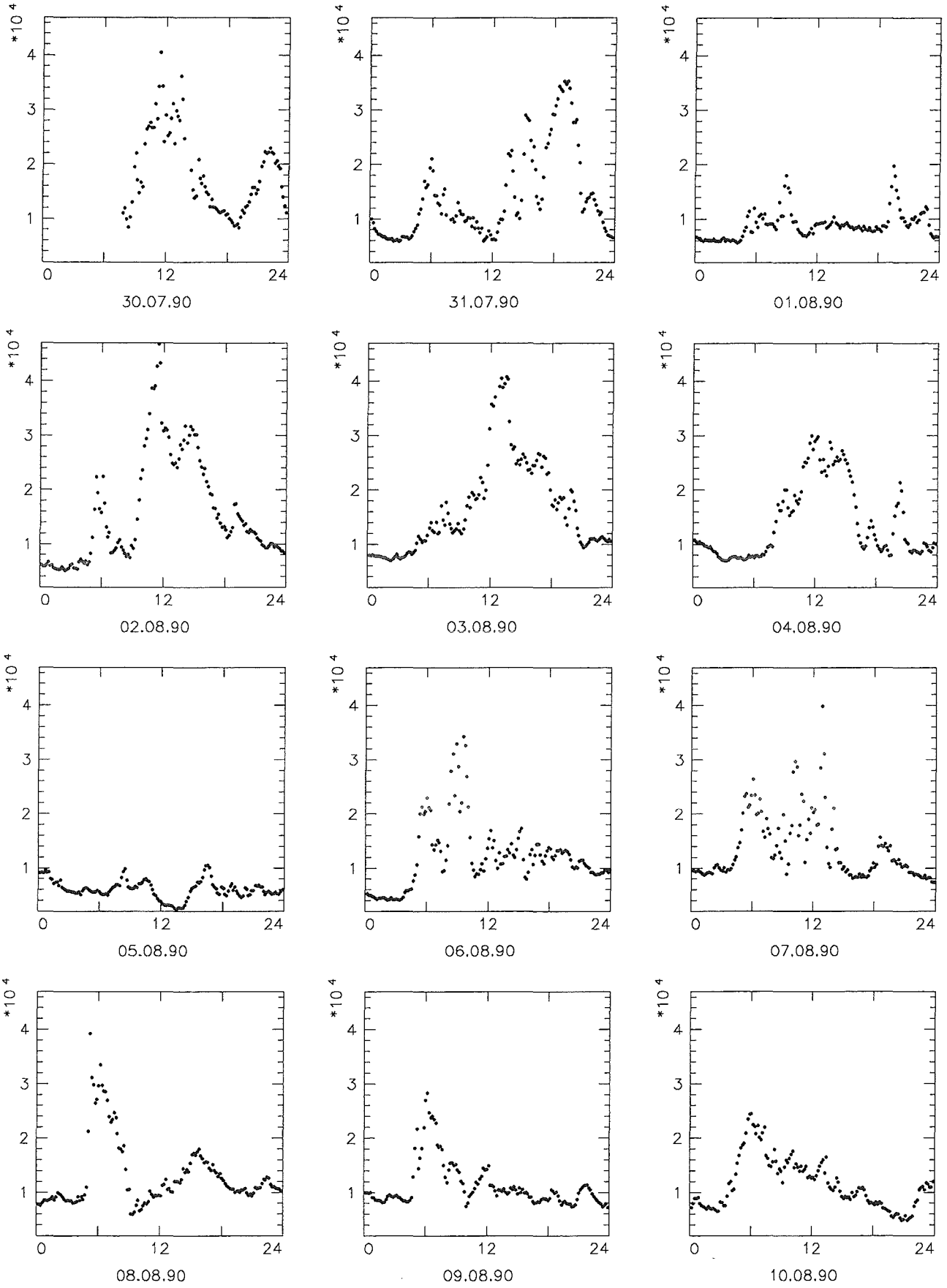

CN/cm^{-3}

File: CONDNNEW ENZ90JUE

Dataset: 42

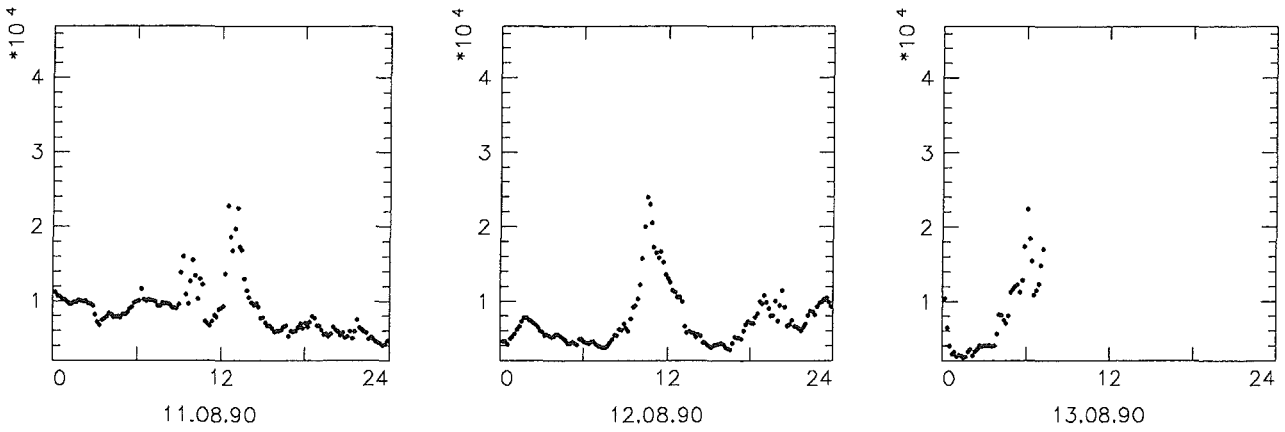

CN/cm^{-3}

File: CONDNNEW ENZ90JUE

Dataset: 42

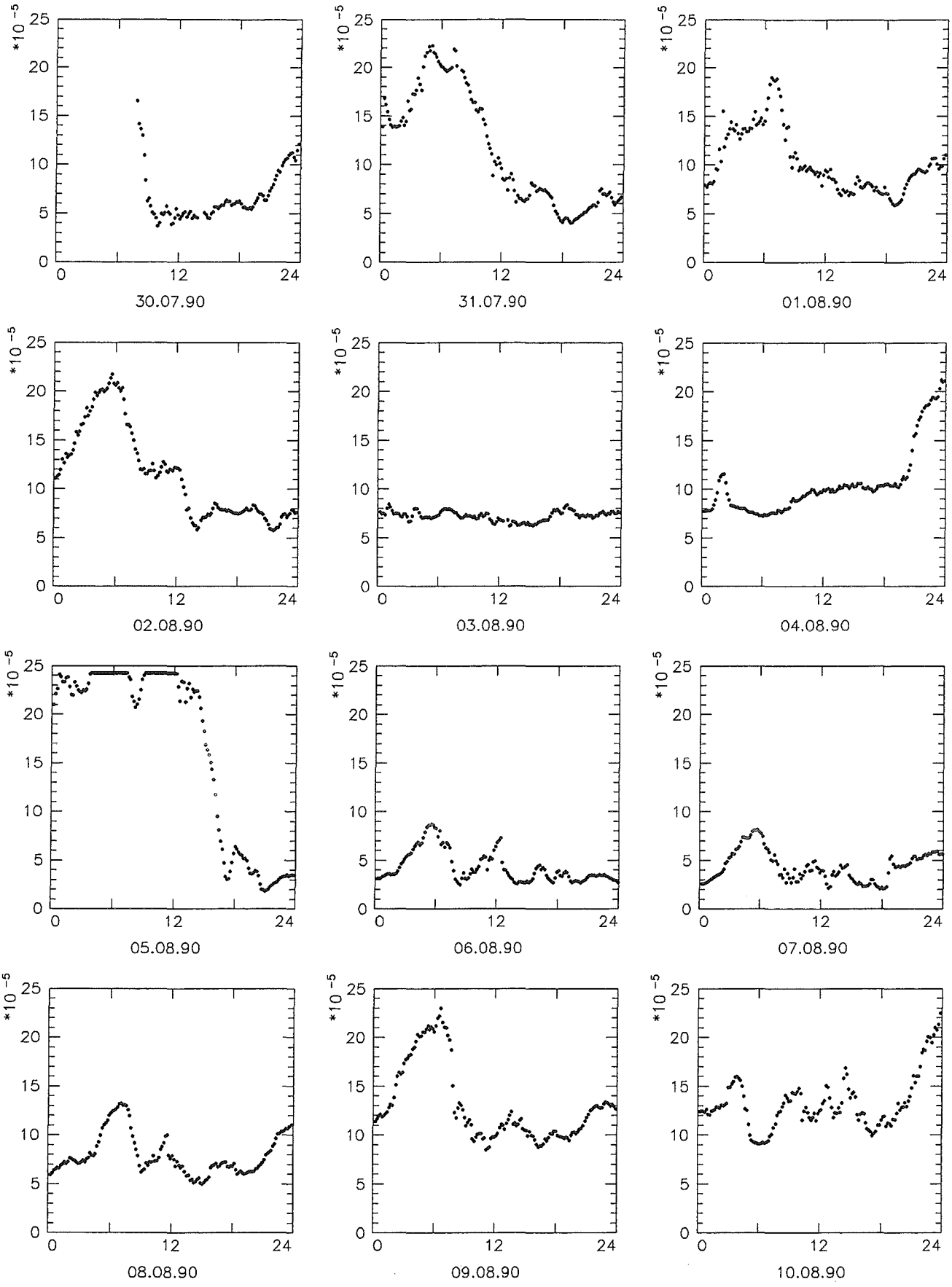

β / m^{-1}

File: NEPH2NEW ENZ90JUE

Dataset: 43

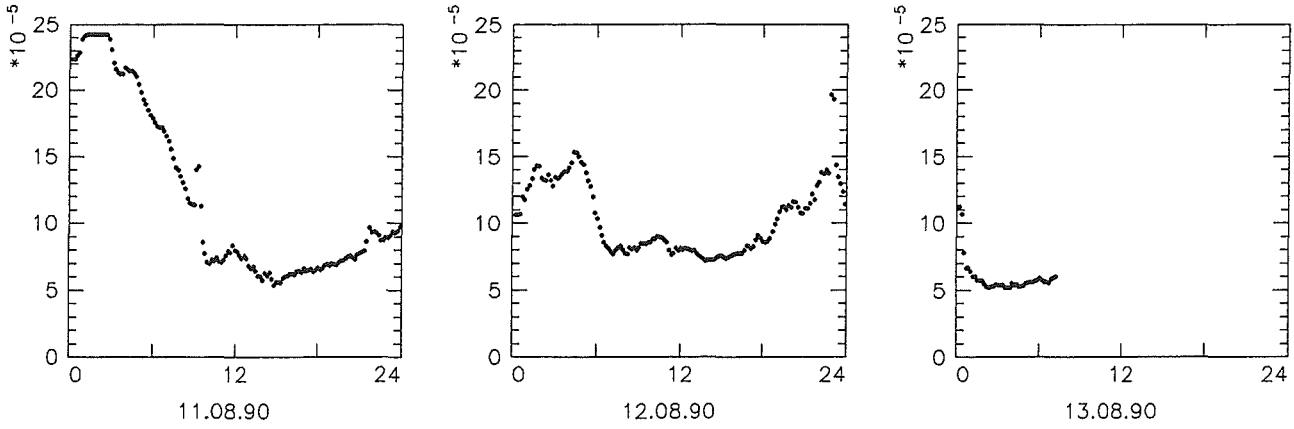

β/m^{-1}

File: NEPH2NEW ENZ90JUE

Dataset: 43

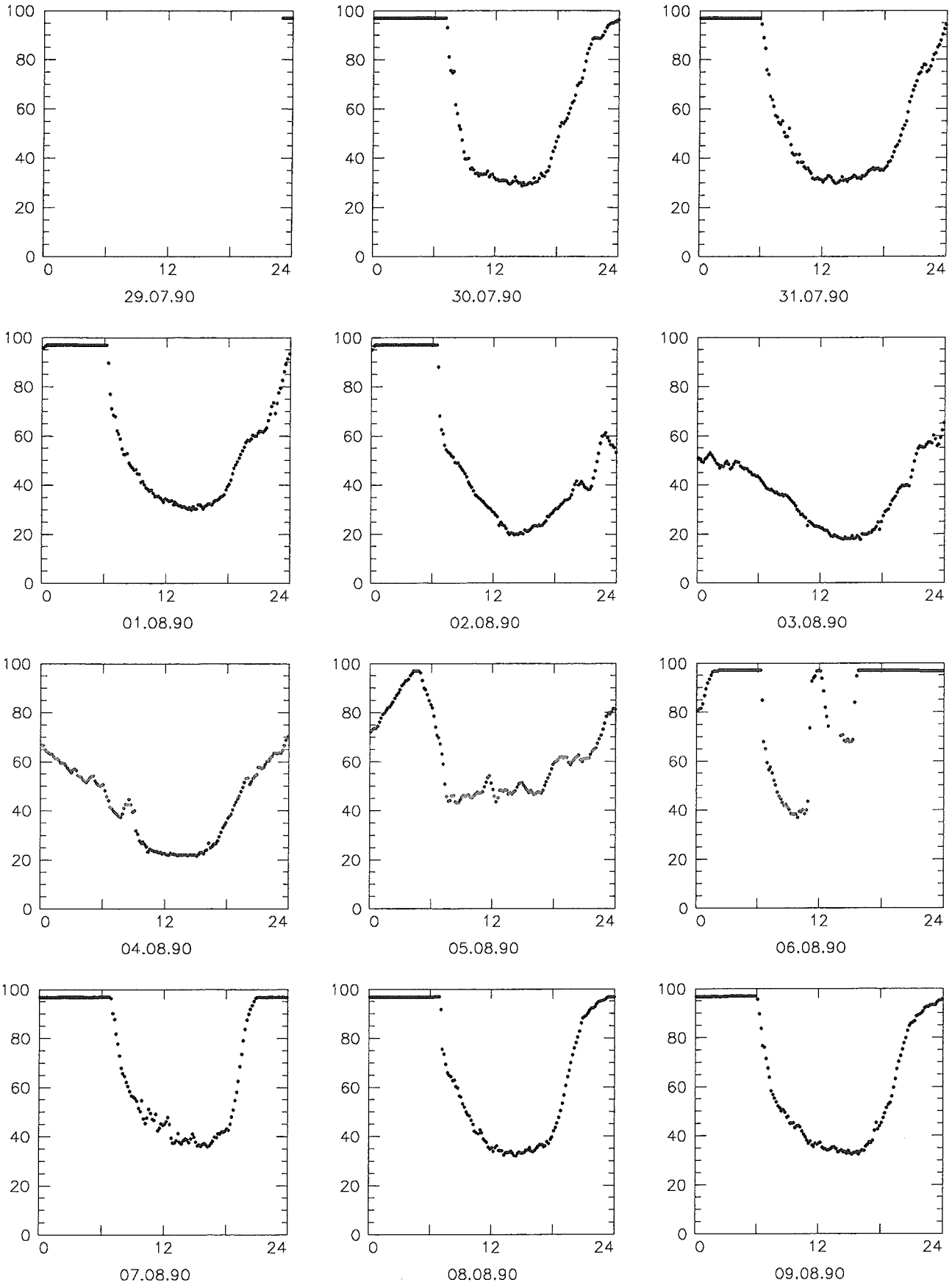

relative humidity / %

File: RF__2 ENZ90JUE

Dataset: 44

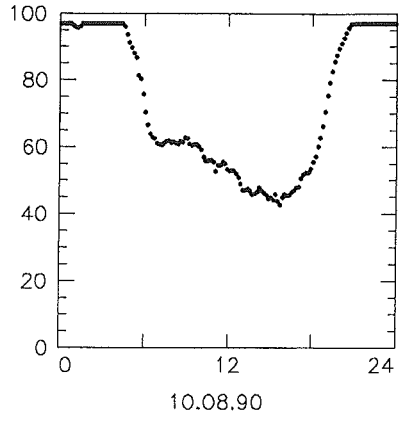

10.08.90

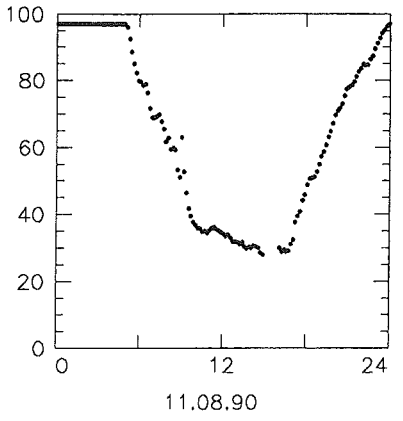

11.08.90

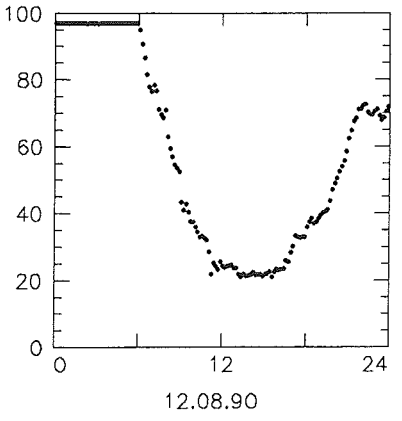

12.08.90

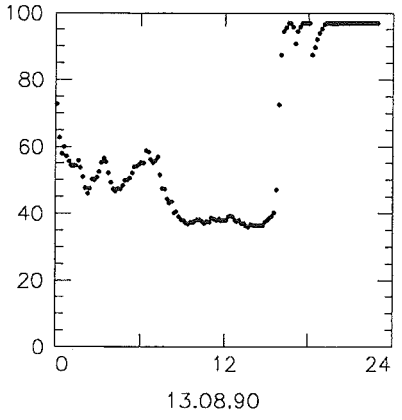

13.08.90

relative humidity / %

File: RF__2 ENZ90JUE

Dataset: 44

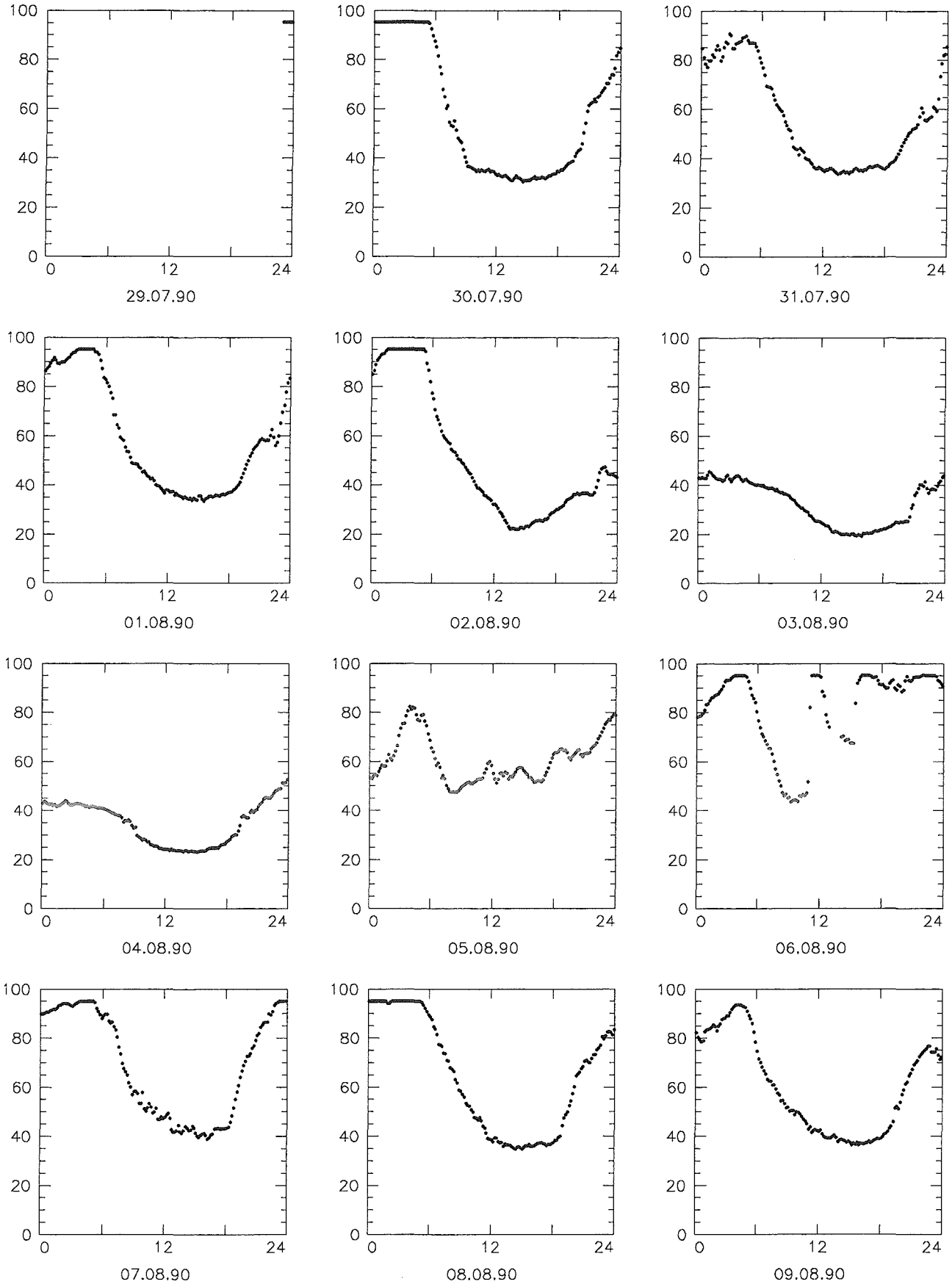

relative humidity / %

File: RF_20 ENZ90JUE

Dataset: 45

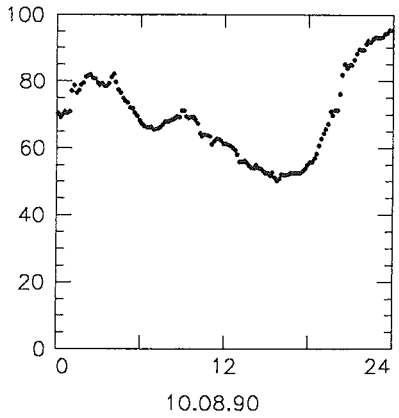

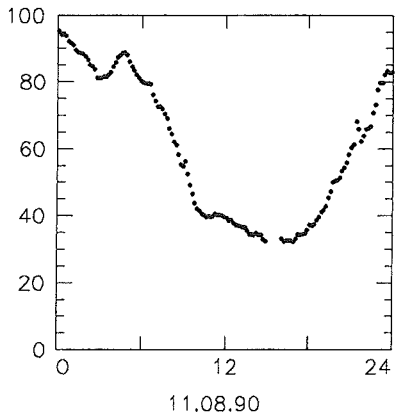

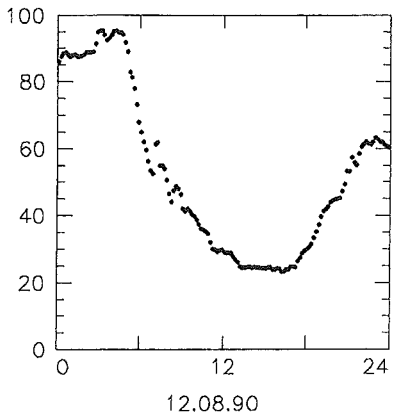

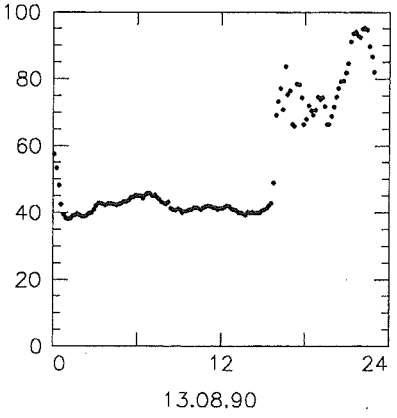

relative humidity / %

File: RF_20 ENZ90JUE

Dataset: 45

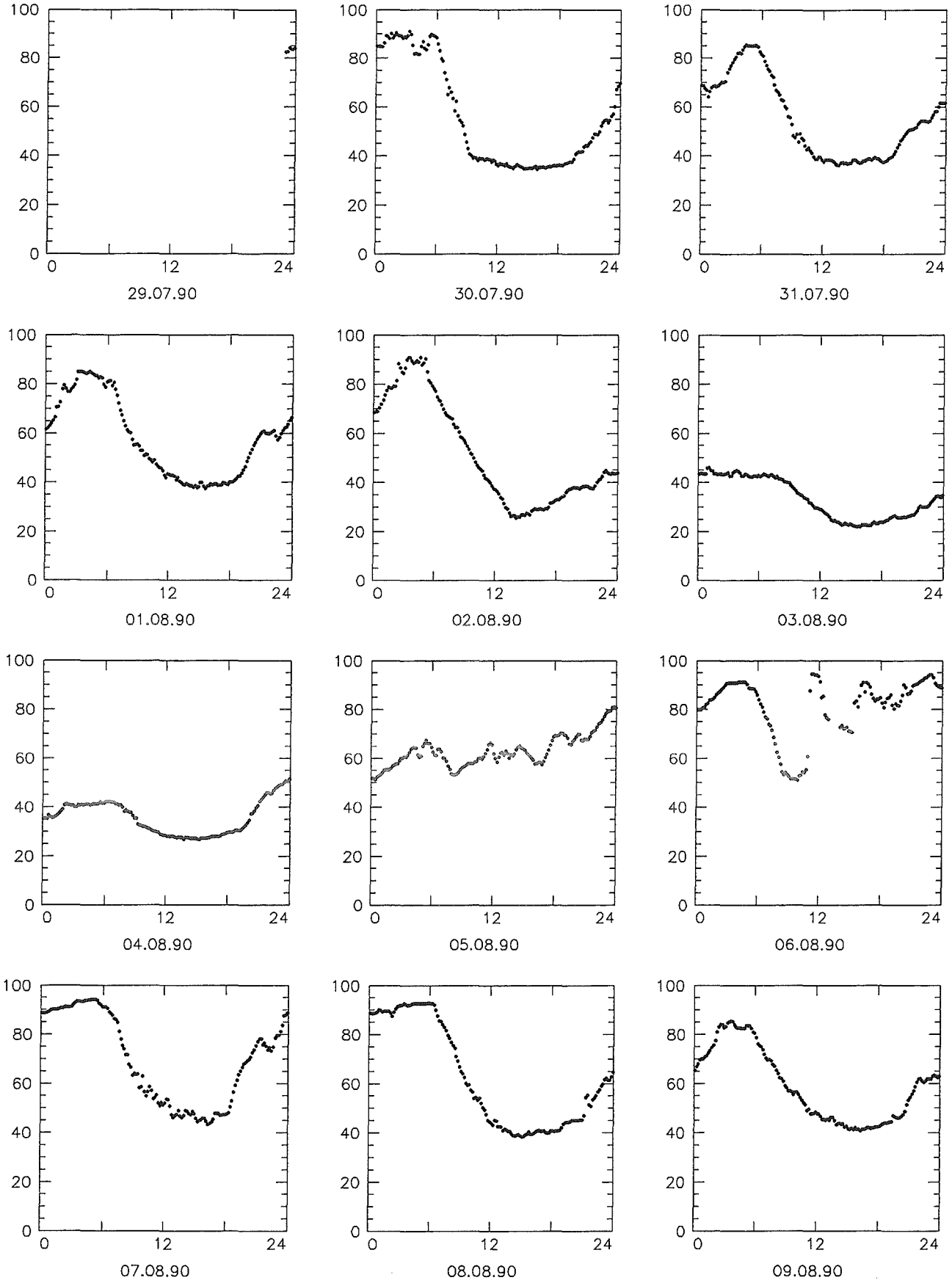

relative humidity / %

File: RF_50 ENZ90JUE

Dataset: 46

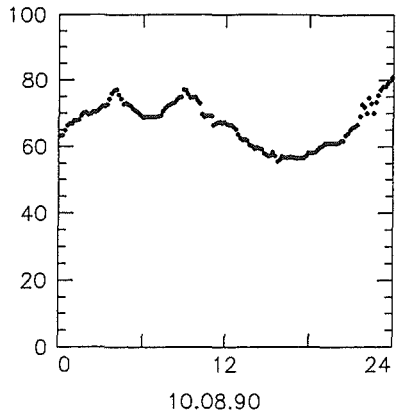

10.08.90

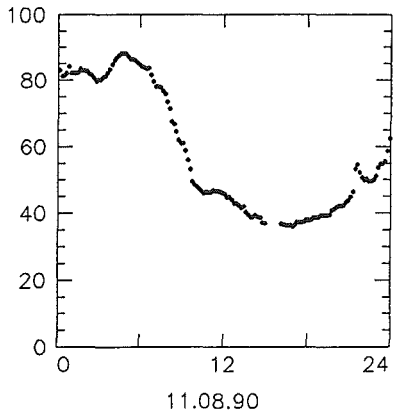

11.08.90

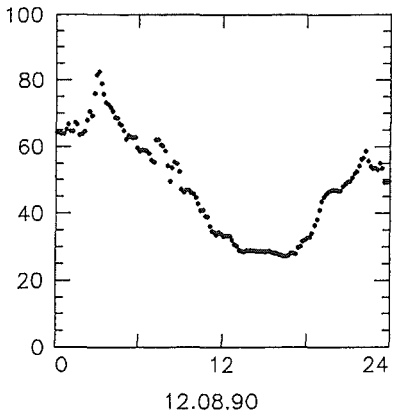

12.08.90

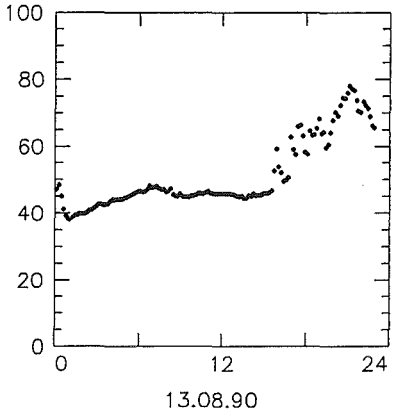

13.08.90

relative humidity / %

File: RF_50 ENZ90JUE

Dataset: 46

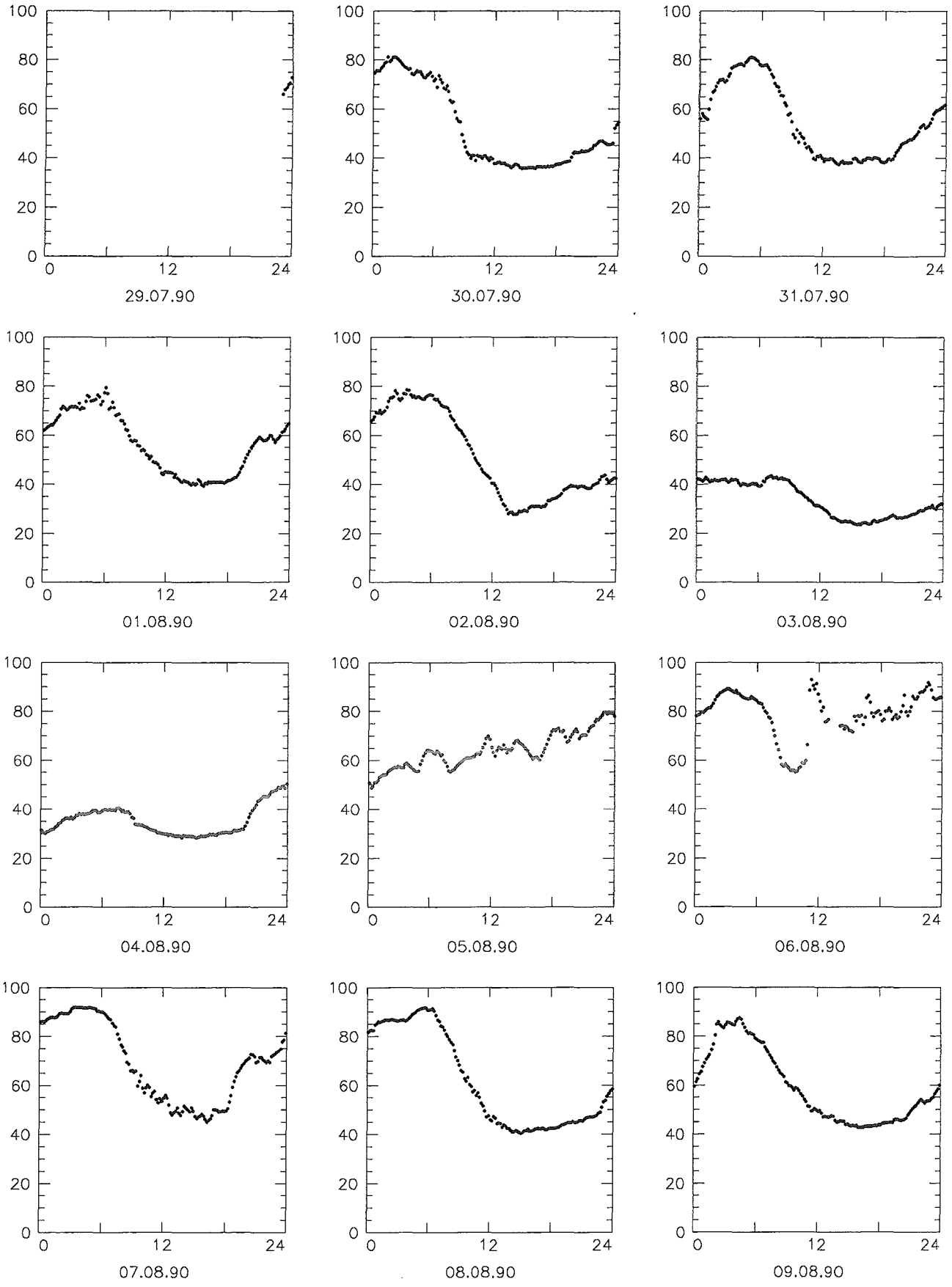

relative humidity / %

File: RF100 ENZ90JUE

Dataset: 47

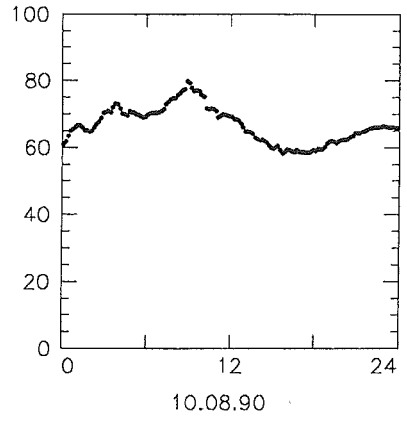

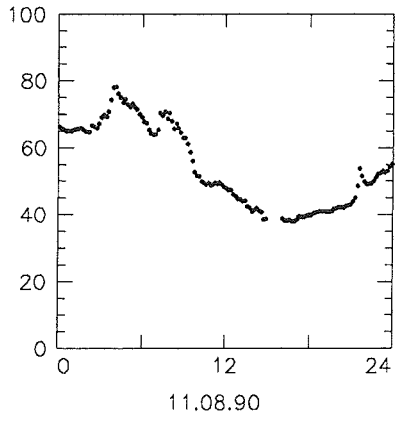

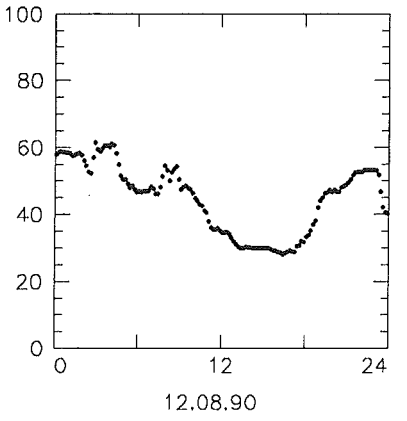

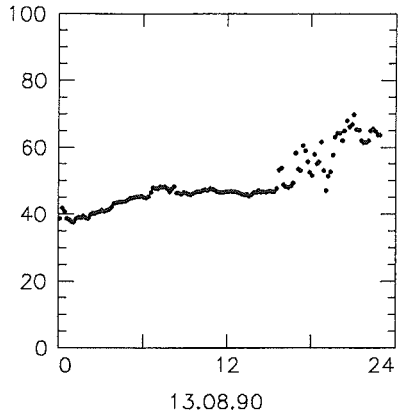

relative humidity / %

File: RF100 ENZ90JUE

Dataset: 47

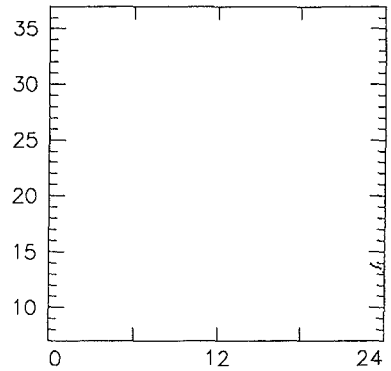

29.07.90

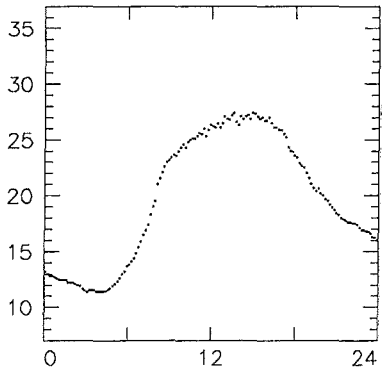

30.07.90

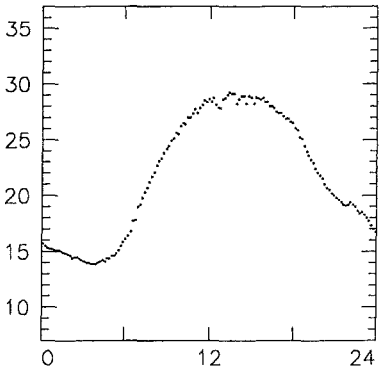

31.07.90

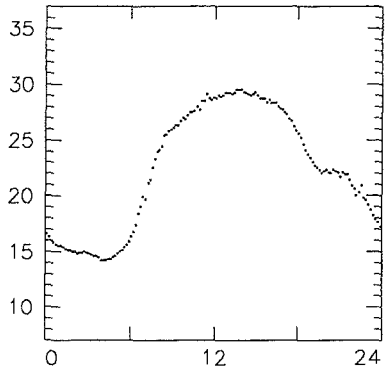

01.08.90

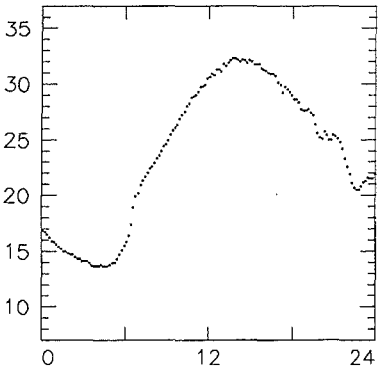

02.08.90

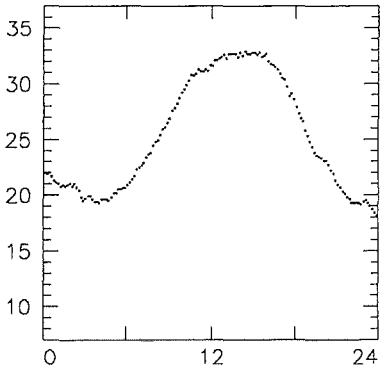

03.08.90

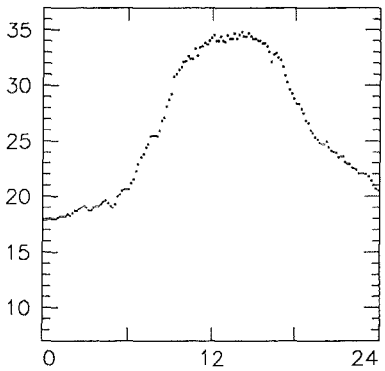

04.08.90

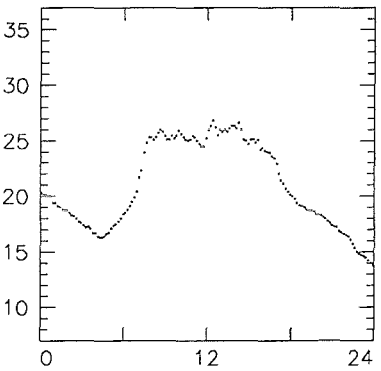

05.08.90

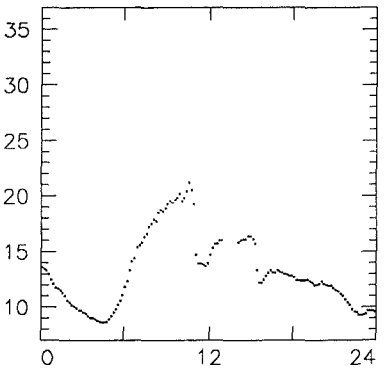

06.08.90

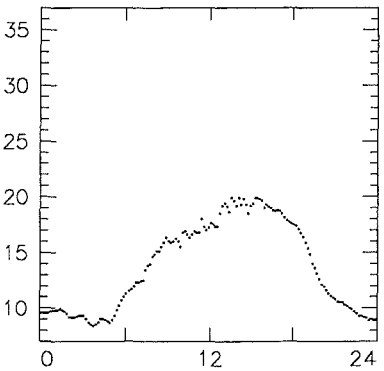

07.08.90

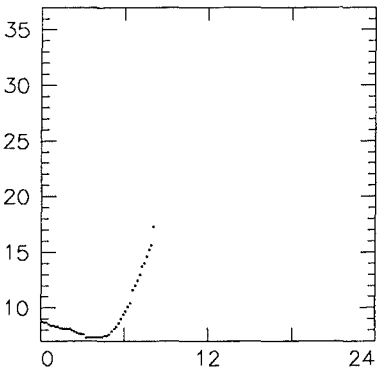

08.08.90

temperature/°C

File: T__2 ENZ90JUE

Dataset: 48

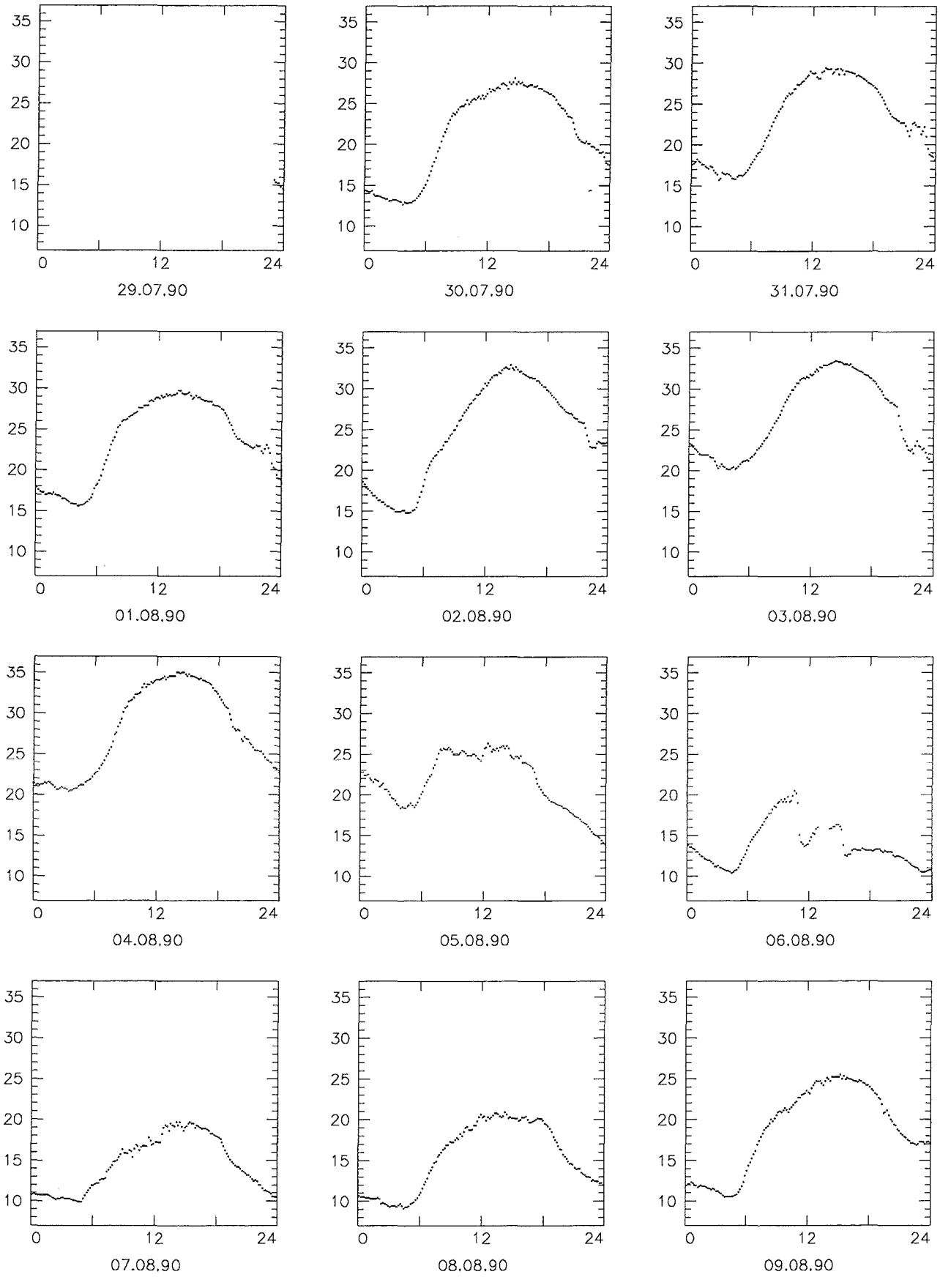

temperature/°C

File: T_20 ENZ90JUE

Dataset: 49

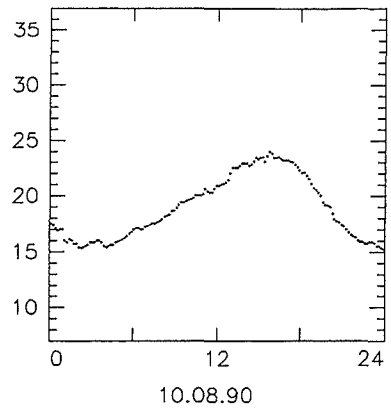

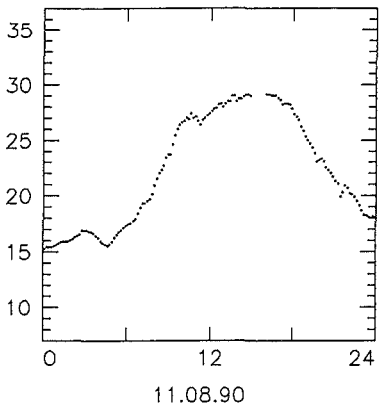

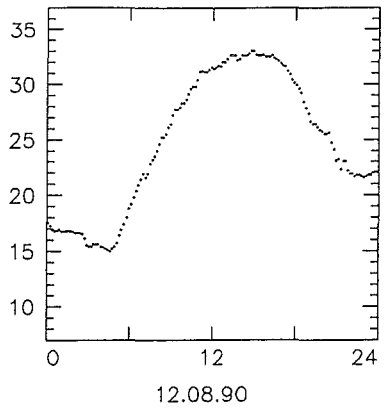

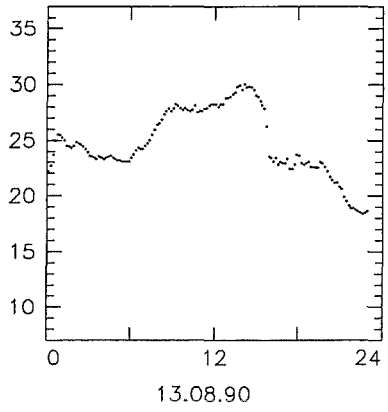

temperature/°C

File: T_20 ENZ90JUE

Dataset: 49

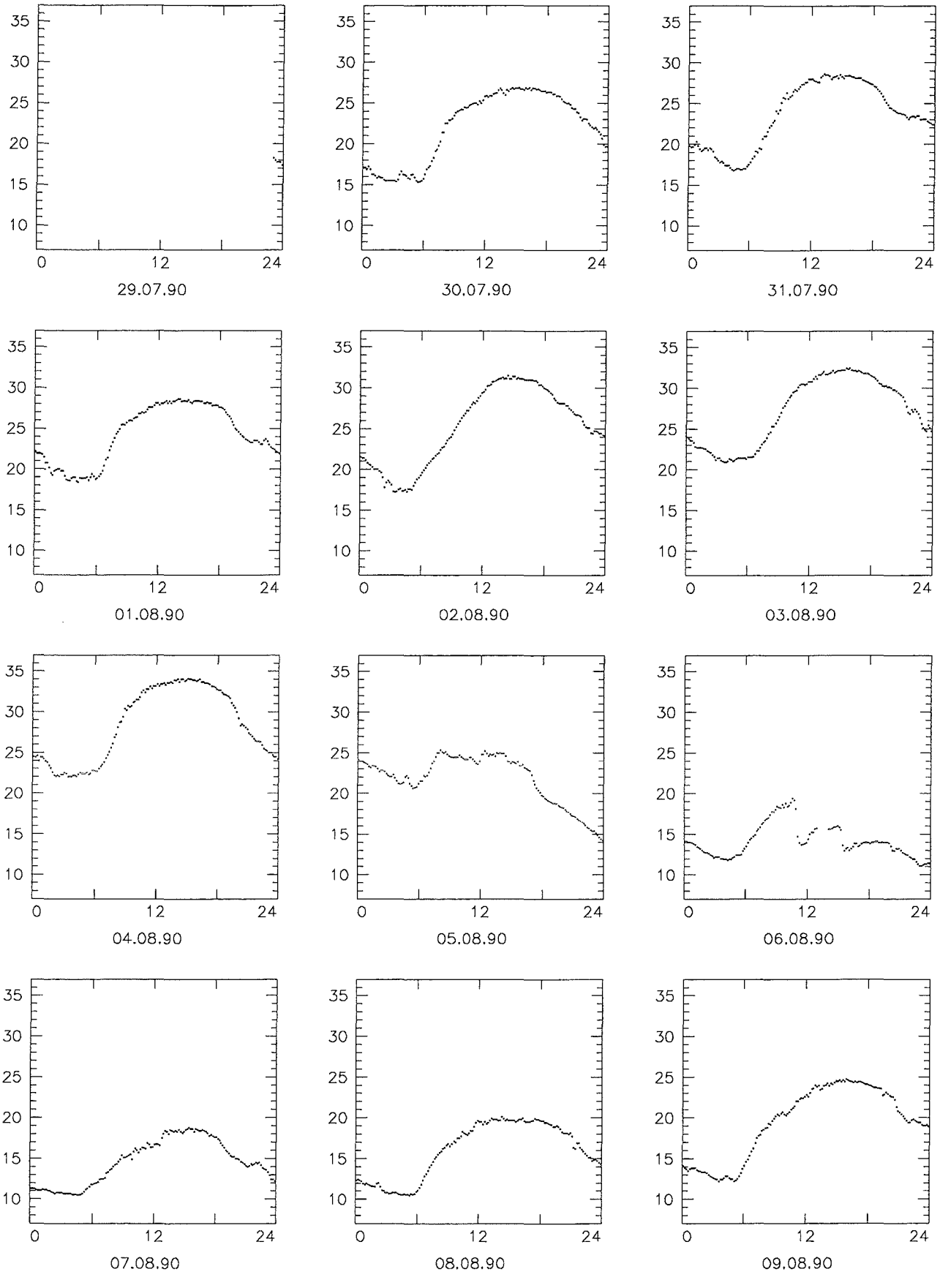

temperature/°C

File: T_50 ENZ90JUE

Dataset: 50

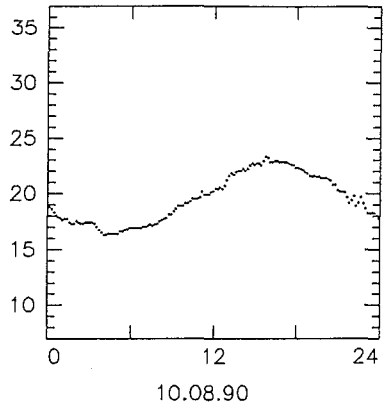

10.08.90

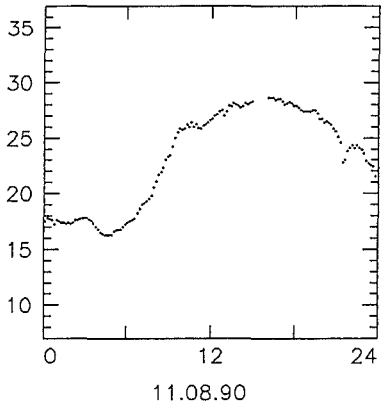

11.08.90

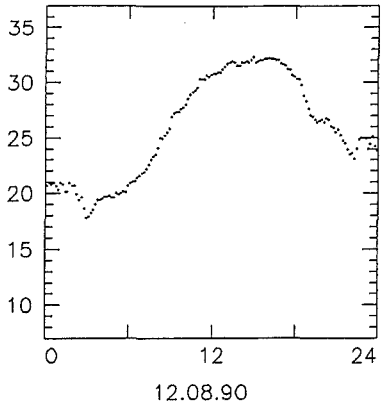

12.08.90

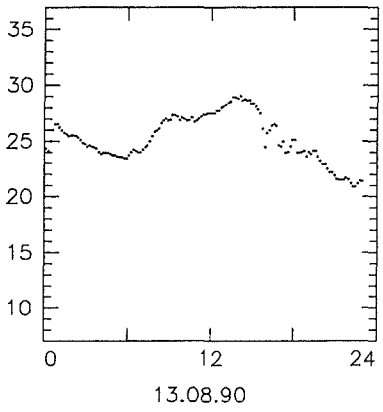

13.08.90

temperature/°C

File: T_50 ENZ90JUE

Dataset: 50

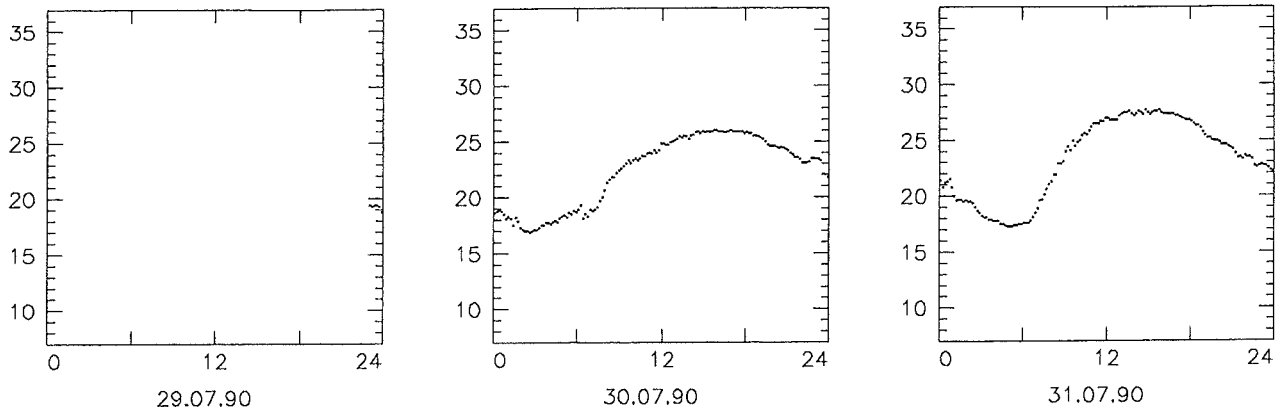

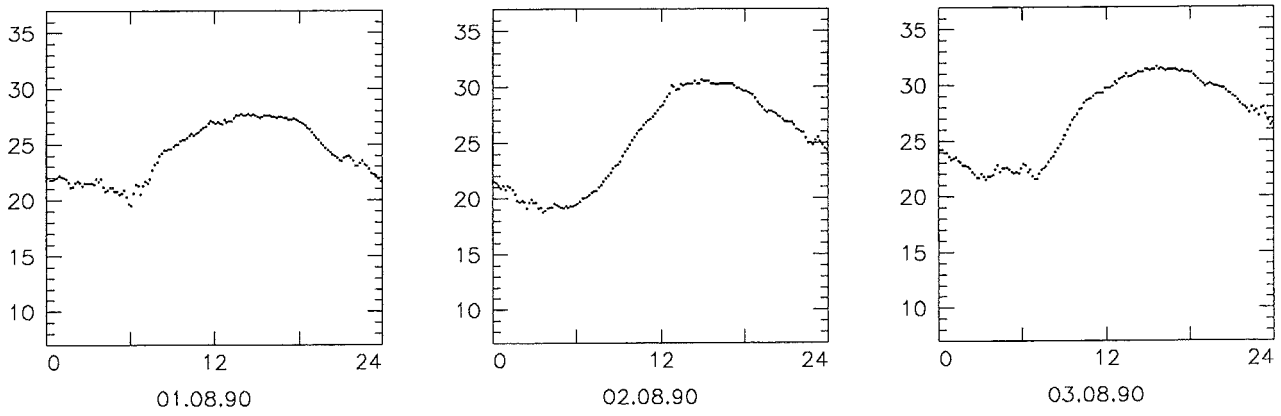

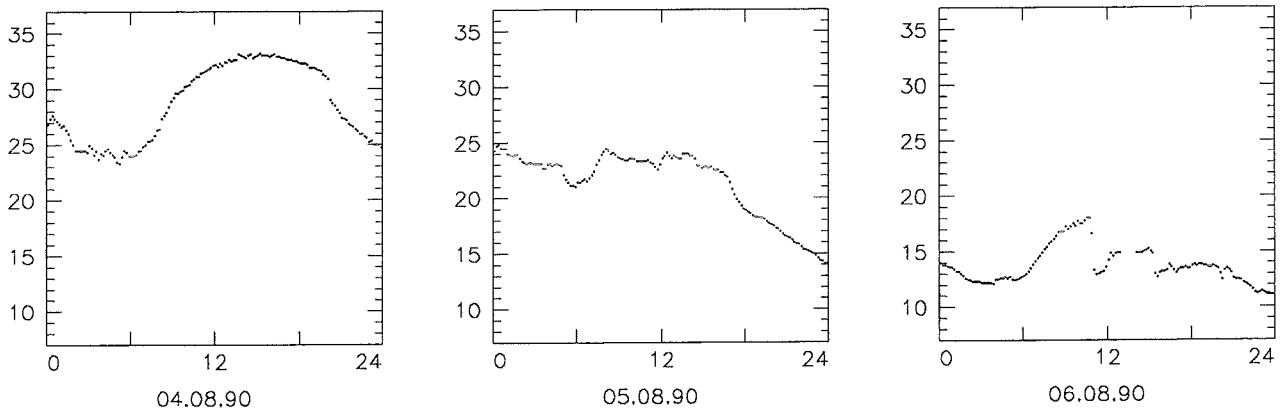

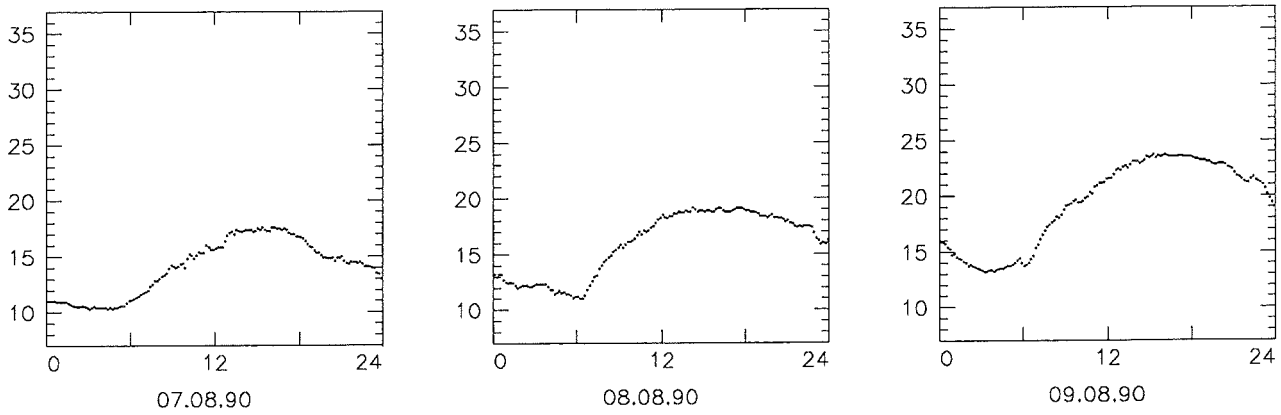

temperature/°C

File: T100 ENZ90JUE

Dataset: 51

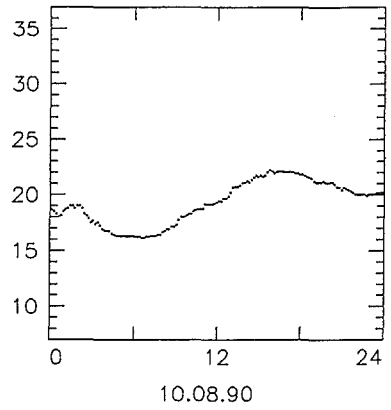

10.08.90

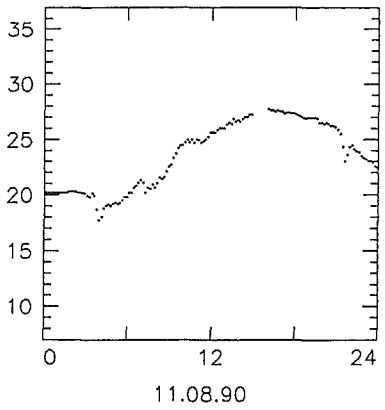

11.08.90

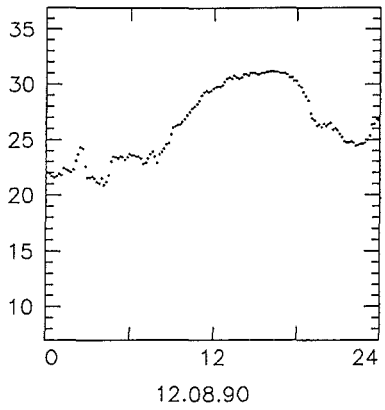

12.08.90

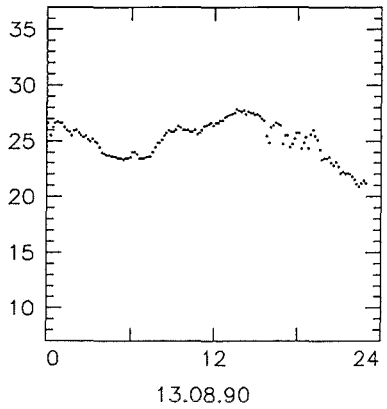

13.08.90

temperature/°C

File: T100 ENZ90JUE

Dataset: 51

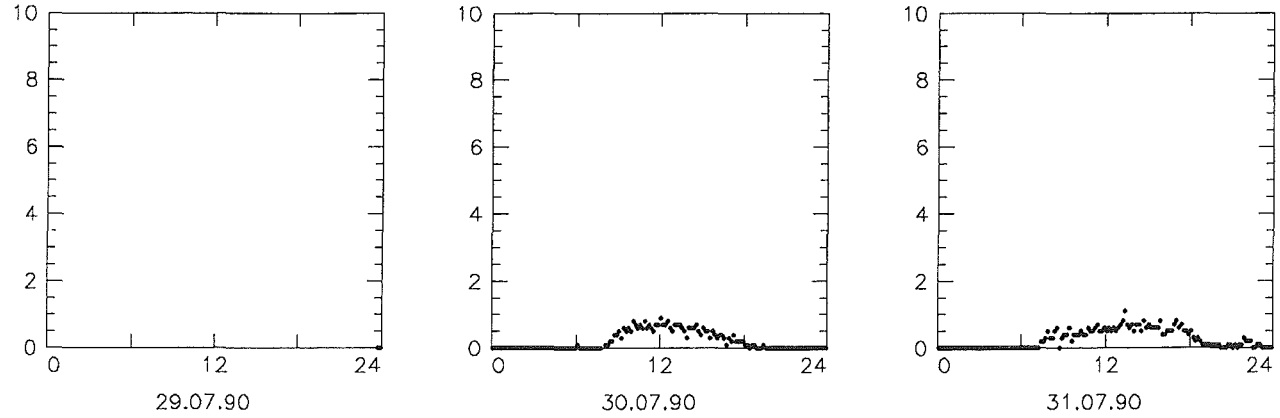

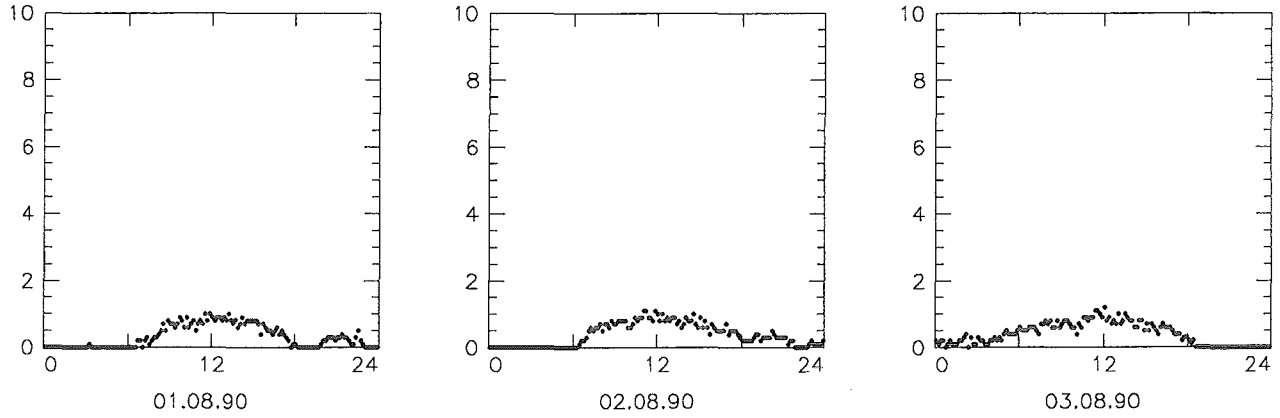

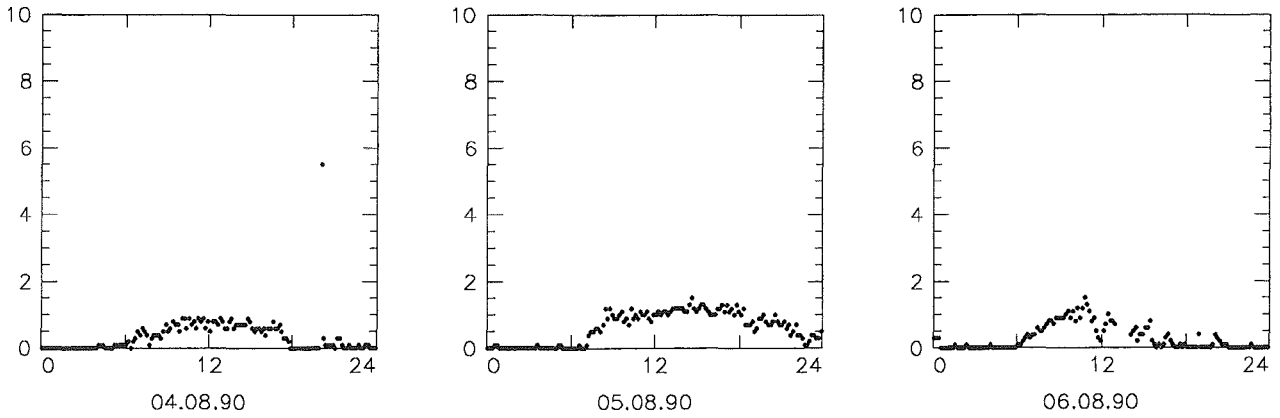

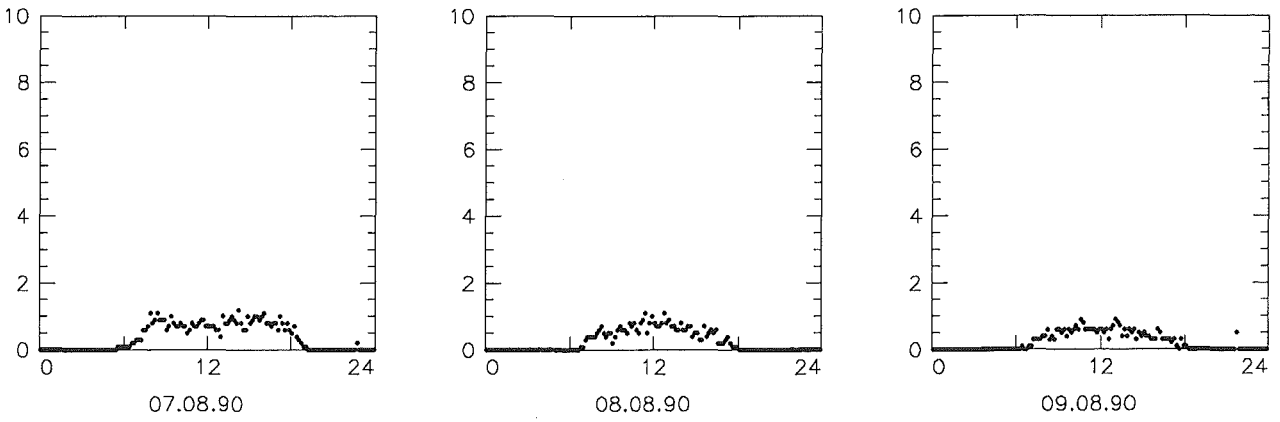

wind speed / ms^{-1}

File: WG__2 ENZ90JUE

Dataset: 52

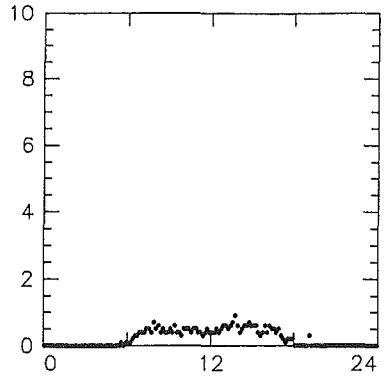

10.08.90

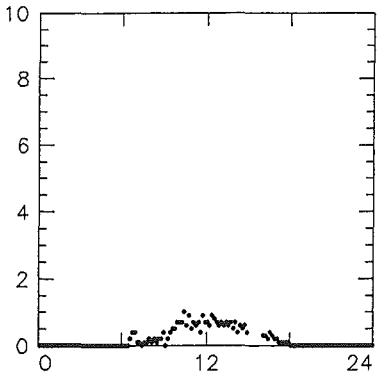

11.08.90

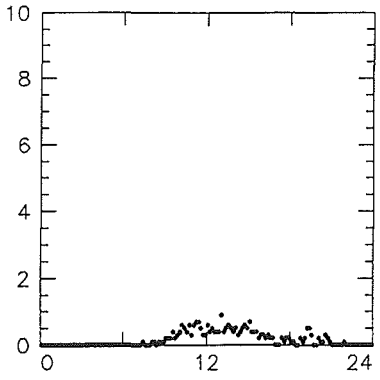

12.08.90

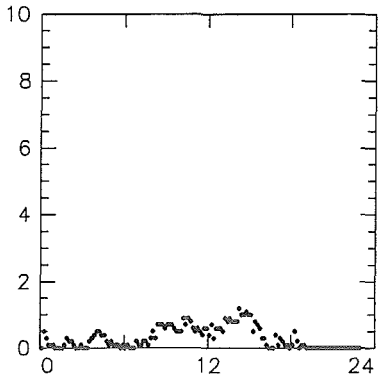

13.08.90

wind speed / ms^{-1}

File: WG__2 ENZ90JUE

Dataset: 52

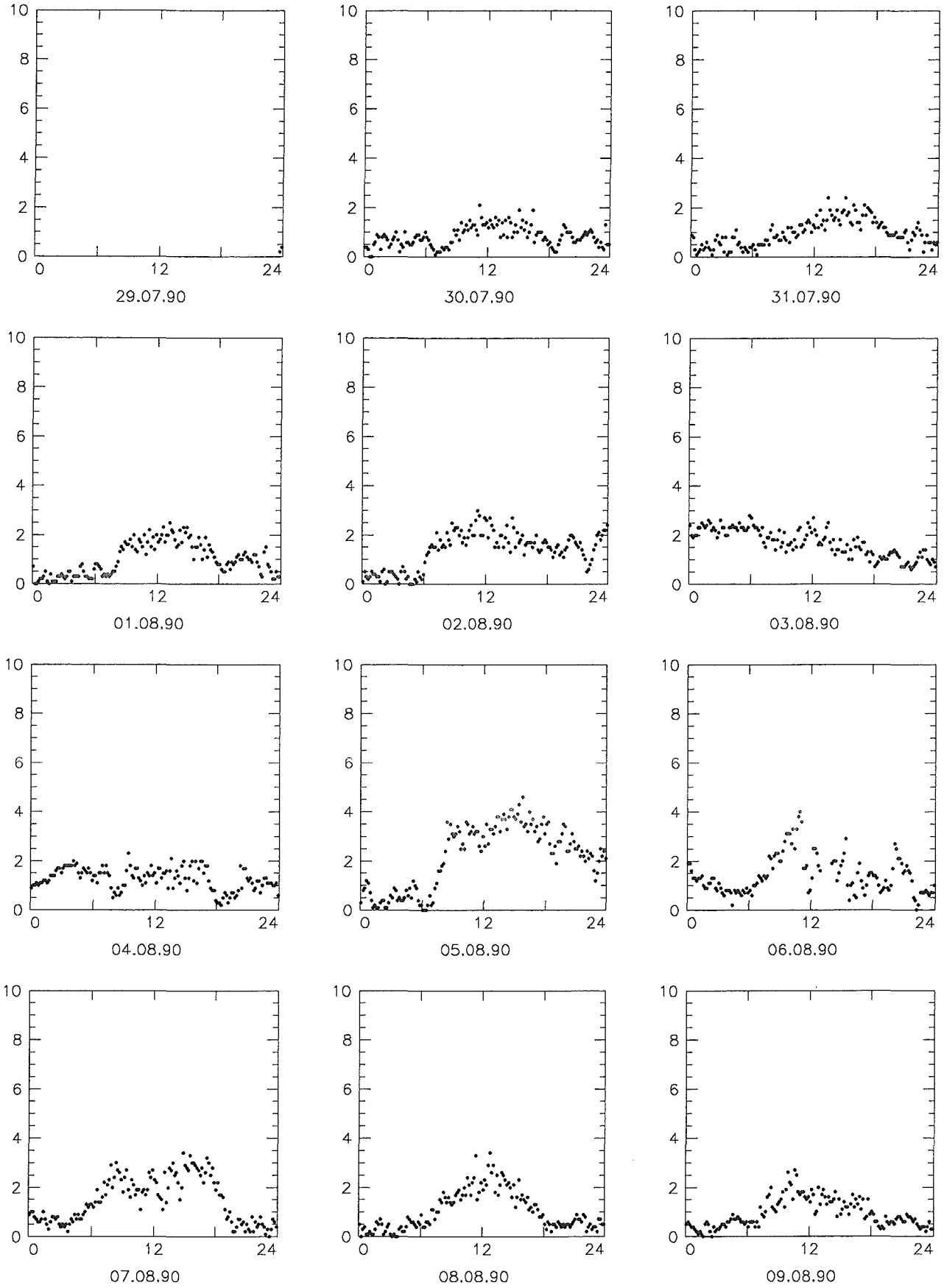

wind speed / ms^{-1}

File: WC_20 ENZ90JUE

Dataset: 53

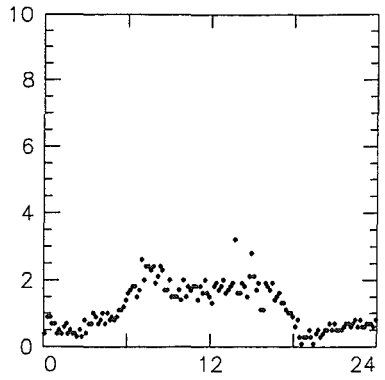

10.08.90

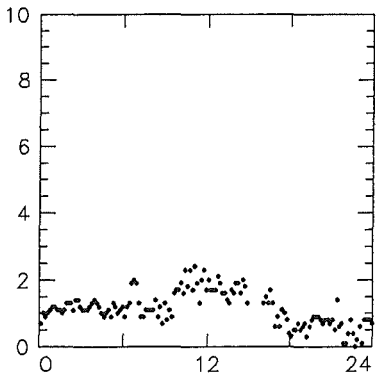

11.08.90

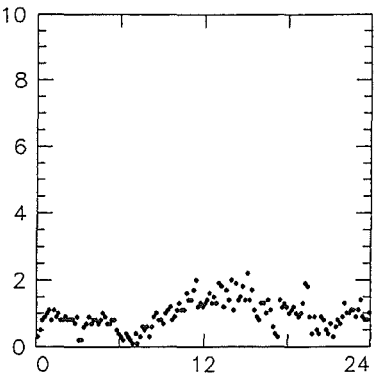

12.08.90

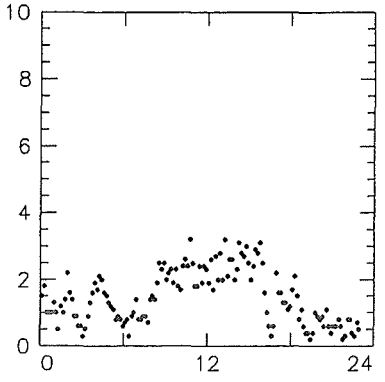

13.08.90

wind speed / ms^{-1}

File: WG_20 ENZ90JUE

Dataset: 53

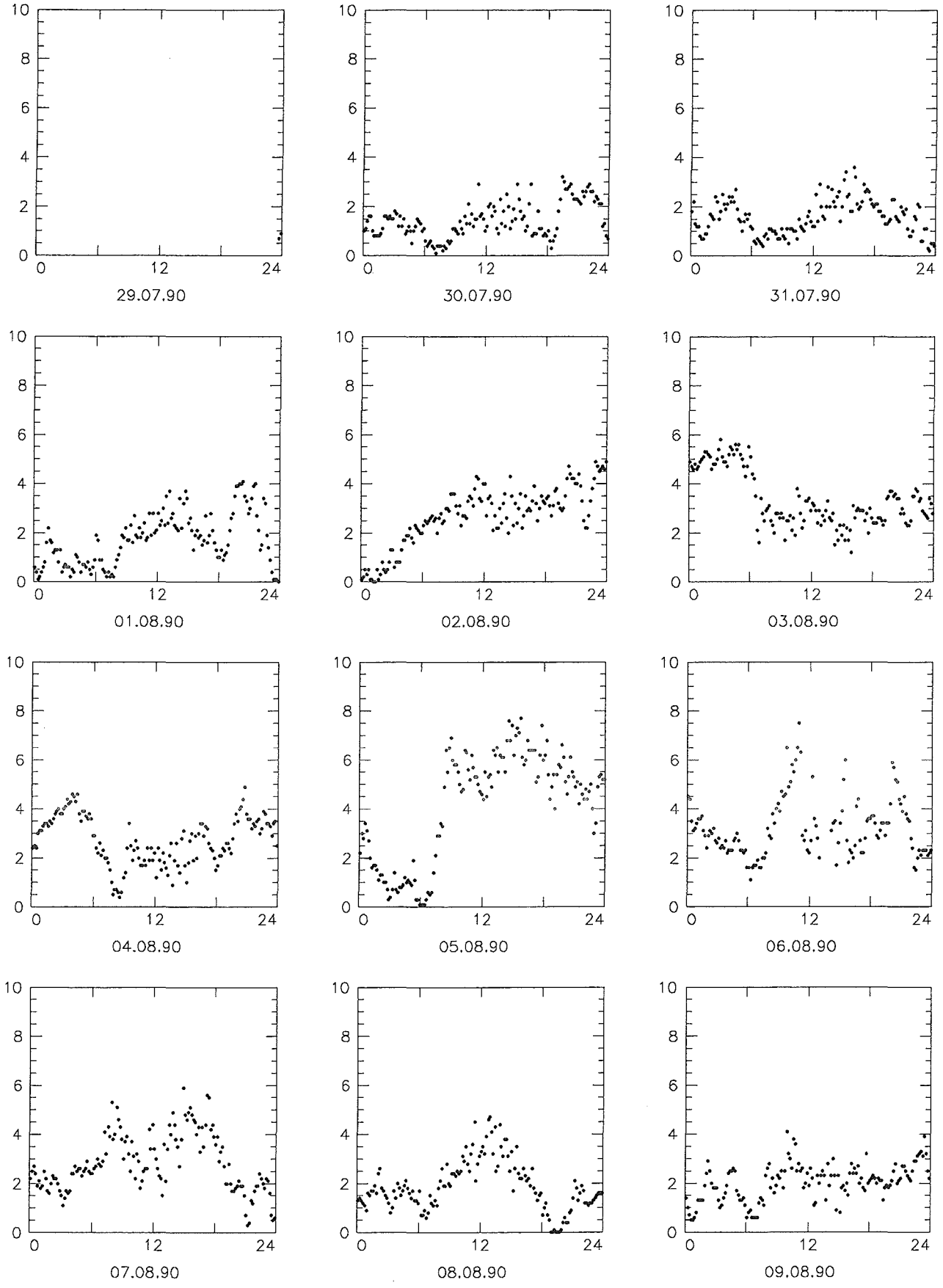

wind speed / ms^{-1}

File: WG_50 ENZ90JUE

Dataset: 54

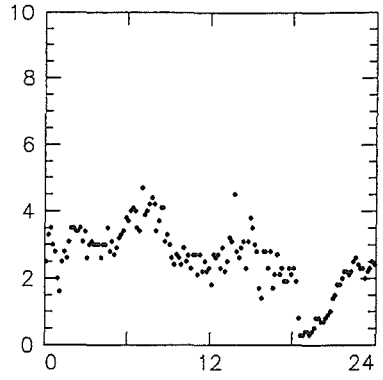

10.08.90

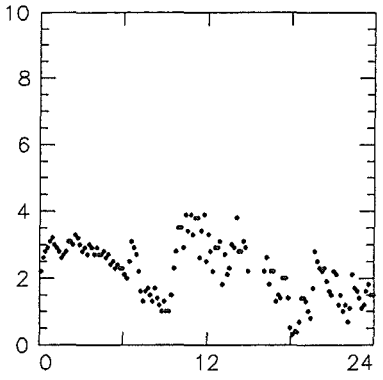

11.08.90

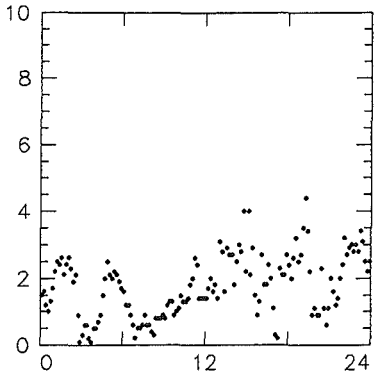

12.08.90

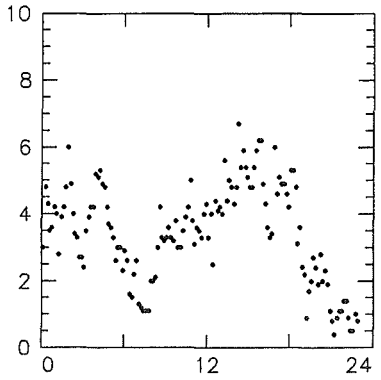

13.08.90

wind speed / ms^{-1}

File: WG_50 ENZ90JUE

Dataset: 54

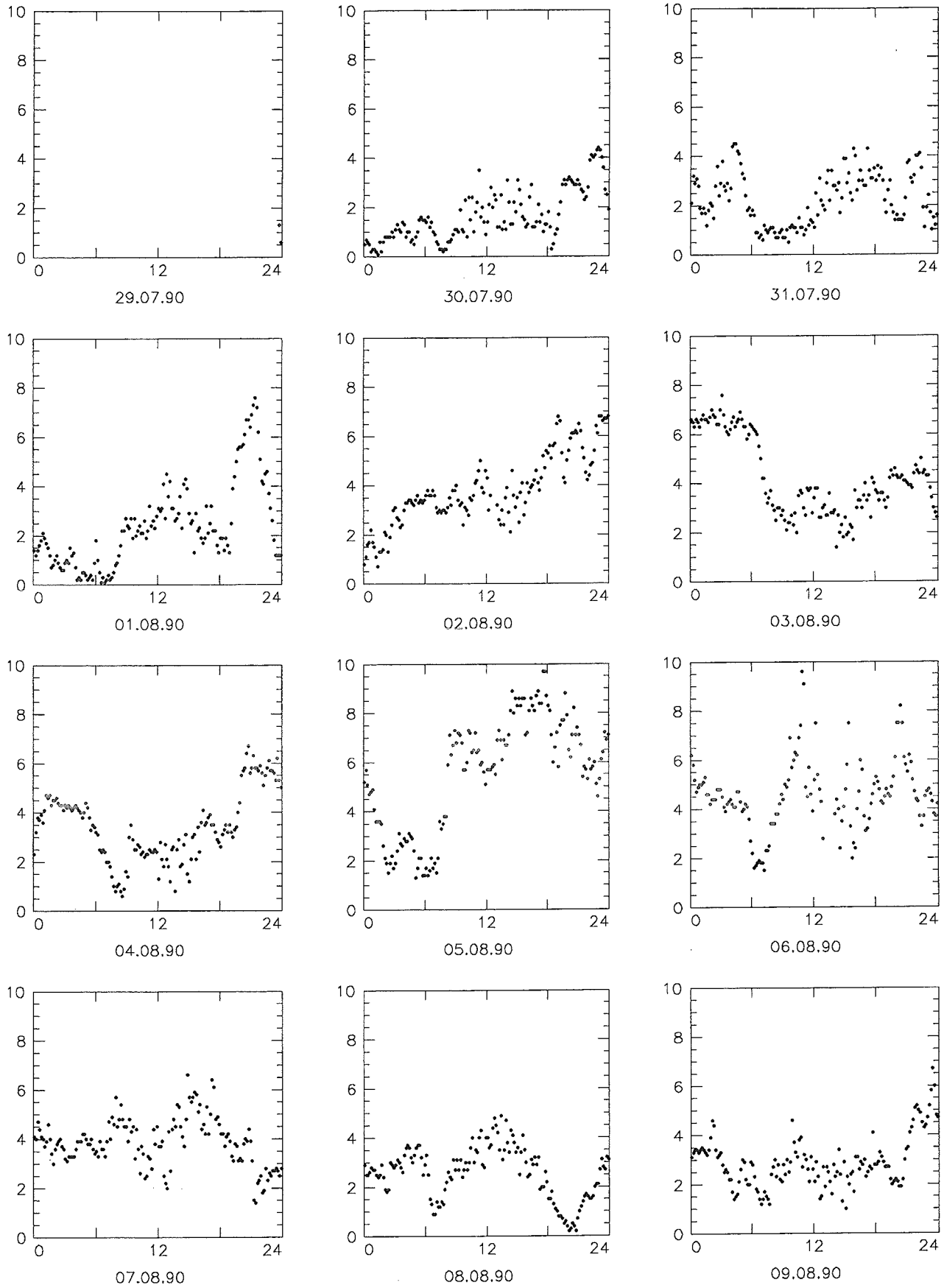

wind speed / ms^{-1}

File: WG100 ENZ90JUE

Dataset: 55

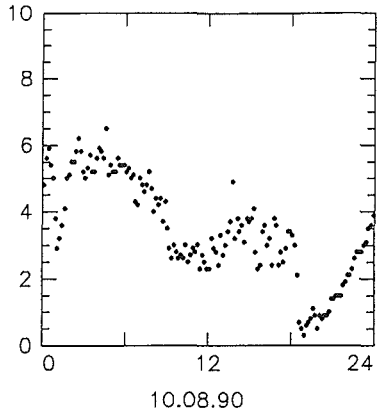

10.08.90

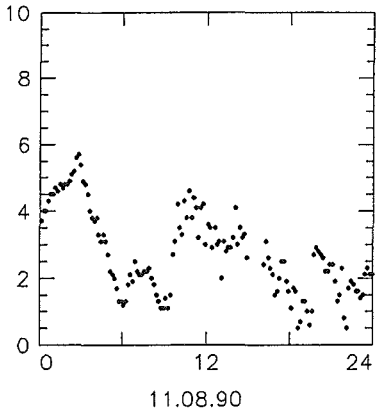

11.08.90

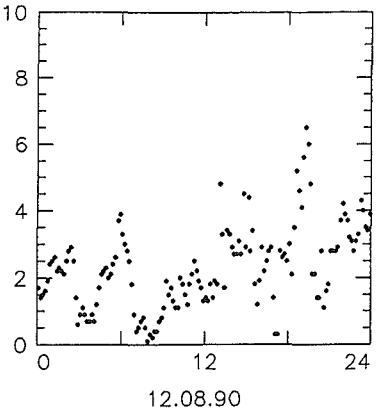

12.08.90

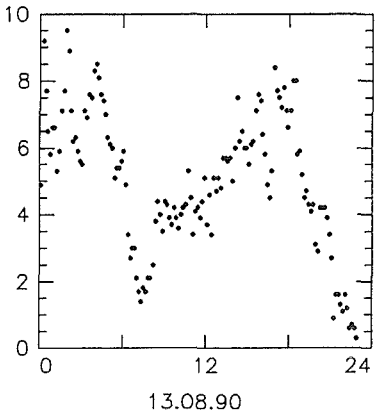

13.08.90

wind speed / ms^{-1}

File: WC100 ENZ90JUE

Dataset: 55

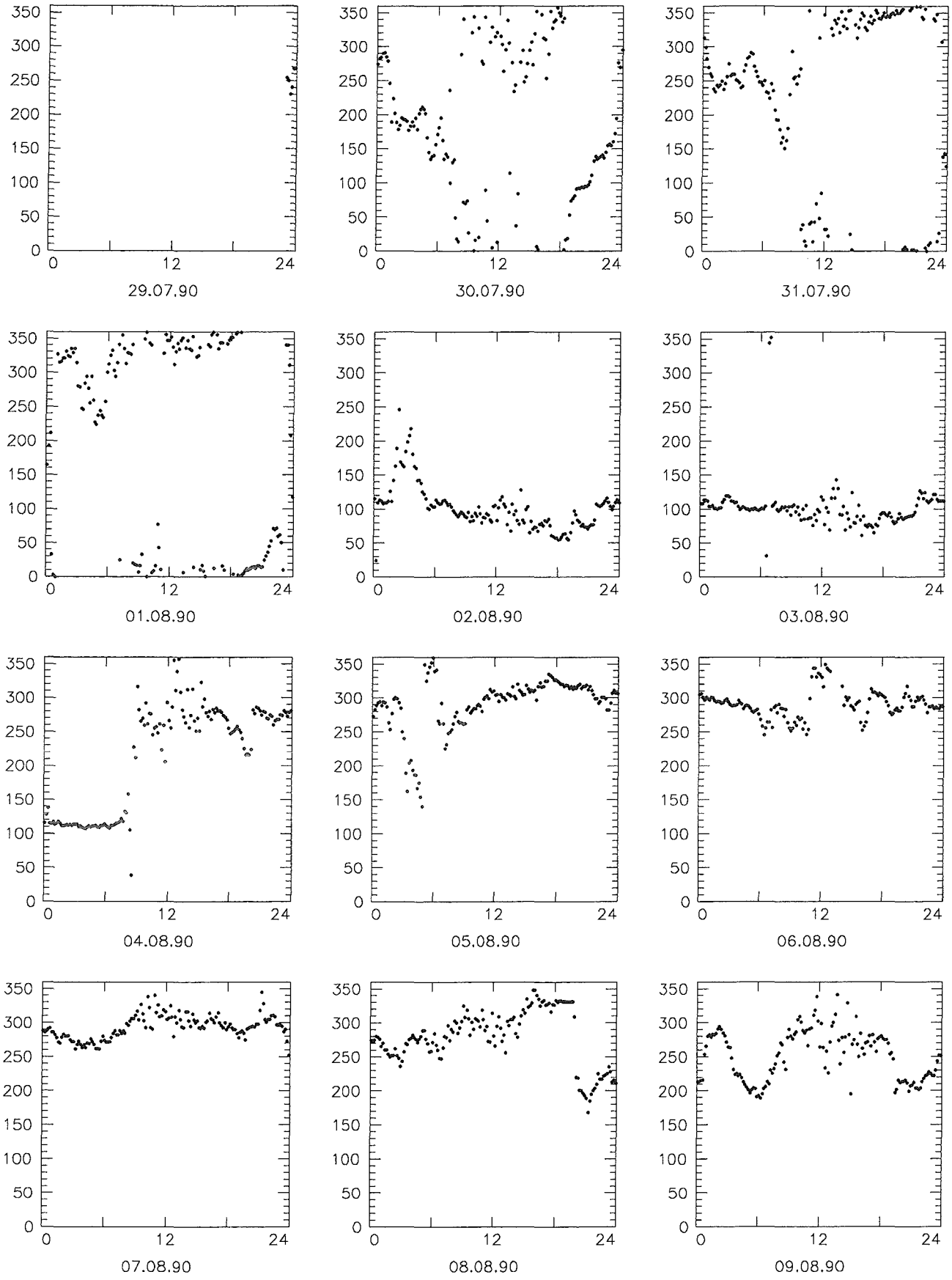

wind direction / °

File: WR_50 ENZ90JUE

Dataset: 56

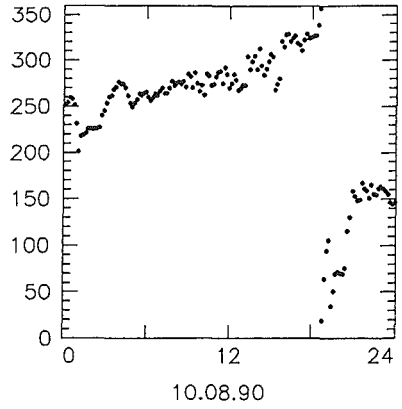

10.08.90

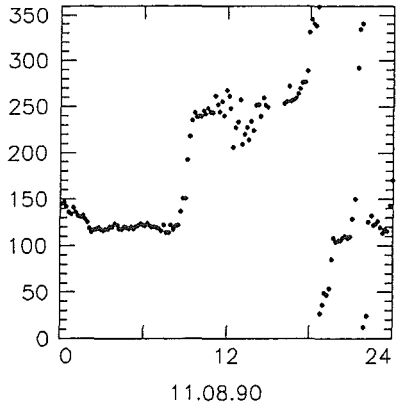

11.08.90

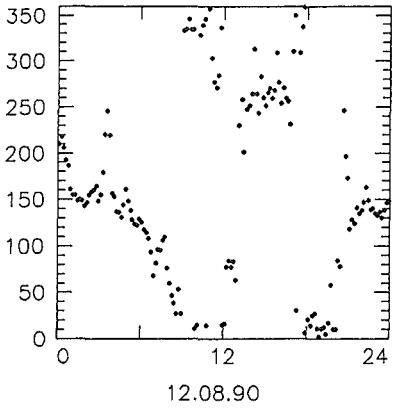

12.08.90

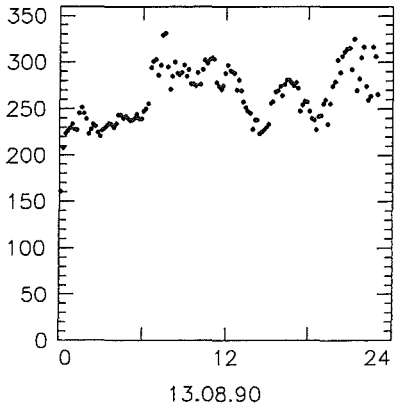

13.08.90

wind direction / °

File: WR_50 ENZ90JUE

Dataset: 56

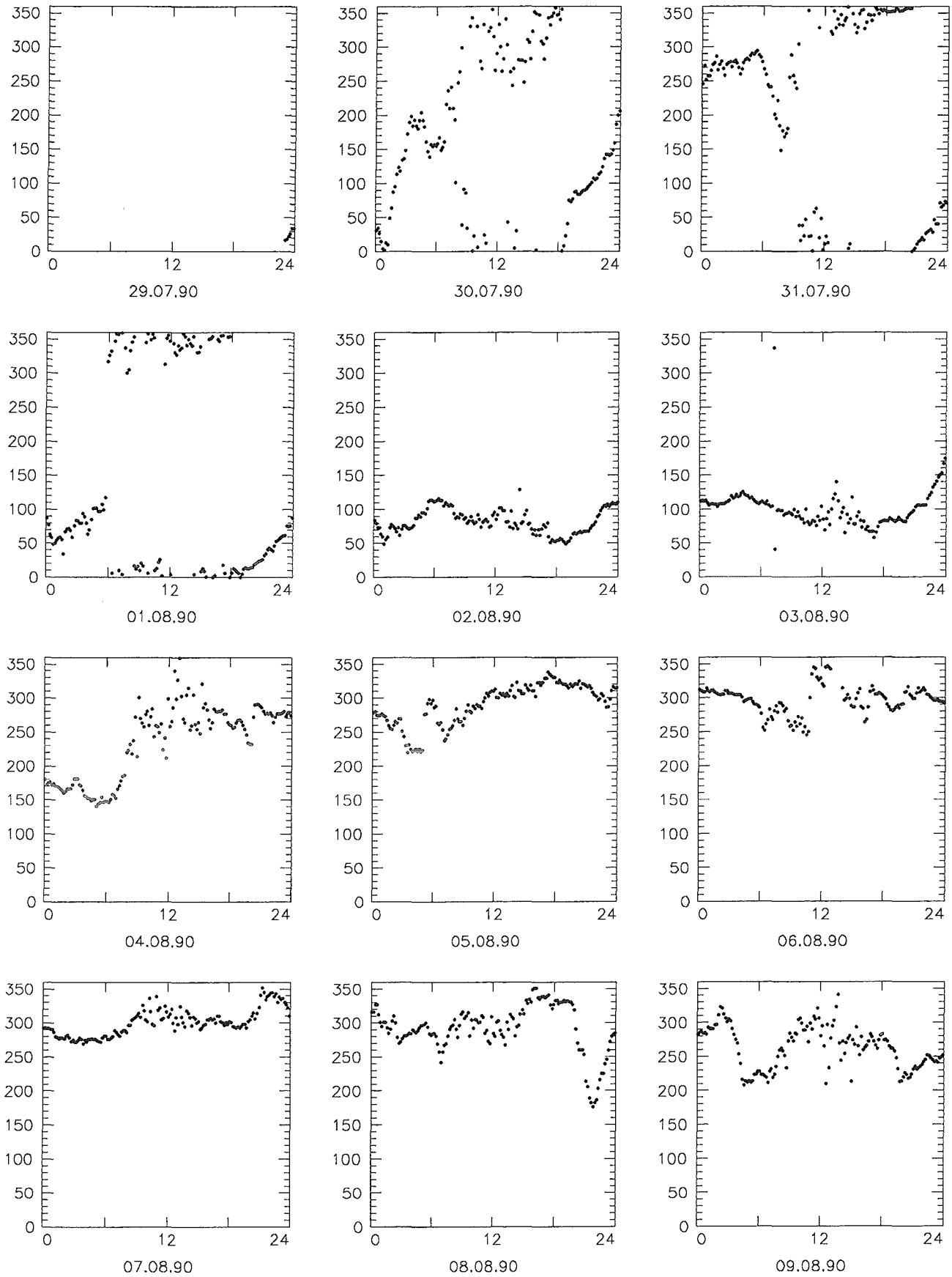

wind direction / °

File: WR120 ENZ90JUE

Dataset: 57

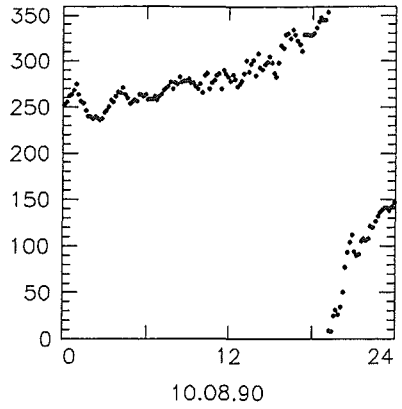

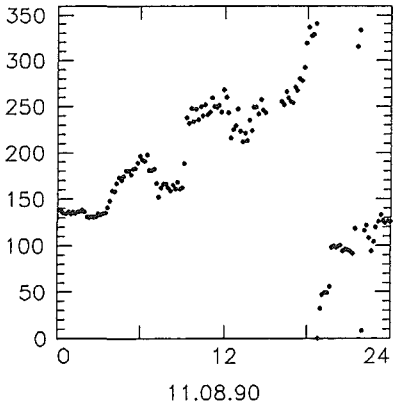

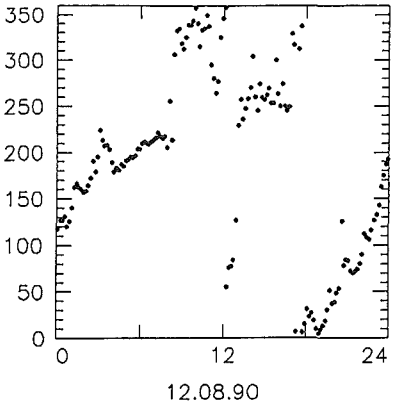

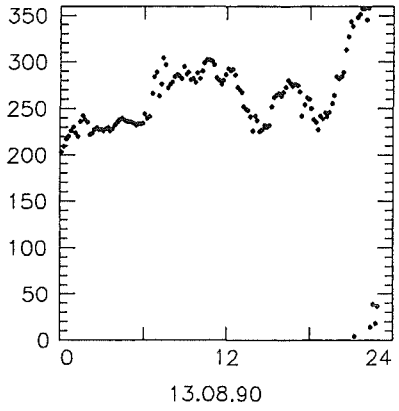

wind direction / °

File: WR120 ENZ90JUE

Dataset: 57

Appendix B **Weather Maps**
(kindly provided by the Deutscher Wetterdienst) for
p = 1000 hPa for all Days during the Campaign.

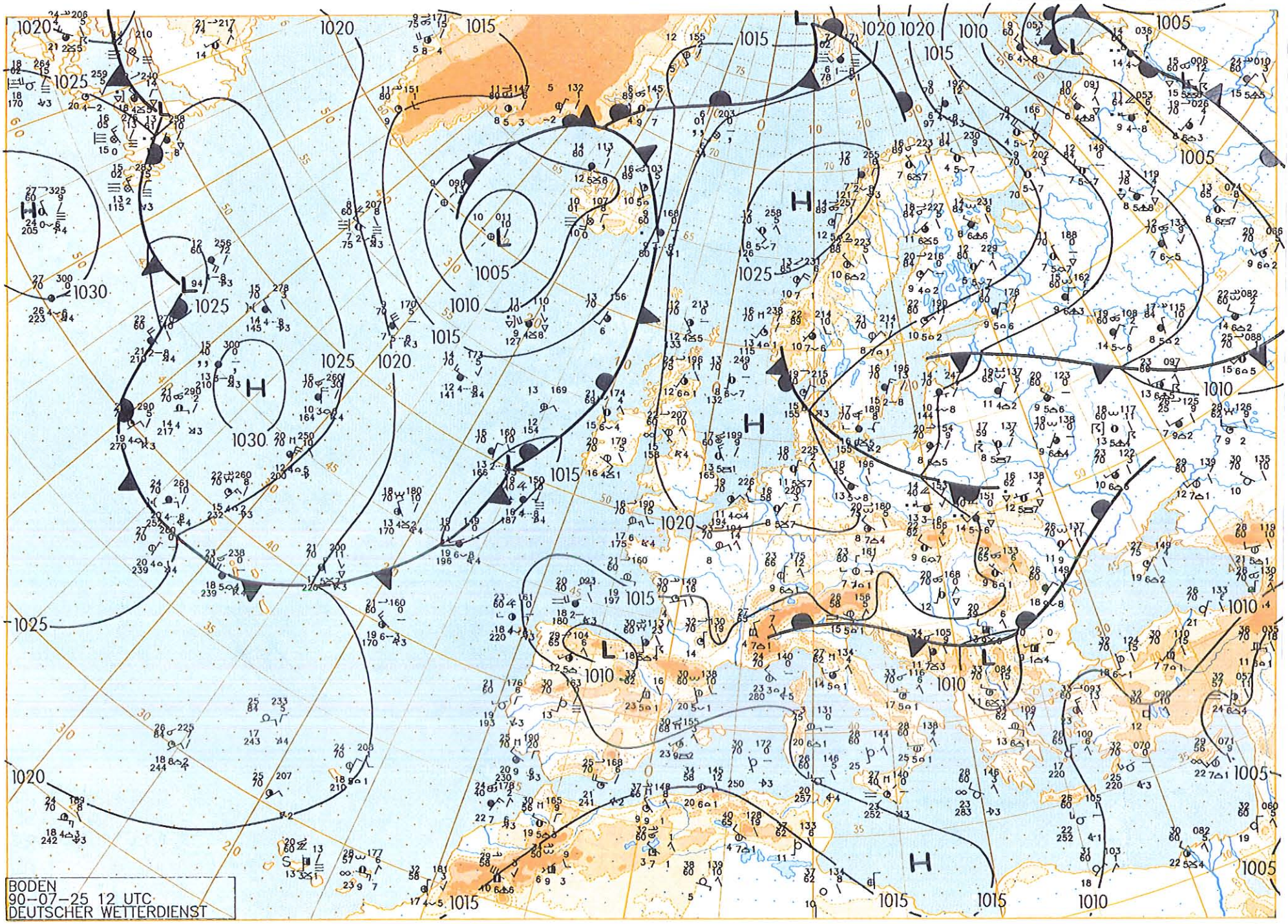
BODEN
90-07-25 12 UTC
DEUTSCHER WETTERDIENST

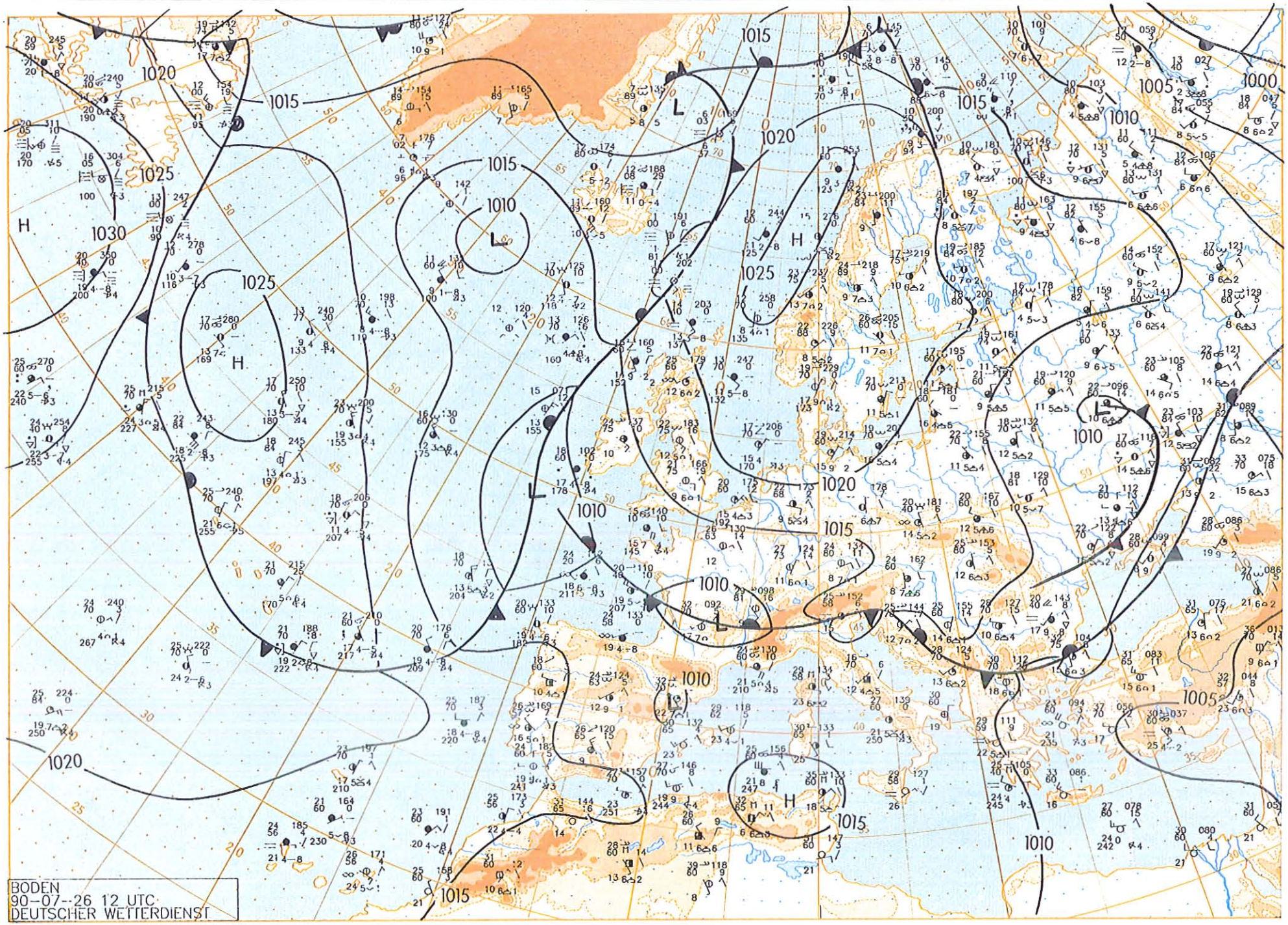
BODEN
90-07--26 12 UTC
DEUTSCHER WETTERDIENST

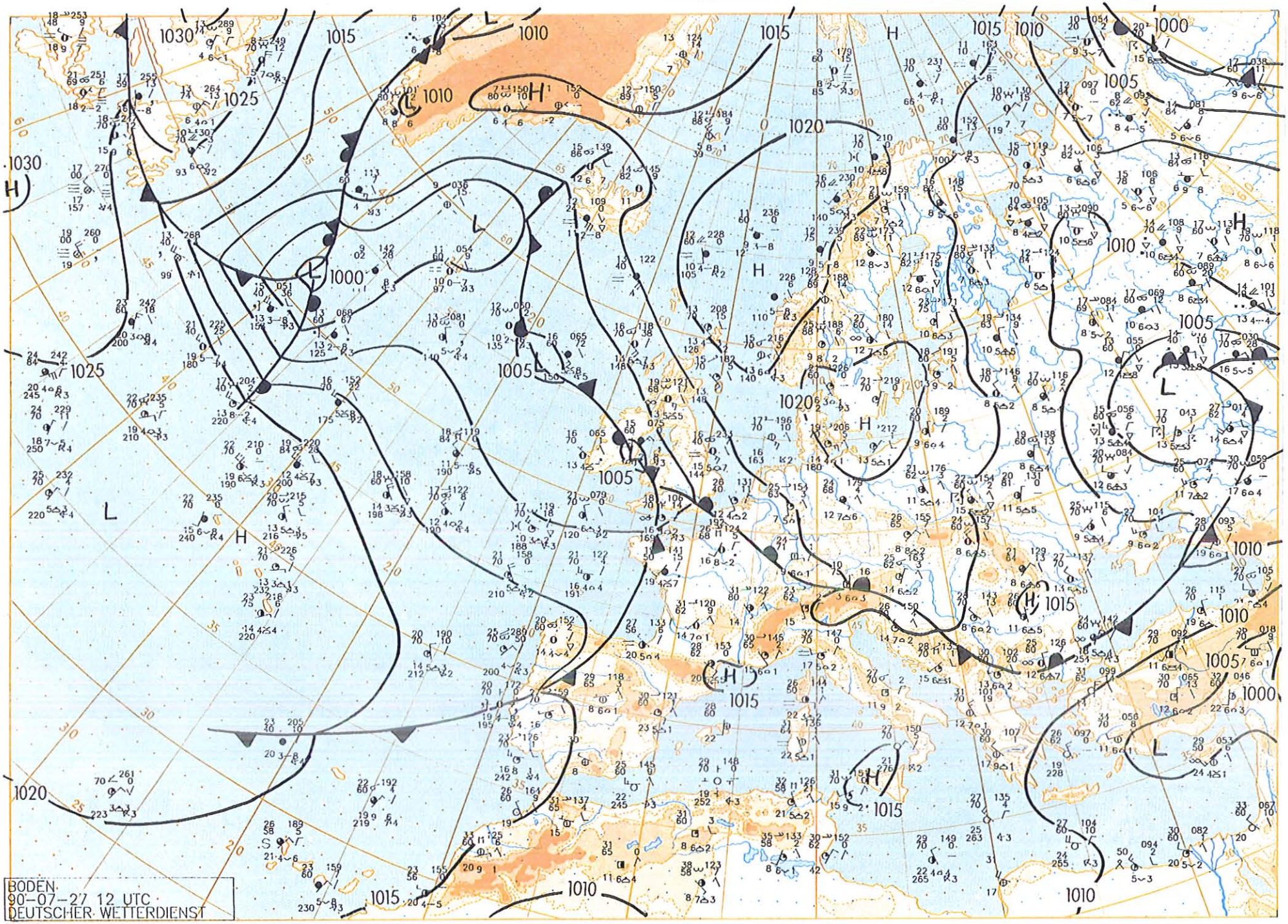
BODEN
90-07-27 12 UTC
DEUTSCHER WETTERDIENST

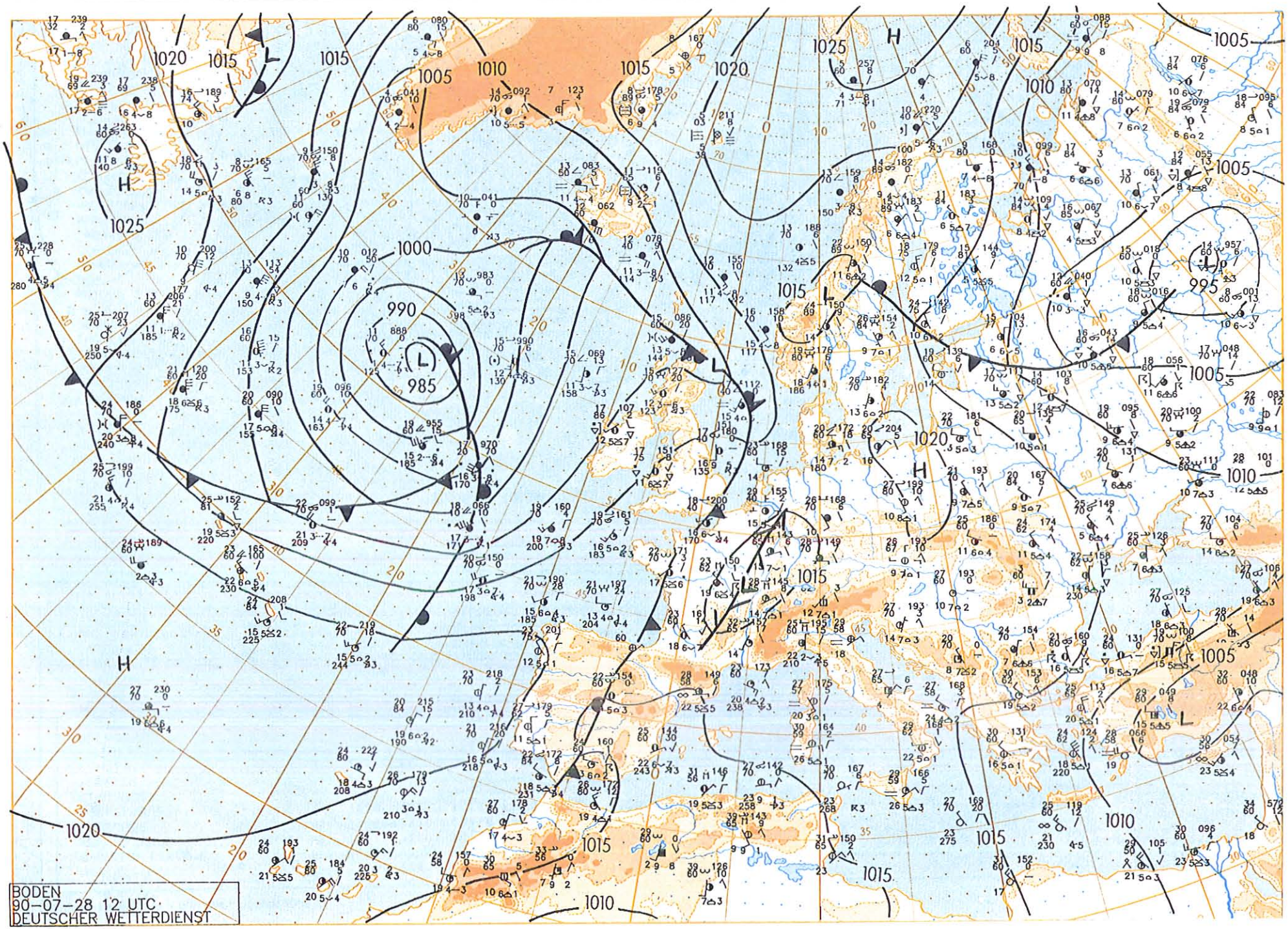
BODEN
90-07-28 12 UTC
DEUTSCHER WETTERDIENST

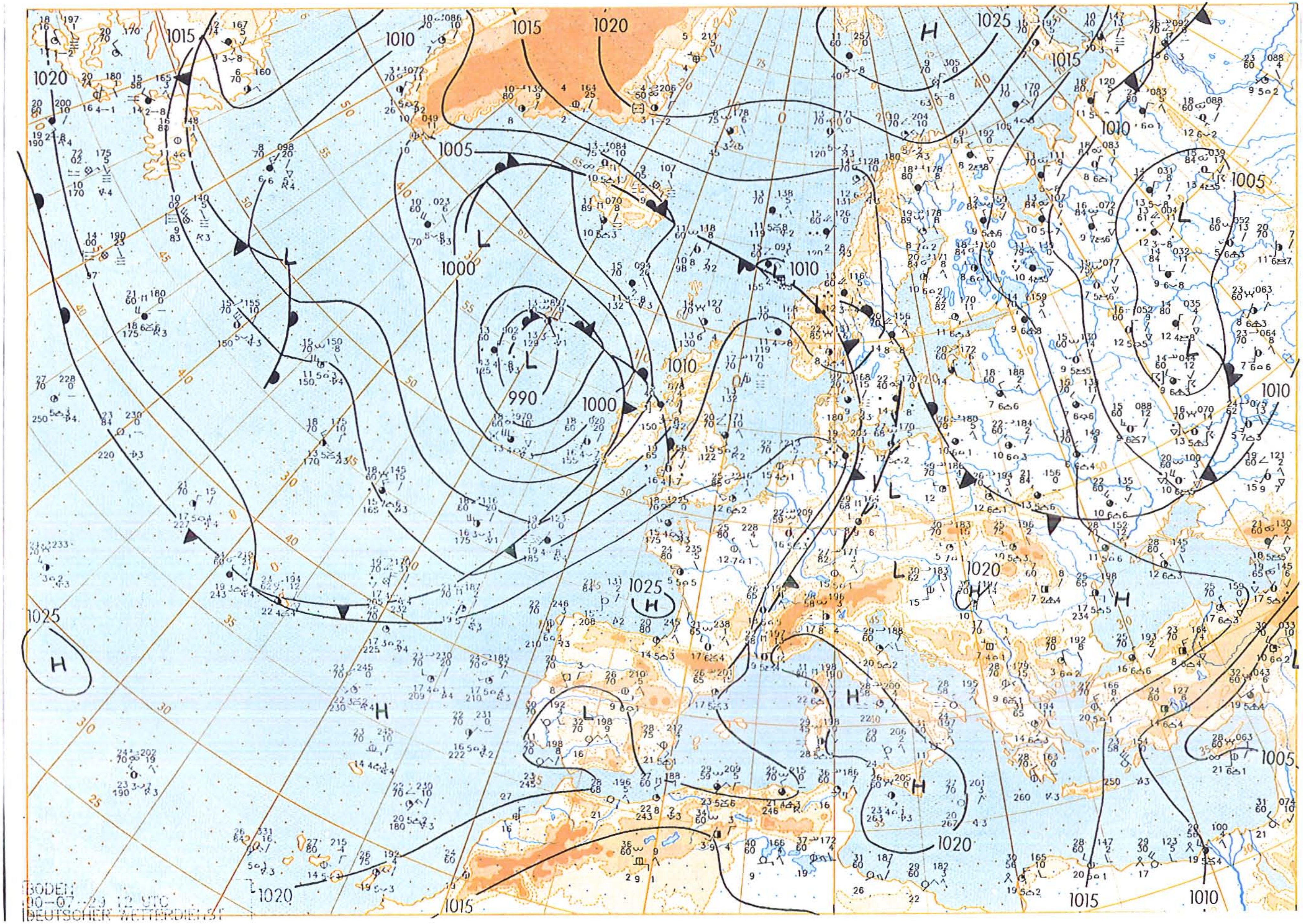
BODEN
90-07-23 12 UTC
DEUTSCHER WETTERDIENST

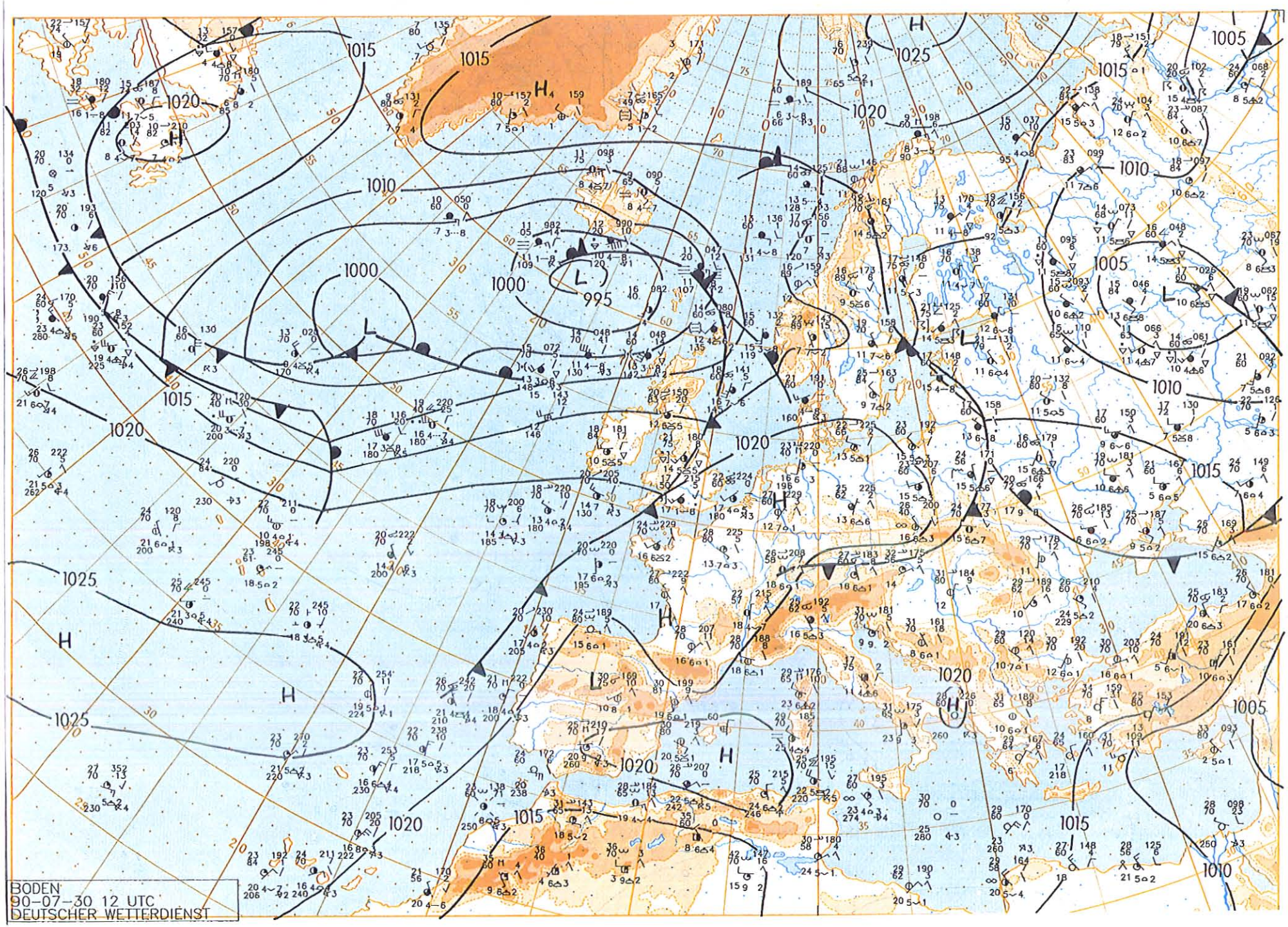
BODEN
90-07-30 12 UTC
DEUTSCHER WETTERDIENST

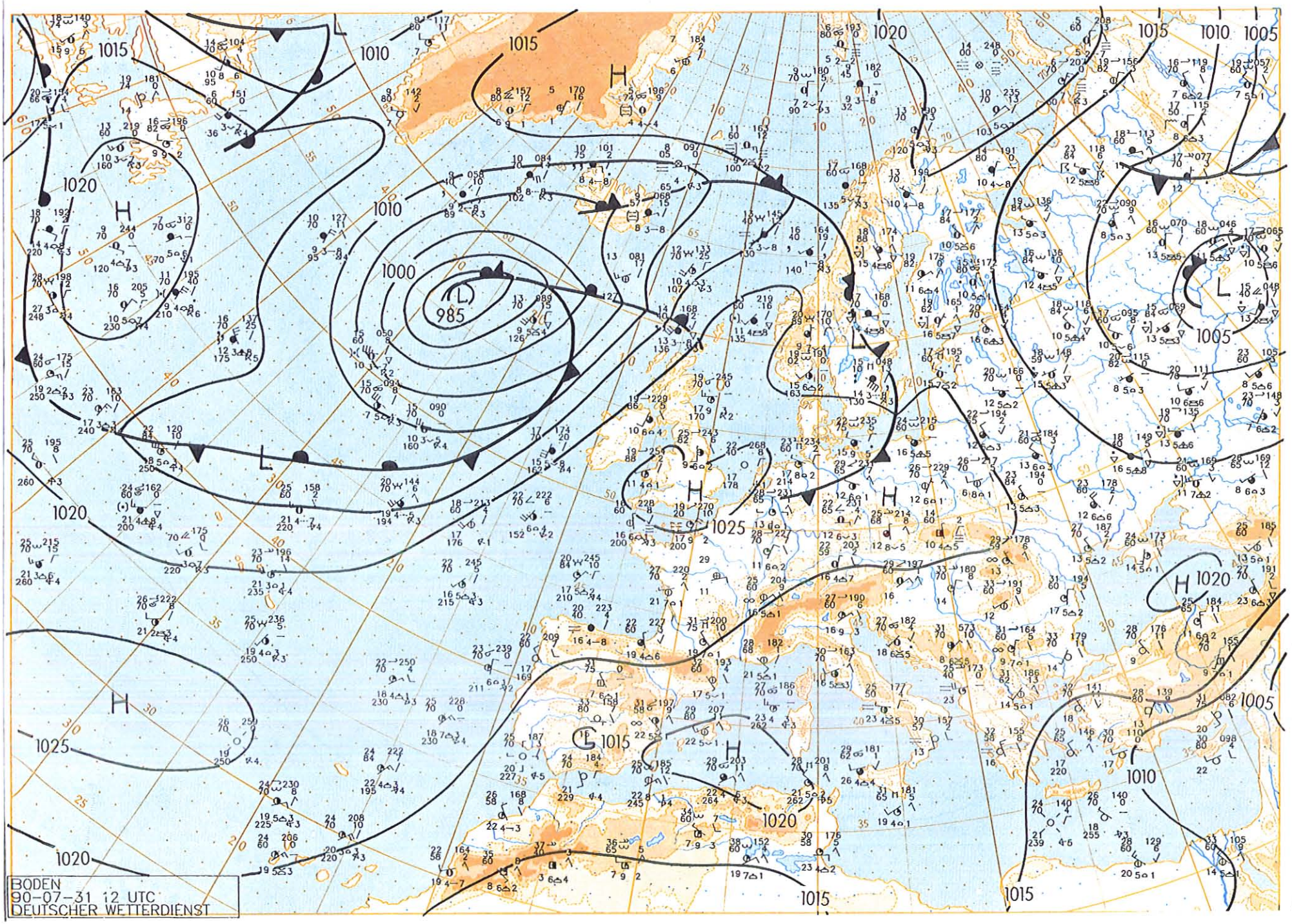
1015
1010
1020
1005
1000
985
1025
BODEN
90-07-31 12 UTC
DEUTSCHER WETTERDIENST

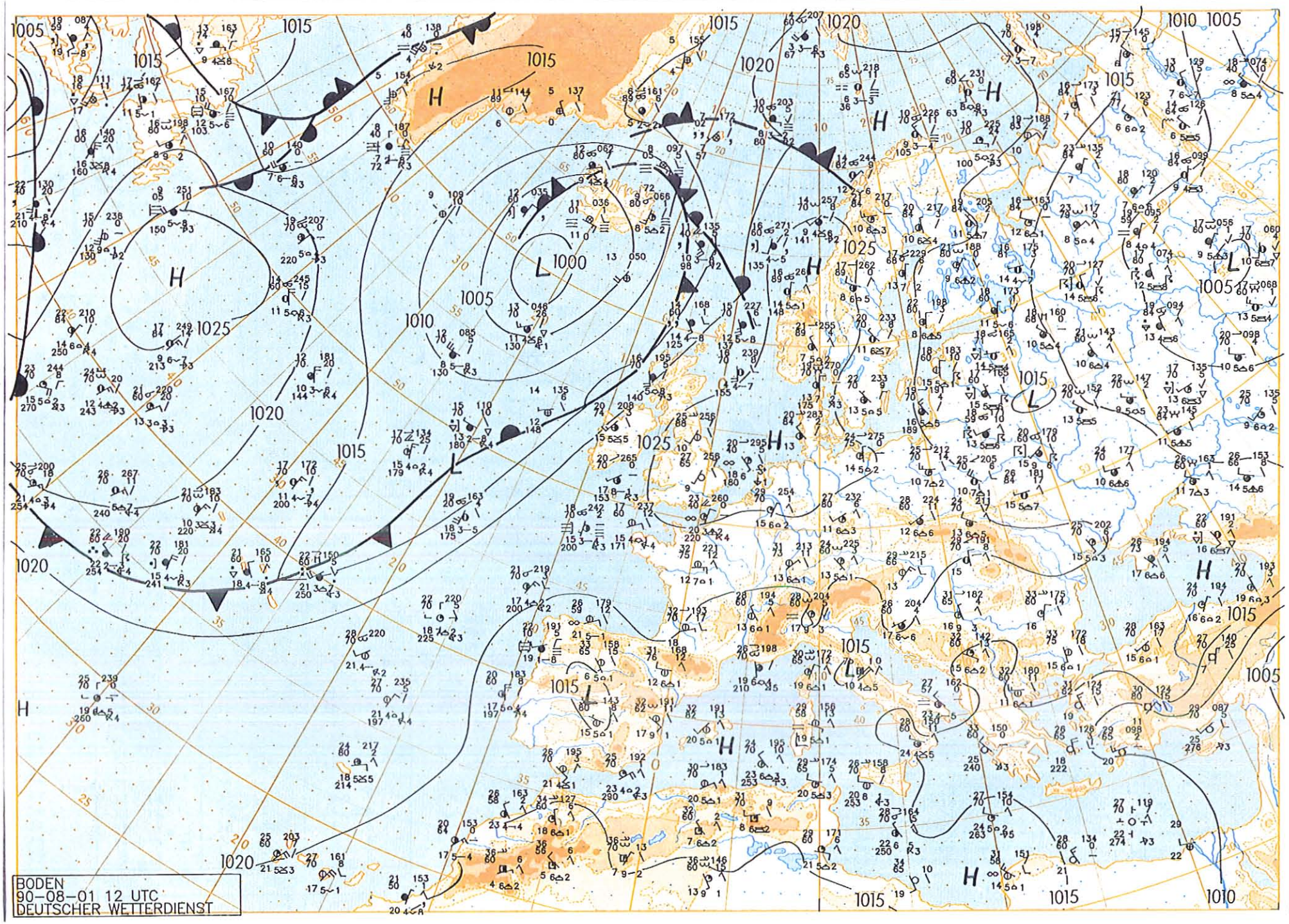
BODEN
90-08-01 12 UTC
DEUTSCHER WETTERDIENST

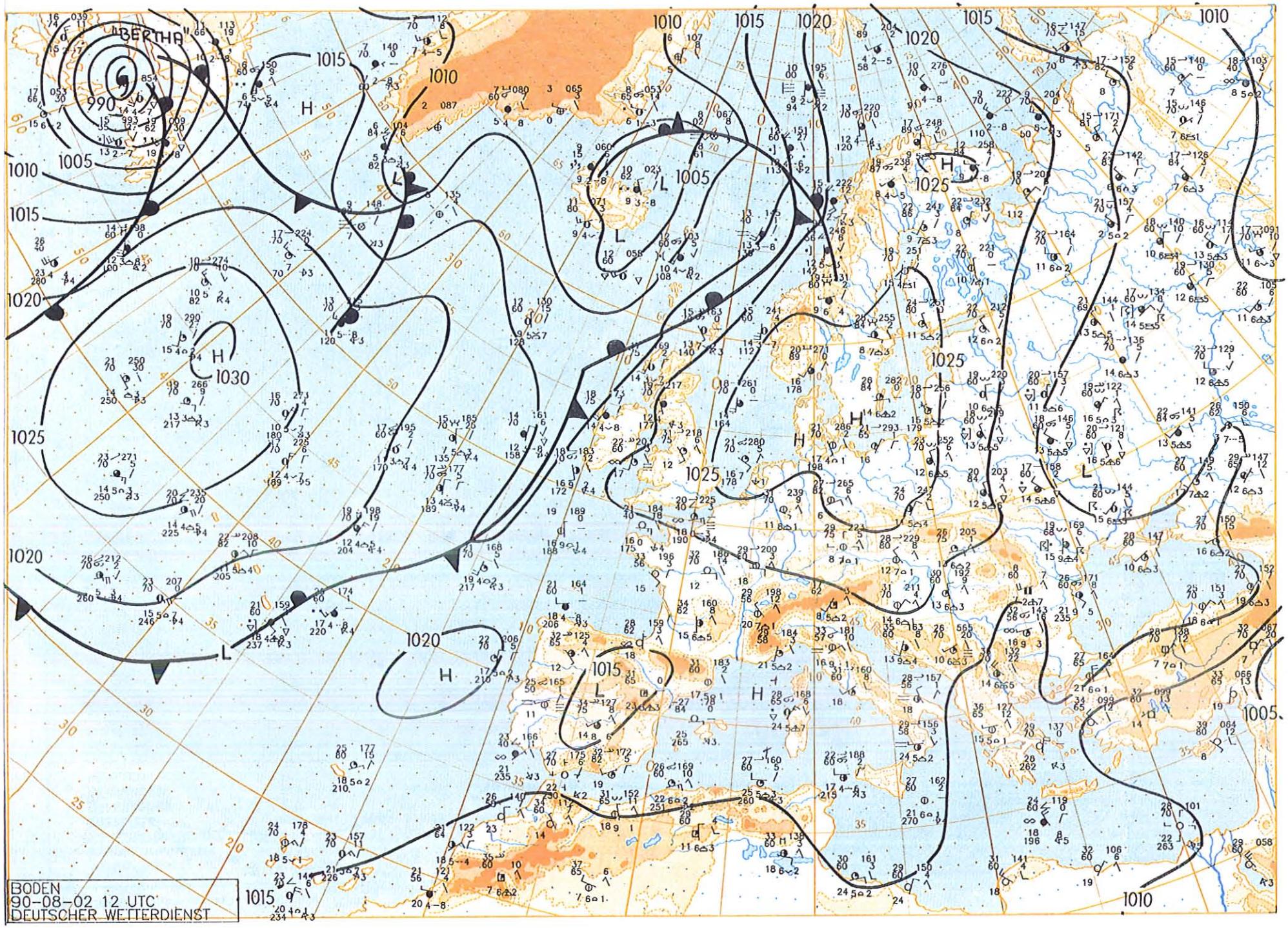
"BERTHA"
990
1030
BODEN
90-08-02 12 UTC
DEUTSCHER WETTERDIENST

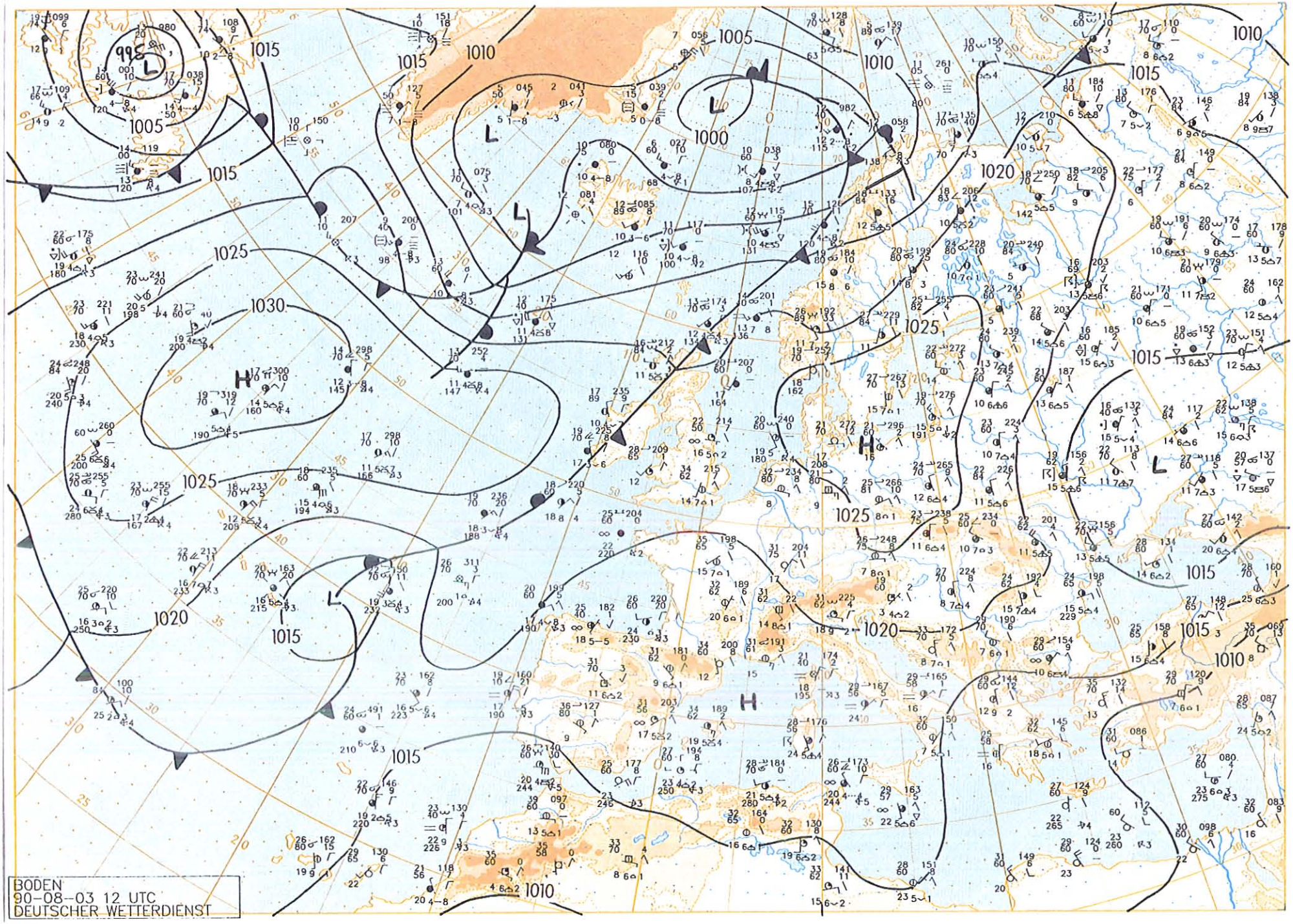
BODEN
90-08-03 12 UTC
DEUTSCHER WETTERDIENST

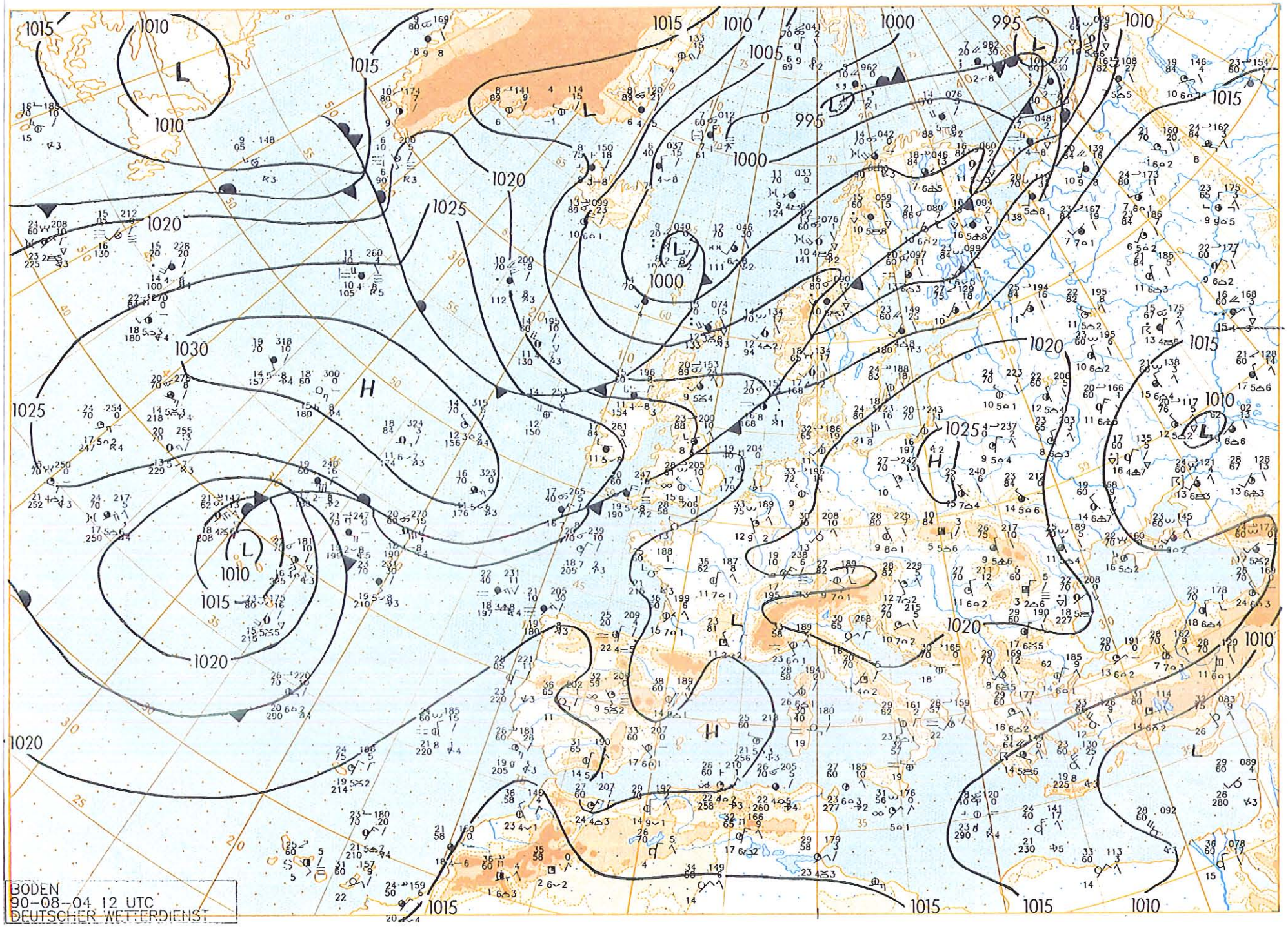
BODEN
90-08-04 12 UTC
DEUTSCHER WETTERDIENST

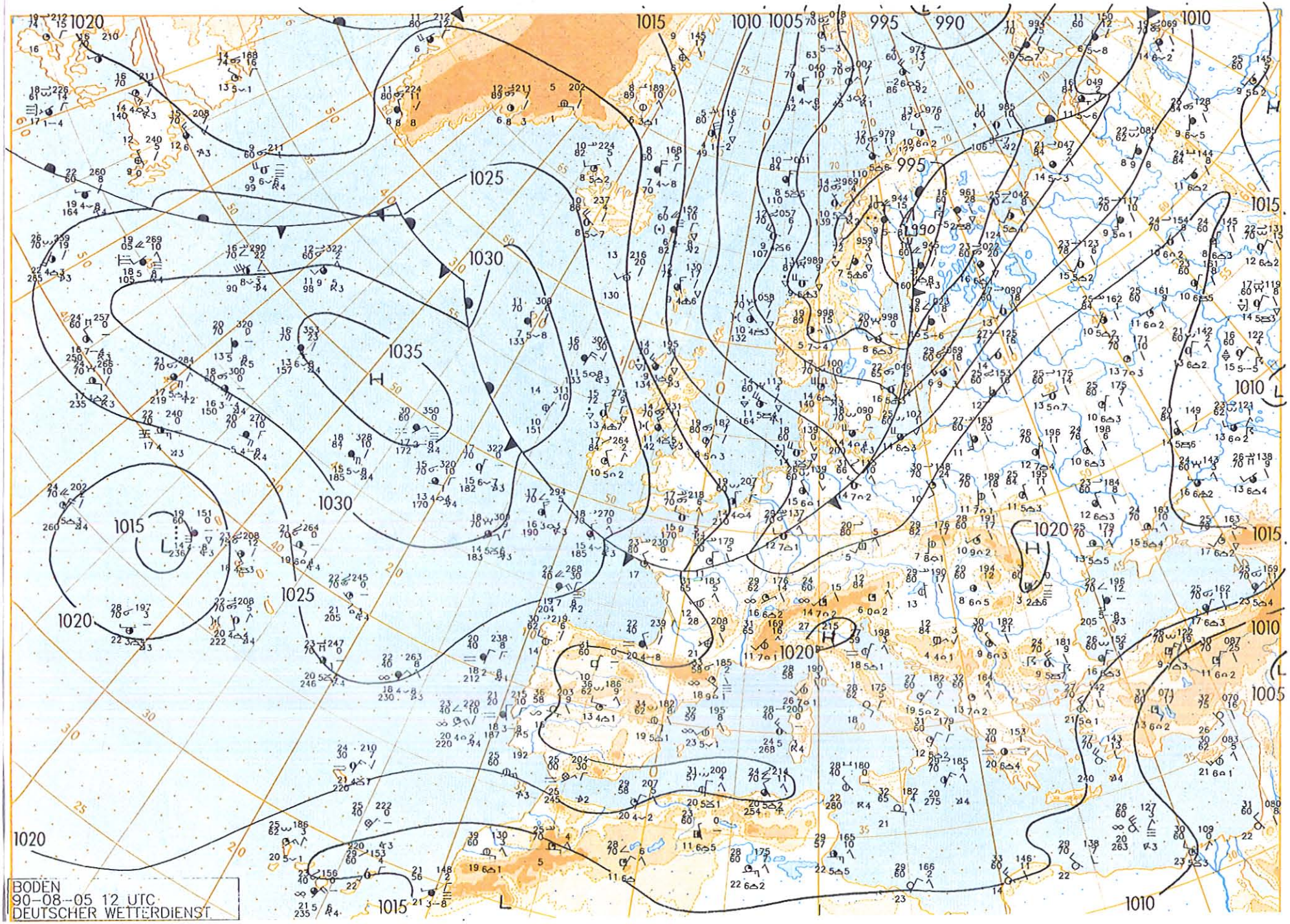
BODEN
90-08-05 12 UTC
DEUTSCHER WETTERDIENST

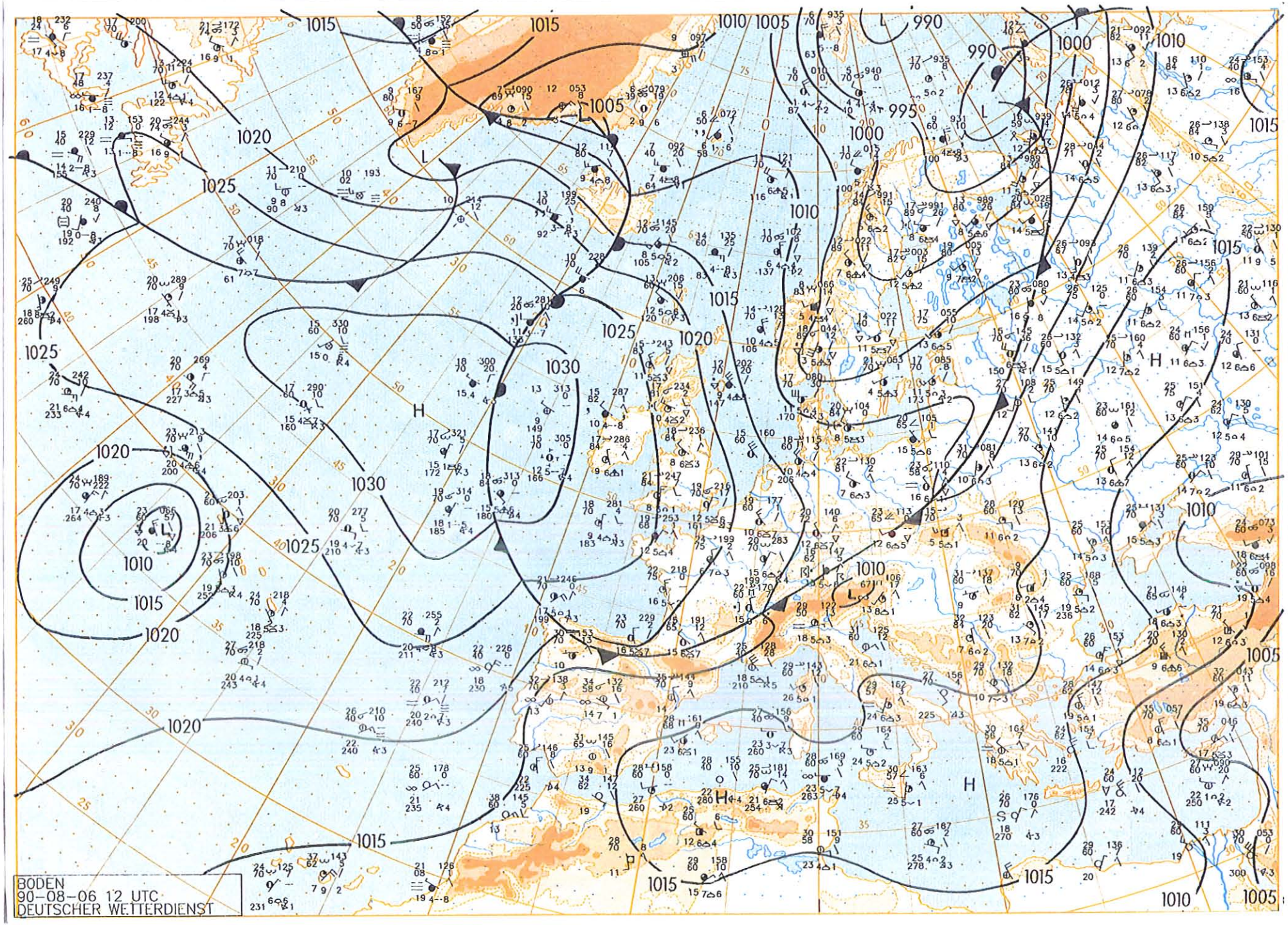
BODEN
90-08-06 12 UTC
DEUTSCHER WETTERDIENST

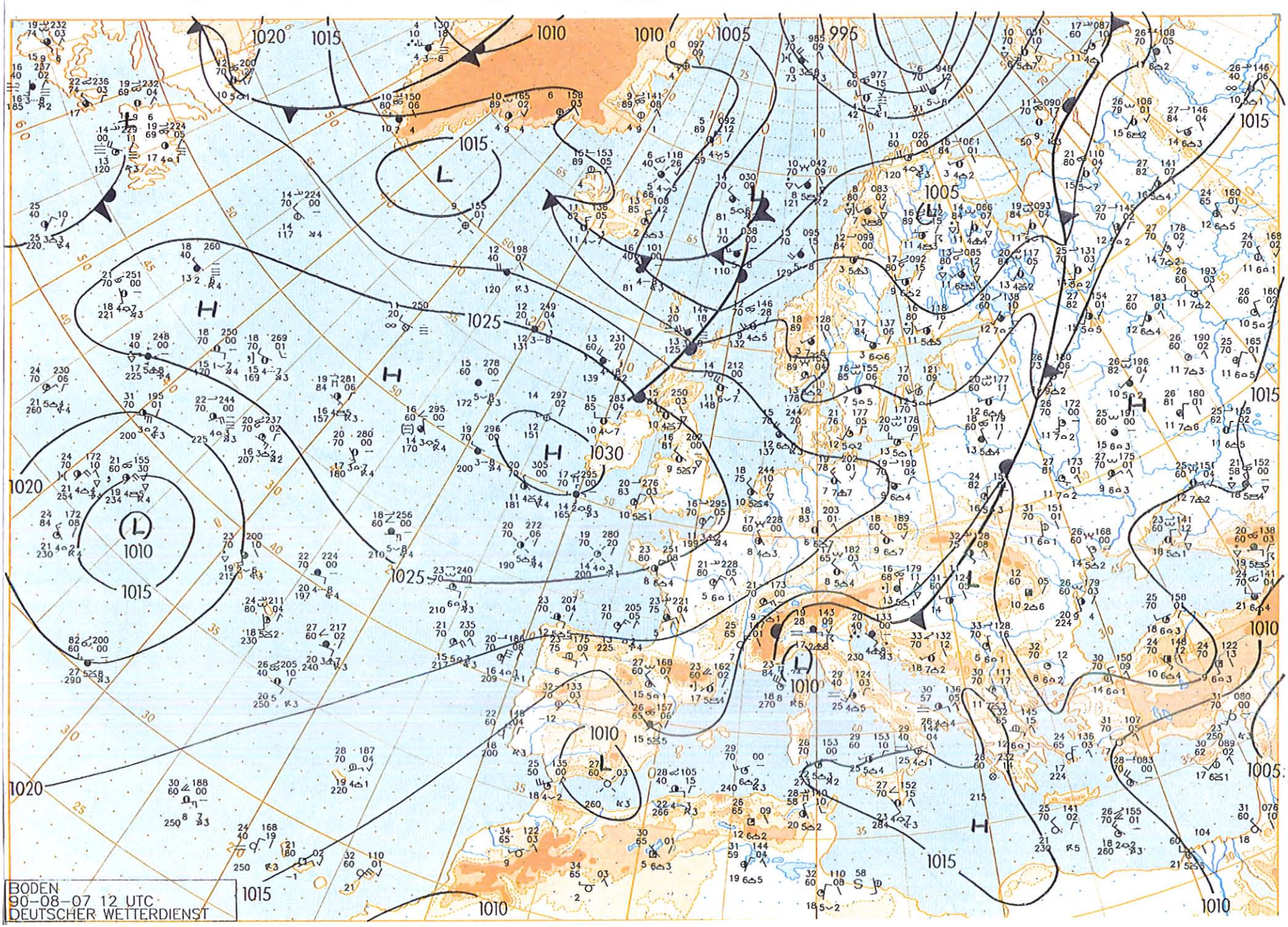
BODEN
90-08-07 12 UTC
DEUTSCHER WETTERDIENST

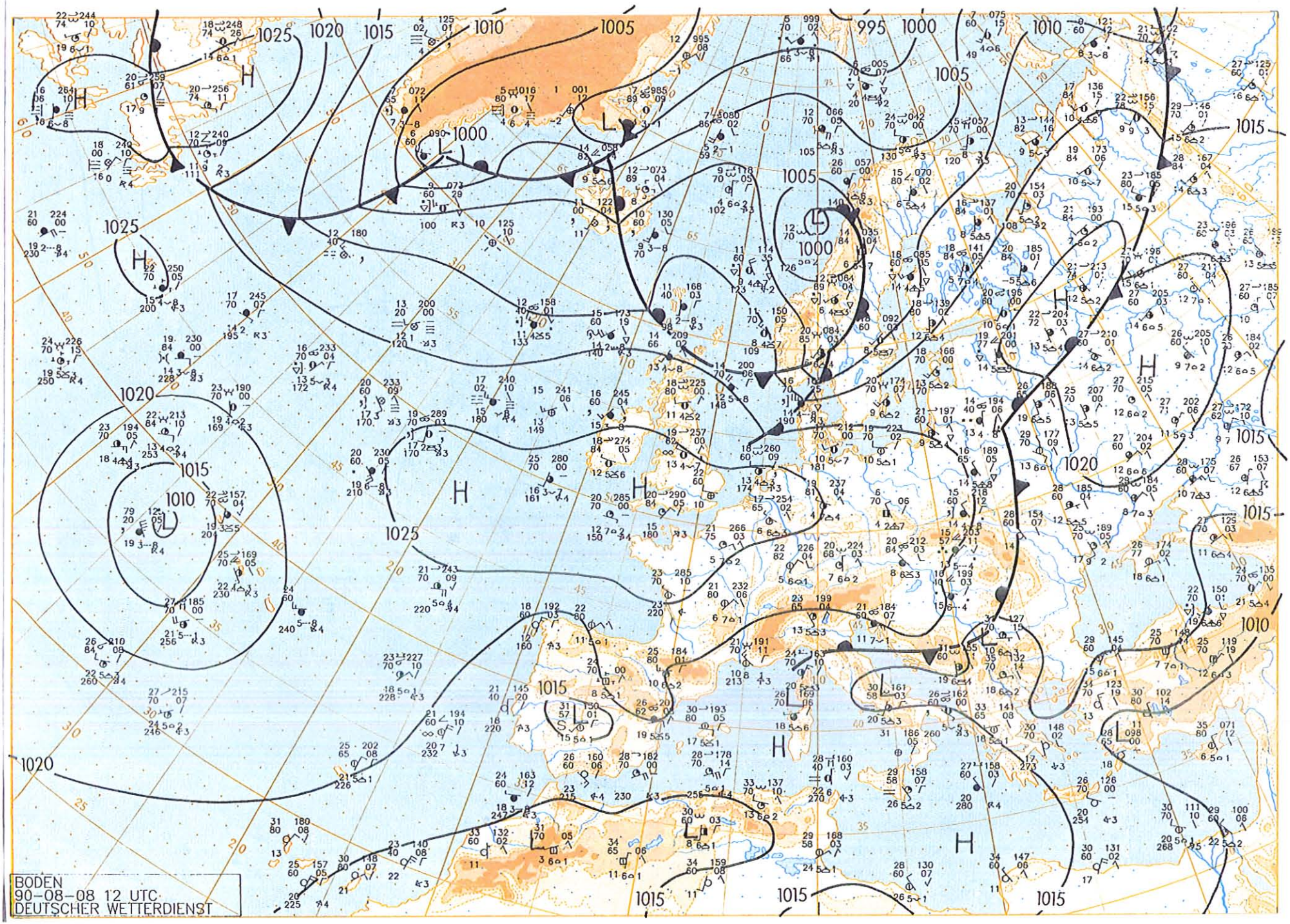
BODEN
90-08-08 12 UTC
DEUTSCHER WETTERDIENST

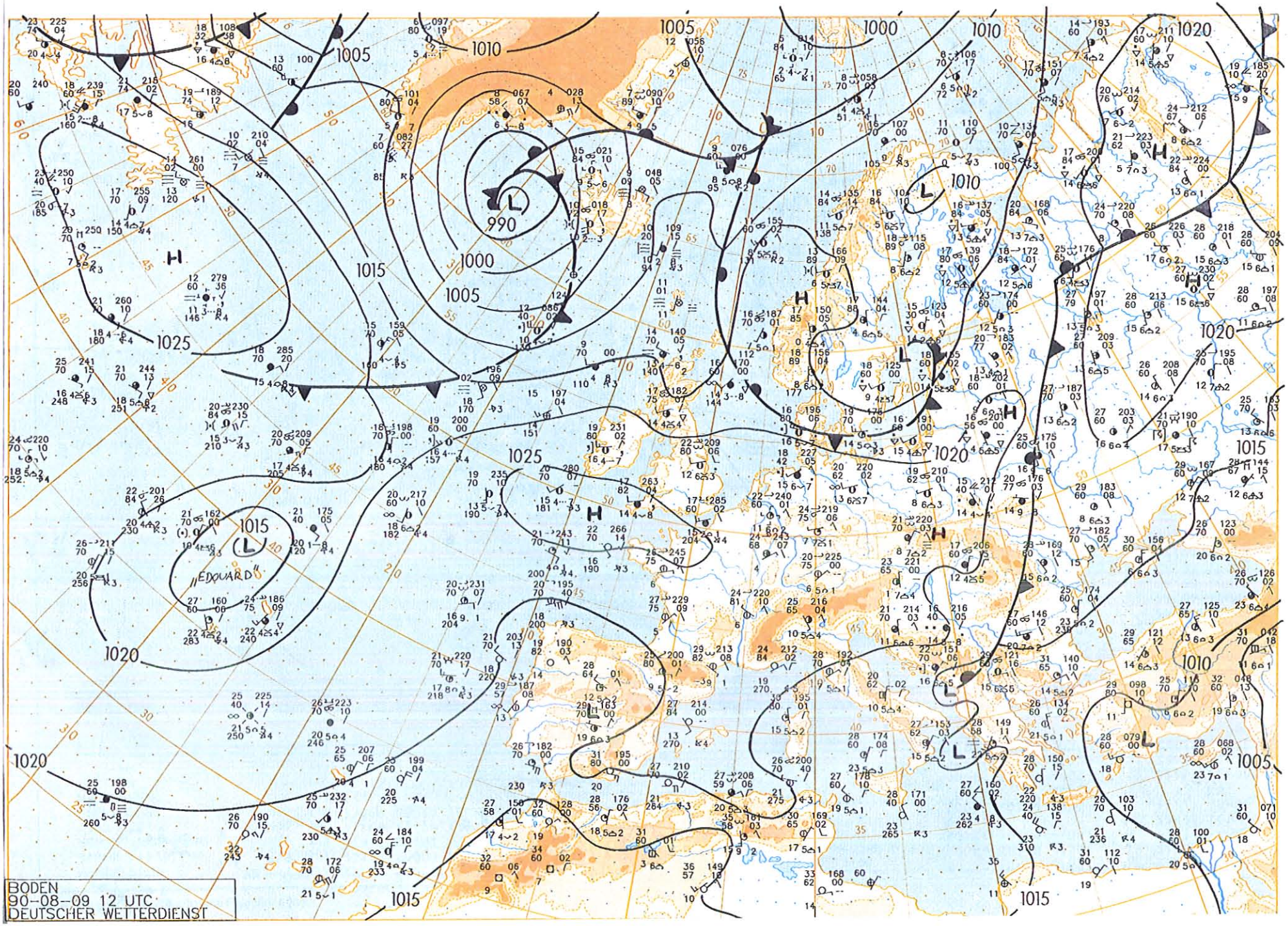
1005
1010
1000
1010
1020
990
1015
1000
1005
1025
1010
1025
1020
1015
1020
"EDOUARD"
1020
1010
1005
1020
1015
1015
BODEN
90-08-09 12 UTC
DEUTSCHER WETTERDIENST

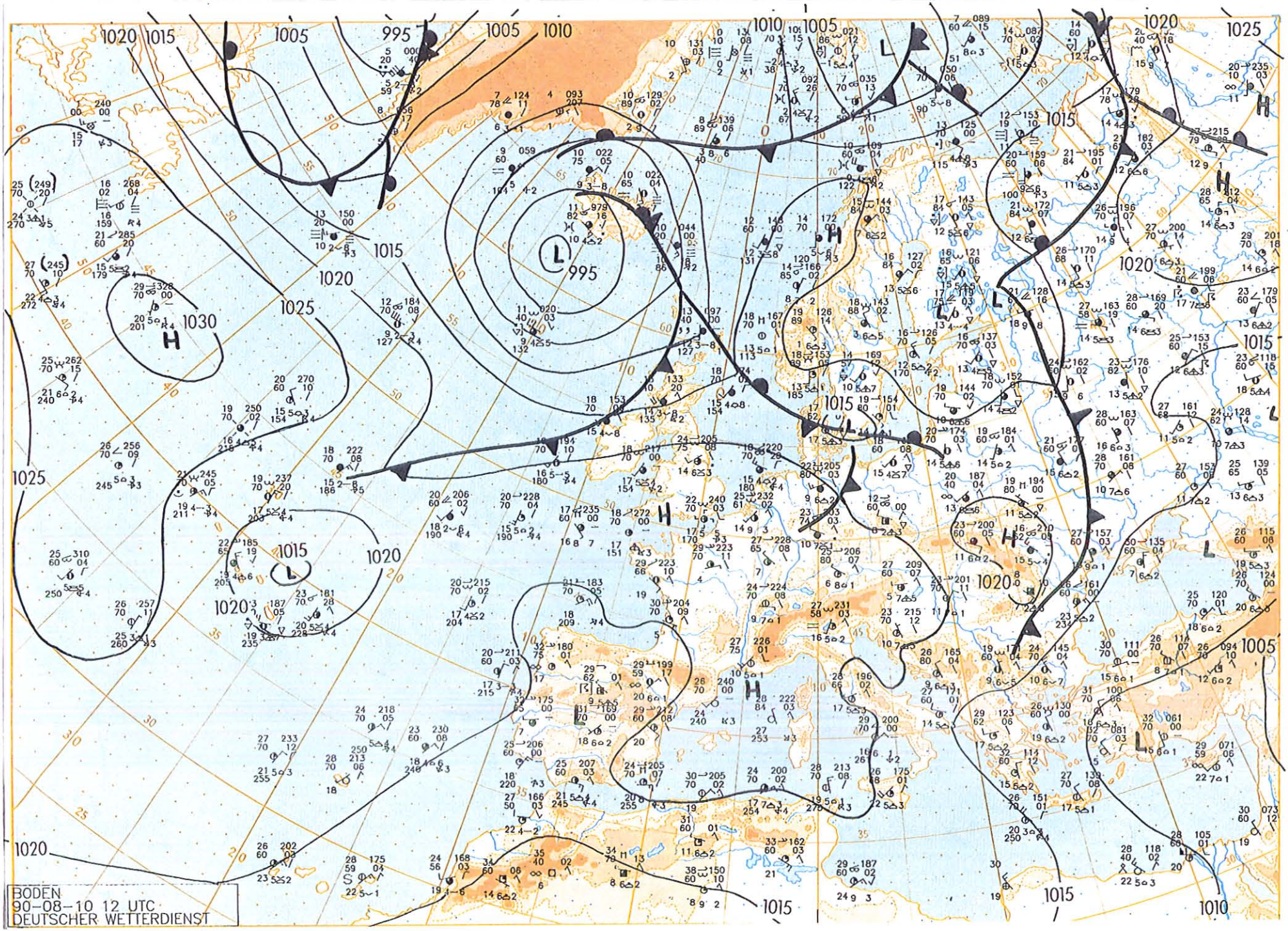
BODEN
90-08-10 12 UTC
DEUTSCHER WETTERDIENST

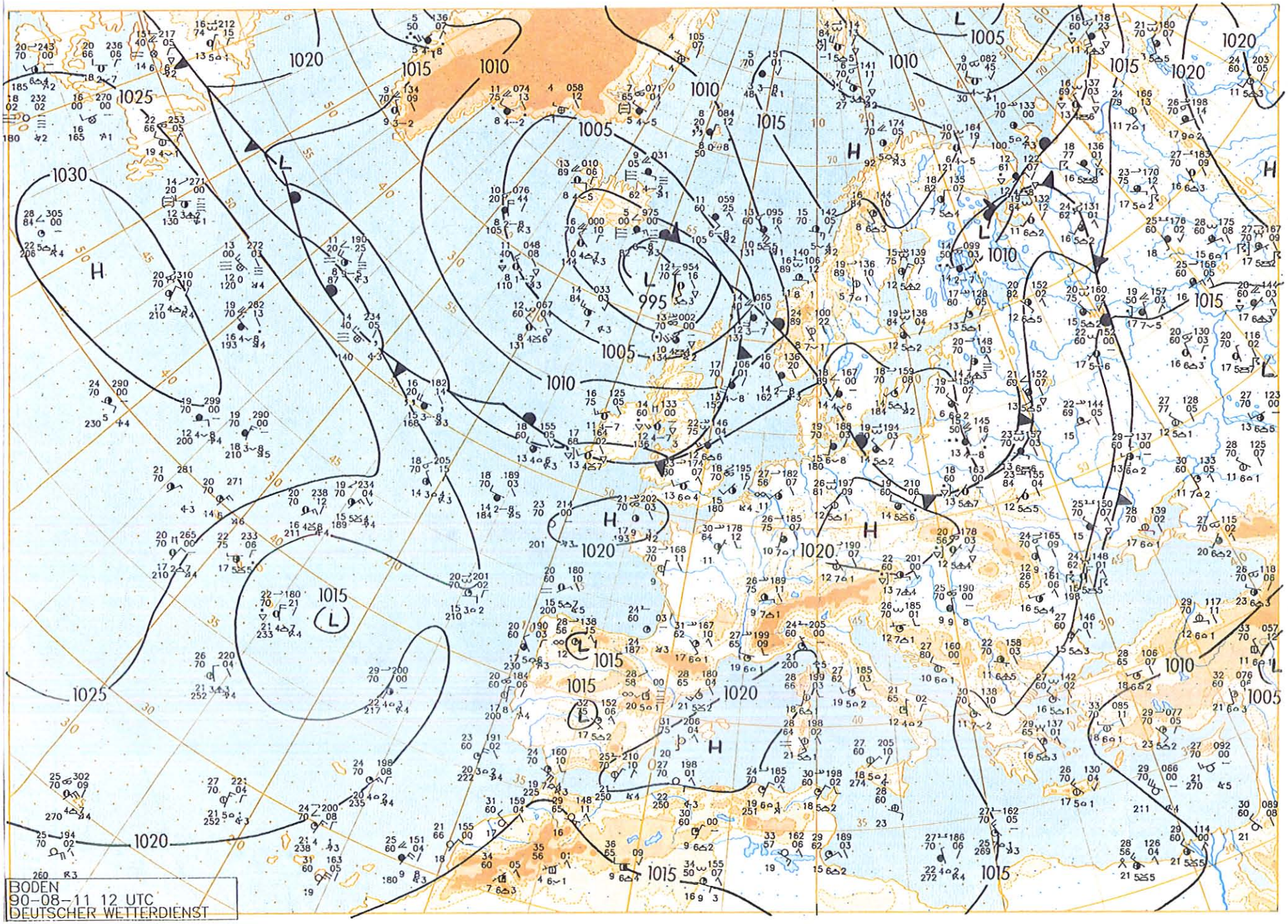
BODEN
90-08-11 12 UTC
DEUTSCHER WETTERDIENST

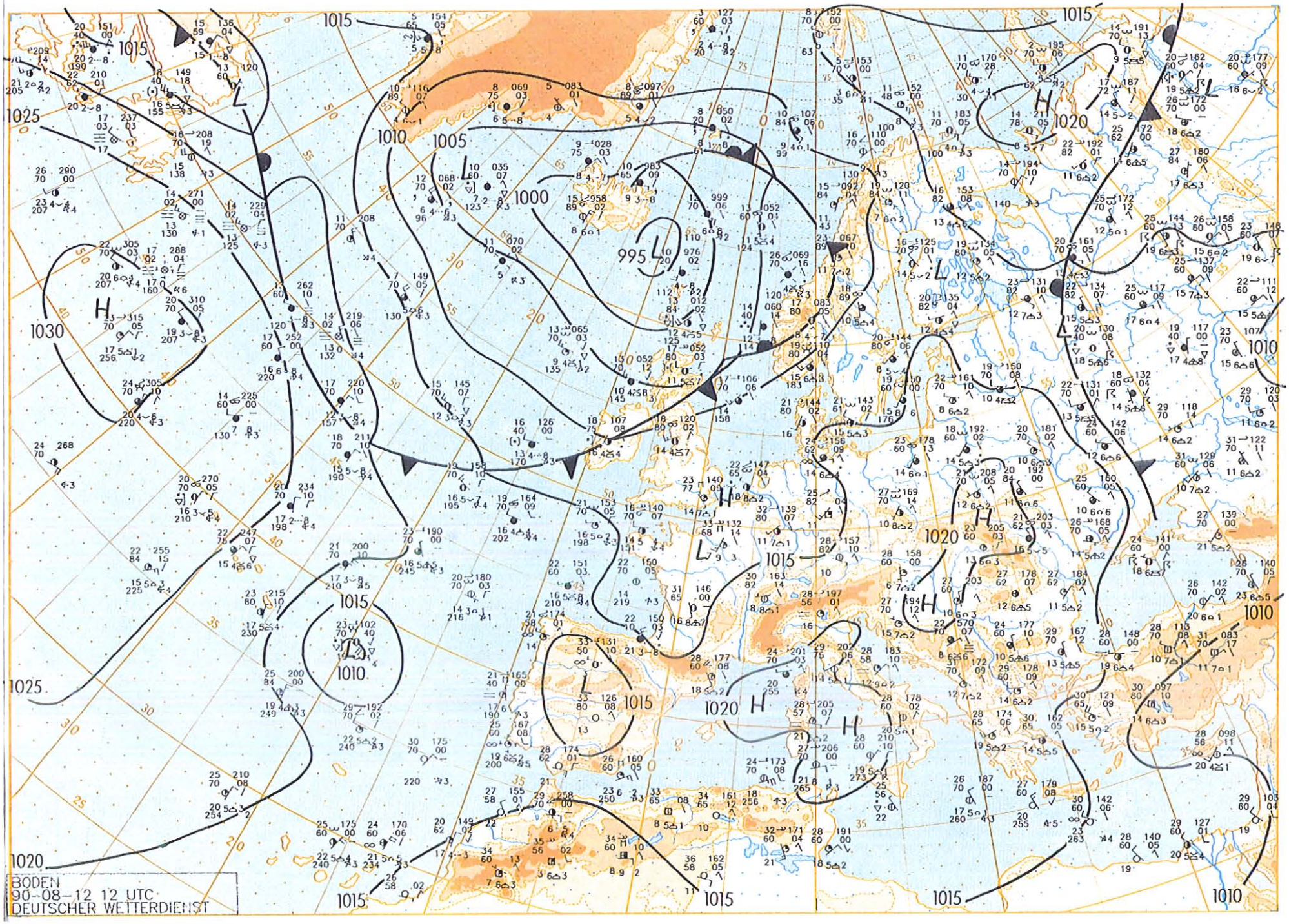
BODEN
90-08-12 12 UTC
DEUTSCHER WETTERDIENST

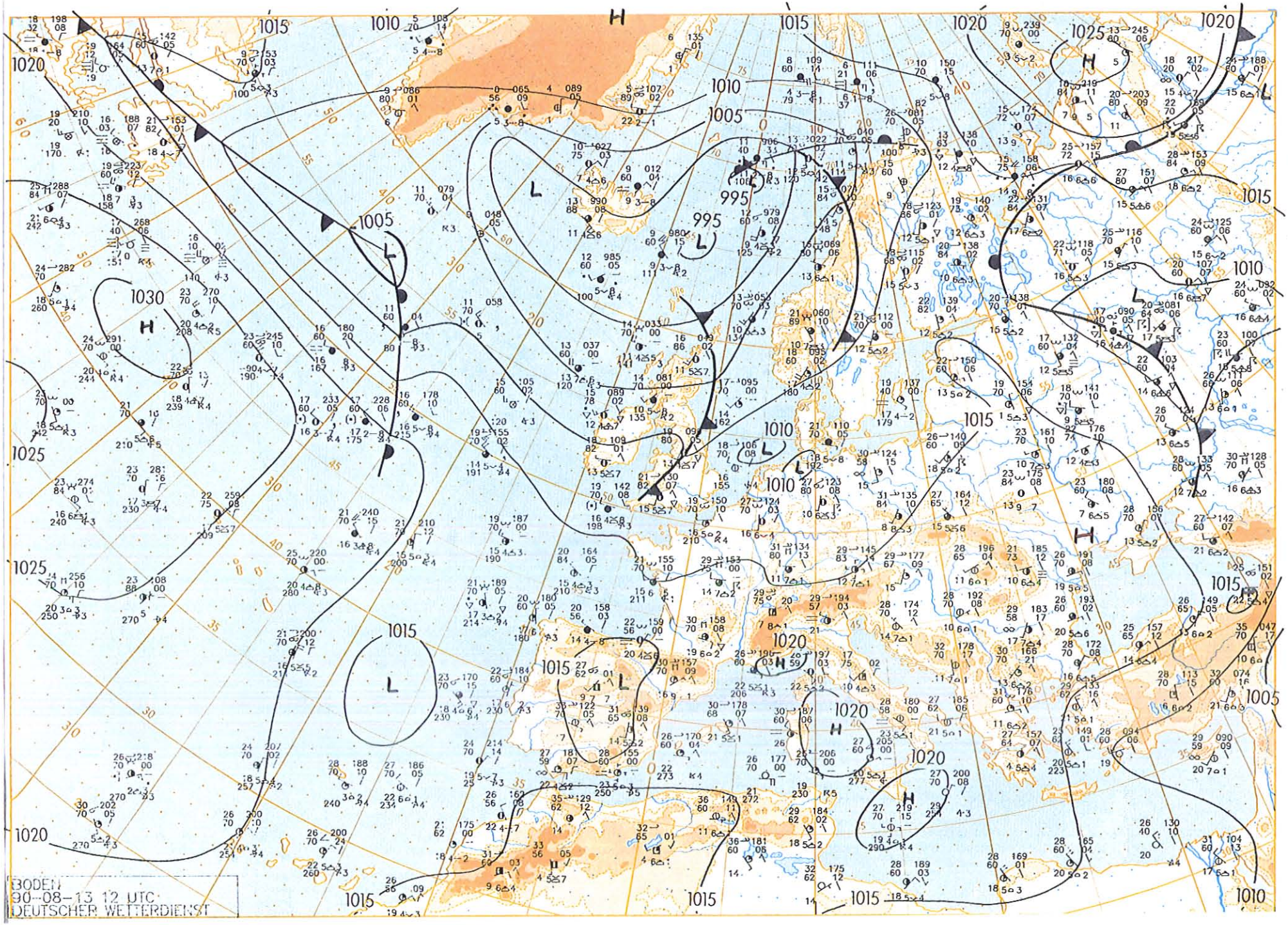
BODEN
30-08-13 12 UTC
DEUTSCHER WETTERDIENST

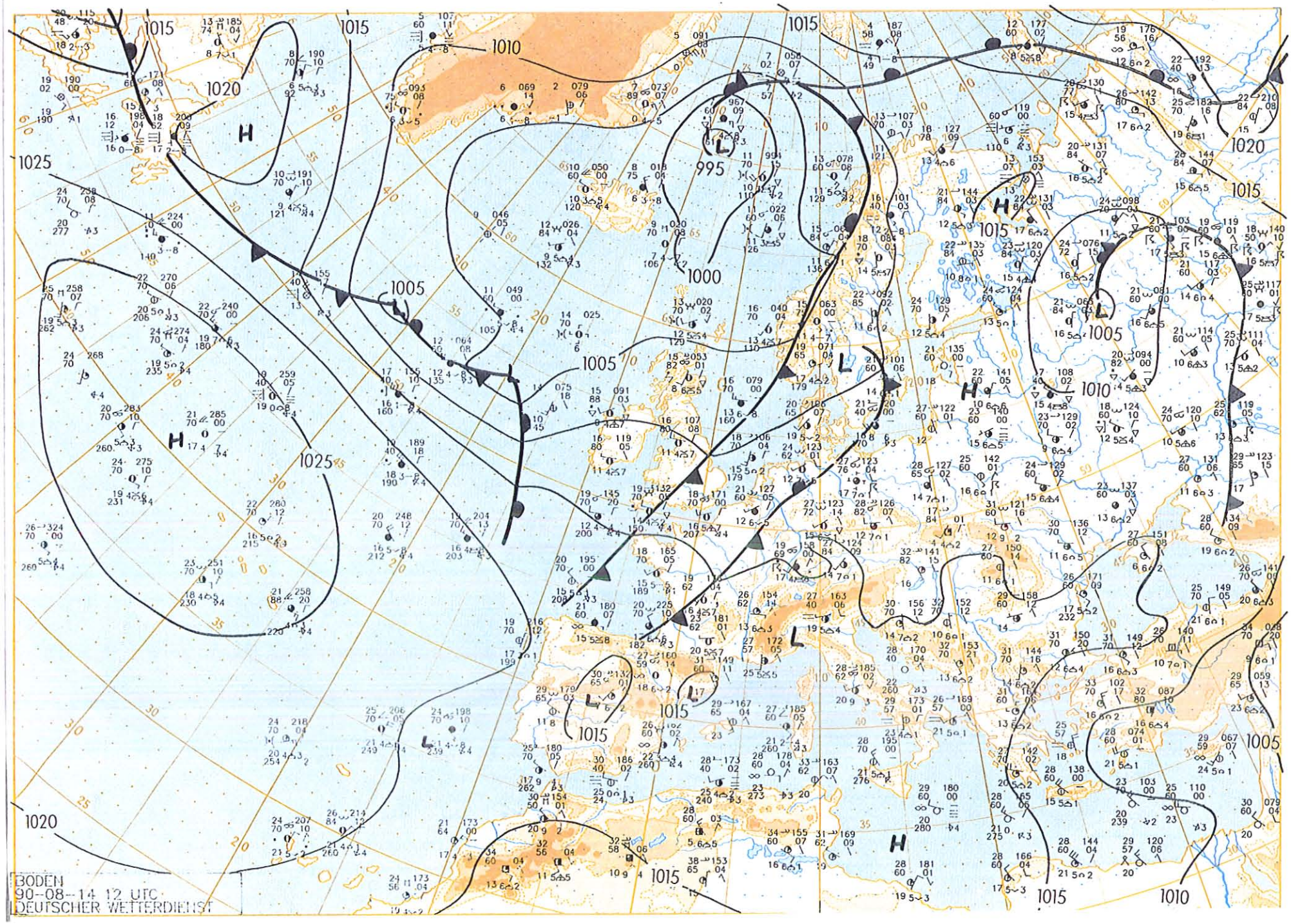
BODEN
90-08-14 12 UTC
DEUTSCHER WETTERDIENST

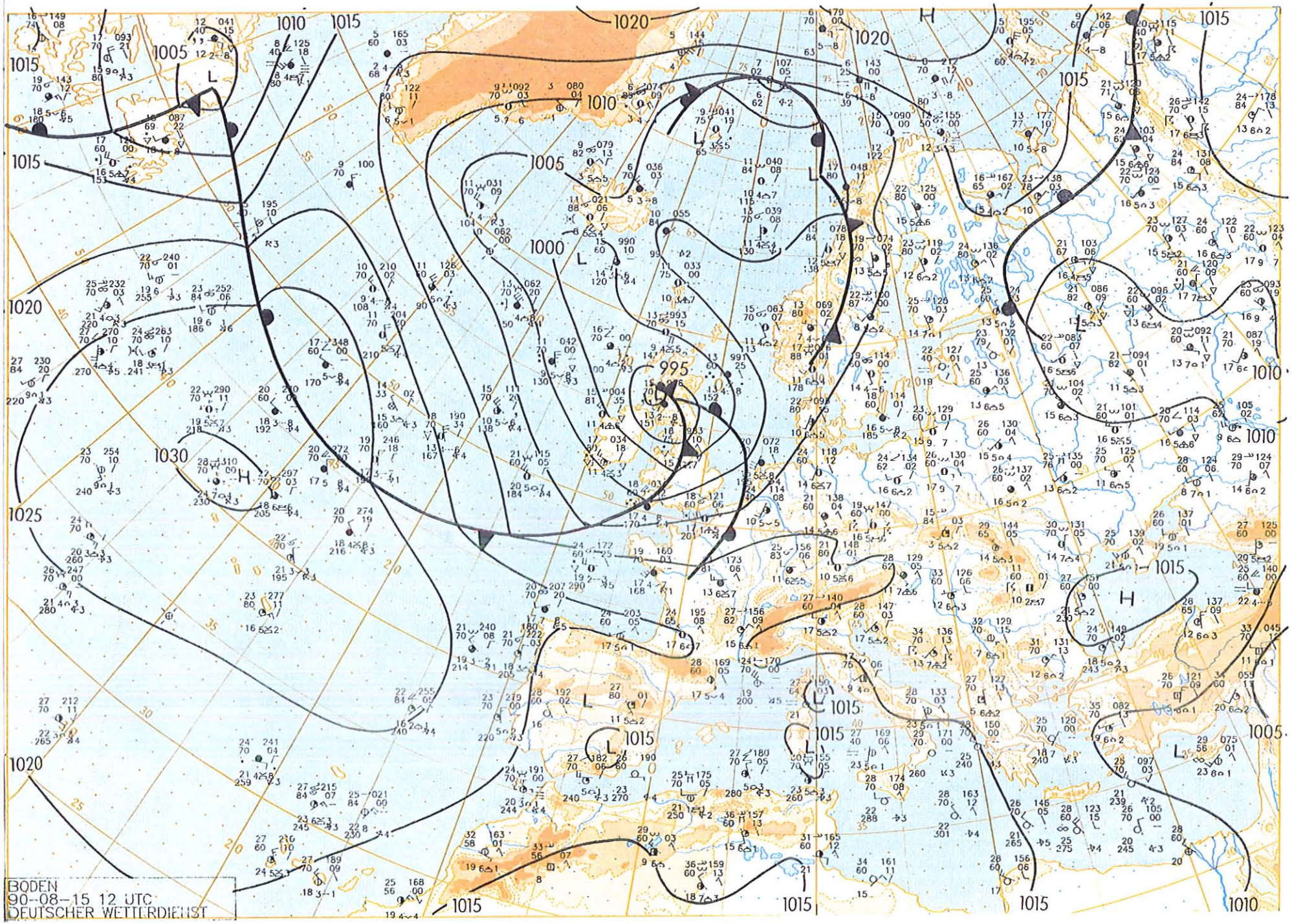
BODEN
90--08--15 12 UTC
DEUTSCHER WETTERDIENST

Forschungszentrum Jülich

Jül-3350
Februar 1997
ISSN 0944-2952